NTNU – Trondheim
Norwegian University of
Science and Technology

Transdermal Delivery of Water Soluble Molecules into Human Skin

Synne Steinsland

Preface

This master thesis was the final work of a Master's Degree Programme (5 year) in biotechnology. The laboratory work was performed during 2011/2012 at the Department of Biotechnology (Gløshaugen) and the Department of Cancer Research and Molecular Medicine (Gastrosenteret, St.Olavs Hospital), at the Norwegian University of Science and Technology (NTNU) in Trondheim.

Abstract

The skin is the largest organ of the human body and it constitutes a great protective barrier against entry of harmful microbial species and foreign materials into the body. The barrier function is a result of the highly hydrophobic nature and compact structure of the outermost skin layer, which makes transdermal delivery of drugs difficult. The aim of this study was to investigate diffusion of hydrophilic fish gelatin peptides and alginate oligomers (G-blocks) into human skin, and to evaluate the effect of skin pretreatments, vehicles and the different characteristics of the test samples on transdermal diffusion.

Fish gelatin was degraded by acid hydrolysis to produce peptides of varying molecular size, and the molecular weight distribution and molecular weight averages of the peptides were determined. Further, peptides were conjugated to fluorescent dyes, and together with fluorescently labeled G-block oligomers, they were utilized as traceable model drugs in the transdermal diffusion experiments. Full-scale skins, from healthy human adults after abdominal plastic surgery, were used and the transdermal diffusion experiments were performed in Franz-type diffusion cells. The surface of the skin tissues mounted in the diffusion cells was either untreated or treated with micro-needles or lasers, to disrupt the skin barrier. The model drugs were applied on the epidermal side of the skins in both a 60% dimethyl sulfoxide (DMSO) and a 10% polyethylene glycol 200 (PEG200) vehicle, and the vehicles were also separately applied on skins as control samples. After the transdermal diffusion experiments, imaging of the skin tissues were performed by confocal laser scanning microscopy.

An incubation time of 22 hours was determined for the transdermal diffusion experiments and pretreatments were necessary for the model drugs to successfully diffuse into the skin. Pretreatments with micro-needles and laser resulted in enhanced diffusion of the test molecules into the skin tissues compared to diffusion into untreated skin. Laser treatment was found to have the most profound enhancing effect on transdermal diffusion, and enabled efficient diffusion both into and through the skin. Of the four model drugs chosen for use in the experiments, the smallest fish gelatin peptide sample, with an estimated average molecular weight of 3000 g/mol, applied on skin tissues in a 10% PEG200 vehicle, showed the most efficient diffusion into and through human skin.

Sammendrag

Huden er kroppens største organ og utgjør en effektiv barriere som forhindrer at skadelige mikroorganismer og fremmed materiale kan gå inn i kroppen. Barrierefunksjonen er et resultat av den svært hydrofobe og kompakte strukturen i hudens ytterste lag, som gjør transdermal levering av legemidler vanskelig. Hensikten med dette studiet var å studere diffusjon av hydrofile fiskegelatinpeptider og alginatoligomerer (G-blokker) inn i hud fra mennesker, og å vurdere hvilken effekt forbehandlinger på huden, vehikler og de molekylære karakteristikkene til testmolekylene (f.eks. molekylvekt, ladning og amfifile/hydrofile egenskaper) har på transdermal diffusjon.

Fiskegelatin ble degradert ved syrehydrolyse til peptider av ulik størrelse, og peptidenes molekylvektsfordeling og molekylvektsgjennomsnitt ble bestemt. Peptidene ble konjugert til fluorescerende fargestoffer, og ble benyttet som modeller for legemidler i de transdermale diffusjonsforsøkene, ettersom de kunne spores i hudvevet. Det ble brukt fullskala hud, fra friske voksne mennesker som hadde fått utført bukplastikk, i de transdermale diffusjonsforsøkene og forsøkene ble utført i diffusjonsceller (Franz-celler). Huden som ble montert i diffusjonscellene var enten ubehandlet eller forbehandlet med mikronåler eller laser, for å forstyrre hudbarrieren. Legemiddelmodellene ble påført på hudens epidermale side både i en 60% dimetylsulfoksid (DMSO) og en 10% polyetylen glykol vehikkel, og vehiklene ble i tillegg påført hudvevene som kontrollprøver. I etterkant av de transdermale diffusjonsforsøkene ble de ulike hudvevene studert ved hjelp av konfokal laser skanning mikroskopi.

En inkubasjonstid på 22 timer ble bestemt for de transdermale diffusjonsforsøkene, og det ble funnet at forbehandling av hud var nødvendig for diffusjon av legemiddelmodellene inn i hudvevene. Sammenlignet med diffusjon inn i ubehandlet hud, førte forbehandling med både mikronåler og laser til økt diffusjon av legemiddelmodellene inn i hudvevene. Forbehandling med laser førte til størst økning i transdermal diffusjon, og gjorde det mulig for effektiv diffusjon både inn i og gjennom hud. Av de fire legemiddelmodellene som ble valgt for bruk i de transdermale diffusjonsforsøkene ble det minste fiskegelatin peptidet, med en gjennomsnittlig molekylvekt estimert til 3000 g/mol, påført huden i en 10 % PEG200 vehikkel, funnet å diffundere raskest inn i og gjennom hud.

Table of contents

Symbols and abbreviations

Alexa 488 HSS	Alexa Fluor® 488 hydrazide, sodium salt
Alexa 488 CASE	Alexa Fluor® 488 carboxylic acid, succinimidyl ester
Alexa 532 CASE	Alexa Fluor® 532 carboxylic acid, succinimidyl ester
Biopsy	Skin sample, tissue removed from a living body
DMSO	Dimethyl sulfoxide
DOL	Degree of labeling
EtOH	Ethanol
F_{HMW}	Fraction of high molecular weight
F_{LMW}	Fraction of low molecular weight
^{1}H-NMR	^{1}H-Nuclear Magnetic Resonance Spectroscopy
I_{auto}	Tissue autofluorescence given as $I_{mean\text{-}control} \pm SD$
$I_{corrected}$	Mean fluorescence intensity in the tissue corrected for DOL, $I_{corrected} \pm SD$
$I_{mean\text{-}control}$	Mean fluorescence intensity in the control tissue, given as $I_{mean\text{-}control} \pm SD$
$I_{mean\text{-}sample}$	Fluorescence intensity in the tissue only due to transdermal diffusion of fluorescently labeled sample, given as $I_{mean\text{-}sample} \pm SD$
$I_{mean\text{-}tissue}$	Fluorescence intensity in the tissue due to both trandermal diffusion of fluorescently labeled sample and tissue autofluorescence, given as $I_{mean\text{-}tissue} \pm SD$
I_{RP}	Fluorescence intensity in the receptor phase
$I_{RP\ corrected}$	Fluorescence intensity in the receptor phase corrected for DOL
KCl	Potassium chloride
KH_2PO_4	Potassium phosphate monobasic
LSCM	Laser Scanning Confocal Microscopy
$\lambda_{emission}$	Fluorescence emission maxima (nm)

λ_{max}	Absorption/Excitation maxima (nm)
MALDI-TOF	Matrix Assisted Laser Desorption-Ionization – Time-Of-Flight
MWCO	Molecular Weight Cut-Off
NaCl	Sodium chloride
$Na_2HPO_4 \cdot 2H_2O$	di-Sodium hydrogen phosphate dehydrate
$NaHCO_3$	Sodium bicarbonate
PBS	Phosphate buffered saline
PEG200	Polyethylene glycol 200
SC	Stratum Corneum
SD	Standard Deviation
SEC-MALLS	Size Exclusion Chromatography - Multi-Angle Laser Light Scattering
µS	Microsimens, unit of measurement for the conductivity of water

1. Introduction

1.1. Aim of the study

The skin is the most accessible organ of the human body and provides a possibility for delivery of drugs for both local and systemic effect. The field of transdermal drug delivery has received increasing interest due to the advantages associated with this route of administration. However, the highly hydrophobic nature of the protective skin barrier limits transdermal delivery of a wide range of drugs, especially large and hydrophilic drug molecules.

In this study the primary aim was to investigate the diffusion of hydrophilic molecules into human skin and the potential effects of physical penetration enhancement, chemically enhancing vehicles, and the molecular and structural characteristics of the applied molecules, such as molecular weight, chain conformation, amphiphilic/hydrophilic properties, and charge. Fish gelatin peptides and G-block oligomers of alginate were used as test molecules in the experiments performed to study transdermal diffusion. The test molecules were chosen for their varying physicochemical properties, and because they could act as model drugs for a range of hydrophilic drugs based on peptides/proteins and polysaccharides.

The secondary aims of this study included molecular characterization of fish gelatin peptides, performance of a pilot study to evaluate the effect of three different laser treatments in regards to both enhancing effect and skin damage and viability, and a study of diffusion kinetics in human skin.

1.2. The human skin

In simplicity, the skin can be described as the organ keeping the "inside in and the outside out" of the human body. The human skin covers an average area of 1.7 m^2, it constitutes 10% of the body mass of an average human being, and is considered to be the largest and heaviest organ of the body (Williams, 2003, Schrieber and Gareis, 2007). The skin functions as an acidic mantle, and has a natural microbial flora, comprising transient, temporary-resident and permanent-resident microbial species. The composition and density of this flora is predominantly pH-dependent. The acidic surface supports the persistence of a normal microbial flora, but limits colonization by pathogenic microbes, and thus prevents entry of

such harmful species into the body (Fluhr et al., 2005, Schrieber and Gareis, 2007). The skin barrier also protects and helps the human body to withstand cold, heat, radiation, external pressure, physical and mechanical injuries, friction and chemicals. It regulates body heat, prevents loss of moisture, and has a major function as a sensory organ (Schrieber and Gareis, 2007). In addition, vitamin D is synthesized in the human skin (Wickett and Visscher, 2006).

1.2.1. Structure of the skin

Healthy human skin can be divided into three main layers: hypodermis (subcutaneous fat layer), dermis (*corium*) and epidermis (cuticle) (Figure 1.1) (Schrieber and Gareis, 2007, McGrath et al., 2010).
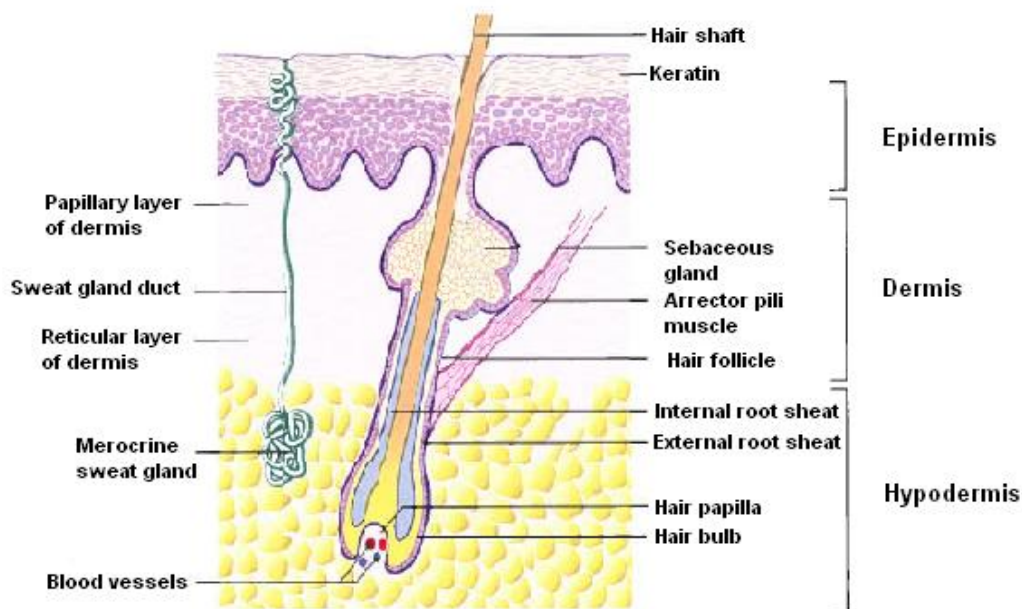
Figure 1.1: The structure of the skin including the three main skin layers: hypodermis, dermis and epidermis (Mitchell and Peel, 2009).

The hypodermis is located between underlying body constituents, such as muscles, bone, fat or cartilage, and the overlying dermis (Williams, 2003, Schrieber and Gareis, 2007). This subcutaneous layer consists of fat pads, closely packed fat cells, surrounded by a loose connective tissue. Fibers which origin in the dermis span the subcutaneous layer and are in direct contact with collagen fibers underlying the sub-cutis (Schrieber and Gareis, 2007). The thickness and structure of the hypodermis varies between individuals, in regards to body site, gender and amount of body fat (Faller et al., 2004, Song et al., 2004). The hypodermis is absent in some areas of the body, such as the eyelids, but mostly it constitute a thick layer in scale of millimeters to centimeters throughout the body (Williams, 2003, Song et al., 2004).

The subcutaneous layer can act as insulation against cold and heat, and as a supply of high-energy molecules. It also provides mechanical protection against physical injuries, and carries blood-vessels and nerve cells to the skin (Williams, 2003, Schrieber and Gareis, 2007).

The dermis is located between the hypodermis and the epidermis, and constitutes the major component of the human skin. The dermis exists of two layers, the deeper reticular dermis and the outer papillary dermis (MacKie, 2003). The reticular dermis is characterized by its irregular, dense and collagen rich connective tissue, and this layer attaches the skin to the underlying hypodermis. The papillary layer consists of a characteristic loose connective tissue that contains collagen, reticulin (a structural protein resembling collagen), elastin and fibroblasts, and it connects the epidermis to the dermis. There are less abundant cells in the reticular dermis compared to in the papillary dermis (Mitchell and Peel, 2009). Fibroblasts, macrophages, and mast cells are the three main cell types comprising the cellular components of the dermis (MacKie, 2003, McGrath et al., 2010). There is a rich blood supply to the dermis, but no blood vessels intersect the junction between the dermis and the epidermis (McGrath et al., 2010). The dermal vasculature supplies the dermis with oxygen and nutrients, removes toxins and waste products, and plays a vital role in the regulation of body temperature (Williams, 2003). In addition to blood vessels, lymphatic vessels, nerve endings, and the skin appendages, including hair follicles, sebaceous glands, and sweat glands are embedded in the dermis (MacKie, 2003, Williams, 2003).

The epidermis is the outermost layer of the human skin. The thickness of the layer varies from roughly 0.006 mm (eyelid) to 0.08 mm (palms and soles) (Aulton, 2007). It is a stratified, squamous and terminal keratinized epithelium, where the majority of cells, making up 95% of the total cell content, are the keratinocytes in the viable epidermis and the corneocytes in the non-viable epidermis (Mitchell and Peel, 2009, McGrath et al., 2010). Other cells are also located in the epidermis, such as melanocytes (pigment producing cells), Merkel cells (mechanoreceptors), and Langerhans cells (dendritic and immunological competent cells) (Williams, 2003, MacKie, 2003, Mitchell and Peel, 2009). The keratinocytes travel from the epidermal basement membrane and outwards to the surface, forming distinct layers throughout the epidermis. From the lower dermal-epidermal interface and towards the outer surface of the skin, the epidermis can be separated into five distinct layers: *stratum basale/stratum germinativum, stratum spinosum, stratum granulosum, stratum lucidium and stratum corneum* (McGrath et al., 2010). All layers are only present in body areas where the skin is considered to be thick (Mitchell and Peel, 2009). In transit, from the basal layer and

outwards to the stratum corneum (SC), the keratinocytes undergo a series of biochemical and morphological changes, including nuclei and organelle disintegration, and replacement of the cell membranes with cell envelopes of cross-linked proteins. These changes leads to the production of dead, flattened and enucleated keratinocytes, called corneocytes, which constitute the stratum corneum (SC). Overall, the continuous transformation of keratinocytes to corneocytes takes 28 days (Williams, 2003, Wickett and Visscher, 2006, Mitchell and Peel, 2009).

The stratum corneum is the last and outermost layer of the epidermis, and is a thin and non-viable membrane typically consisting of 10-15 layers of corneocytes (Williams, 2003, Benson and Namjoshi, 2008). The structure of the SC is often represented as a "brick and mortar" model. The keratin-filled corneocytes constitute the bricks, and are connected to one another through corneosomes, which originates from desmosomes (cellular bridges) in the viable epidermis. The lipid matrix in the intercellular space surrounding the corneocytes is the mortar. This matrix consists of ceramides ($\approx$50%), cholesterol (25%), free fatty acids (10-12%) and a small moiety of cholesterol sulfate ($\approx$5%) and cholesterol esters ($\approx$2%) organized in multiple bilayers. The lipid composition in the SC is different from the one found in the underlying viable epidermis, primarily consisting of phospholipids (Downing, 1992, Williams, 2003, Wickett and Visscher, 2006, Benson and Namjoshi, 2008). The constituents of the mortar comprise a lipid lamellae consisting of both crystalline and liquid domains. The combination of the corneocyte structure and the hydrophobic lipid composition form a flexible and excellent protective barrier in healthy human skin (Bouwstra et al., 2002, Wickett and Visscher, 2006).

Water also plays an important role in maintaining the integrity of the SC barrier. The continuous desquamation, or shedding, of old corneocytes from the skin surface is dependent on the activity of hydrolytic enzymes. The activity of the enzymes is further affected by the humidity in their surroundings. Thus, water is essential for the degradation of corneodesmosomes leading to detachment and shedding of corneocytes. The water activity of keratinocytes also regulates enzymes involved in the formation of natural moisturizing factor (NMF), which is the skin's natural hydration mechanism located in the SC. NMF consist of a hygroscopic mixture of roughly 50 % amino acids and 50 % salts, including lactic acid and urea. As a result of its composition, NMF function as a water-binding mechanism in the SC and assist in the maintenance of skin elasticity. A hydrated SC also reduces the risk of skin cracking (Williams, 2003, Draelos, 2005).

1.3. Transdermal administration of drugs

The transdermal route of drug administration presents an appealing alternative to other drug delivery routes. Today around 35 transdermal drug products, comprising around 20 drug molecules, are on the market. An increase in both the development of new products and the value on the global market is expected (Tanner and Marks, 2008, Subedi et al., 2010). The transdermal administration route can be used for delivery of drugs for both local effect, such as local pain relief (e.g. Ibux), and systemic effect (Thomas and Finnin, 2004, Weifa, 2012). Transdermal delivery of drugs to the systemic circulation offers a series of advantages compared to its administration counterparts. Orally delivered drugs are observed to cause gastrointestinal irritation, and during delivery the drugs are affected by variables such as enzymes, pH and gastric emptying. In addition, the liver contributes to the first pass metabolism of the drugs. Drugs delivered by the transdermal route avoid the gastrointestinal tract and are exposed to reduced first pass metabolism. Transdermal delivery potentially improves patient compliance, as a result of painless and easy treatment (in contrast to hypodermic injections or tablets). Other benefits with this route of administration are controlled and sustained delivery, reduced frequency and amount of dose, which conduce to a reduced risk of side effects, and the possibility of immediately and easy termination of treatment (Prausnitz et al., 2004, Thomas and Finnin, 2004, Tanner and Marks, 2008, Subedi et al., 2010). However, despite the great advantages of transdermal drug delivery there are few available products, which reflect the limitations associated with this route of administration, as will be described later in this section.

In transdermal drug delivery the drugs applied on the skin have three possible penetration routes. The molecules can penetrate 1) through the sweat ducts, 2) across the stratum corneum or 3) via the hair follicles and their associated sebaceous glands (Figure 1.2) (Benson and Namjoshi, 2008). The appendages only comprise about 0.1 % of the area available for transdermal penetration and are therefore generally considered as negligible (Barry, 2001, Benson and Namjoshi, 2008).
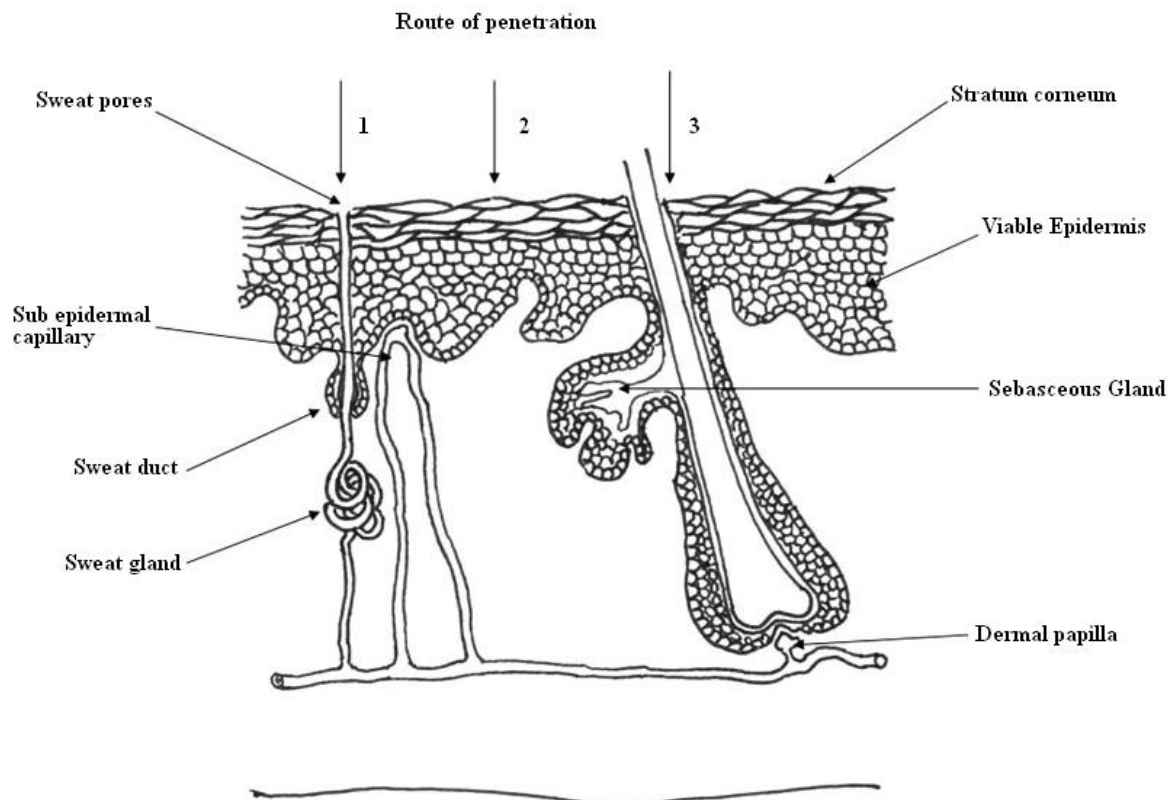
Figure 1.2: In transdermal drug delivery the drugs applied on the skin have three possible penetration routes: through the sweat ducts (1), across the stratum corneum (2) or via the hair follicles and their associated sebaceous glands (3) (Benson, 2005).

The penetration route across the SC can be divided into the transcellular route and the intercellular route (figure 1.3). The transcellular route is considered unfavorable because the drugs not only have to partition and diffuse through the corneocytes, they also have to traverse to adjacent corneocytes through the intercellular lipid matrix (Benson, 2005). This suggests that the intercellular route is the predominant route of penetration across the SC, which provides a tortuous path of diffusion much longer (500 µm) than the thickness of SC (Hadgraft, 2004, Benson and Namjoshi, 2008). After overcoming the SC barrier drug molecules must diffuse deeper into viable epidermis to reach the vasculature in the dermis, and hence the systemic circulation. Small and moderately lipophilic molecules overcome the SC and can continue their diffusion into the deeper skin layers. For hydrophilic and high molecular weight drug molecules, such as proteins and peptides, the ability to diffuse through viable epidermis and into the dermis are solely restricted by the outermost barrier of SC (Benson and Namjoshi, 2008, Karande and Mitragotri, 2009, Kalluri and Banga, 2011).
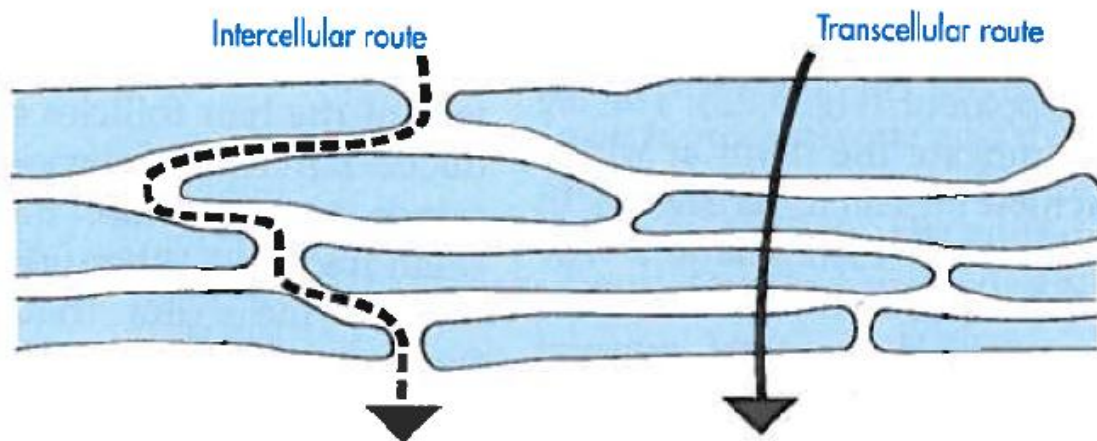
Figure 1.3: A simple illustration of the intercellular and the transcellular penetration routes across the SC barrier (Florence and Attwood, 2006).

There are several factors that influence the rate of transdermal drug delivery to and through healthy human skin. Physicochemical factors include the chemistry of the drug, skin hydration, temperature and pH, drug concentration, and molecular size and shape. Physiological factors include skin condition, skin metabolism, skin age and sites of drug application (Williams, 2003, Aulton, 2007). The hydrophobic layer of stratum corneum is considered to be the rate limiting step in transdermal drug delivery. For a molecule to passively diffuse and partition across the barrier, it must possess several physical and chemical properties. Only pharmacologically potent and low molecular weight compounds (<500 Da) with low melting points (>200˚C), and moderate lipophilicity and water solubility are allowed to passively move across the SC (Benson and Namjoshi, 2008, Kalluri and Banga, 2011). In regards to molecular size, it has been shown a correlation between molecular size and skin absorption, and for molecular weights above 500 Dalton (Da) absorption starts to rapidly decrease (Bos and Meinardi, 2000). Local skin irritation and additional adverse effects, caused by the drugs, excipients or components associated with the delivery devices, and delay in onset of action, are associated with this route of delivery. The limited drug doses that can be applied are also a disadvantageous and limiting factor in transdermal drug delivery (Brown et al., 2006, Tanner and Marks, 2008).

Intact and healthy skin holds the strong barrier of SC. However, skin disorders can affect the permeability of the barrier and in diseases where SC is defect, absorption will tend to increase. An increase in absorption can also be a result of physical injuries, such as cuts and abrasions (Aulton, 2007). Skin age show little difference in transdermal drug delivery, but both structural and functional alterations occur with aging. The moisture content of the skin is

known to decrease with age and therefore younger and more hydrated skin is more permeable compared to older skin. Blood flow also tends to decrease with age and can further reduce the transdermal flux of topically applied drugs (Williams, 2003). The thickness and nature of the SC and density of body appendages varies throughout the human body. Differences in permeation occur both between different body sites of an individual and between identical body sites in different individuals, illustrating that permeation is not only affected by the thickness of the SC (Williams, 2003, Aulton, 2007, Tanner and Marks, 2008). Race, gender and amount of body fat may also contribute to variation in drug absorption and transdermal drug delivery among individuals (Williams, 2003, Robinson, 2005).

For drug molecules unable to passively diffuse through the SC, a possibility is to increase skin permeability by chemical, enzymatic or physical modifications. The challenge is to modify SC in a safe and reversible fashion to avoid permanent skin damage or introduction of pathogens to the body (Karande and Mitragotri, 2009, Pathan and Setty, 2009). Penetration enhancement techniques can be divided into chemical and physical methods (Karande and Mitragotri, 2009, Subedi et al., 2010). Chemical methods include prodrugs, salt formation, ion pairs, eutectic systems, liposomes, vesicles and particles, and the use of chemical enhancing vehicles and other chemical enhancers (Benson, 2005, Subedi et al., 2010). For both lipophilic and hydrophilic drugs water is the most natural and safe penetration enhancer, and in addition to altered solubility of the drug and partitioning from the vehicle, it is a possibility that hydration of the skin results in increased penetration due to swelling and opening of the SC (Benson, 2005). Skin hydration can be increased by the use of occlusive dressings, which lower the transepidermal water loss and increase the skins capacity of water holding (Praessler and Fluhr, 2005).

Chemical enhancers reduce the barrier properties and increase the permeability by altering the structure of the intercellular lipid matrix in the SC (Kalluri and Banga, 2011, Karande and Mitragotri, 2009). Chemical enhancers can be grouped into hydrocarbons, alcohols, acids, amines, amides, esters, surfactants, terpenes, sulfoxides, lipids and miscellaneous complexes. Polyethylene glycol (PEG) is a solvent in the group of alcohols that has been found to increase skin permeability. Alcohols may enhance skin diffusion through different mechanisms, including extraction of lipids, swelling of the SC or improving drug partitioning into the skin (Karande and Mitragotri, 2009). PEG is non-toxic and non-immunogenic, and is known to have an amphiphilic nature, which makes the polymers soluble both in water and organic solvents. Further, it is widely used in pharmaceutical formulations such as oral

solvents in liquid-filled capsules, and dermal ointments and creams (Barnes et al., 2008). The aprotic solvent dimethyl sulphoxide (DMSO), which tends to form hydrogen bonds with itself rather than with water, is considered to be a "universal solvent" (Pathan and Setty, 2009). DMSO increases the lipid fluidity, and hence the permeability of SC due to the alterations in the lipid matrix, and is found to enhance penetration of both hydrophilic and hydrophobic molecules. This solvent is concentration-dependent and to achieve optimal penetration enhancement, concentrations of > 60% is required (Williams and Barry, 2004, Notman et al., 2007, Pathan and Setty, 2009). The high concentration dependency of DMSO can, however, cause skin irritation and cutaneous eruptions (Williams and Barry, 2004, Benson, 2005, Pathan and Setty, 2009).

Physical penetration enhancement methods disrupt the skin barrier, and include the use of micro-needles, iontophoresis, electroporation, sonophoresis, jet injectors, lasers, thermal and radiofrequency ablation, and ablation by tape stripping. Both chemical enhancers and physical methods act individually, but they can also be combined to produce a synergistic enhancement effect (Benson, 2005, Karande and Mitragotri, 2009, Kalluri and Banga, 2011). Physical penetration enhancement techniques based on micro-needles and laser treatment were of particular interest in this study.

1.3.1. Micro-needles

Micro-needles are a minimally invasive technique where needles in the size range of microns create channels or holes in the skin/SC, through which skin-impermeant molecules can be transported (Prausnitz, 2004, Kalluri and Banga, 2011). Micro-needle devices consist of a plurality of needles with a general length range from 25-2000 μm attached to a base support (Donnelly et al., 2010). The micron-sized pores created by micro-needles can allow for transport of macromolecules, supramolecular complexes and micro-particles across the SC barrier and into deeper layers of the skin (Prausnitz, 2004). Micro-needles can either be categorized as solid or hollow. Solid micro-needles can be utilized either to porate the skin before a drug molecule is applied or can be coated with the drug prior to poration (Figure 1.4a and b). Hollow micro-needles can be used to infuse or inject a liquid drug formulation (Figure 1.4c). Another possibility is to encapsulate the drug in biodegradable micro-needles that will dissolve and release the drug in the skin after poration (Figure 1.4d) (Benson and Namjoshi, 2008, Kalluri and Banga, 2011). Perforation by micro-needles, followed by removal of the device results in higher skin permeability compared to micro-needles that remain in the skin.

This is probably due to a blockage of the pores, either by the supporting material from which the needles project or by the needles themselves (Henry et al., 1998). A drawback associated with micro-needles is the limited amount of dose that can be coated on solid micro-needles or loaded in biodegradable micro-needles (Kalluri and Banga, 2011).
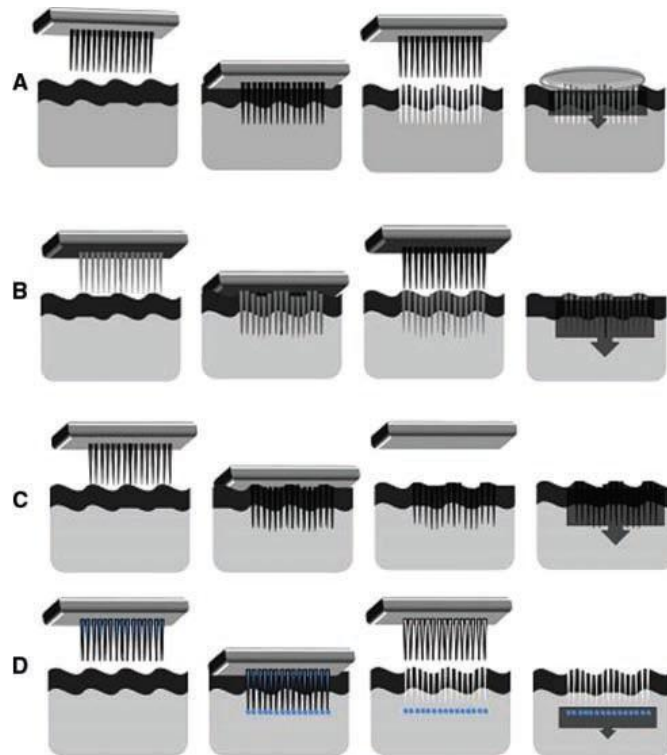
Figure 1.4: A schematic overview of micro-needle design and mode of application in transdermal drug delivery: a) Solid micro-needles porate the skin prior to drug application, b) solid micro-needles coated with drug prior to skin poration, c) biodegradable micro-needles with encapsulated drug that dissolve and release the active substance in the skin, d) hollow micro-needles that infuse or inject the drug (Escobar-Chavez et al., 2011).

During poration of the skin, small micro-needles avoid the nerves and blood vessels found in deeper layers of the skin and are therefore not associated with pain, and cause minimal skin irritation. This is because they generally only penetrate the SC and the epidermis (Henry et al., 1998, Kaushik et al., 2001, Bal et al., 2008). Though, the needles penetrating the skin may also be inserted into both the epidermis and the superficial layers of the dermis, depending of the micro-needle device used. The painless conception of micro-needles can therefore also be explained by the reduced risk of the small needles to encounter nerves and stimulate a response causing pain (Prausnitz, 2004). However, micro-needle devices consisting of longer

needles, such as the one used in this study (1500 µm), reach deeper into the skin and increases the risk of pain and damage of blood capillaries, causing bleeds (Badran et al., 2009).

The use of micro-needles in transdermal drug delivery gives rise to different safety concerns. The risk of needle fracture in the skin indicates a need for micro-needles with appropriate geometry and physical properties. Micro-needles with a safety margin value, defined as the ratio between the fracture force and the insertion force, greater than one, will not fracture when inserted into the skin. Needles with a small tip radius strengthen by a thick wall achieve the highest safety margin values (Prausnitz, 2004). In addition sterility and time until pore closure is important parameters affecting the possibilities of skin infections and irritation (Kalluri and Banga, 2011). The pore size after micro-needle perforation decreases with time and for the method to be fully reversible the pores must eventually be closed (Badran et al., 2009). Recovery of the barrier function of SC in the micro-pores is reported to occur as early as 2 hours after poration in absence of occlusion. Resealing of micro-pores in occluded sites ranges from 3-40 hours, depending on the geometry of the utilized micro-needles (Gupta et al., 2011). Others have reported evidence of repair and pore closure after 8-24 hours (Haq et al., 2009).

Micro-needle based applicator designs exist on the market, including different micro-needle patches utilizing the different designs and application modes given in Figure 1.3. These patches differ from the traditional patch delivery systems because they require external energy or pressure to ensure sufficient and desired depths of penetration through the skin barrier. Applicator devices, providing consistent penetration, or manual application methods can be used for this purpose. However, consistent depths of penetration and constant pressure are more difficult to obtain with manual methods of application. Micro-needle rollers (MTS-Rollers™, Dermaroller®) are available in different models for both personal and clinical use, and are primarily developed for cosmetical and dermatological applications (Donnelly et al., 2010). Due to the already existing market of micro-needle based technology and its promising prospects in transdermal drug delivery, a micro-needle device of the type Dermaroller® (Dermaroller LLC, USA) was chosen as a physical enhancement method in this study.

1.3.2. Laser treatment

Lasers are widely used in the treatment of dermatological conditions and in cosmetic resurfacing of the skin, and include treatment of acne, acne scars, aging, photodamage, depigmentation, wrinkles and general smoothing of the skin (Fernandes, 2005, Brown et al.,

2006, Benson and Namjoshi, 2008). In laser treatment high energy laser beams are directly applied on the skin and results in controlled ablation of the SC. The heat generated at the skin surface cause a rapid evaporation of water molecules and formation of vertical holes in the size range of microns, functioning as channels through SC and into deeper skin layers of the skin (Brown et al., 2006, Benson and Namjoshi, 2008). A laser can create a pattern of multiple spots or channels through skin, where only a fraction of the treated area is damaged and surrounded by intermediate undamaged and unexposed skin. This can be described as ablative fractional resurfacing, and both CO_2 and low intensity erbium YAG (yttrium-aluminum-garnet) lasers are utilized (Hædersdal et al., 2010).

In addition to skin treatment, laser ablation is suggested as a possible physical penetration enhancement method in transdermal drug delivery (Benson and Namjoshi, 2008, Kalluri and Banga, 2011). Laser treatment increases the skin permeability of both hydrophilic and lipophilic drugs. However, a more significant increase in the permeation of hydrophilic drugs compared to lipophilic drugs has been found, indicating a correlation between the chemical nature of the drug molecule and the impact of the SC barrier on transdermal drug delivery (Lee et al., 2001). Different parameters, such as the wavelength of the laser light emitted, pulse energy applied, laser power, duration of radiation, pulse repetitions, spot size and number and density of spots, influence the degree of barrier disruption (Lee et al., 2001, Brown et al., 2006, Hædersdal et al., 2010). The advantages of laser treatment in drug delivery are reported to be the short treatment time, controlled removal of tissue, minor adverse effects and minimal pain (Brown et al., 2006). However, laser treatments used in dermatology are basically described as burns, which can cause a variety of adverse effects. These effects include pain, persistent redness, blistering (edema), infections and pigment changes (Gold, 2010). The high costs apparatus and need for expert operation to minimize safety risks such as burns, restricts the use of laser to clinical settings. In terms of transdermal drug delivery this means a poor patient compliance when it comes to self administration and home use (Barry, 2001).

Laser treatment was included in this study only to provide a standardized method to penetrate human skin. This standardization was of great value in studying the transdermal diffusion of hydrophilic molecules through human skin from different donors. The treatment provided identical patterns of laser spots, including identical laser spot density, distance between spots, and spot depth and diameter at the site of application of test molecules.

1.4. Diffusion through skin

For a topically applied drug to act either locally or systematically it must penetrate the SC barrier of the skin (figure 1.3). The SC is a passive diffusion barrier that show no evidence of metabolic transport processes (Florence and Attwood, 2006). Passive diffusion occurs when matter moves from one region of a system to another through random molecular motion. The diffusion of isotropic materials, materials with identical structural and diffusional properties in all directions, can be described by Fick's first law of diffusion (Equation 1.1) (Aulton, 2007).

$$\mathbf{J} = -\mathbf{D}\frac{\partial \mathbf{C}}{\partial \mathbf{x}}$$ (1.1)

In the equation, J is the flux of the drug, D is the diffusion coefficient, C is the concentration and x is the measured diffusion distance. The negative sign indicates that the flux moves down the concentration gradient, thus in the direction of decreasing concentration (Aulton, 2007). Passive diffusion of water and non-electrolytes of low molecular weight through the epidermis is proportional to concentration and the solute partition coefficient between the tissue and the vehicle. Steady state transport through the skin can be described by the form of Fick's first law given in Equation 1.2 (Florence and Attwood, 2006).

$$\mathbf{J} = \left(\frac{\mathbf{DP}}{\delta}\right)\Delta \mathbf{C_v}$$ (1.2)

Here, P is the partition coefficient of the solute between the vehicle and the skin, δ is the thickness of SC and ΔC_v is the concentration difference between the vehicle and the tissue (Florence and Attwood, 2006). The drug diffusion coefficient in the skin will be determined by physicochemical factors such as molecular size, shape and charge, and the partitioning coefficient will be determined by the properties of both the drug and the vehicle used.

1.5. Biopolymers as model drugs and potential candidates for transdermal drug delivery

Polymers are macromolecules built up from small residues called monomers. A molecule is commonly regarded as an oligomer if it contains 2-20 such monomer residues and as a polymer if the molecules contain >20 monomers and have a molecular weight above 10000 g/mol. Biopolymers are biologically occurring polymers, and the most important biopolymers are normally divided into nucleic acids and nucleotides, proteins and amino acids, carbohydrates and lipids. Biopolymers can also be divided either by their chemical properties or their function (Smidsrød and Moe, 2008).

Proteins and peptides are polymers constructed from 20 different amino acids. The amino acids are linked together through peptide bonds between the α-carboxyl group of one amino acid and the α-amino group of another. The amino acid composition and sequence of proteins and peptides determine their properties and function. Peptides can be regarded as fragments of larger proteins or polypeptides obtained by cleavage of peptide bonds in the amino acid sequence (Nelson et al., 2008). The amino acids, and thus proteins and peptides, have zwitterionic nature, which means that they contain both positive and negative charges at physiological pH. This feature strongly affect their physical properties (Smidsrød and Moe, 2008). Proteins and peptides are approved for medical use and are classified as biopharmaceuticals (Benson and Namjoshi, 2008, Antosova et al., 2009). Drugs based on proteins and peptides are predominantly delivered through the parenteral route (injections and intravenous infusion). This route is disadvantageous due to a need for repeated administration and low patient compliance (Kalluri and Banga, 2011). Transdermal delivery (section 1.3) has therefore been suggested as an attractive alternative.

Proteins and peptides are generally high molecular weight molecules with amphiphilic, hydrophilic, and/or charged nature (Benson and Namjoshi, 2008). A consequence of this is poor permeation through the skin barrier and the need for penetration enhancement techniques to overcome the skin barrier, as described in section 1.3. A majority of proteins and peptides are intended for systemic effect. However, administration through the transdermal route to target sites in the skin also provides a great potential for local therapeutic effect (Benson and Namjoshi, 2008, Namjoshi et al., 2008). In this study, fish gelatin peptides, representing peptides in general, were utilized as model drugs.

Polysaccharides are biopolymers built up by monosaccharide residues linked together by glycosidic linkages. They have diverse chemical structures, giving rise to diverse properties, as polysaccharides differ from each other in the identity of their repetitive monosaccharide residues, chain length, types of glycosidic bonds in the polysaccharide chain and degree of branching (Smidsrød and Moe, 2008, Nelson et al., 2008). In this study, oligomers of the polysaccharide alginate were also utilized as hydrophilic model drugs in this study.

1.5.1. Fish gelatin – an amphiphilic model drug

Gelatin in general is a very versatile biopolymer derived from the fibrous protein collagen, the most abundant protein found in animals (Veis, 1964, Babel, 1996). Collagen is the major component of connective tissues and bones, and its molecular structure is made up by three parallel α-chains that constitute a right-handed triple helical rod. The three α-chains have the general amino acid sequence Gly-X-Y, where X often is proline (Pro) and Y often is hydroxyproline (Hyp), but yet each chain in a collagen molecule have a singular amino acid composition (Haug and Draget, 2009, Eysturskaro et al., 2009). The imino acids proline and hypdroxyproline cause a left-handed helical structure. Hydrogen bonds stabilize the collagen triple helix, and covalent cross-linking between the three α-chains gives collagen its super-helical structure. Gelatin is derived from collagen through partial hydrolysis and gives rise to a polydisperse gelatin product (Haug et al., 2004, Eysturskard et al., 2009).

The raw material sources for gelatin production can be mammalian sources, such as bovine or porcine, or marine sources, including both warm and cold water fish species (Haug and Draget, 2009). Gelatin (mainly mammalian) is utilized in a variety of applications in the food, pharmaceutical, medical and cosmetic industries, reflecting their diverse properties and their non-toxic and biodegradable nature (Haug and Draget, 2009). Gelatins from marine sources are suggested as potential alternatives to mammalian gelatins and they have several appealing advantages. Utilization of marine gelatins is not associated with the risk of "mad cow disease" (bovine spongiform encephalopathy, BSE), and their use are in fully acceptance with Islam and minimally restricted by other religions compared to bovine and porcine gelatins. The fishery industry generates a large biomass of fish waste that, rather than being discarded, can serve as a rich marine sources for fish gelatin. Thus, fish gelatin can be provided at low costs (Karim and Bhat, 2009). Other factors, however, restrict the range of use of fish gelatin in industrial applications, such as low manufacturing efficiency, due to low concentrations of collagen in fish skin. Fish gelatin may also be a potential allergen, and they have physical

properties that are sub-optimal compared to mammalian gelatin (Haug et al., 2004, Schrieber and Gareis, 2007).

Amphiphilic gelatin peptides obtained by acid hydrolysis of cold water fish gelatin were chosen as model drugs in this study. Fish gelatins from cold water species, such as cod and pollock, have a different amino acid composition compared to gelatins from mammalian sources and warm water fish species, as illustrated by Table 1.1 (Haug and Draget, 2009).

Table 1.1: The composition of amino acids in collagen, type A and type B gelatins from bovine sources and in fish gelatins from both cold water and warm water species, given as number of amino acid residues per 1000 residues (Haug and Draget, 2009).

Amino acid	Type I collagen (bovine)	Type A gelatin	Type B gelatin	Cold water fish gelatin	Warm water fish gelatin
Alanine	114	112	117	112	123
Arginine	51	49	48	49	47
Aspargine	16	16	46	48	48
Aspartic acid	29	29			
Glutamine	48	48	72	72	69
Glutamic acid	25	25			
Glycine	332	330	335	347	347
Histidine	4	4	4	11	6
4-Hydroxyproline	104	91	93	60	79
Hydroxylysine	5	6	4	5	8
Isoleucine	11	10	11	11	8
Leucine	24	24	24	21	23
Lysine	28	27	28	28	25
Methionine	6	4	4	3	9
Phenylalanine	13	14	14	13	13
Proline	115	132	124	96	119
Serine	35	35	33	63	35
Threonine	17	18	18	24	24
Tyrosine	4	3	1	9	2
Valine	22	26	22	18	15

The content of the imino acids Pro and Hyp are responsible for the differing physical properties between mammalian gelatins and cold water fish gelatins (Table 1.1). The low gelling modulus and low gelling and melting temperatures of cold water fish gelatin is a result of a lower content of Pro and Hyp compared to mammalian gelatin (Haug et al., 2004). The imino acids Pro and Hyp have aliphatic side chains with characteristic cyclic structures. The imino group that participates in peptide linkage is held in a rigid conformation that reduces the structural flexibility in regions of proteins and peptides containing Pro and Hyp (Nelson et al., 2008). The lower content of Pro and Hyp is therefore likely to give cold water fish gelatin a less rigid and more flexible chain conformation compared to mammalian gelatins with

higher imino acid content. Cold water fish gelatin has an isoelectric point (IEP) around 8-9.5, and thus a weak net positive charge at physiological pH (Gudmundsson, 2002).

Cold water fish gelatins were considered a good choice as model drugs based on that gelatin is derived from collagen, which is a naturally occurring protein in skin. In addition, cold water fish gelatins were chosen due to the possibly reduced chain rigidity in solution compared to mammalian gelatins. These structural features were believed to make fish gelatin applicable as vectors for transportation into the skin layers, and thus as model drugs in the transdermal diffusion experiments.

1.5.2. Alginate – a polyanionic model drug

The alginate polymer have been used as device in human health applications, including excipients in drug delivery, immobilization of cells for possible use in human transplantation and cell therapy, drug delivery and wound dressings (Ertesvåg and Valla, 1998, Dettmar et al., 2011, Draget and Taylor, 2011). Alginate is a linear polysaccharide primarily found in marine brown algae, where it constitute close to 40 % of the dry weight of the seaweed and function as a structural substance providing strength and flexibility to the tissue of the algae. In addition, soil bacteria, such as *Azotobacter vinelandii*, and a selection of *Pseudomonas* species, produce alginate for capsular protection and surface adhesion.

The alginate molecule is a copolymer with a varying composition and sequence of (1→4)-linked β-D-mannuronic acid (M) and α-L-guluronic acid (G) monomers (Figure 1.5a) (Draget et al., 2006, Smidsrød and Moe, 2008). The extended and stiff structure of alginate is a result of rotational hindrance caused by diaxial bonds in G-blocks (Draget et al., 2005, Draget and Taylor, 2011).
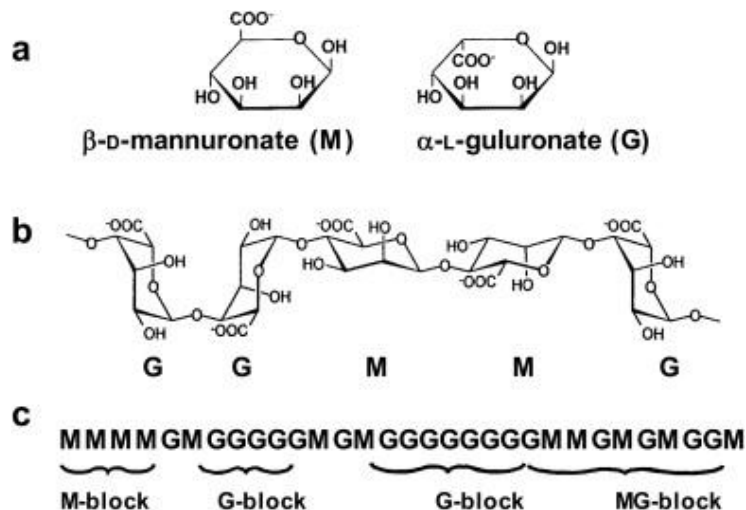
Figure 1.5: The structural characteristics of alginate. **a)** The two monomers β-D-mannuronic acid (M) and α-L-guluronic acid (G), **b)** the alginate chain presented in chair conformation and **c)** an alginate chain represented by the symbols of the monomers illustrating the block sequence (Draget et al., 2006).

It is common to describe alginate as a block copolymer that contain M-blocks, G-blocks, and MG-blocks, where the former two are homopolymeric regions of M and G, respectively, and the third represents an alternating sequence of both monomers (Figure 1.5b and c). Both the fraction of M and G residues (F_M and F_G) and the length of the block sequences can vary greatly in an alginate molecule, ranging from a fully homopolymeric β-D-mannuronat polymer ($F_M = 1$) to a polymer with a α-L-guluronate content of >70% ($F_G = 0.7$). This variation in chemistry are reflected by alginates with various physical properties (Draget et al., 2006, Smidsrød and Moe, 2008).

The pKa values of the carboxylic groups of M and G monomers are 3.38 and 3.65, respectively (Draget et al., 2006). This means that alginate is negatively charged at physiological pH and characterized as a polyelectrolyte (Smidsrød and Moe, 2008). The polyelectrolyte nature at pH > pKa make it possible for alginate to interact electrostatically with other charged polymers in a mixed system, resulting in phase transitions and altered rheological behavior (Draget et al., 2006). Recently, low molecular weight G-blocks have been found to enhance mucosal drug delivery. Interactions between mucin (negatively charged glycosylated proteins) and other macromolecules lead to increased mechanical properties in the mucus barrier. However, charged G-block oligoelectrolytes, which are too small to create intermolecular cross-links, can eliminate these types of interactions through electrostatic competitive inhibition. This elimination of interactions modifies the mucin network to such an extent that the structure opens up and drug bioavailability increases due to

increased mucosal uptake (Draget and Taylor, 2011). The negatively charged glycoproteins that constitute the mucin fibres in mucus can be compared to the components of the extracellular matrix throughout the human body (Alberts et al., 2002, Cone, 2009). G-blocks may therefore lead to the same alterations in the extracellular matrix as in the mucin network, and may thus enhance the delivery of drugs through transdermal administration. In addition, alginates of high G content are known to be non-immunogenic, while the opposite is true for a high content of M (Otterlei et al., 1991). For these reasons G-blocks were chosen as an appropriate model drug in transdermal diffusion experiments, giving rise to test molecules that possibly would behave very different in combination with skin compared to the cold water fish gelatins also used as model drugs.

1.6. Fluorescence

The process resulting in fluorescence occurs in certain molecules called fluorophores or fluorescent dyes, and comprises three stages: excitation, the lifetime of the exited state and emission (Haugland et al., 2005). This three-stage process is illustrated in Figure 1.6. (Haugland et al., 2005).
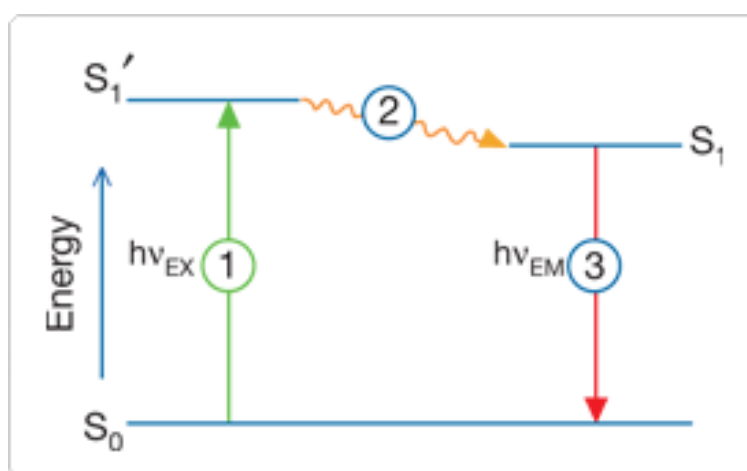
Figure 1.6: Figure 1.7: Jablonski diagram, an electronic-state diagram, which illustrates the three processes excitation (1), the exited-state lifetime (2) and emission (3), which result in fluorescence (Haugland et al., 2005)

In the first stage of the process leading to fluorescence, an external source of light provides a photon of energy, $h\upsilon_{EX}$, that is absorbed by a fluorophore causing it to shift from its ground state (S_0) to an exited state (S_1) (Haugland et al., 2005). Stage two of the process is the exited-state's lifetime; a short period of time that equals the time an excited molecule remains in the excited state. This lifetime is also called the fluorescent lifetime and is usually in the

range of nanoseconds (10^{-9} s) to picoseconds (10^{-12} s)(Albani, 2007). During the excited-state lifetime the fluorophore undergoes the phenomenon of internal conversion, where a loss in energy to the environment results in the return of the excited fluorophore to its lowest or relaxed excited state (S_1), which is the origin of fluorescence emission. From this state the fluorophore can return to its ground state (S_0), through different competitive processes, including fluorescence emission, such as loss of energy as heat, release of energy to nearby molecules by collisional quenching or fluorescence resonance energy transfer (FRET), and intersystem crossing (Haugland et al., 2005, Albani, 2007). Fluorescence emission is the third and last stage, and when a photon of energy, $h\upsilon_{EM}$, is emitted, the fluorophore returns to its ground state. Because of the energy loss during the exited-state lifetime the emitted photon, $h\upsilon_{EM}$, have a lower energy level resulting in a longer wavelength compared to the excited photon, $h\upsilon_{EX}$. The difference in wavelength between the excited and the emitted photon, $h\upsilon_{EX}$ - $h\upsilon_{EM}$, is called the Stokes shift (Haugland et al., 2005).

The three-stage process of fluorescence is cyclical, meaning that one fluorophore can be excited and detected repeatedly. As long as the fluorophore avoids irreversible damage in the excited state, it can give rise to thousands of photons, a property essential for the high sensitivity provided by fluorescence detection techniques. Molecules consisting of multiple atoms in solution replace the single electronic transitions $h\upsilon_{EX}$ and $h\upsilon_{EM}$ with two broad energy spectra, namely a fluorescence excitation spectrum and a fluorescence emission spectrum. For a single fluorophore the excitation spectrum is, almost without exception, identical to the absorption spectrum, and at the excitation wavelength the intensity of emission is proportional to the amplitude of excitation in the fluorescence excitation spectrum (Haugland et al., 2005).

In all applications where fluorescent probes function as detection tools, such as in this study, the detection sensitivity can be affected by background signals. Interfering background signals can be a result of reagent background, where the signals are caused by unbound probes or probes bound nonspecific, or they can arise from endogenous sample constituents, a phenomena called autofluorescence (Haugland et al., 2005). The impact of autofluorescence can be studied by using longer wavelengths, as autofluorescence generally decreases when imaging at wavelengths greater than 550 nm (Zeiss et al., 2012). In human tissue autofluorescence is caused by endogenous fluorophores, and in human skin the known fluorophores are collagen, elastin, NADH, tryptophan, flavins and porphyrins. All of these fluorophores have certain excitation and emission wavelengths. Collagen-linked fluorescence

has excitation and emission bands in the region 330-500 nm, and has received increased interest due to its role in skin changes during aging and photoaging. Fluorescence from elastin is less studied due to its relatively weak signals, which is highly overlapped by the emission of other fluorophores (Na et al., 2001). When studying transdermal diffusion of fluorescently labeled molecules the contribution of autofluorescence should be taken into account. Autofluorescence corrections are of particular relevance when comparing transdermal diffusion in human skin from different donors or in skin retrieved from different body sites of a donor.

2. Materials and methods

2.1. Materials

2.1.1. Fish gelatin - precursor for the fish gelatin peptides

The cold water fish gelatin used as a model drug in skin diffusion experiments was provided by Norland Products Inc., USA (FG6, Batch 8004). It is a type A fish gelatin with a high molecular weight distribution (HMWD), produced from the skins of cod, haddock and pollock.

2.1.2. Alginate - precursor for the G-blocks

High guluronic acid Na-alginate (degraded alginate) was provided by FMC BioPolymer AS, Norway (Batch 907-255-01).

2.1.3. Alexa Fluor® dyes

The spectral properties of the three fluorophores applied in the fluorescence labeling of the fish gelatin peptides and G-block samples, are given in Table 2.1. All the dyes were purchased from Invitrogen, Norway.

The Alexa 488/532 carboxylic acid, succinimidyl ester (CASE) fluorophores bind to primary amines in proteins, peptides and amine-modified nucleic acids via a Shiff base reaction and results in an amine bond that exhibit the stability of a peptide bond. The Alexa Fluor® 488 hydrazide, sodium salt (HSS) fluorophore binds to the reducing end of polysaccharides through an aldehyde linkage (Invitrogen, 2010).

Table 2.1: An overview of the spectral properties of the Alexa Fluor® dyes, which include molecular weight (M_w), absorption/excitation maxima (λ_{max}), emission maxima ($\lambda_{emission}$) and extinction coefficient (ε) (Invitrogen, 2010).

Fluorescent dye	M_W [g/mol]	λ_{max} [nm]	$\lambda_{emission}$ [nm]	ε [cm^{-1}M^{-1}]
Alexa Fluor® 488 carboxylic acid, succinimidyl ester	643,41	494	517	73000
Alexa Fluor® 532 carboxylic acid, succinimidyl ester	723,77	530	554	81000
Alexa Fluor® 488 hydrazide, sodium salt	570,48	493	517	73000

2.1.4. NaHCO$_3$ - buffer

Sodium bicarbonate (NaHCO$_3$, 8.4 g) was dissolved in MQ-water and adjusted to pH 8.3 and 500mL. The solution was applied in the conjugation of fish gelatin peptides to the Alexa Fluor® dyes.

2.1.5. DMSO

Dimethyl sulfoxide (DMSO) is an aprotic solvent that was used both as solvent and as a chemically enhancing vehicle in the transdermal diffusion experiments (Sigma-Aldrich, France).

2.1.6. PEG200

A polyethylene glycol with an average degree of polymerization of 200 (PEG200) was used as a chemically enhancing vehicle in transdermal diffusion experiments (Batch 81150, Sigma-Aldrich, Germany).

2.1.7. PBS-buffer

The phosphate buffered saline (PBS) was prepared by dissolving NaCl (8.0 g, M_W = 58.44 g/mol), Na$_2$HPO$_4$ · 2H$_2$O (1.44 g, M_W = 177.99 g/mol), KCl (0.2 g, M_W = 74.55) and KH$_2$PO$_4$ (0.2 g, M_W = 136.09 g/mol) in MQ water. The pH of the buffer was adjusted to 7.4, and the volume to 1000mL. This buffer constituted the receptor phase in the transdermal diffusion experiments.

2.1.8. TissueTek®, O.C.T^{TM}

TissueTek® is a tissue glue, which is a formulation of water-soluble glycols and resins that provide a convenient specimen matrix for cryostat sectioning at temperatures of -10°C and below (Sakura, Netherland). This material was used to attach skin biopsies on cork for transportation, and on a specimen disc to enable cryo sectioning.

2.2. Methods

2.2.1. Preparation of fish gelatin peptide samples

Fish gelatin (FG) peptides were prepared for two purposes; a general experiment to examine the kinetics of fish gelatin degradation to obtain FG peptides, and for preparation of FG peptides for further use in transdermal diffusion experiments.

#### 2.2.1.1. Degradation by acid hydrolysis - kinetics

Fish gelatin (0.75 g) was dissolved in hydrochloric acid (HCl; 0.2 M, 5 mL). To obtain complete dissolution the fish gelatin was added into the liquid under stirring conditions at room temperature. This procedure was repeated for eleven different samples. The degradation was performed at 90°C, and sampling was performed after 1, 2, 4, 6, 8, 12, 16, 18, 20, 24 and 36 hours, yielding eleven samples with different degradation time (Figure 2.1). Each sample was cooled to room temperature and adjusted to pH 6-7 with sodium hydroxide (NaOH; 1 M) to stop further degradation. Salt and small FG peptides were removed from the samples by dialysis (MWCO 100-500 Da) against MQ-water (8 L) at 4 °C. The MQ-water was changed every four hours during the day until the conductivity of the dialysis water was below 10 µS (µS), and as close as possible to 5 µS. All the degraded samples of fish gelatin were lyophilized and stored at - 40°C.
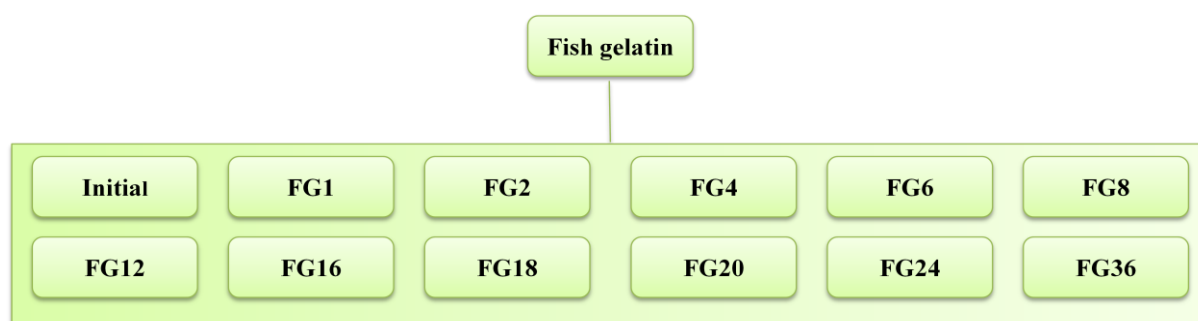
Figure 2.1: Degradation of fish gelatin at 90°C, where each sample has different degradation time, providing in total eleven samples. An initial sample of fish gelatin is also represented in the scheme to illustrate a total of 12 samples in studying the kinetics of fish gelatin degradation by acid hydrolysis.

2.2.1.2. Degradation by acid hydrolysis

Fish gelatin (5 g) was dissolved in HCl (0.2 M, 33.3 mL). The degradation was performed at 90°C, and sampling was performed after 4, 12, 24 hours, yielding three samples with different degradation time (Figure 2.2). The degradation procedure was identical to the one performed during the kinetics experiment, including the purification by dialysis and the following lyophilization.
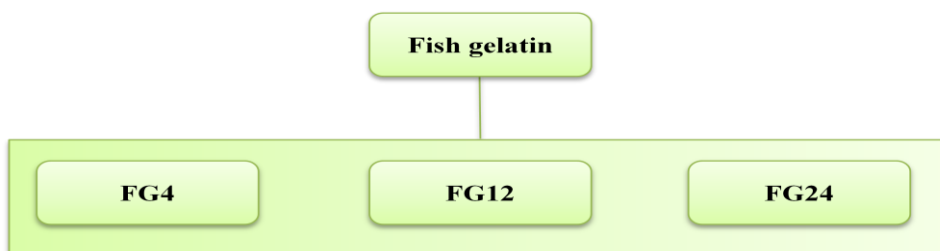
Figure 2.2: Degradation of fish gelatin at 90°C, where each sample has different degradation time, yielding in total three samples.
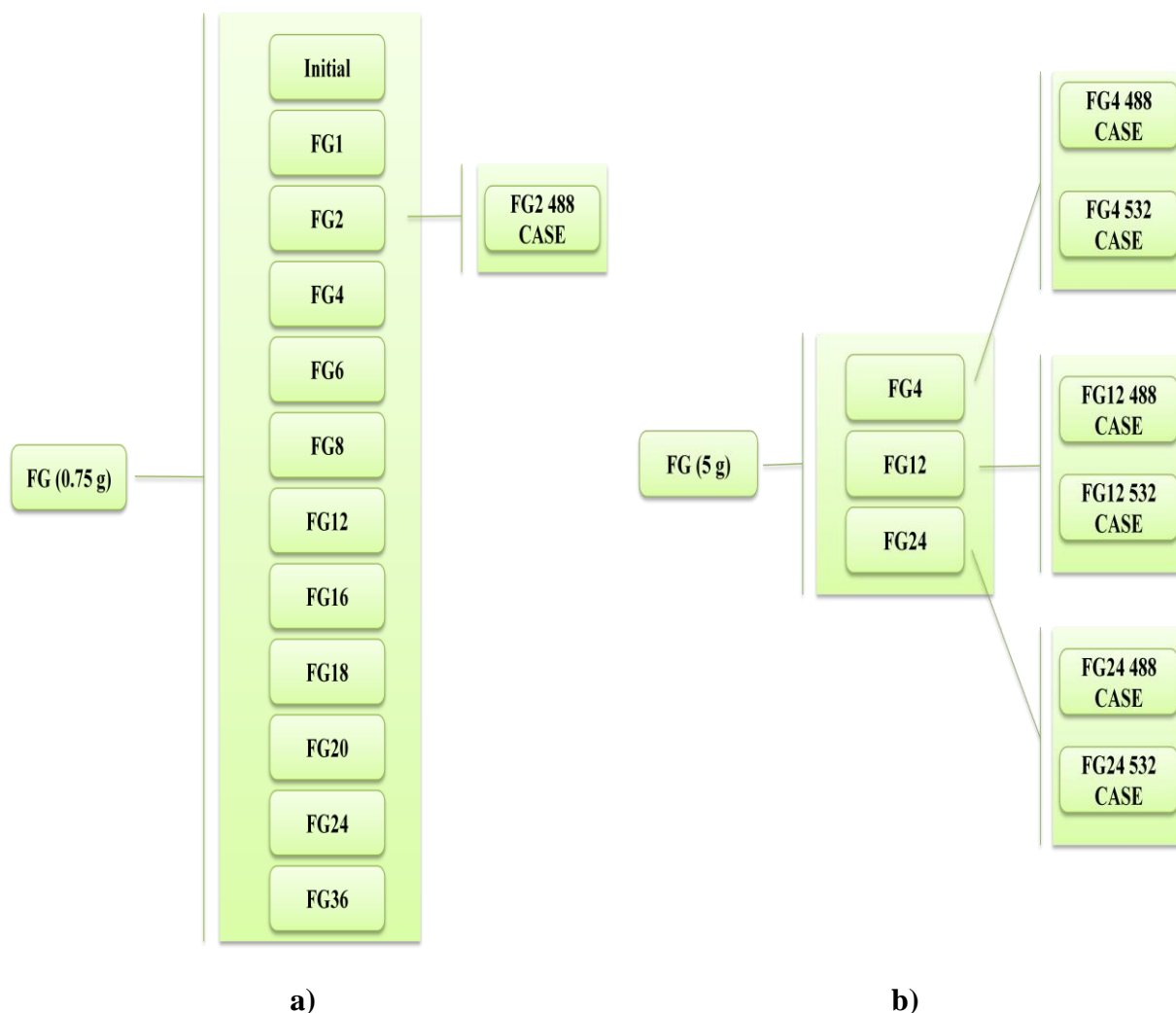
2.2.1.3. Conjugation of fish gelatin to Alexa Fluor® CASE dyes

Fish gelatin peptides (100-500 mg) were dissolved in MQ-water (1-2.5 mL), and mixed with NaHCO$_3$ buffer (0,2 M, pH 8,3) in the ratio 1:1. To ensure uncharged amino groups in the fish gelatin samples, enabling reaction with the carboxylic groups found in the fluorophores, the pH of the solutions should be >7.

The Alexa 488/532 CASE (1 mg) (Table 2.1) was first dissolved in 99% DMSO (0.2 mL) and mixed using a vortex mixer. Further the fluorescent dye (50 µL) was added drop wise to the respective peptide sample, and the mixture was covered by aluminum foil and incubated for nineteen hours under stirring conditions at room temperature. Aluminum foil was used to minimize light exposure of the fluorescent dyes.

Excess fluorescent dye in the protein-dye mixtures was removed by dialysis (MWCO 1000 Da) against MQ-water (8 L). The MQ-water was changed every four hours during the day until the fluorescence intensity of the dialysis water, measured by a Perkin Elmer LS 50B fluorescence spectrometer (PerkinElmer, Inc., Massachusetts, USA), was below 2 (I<2). Dialysis was followed by lyophilization, without exposure to light, and the lyophilized samples were stored at -40°C.

The flow diagrams below (Figure 2.3) give an overview of the different fish gelatin peptides generated by acid hydrolysis, each named FG# where # represents the degradation time in hours, and of the samples selected for conjugation to Alexa Fluor® CASE dyes.

a)   b)

Figure 2.3: Flow diagrams illustrating the initial source of fish gelatin, fish gelatin peptides with different degradation times, and the samples conjugated to Alexa Fluor® dyes. In **a)** the amount of initial material was 0.75 g, and in **b)** the initial amount was 5 g.

Initially, the fish gelatin samples FG4, FG12 and FG24, prepared for further use in transdermal diffusion experiments, were the only samples to be fluorescently labeled with Alexa Fluor® 488/532 CASE. However, as the experiments proceeded it was discovered that the difference in molecular weight among the three samples were much smaller than expected (Table 3.3). Therefore, FG2, with a higher estimated molecular weight was conjugated to Alexa Fluor® 488 CASE.

2.2.2. Preparation of G-block samples

G-blocks with two different molecular weight distributions were used as model drugs in transdermal diffusion experiments. The two different G-block samples were prepared from acid precipitation of high guluronic acid NA-alginate, performed in two separate master's thesis, by Karianne Birkestøl Eiken (Eiken, 2011) (G-DP22) and Tone Aspevik (Aspevik, 2010) (G-DP18), respectively. Conjugation of G-DP18 and G-DP22 to Alexa Fluor® 488 HSS was performed by Karianne Birkestøl Eiken (Eiken, 2011). The number average degree of polymerization (DP_n) of the two samples was determined by ¹H-NMR, as described in section 2.2.3.3.

2.2.3. Determination of molecular weight and molecular weight distribution

Polymers consist of varying amounts of monomers and to determine their molecular weights it is necessary to use defined equations for calculation of weight averages. The number average molecular weight (M_n) and the weight average molecular weight (M_w) are defined in Equations (2.1) and (2.2) (Smidsrød and Moe, 2008).

$$\mathbf{M_n} = \frac{\sum_i \mathbf{N_i} \cdot \mathbf{M_i}}{\sum_i \mathbf{N_i}} = \frac{\sum_i \mathbf{c_i}}{\sum_i (\mathbf{c_i}/\mathbf{M_i})} \tag{2.1}$$

$$\mathbf{M_w} = \frac{\sum_i \mathbf{N_i} \cdot \mathbf{M_i}^2}{\sum_i \mathbf{N_i} \cdot \mathbf{M_i}} = \frac{\sum_i \mathbf{c_i} \cdot \mathbf{M_i}}{\sum_i \mathbf{c_i}} \tag{2.2}$$

In the equations, c_i is the concentration of molecules, and N_i is the number of molecules with molecular weight M_i. Each molecule influences the two different averages M_n and M_w in proportion to their number or their weight, respectively. In the number average molecular weight all molecules will have the same influence on the average value. In the weight average molecular weight the large molecules will contribute to an increase in the average value due to the square root of the molecular weight in Equation (2.2) (Smidsrød and Moe, 2008).

Polymer solutions are either monodisperse or polydisperse. In a monodisperse solution all molecules have the same weight, and per definition M_n equals M_w. The situation is somewhat different for a polydisperse solution, where the molecules are of varying molecular weights,

and M_n has a lower value compared to M_w. The ratio between M_w and M_n is the definition of the polydispersity index (p.i) used to roughly measure the polydispersity in a sample (Smidsrød and Moe, 2008).

M_n and M_w of the FG samples were determined by both size-exclusion chromatography coupled to multi-angle laser light scattering (SEC-MALLS) and matrix-assisted laser desorption/ionization – time-of-flight (MALDI-TOF). M_n of the G-block oligomer samples were determined from data obtained from ^{1}H-NMR.

2.2.3.1. SEC-MALLS

Size-exclusion chromatography coupled to multi-angle light scattering (SEC-MALLS) is a widespread method for the absolute determination of the molecular weight averages and molecular weight distributions. In SEC-MALLS two on-line detectors are used: a concentration sensitive detector (refractive index (RI) or UV detector) and a light scattering detector, which is able to monitor up to 18 laser angles simultaneously (Christensen, 2010b). M_n and M_w of the FG samples were determined from SEC-MALLS. The 15 different gelatin samples were dissolved in MQ-water. The initial fish gelatin sample, and samples degraded for 1, 2 and 4 hours were dissolved to 2 mg/mL, samples degraded for 6, 8, 12 and 16 hours were dissolved to 6 mg/mL, and samples degraded for 18, 20, 24 and 36 hours were dissolved to 10 mg/mL. All the dissolved samples were filtered (pore size 0.2 μm, low protein binding membrane; Acrodisc[®] Syringe Filters with GHP membrane, PALL Corp., USA). The eluting buffer consisted of Na_2SO_4 (0.1 M) and Na_2EDTA (0.02 M) and was adjusted to pH 9. The experimental procedure was described by Eysturskarð et al. (2009), and the analysis was performed by Ann-Sissel Teialeret Ulset, Staff Engineer at the Department of biotechnology, NTNU.

2.2.3.2. MALDI-TOF

In mass spectrometry the mass to charge ratio (m/z) of ions are measured and allows for the molecular weight to be determined. In matrix-assisted laser desorption/ionization – time-of-flight (MALDI-TOF) proteins or peptides are crystallized in a matrix that absorbs at the wavelengths of a high energy pulsed laser. When the matrix is irradiated by this laser the energy is transferred to the molecules to be analyzed. The resulting ions, with unique size and charge, are accelerated by a high voltage electric field through a vacuum tube and towards a

detector. The TOF-detector measures the time it takes for the ion to fly to the detector, and this time-of-flight is proportional to the square root of m/z (Clark, 2005).

The fish gelatin peptides FG1-FG36 (1 mg) were dissolved in MQ-water (1 mL). 2μL of each sample solution was mixed with 2μL of a sinapinic acid (SA) matrix, dissolved in acetonitrile (ACN) and trifluoroacetic acid (0.1% TFA) (ratio 3:1). 1 μL of the sample-matrix mix was applied onto a MALDI target plate (AnchorChip[TM] Technology) and was allowed to dry. A N2 nitrogen laser with 337 nm wavelength (pulse energy of 100μJ) was utilized to irradiate the matrix and the analyses were performed in a linear positive mode. The experimental procedure was described by the autoflex[®] Operator Manual (Bruker Daltonik GmbH, 2001, Germany) (given on the enclosed cd) and by Webster and Oxley (2005), and was performed by Kåre Andre Kristiansen, Senior Engineer at the Department of biotechnology, NTNU.

2.2.3.3.   ^{1}H-NMR

[1]H-Nuclear Magnetic Resonance Spectroscopy (^{1}H-NMR) is a method utilizing a samples ability to absorb electromagnetic energy in a magnetic field in order to determine its structural and chemical composition. The average degree of polymerization (DP_n) and the fractions of M and G monomers (F_M and F_G) of the G-block samples, used as model drugs in the transdermal diffusion experiments, were determined by ^{1}H-NMR prior to this study. The ^{1}H-NMR analysis was performed according to Holtan (2006), with the exception of acid hydrolysis, and was carried out by Wenche Iren Strand, Staff Engineer at the Department of biotechnology, NTNU. ^{1}H-NMR spectra were recorded on a Bruker Avance DPX 300 and the spectra peaks were determined according to Grasdalen (1983).

2.2.4.   Determination of the degree of labeling

The degree of labeling (DOL) (Equation 2.3) specifies the number of moles of Alexa Fluor[®] dyes conjugated to one mole of peptide or oligomer. In order to determine DOL, fluorescently labeled FG and G-block samples were diluted in MQ-water to a concentration of 0.1 mg/mL, and the absorbance was measured with a Lambda 25 UV/VIS Spectrometer (Perkin Elmer Inc., Massachusetts, USA) at the absorbance maximum (λ_{max}) of the respective dyes (Table 2.1).

$$DOL = \frac{A_{max} \cdot M_w}{c_{protein} \cdot \varepsilon_{dye}} \qquad (2.3)$$

In the equation, which originally is defined for labeling of proteins, A_{max} is the absorbance of the protein-dye complex measured at the λ_{max} of the dye and M_w is the molecular weight of the protein (g/mol). ε_{dye} is the extinction coefficient of the dye at its absorbance maximum $(cm^{-1} \cdot M^{-1})$ (Table 2.1). The concentration of dye in the protein-dye complex can be considered negligible giving a protein concentration, $c_{protein}$, equal to the $c_{protein\text{-}dye\ complex}$ of 0.1 mg/mL.

2.2.5. Transdermal diffusion experiments

The full-scale skins used in the transdermal diffusion experiments were donated from healthy female adults who had undergone abdominal plastic surgery at Clinic Stokkan in Trondheim. This study was approved by the local ethics committee, and all skin donors signed an informed consent. In total, skin samples from 11 donors were used in the experiments, and each donor was labeled alphabetically from A to K. The skin was transported to the laboratory at NTNU Gløshaugen immediately after pick up at Clinic Stokkan, to prepare it for use in transdermal diffusion experiments. The experiments were performed in a laboratory approved for experiments utilizing human skins and cells, classified as biohazard level 2, and entry was only allowed for students/staff vaccinated for hepatitis A/B. The preparation procedure started with removal of the subcutaneous fat applying surgical scissors. Skin thickness measurements were performed by measuring the thickness at 10 different locations on the skin samples from each donor with a digital slide gauge (micromaster®, capa μ system, Swiss Instruments Ltd, Ontario, Canada). All skin samples were investigated for areas with a lot of hair, stretch marks, tattoos and perforations that potentially could affect the diffusion of the test molecules into the skin.

2.2.5.1. Pretreatment of the skin

The skin samples from all the different donors were either untreated, or pretreated with micro-needles or laser. The surface and structure of untreated skin was not altered prior to applying the test molecules. A solid micro-needle device, Dermaroller® MC915 (1.5 mm, Dermaroller LLC, California, USA) (Figure 2.4a), was used to porate the stratum corneum, creating small channels to enhance the diffusion of macromolecules across the outermost barrier of the skin.

Pretreatment with micro-needles was performed by rolling the Dermaroller® MC915 over the skin surface once with a constant pressure (Figure 2.4b).

Three different laser treatments were applied (Table 2.2). The laser pretreatment was performed with the ablative CO_2 fractional laser eCO_2^{TM} (Lutronic Inc., Seoul, Korea) by Dr. MD Ole Martin Rørdam (Figure 2.4c). However, the laser pretreatment applied in skin diffusion kinetics experiments was performed with a fractional erbium:YAG laser (Sciton Inc., California, USA), mimicking laser treatment 1 (Table 2.2) . For practical reasons the skins were treated with laser before removal of the subcutaneous fat tissue. Each of the three different laser treatments resulted in spherical points consisting of multiple laser spots with identical diameters and depths (Figure 2.4d). The spot density varied between the three different laser treatments, and the depth of the laser spots increased with increasing pulse energy. All three laser treatments were first applied in a pilot study to investigate the effect of laser radiation regarding both transdermal diffusion of model drugs and skin damage, and laser treatment 1 (L1) was chosen for further use in transdermal diffusion experiments.

Table 2.2: Overview of the three different laser treatments performed on human skin, including the pulse energy, laser strength and density of spots.

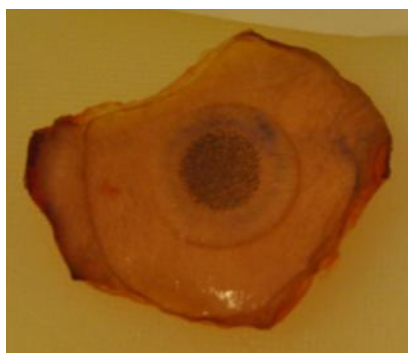| Laser treatment	Pulse energy (mJ)	Laser power (W)	Density (Spots/cm^2)
L1	14	30	400
L2	30	30	300
L3	40	30	600

a)
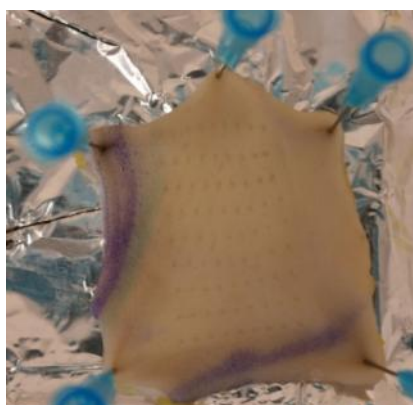
b)

c)

d)

Figure 2.4: a) The Dermaroller® MC915 used to porate the stratum corneum to enhance the diffusion of macromolecules through skin, **b)** a tissue sample pretreated with Dermaroller® MC915 illustrating the poration of the skin surface, **c)** the CO_2 fractional laser eCO_2^{TM} used for laser treatments (Lutronic, Seoul, Korea), **d)** a tissue sample pretreated with laser treatment 3 (picture taken after the diffusion experiment).

2.2.5.2. The general experimental design of transdermal diffusion experiments

The general experimental design was identical for all the different transdermal diffusion experiments, regardless of pretreatment of the skin and the test samples applied. After the initial removal of subcutaneous fat and redundant liquids, the skin was placed on a plate of polystyrene covered with aluminum foil. Further, the skin was cut into smaller tissue samples ($\approx$ 3x3 cm) that fitted onto a Franz-type diffusion cell (PermeGear, Inc, Pennsylvania, USA), used to investigate transdermal diffusion. The diffusion cell consisted of an application chamber and a receptor chamber, both with a diameter of 20 mm. The receptor chamber (15 mL) was filled with PBS (pH 7.4), which constituted the receptor phase. Each tissue sample

was mounted between the application and the receptor chamber by a screw clamp, with the epidermal side facing the application chamber and the dermal side facing the receptor chamber, (Figure 2.5). The receptor phase volume was adjusted through the sampling port, and the test samples were deposited on the epidermal side of the tissue sample in the application chamber (4 (w/v)%, 30 µL) with an automatic pipette. For pretreated skins it was important that the treated area was accessible for test sample deposition in the application chamber. Both the application chamber and the sampling port were closed by parafilm, and in addition the application chamber was covered with aluminum foil to prevent evaporation and exposure to light. The Franz cells were placed in small water baths, where the water covered approximately half of the receptor chamber, and the units were incubated in darkness at 30°C for 22 hours. To study the diffusion kinetics the incubation time was varied, depending on the pretreatment of the skin and the fluorescently labeled model drugs used. In the pilot study, performed to investigate the effect of laser treatments, the Franz cells were incubated for 48 hours due to practical reasons.

a)   **b)**
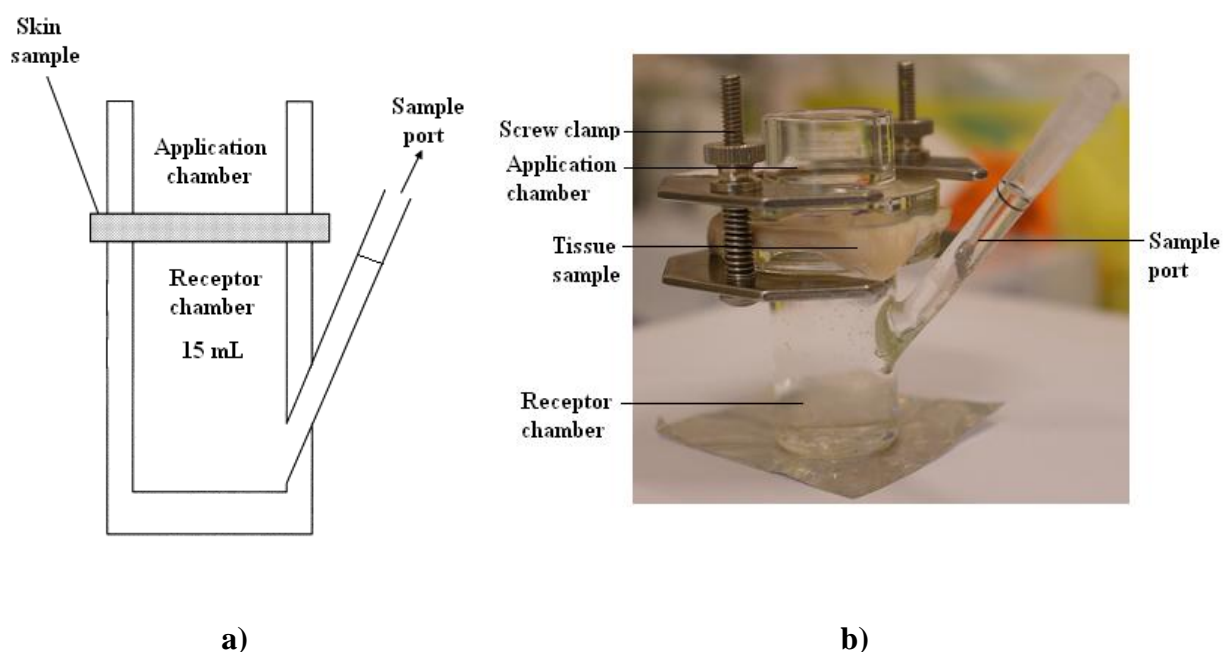
Figure 2.5: a) Schematic representation of a Franz-type diffusion cell, where a skin sample is mounted between the application and the receptor chamber (Adapted from (Moser et al., 2001)), **b)** a real life Franz-cell unit with a tissue sample from human skin mounted between the application and the receptor chamber by a screw clamp.

2.2.5.3. Measure of fluorescence intensity in the receptor phase (I_{RP})

After incubation the skin samples were carefully removed from the Franz cells, and the receptor phase transferred to a test tube. The fluorescence intensities in each individual receptor phase were measured using a Perkin Elmer LS 50B fluorescence spectrometer (PerkinElmer, Inc., Massachusetts, USA). For receptor phases collected from experiments involving molecules conjugated to Alexa Fluor® 488 CASE or HSS the fluorescence intensity was measured at the excitation/emission wavelengths 495/519 nm. For receptor phases collected from experiments involving test samples conjugated to Alexa Fluor® 532 CASE the same measurements were made at wavelengths 514/532 nm.

The maximum possible fluorescence intensity in the receptor phase was determined, by adding test samples (10 µL) directly into PBS (5 mL, pH 7.4).

2.2.5.4. Biopsy punching

The skin samples removed from the diffusion cells were attached to a polystyrene plate by the help of hypodermic needles. Excess test sample was removed from the skin surface by tissue paper, and a biopsy was collected for each tissue sample using a biopsy puncher with a diameter of 5mm. Between each biopsy punch the puncher was washed in 70% EtOH to avoid transfer of fluorescence from one biopsy to another. By using TissueTek® O.C.T™ (Sakura Finetek Europe B.V., Netherlands) every biopsy specimen was attached to a small, rectangular piece of cork followed by deep-freezing in liquid nitrogen. The frozen biopsies were completely covered by TissueTek® O.C.T™, deep-frozen, and stored in cryo tubes (1.8 mL) at - 40˚C until cryo sectioning

2.2.5.5. Cryo sectioning

Cryo sectioning basically means sectioning under cold conditions, and all the biopsies were sectioned using a Leica CM 3050 S cryostat (Leica Microsystems, Wetzlar, Germany) (Figure 2.6a). The cryo sectioning was performed at the Department of cancer research and molecular medicine at Gastrosenteret, St.Olavs Hospital, in Trondheim. In the cryostat the cryochamber temperature was set to -25˚C and the specimen temperature to -12˚C. Each biopsy was removed from the cork material and mounted with TissueTek® O.C.T™ on a specimen disc (Figure 2.6b). After deep-freezing in the cryochamber the biopsies were prepared for sectioning (Figure 2.6c), and the sectioning thickness was set to 20 µm. During cryo sectioning thin slices of the biopsies were transferred to SuperFrost® microscope slides

(Menzel-Glaser GmbH, ThermoFischerScientific Inc., USA) (Figure 2.6d). The microscope slides were stored in light-proof boxes under dry conditions at room temperature.
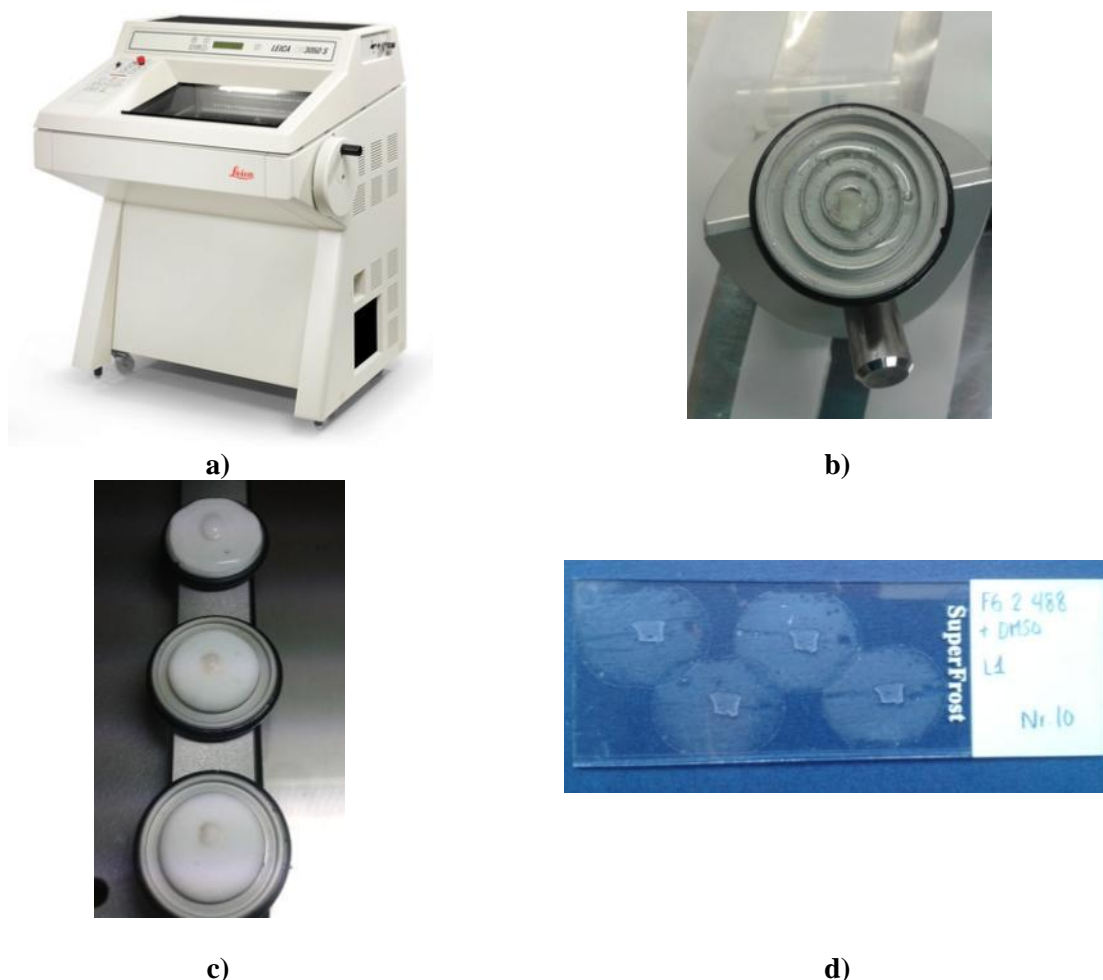
Figure 2.6: a) The Leica CM 3050 S Cryostat (Leica Microsystems, Germany), **b)** a skin biopsy mounted with TissueTek® O.C.T™ on a specimen disc, **c)** deep-freezing of biopsies in the cryochamber, prepared for cryo sectioning, **d)** slices (20 µm) of skin biopsy on a microscopic slide.

2.2.6. Overview of the performed diffusion experiments

Table 2.3 gives an overview of the transdermal diffusion experiments performed to study the diffusion of fish gelatin peptides and G-block oligomers into human skin. In all the transdermal experiments, with exception of the pilot study and the skin diffusion kinetics experiments, diffusion of pure Alexa Fluor® 488 CASE/HSS was also studied, to provide "positive" control tissues giving rise to fluorescence. "Negative" control tissues were obtained by applying only the vehicles on the skin. These control experiments were performed

simultaneously with the peptide and oligomer samples to be studied, and thus, the same vehicles and skin pre-treatments were utilized.

Table 2.3: Overview over the performed transdermal diffusion experiments, including skin donor, the sample and vehicle applied, and skin pretreatment.

Donor	Sample	Vehicle(s)	Skin pretreatment(s)	Comment
A	FG24 488 CASE FG24 532 CASE	60% DMSO	L1, L2 and L3	Pilot study – effect of laser pretreatment
B	FG 24 488 CASE	60% DMSO	L1	Transdermal diffusion experiment
E	FG24 488 CASE Alexa 488 CASE	60% DMSO	Micro-needles	Skin diffusion kinetics experiment
F	FG24 488 CASE Alexa 488 CASE	60% DMSO	Micro-needles	Skin diffusion kinetics experiment
G	G-DP18 488 HSS G-DP22 488 HSS	10% PEG200	Untreated Micro-needles	Transdermal diffusion experiment
H	FG24 488 CASE	60% DMSO 10% PEG200	Untreated Micro-needles	Transdermal diffusion experiment
I	G-DP18 488 HSS G-DP22 488 HSS	60% DMSO	Untreated Micro-needles	Transdermal diffusion experiments
J	FG24 488 CASE Alexa 488 CASE	60% DMSO	L1 (Sciton laser)	Skin diffusion kinetics experiment
K	FG2 488 CASE FG24 488 CASE*	60% DMSO 10%PEG200	Untreated Micro-needles L1	Transdermal diffusion experiment

*The FG24 488 sample was applied in a 10% DMSO vehicle on skin from donor K after pretreatment with L1

2.2.7. Imaging of the skin tissues; confocal laser scanning microscopy

In confocal laser scanning microscopy (CLSM) laser light of defined wavelengths are used as light source and is directed as a laser spot towards the sample. An illustration of a confocal optical system is given in Figure 2.7. When the laser light reaches the sample the fluorescently labeled molecules are excited and the emitted light is collected by the objective lens. This brings the light towards a photomultiplier tube (PMT) detector. A pinhole is placed in front of the detector, where only light from the focal plane is allowed to pass. Out-of-focus light will spread over a larger area at the pinhole, allowing only a small fraction to pass through it and thereby out-of-focus light is excluded from contributing in creating the final image. This feature of LSCM enables capturing of clear images of thick samples, and imaging of individual planes of thick objects, called optical sectioning (Cox, 2007).
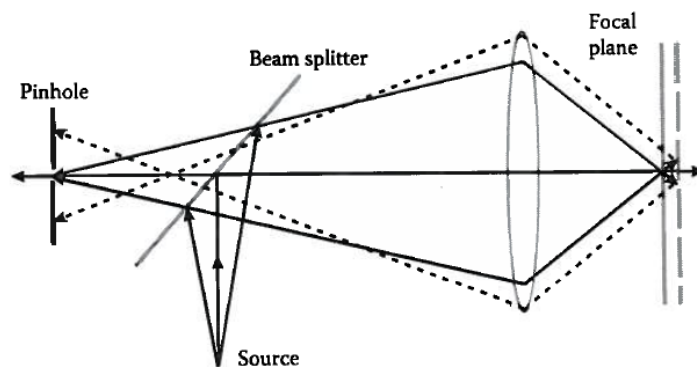
Figure 2.7: Illustration of a confocal optical system, where the laser light is directed towards confocal plane of the sample. Solid lines indicate in-focus light, dotted lines indicate out-of-focus light.

The microscope slides were studied using a Leica TCS SP5 confocal laser scanning microscope coupled to the Leica LAS AF software (Leica Microsystems, Wetzlar, Germany). Cover glasses (Menzel-Glaser GmbH, ThermoFischerScientific Inc., USA) were placed over the tissues on the microscope slides right before imaging. Standardized settings were determined and applied during imaging of all the tissue samples to obtain comparable images. For the study of samples conjugated to Alexa Fluor® 488 CASE/HSS an argon laser was used, and the standardized settings are given in Table 2.4. The FG24 sample conjugated to Alexa Fluor® 532 CASE were studied by applying a combination of an argon and a DPSS 561 laser, and the standardized settings are given in Table 2.5.

Table 2.4: Standardized settings applied for imaging of skin tissue after transdermal diffusion of sample molecules conjugated to Alexa Fluor® 488 CASE/HSS by CLSM.

Laser	Argon (17%)	
Beam path setting	488	
PMTs **(photo multiplier tubes)**	PMT 1 (system 1)	
	Mode	Leica/Alexa 488
	Gain	774.2
	Offset	0%
	PMT Trans (transmitted light channel)	
	Mode	Leica/BF Scan
	Gain	208.1
	Offset	0%
Image resolution	1024x1024 pixels (1550x1550 microns)	
Scan speed	400 Hz	
Zoom factor	1	
Pinhole	Airy 1	
Line average	4	
Frame average	1	
z-stack	Wide	
Objective	HC PLAPO CS 10x0.4 DRY	

Table 2.5: Standardized settings applied for imaging of skin tissue after transdermal diffusion of sample molecules conjugated to Alexa Fluor® 532 CASE by CLSM.

Laser	Argon (17%) and DPSS 561	
Beam path setting	488 and 561	
PMTs **(photo multiplier tubes)**	PMT 2 (system 2)	
	Mode	Leica/Cy3
	Gain	774.2
	Offset	0%
	PMT Trans (transmitted light channel)	
	Mode	Leica/BF Scan
	Gain	206
	Offset	-11%
Image resolution	1024x1024 pixels (1550x1550 microns)	
Scan speed	400 Hz	
Zoom factor	1	
Pinhole	Airy 1	
Line average	4	
Frame average	1	
z-stack	Wide	
Objective	HC PLAPO CS 10x0.4 DRY	

The images captured by the CLSM were exported to the Java-based image processing program ImageJ 1.45 (ImageJ, U.S, Maryland, USA), where tissue fluorescence intensity measurements were performed. The intensity values were detected within a range of 0-255 (where 0 (minimum) = black and 255 (maximum) = bright green/red). The mean fluorescence intensity in the tissue ($I_{mean-tissue}$) was determined using the polygon selection tool in the ImageJ toolbar. Three intensity profiles were drawn in the longitudinal direction in the tissue, from the outer edge of SC to the deepest skin layers captured in the image. The average fluorescence intensities obtained from the three plot profiles resulted in intensity plots with fluorescence intensity as a function of tissue depth. 3D surface plots were made using an interactive 3D surface plot plugin, illustrating the distribution and intensity of fluorescence in the tissue.

The mean autofluorescence intensity (I_{auto}) in the tissue was measured using the same polygon selection as for $I_{mean-tissue}$ in the control tissues. $I_{mean-tissue}$ could therefore be corrected for I_{auto}, to yield $I_{mean-sample}$, according to Equation (2.4).

$$\mathbf{I_{mean\text{-}sample} = I_{mean\text{-}tissue} \pm SD - I_{auto} \pm SD} \qquad\qquad (2.4)$$

$I_{mean-sample}$: Fluorescence intensity in the tissue only due to transdermal diffusion of fluorescently labeled sample, given as $I_{mean-sample} \pm SD$

$I_{mean-tissue}$: Fluorescence intensity in the tissue due to both trandermal diffusion of fluorescently labeled sample and tissue autofluorescence, given as $I_{mean-tissue} \pm SD$

I_{auto} : Tissue autofluorescence given as $I_{mean-control} \pm SD$

$I_{mean-control}$: Mean fluorescence intensity in the control tissue, given as $I_{mean-control} \pm SD$

All the fluorescence intensity values in Equation (2.4) are given as mean values $\pm$ SD. Because the measured $I_{mean\text{-}tissue}$ and I_{auto} values are not independent of each other the standard deviation from both measurements are added together, resulting in a higher SD for $I_{mean\text{-}sample}$, as given in Equation (2.5) (Taylor, 1997).

$$I_{mean\text{-}sample} = I_{mean\text{-}tissue} - I_{auto} \pm (SD_{tissue} + SD_{auto}) \qquad (2.5)$$

3. Results and discussion

3.1. Molecular weight determination

The weight average molecular weight (M_w) and the number average molecular weight (M_n) of fish gelatin (FG) peptides were determined by both SEC-MALLS and MALDI-TOF analyses. An estimation of the mean molecular weights of the different FG peptides was performed by combining the results from the SEC-MALLS and MALDI-TOF analyses. The results from the ^{1}H-NMR analyses were used to determine the number average molecular weight for the G-block oligomers.

3.1.1. Molecular weight determination of fish gelatin by SEC-MALLS

The results of the SEC-MALLS analyses for determination of M_n and M_w are given in Table 3.1, and the raw data are given in Appendix A. The calculated mass (m_{calc}) is the amount of the injected fish gelatin molecules, detected by the RI-detector. The M_w and M_n were determined for the molecules comprising the m_{calc}, which is the fish gelatin molecules eluted from the SEC column prior to the buffer salt void. The difference between the injected mass of fish gelatin molecules ($m_{injected}$) and m_{calc} provides information about the separation of the molecules. The lower m_{calc} compared to $m_{injected}$ (Table 3.1) indicated that not all molecules injected into the SEC-columns were eluted before the buffer salts. This may further indicate that small fish gelatin molecules were lost in the salt signal. The molecular weight distribution for a selection of the degraded fish gelatin samples are given in Figure 3.1.

Table 3.1: Results from the SEC-MALLS analyses of fish gelatin samples. The calculated mass (m_{calc}) represents the mass of the injected fish gelatin molecules eluted before the salt signal, from which M_w and M_n were determined.

Sample	$m_{injected}$ (g)	m_{calc} (g)	M_w [g/mol]	M_n [g/mol]
Initial	$2.00 \cdot 10^{-4}$	$1.12 \cdot 10^{-4}$	119700	117200
FG1	$2.00 \cdot 10^{-4}$	$1.274 \cdot 10^{-4}$	14080	12570
FG2	$2.00 \cdot 10^{-4}$	$1.09 \cdot 10^{-4}$	10000	9025
FG4	$2.00 \cdot 10^{-4}$	$1.005 \cdot 10^{-4}$	6452	6083
FG6	$6.00 \cdot 10^{-4}$	$4.07 \cdot 10^{-4}$	4218	4078
FG8	$6.00 \cdot 10^{-4}$	$3.90 \cdot 10^{-4}$	4134	3990
FG12	$6.00 \cdot 10^{-4}$	$4.03 \cdot 10^{-4}$	3484	3391
FG16	$6.00 \cdot 10^{-4}$	$4.35 \cdot 10^{-4}$	2764	2641
FG18	$1.00 \cdot 10^{-3}$	$6.94 \cdot 10^{-4}$	2708	2537
FG20	$5.00 \cdot 10^{-4}$	$4.80 \cdot 10^{-4}$	2947	2839
FG24	$1.00 \cdot 10^{-3}$	$7.46 \cdot 10^{-4}$	2594	2409
FG36t	$1.00 \cdot 10^{-3}$	$7.41 \cdot 10^{-4}$	2324	2248

The molecular weight averages determined by SEC-MALLS (Table 3.1) indicated a trend of decreasing molecular weight with increasing degradation time. During the first hour the degradation was more extensive, but as the degradation time increased, the rate of degradation seemed to decrease. This resulted in low molecular weight gelatin peptides with a wide molecular weight distribution indicating that the samples were polydisperse (Figure 3.1).
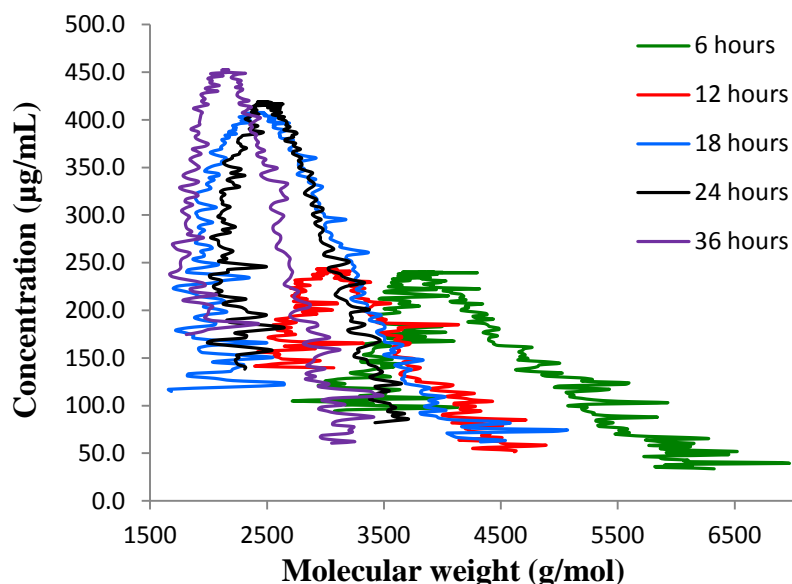
Figure 3.1: The molecular weight distributions of FG peptides obtained from acid hydrolysis of the initial FG after 6, 12, 18, 24 and 36 hours of degradation.

As mentioned above, the m_{calc} indicated that a proportion of each sample was excluded in the salt cut-off range of the MALLS integration, and therefore did not contribute in the molecular weight determination. Due to the columns applied in the analyses it was likely to believe that the low molecular weight peptides in the samples to a large extent were eluted in the salt void, and thus the high molecular weight fractions of the samples were overestimated. Because of this the molecular weight averages determined from SEC-MALLS were considered to represent a high molecular weight fraction of the FG samples (F_{HMW}). The F_{HMW} corresponded to the ratio between m_{calc} and $m_{injected}$, as given in Equation (3.1). The remaining portions of the samples, assumed to be excluded in the salt void during separation, were consequently considered to constitute the low molecular weight fraction of the FG peptides (F_{LMW}), and were calculated according to Equation (3.2).

$$F_{HMW} = \frac{\text{Calculated mass (g)}}{\text{Injected mass (g)}} \qquad (3.1)$$

$$F_{LMW} = 1 - F_{HMW} \qquad\qquad (3.2)$$

The $m_{injected}$ for the FG peptides may have been misleading, as the water content of the gelatins was unknown. Presence of water in the FG peptides would be expected to contribute to a deviation from the actual weight of the FG peptide samples, prepared for dissolution in MQ-water and injection into the SEC column (subsection 2.2.3.1). The actual amount of FG peptides injected into the column was therefore believed to be somewhat smaller than the $m_{injected}$ obtained from the SEC-MALLS raw data. This may further have had an impact on the calculated ratio between m_{calc} and $m_{injected}$ (Equation 3.1).

In MALLS there is a lower detection limit in the range of $\lambda/20$, meaning that for a laser wavelength of 658 nm, which was applied in the analyses, only peptide molecules with a $R_G >$ ~30 nm (radius of gyration) can be considered. For molecules where R_G is small compared to the laser wavelength, the laser light is unable to resolve the structure of the molecules, and it can be considered as point scattering rather than multi-angled light scattering (Christensen, 2010a). From the SEC-MALLS results (Appendix A) none of the measured radius moments were above this limit and for many of the samples the radius were undetectable. A low R_G represents a low degree of chain extension, and highly contracted FG molecules could therefore also contribute to give small low molecular FG peptides that are eluted with the salt.

3.1.2. Molecular weight determination of fish gelatin by MALDI-TOF

The results of the MALDI-TOF analyses for determination of molecular weight are given in Table 3.2. The mass spectra are given in Appendix B and the raw material on the enclosed cd. The initial FG sample was not included in the MALDI-TOF analyses due to its high molecular weight, and was only analyzed by SEC-MALLS.

Table 3.2: M_w and M_n determined by MALDI-TOF. The molecular weight averages are based on intensity.

Sample	M_w [g/mol]	M_n [g/mol]
FG1t	5506	3983
FG2t	5131	4145
FG4t	4618	3812
FG6t	5246	3961
FG8t	4584	3484
FG12t	4488	3679
FG16t	4525	3681
FG18t	4427	3679
FG20t	4716	3944
FG24t	3951	2990
FG36t	4683	3738

The results from the MALDI-TOF analyses indicated no clear correlation between molecular weight and degradation time, instead all samples, regardless of degradation time, seemed to be in the same low molecular weight range. This is in accordance with the fact that high-mass ions are underestimated in cases of high polydispersity (PI >1.1) (Gross, 2011), which seems to be true in this case. The underestimation of the high molecular weight molecules, and thus overestimation of the low molecular weight molecules, was the opposite of what was found in the SEC-MALLS analyses. Therefore, the molecular weights given in Table 3.2 were considered to constitute the F_{LMW} (Equation 3.2) of the FG peptide samples.

3.1.3. Estimated weight average molecular weight (M_w) by combining the results from SEC-MALLS and MALDI-TOF

The weight average molecular weight (M_w) was the molecular weight average of interest when performing molecular weight determination by SEC-MALLS and MALDI-TOF. This parameter is required in determining the degree of labeling, and is of experimental value with regards to the size-dependency of molecules diffusing into the skin. Because of the overestimation of the high molecular weight compounds in SEC-MALLS and the overestimation of low molecular weight compounds in MALDI-TOF, an estimated average weight of each FG sample was determined by combining the results from SEC-MALLS and MALDI-TOF. The average molecular weights were calculated in accordance with Equation (3.3) and the estimated average M_w of the 12 FG samples are given in Table 3.3.

$$\overline{M}_w = \left(F_{HMW} \cdot M_{w\,(SEC\text{-}MALLS)} \right) + \left(F_{LMW} \cdot M_{w\,(MALDI\text{-}TOF)} \right) \qquad\qquad (3.3)$$

Table 3.3: The estimated average M_w of the 12 FG samples after combining the results from the SEC-MALLS and MALDI-TOF analyses.

Sample	$\overline{M}_W$
FG0	120000
FG1	11000
FG2	8000
FG4	6000
FG6	5000
FG8	4000
FG12	4000
FG16	3000
FG18	3000
FG20	3000
FG24	3000
FG36	3000

The results given in Table 3.3 show a correlation between duration of acid hydrolysis and average molecular weights, and longer time of acid hydrolysis gave FG peptides with lower average molecular weights, as expected. After 16 hours all the unstable peptide linkages appeared to be broken, and the peptides degraded for 16-36 hours obtained the same molecular weight. Further depolymerization would therefore not be possible unless the experimental conditions were changed, such as acid concentration, type of acid and/or temperature. The weight average molecular weights determined from Equation (3.3) are not absolutely correct since the low and high molecular weight cut offs in the two applied test methods are not known. This means that both the high and low molecular weight fractions may include some of the same molecules. Still, the calculated molecular averages are assumed to provide DOL data, which are more correct than applying M_w from either the SEC-MALLS or MALDI-TOF analyses. The molecular weight values given in Table 3.3 are rounded to the nearest 1000, and are solely regarded as rough estimates due to the uncertainties related to each of the analyses and the combination of the results.

3.1.4. Molecular weight determination of G-block

The M_n of G-DP18 and G-DP22 were determined from the results of the ^{1}H-NMR analyses performed prior to this study. The analyses resulted in two ^{1}H-NMR spectra, one for G-DP18 and one for G-DP22, respectively. The spectra are given in Appendix C. The fractions of G- and M monomers, and the number average degree of polymerization (DP_n) of the samples determined from the ^{1}H-NMR spectra, are given in Table C.1 in Appendix C.

The DP_n of the two G-block samples were determined to be 18 and 22, respectively. The molecular weight of the Na-alginate monomers (guluronic and mannuronic acid) are 198.1 g/mol. The M_n of G-DP18 and G-DP22 was calculated in accordance to Equation (3.4) and are given in Table 3.4.

$$\overline{M}_n = 198.1 \text{ g/mol} \cdot DP_n \qquad (3.4)$$

Table 3.4: The $_n$ of G-DP18 and G-DP22.

Sample	$_n$ (g/mol)
G-DP18	3600
G-DP22	4400

3.1.5. Degree of labeling (DOL)

The degree of labeling was calculated (Equation 2.3) for the FG and G-block samples selected as model drugs in the transdermal diffusion experiments (Table 2.3), and are presented in Figure 3.2. The A_{max} values for the samples, measured at the λ_{max} of the respective dyes, are given in Appendix D. M_n was used instead of M_w in Equation (2.3) for the G-block oligomers. From the performed ^{1}H-NMR analyses only M_n could be determined for these samples. The relationship $M_w/M_n \approx 2$ is applicable for randomly degraded polymer chains (Smidsrød and Moe, 2008), but this relationship could not be used to find M_w for the two G-block samples. The reason for this was that the glycosidic linkages in alginate molecules are hydrolyzed by acids at different rates, and thus, acid hydrolysis of alginate results in a non-random depolymerization of the molecules (Haug et al., 1967). In a polydisperse system $M_n < M_w$, and therefore the DOL values for G-DP18 and G-DP22 were underestimated.
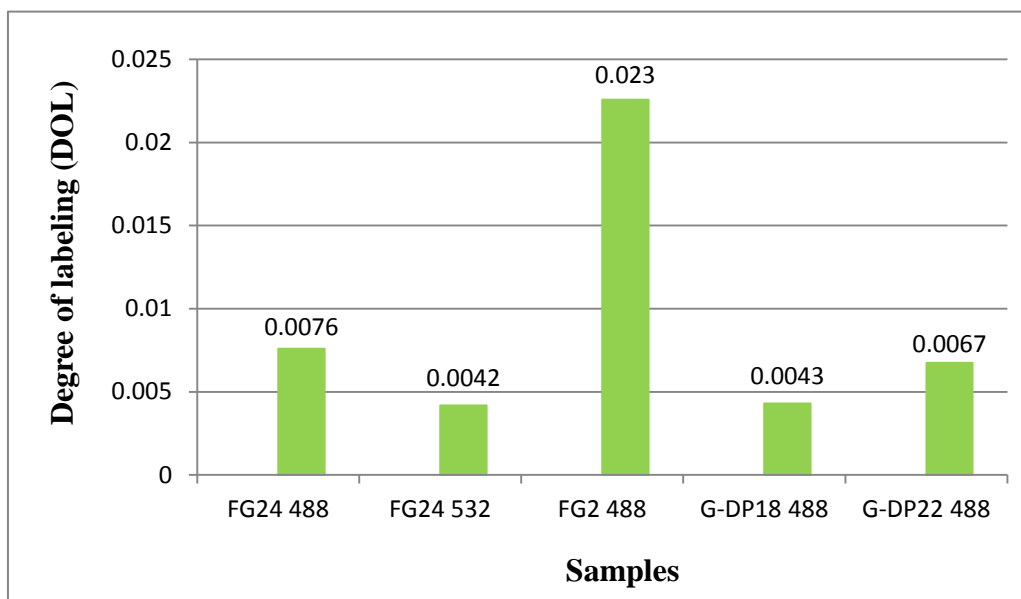
Figure 3.2: The degree of labeling of the fish gelatin peptide samples FG24 488 CASE, FG24 532 CASE and FG2 488 CASE, and of the two G-block samples G-DP18 488 HSS and G-DP22 488 HSS.

Figure 3.2 shows a varying DOL for the different samples. In the comparison of FG24 488 CASE, having the highest calculated DOL, with FG2 488 CASE, and G-DP18 HSS with G-DP22 HSS, the differences in DOL between samples conjugated to the same fluorescent dye indicated a size dependency. Both FG2 488 CASE and G-DP22 HSS had higher DOL compared to FG24 488 CASE and G-DP22 HSS, respectively. A reason for this could be that longer peptide and oligomer chains make it possible for more Alexa Fluor® fluorophores to react with the molecule. The lower DOL calculated for FG24 532 CASE compared to FG24 488 CASE may indicate a lower reactivity of the Alexa Fluor® 532 CASE dye, and thus, a lower affinity towards the primary amines in the FG peptides.

The variations in DOL between the different samples may also be due to experimental errors, such as too low pH in the solution during the conjugation of FG to the amine reactive dyes. The amine reactive dyes bind to the primary amines in proteins via a Schiff base reaction (Invitrogen, 2010), but this reaction will only occur if the amine group is uncharged and therefore pH must be >7 in the reaction buffer.

During transdermal diffusion, a sample with high DOL will give rise to higher fluorescence intensities in the tissue, due to more fluorescent dye per mole molecule, compared to a sample of molecules with low DOL. This is not synonymous with low DOL molecules providing lower penetration ability or diffusion efficiency, but rather with the fact that only the labeled molecules, representing only a minority of the sample, are detected in post diffusion studies.

The difference in DOL between samples, particularly if they are to be compared, can give inaccurate results in the evaluation of fluorescence intensity distribution in skin tissue, and therefore the fluorescence intensity values found in skin tissues after the transdermal diffusion experiments should be corrected for DOL. By assuming a linear correlation between DOL and the fluorescence intensity values obtained from post diffusion studies in human skin, fluorescence intensity values were corrected for DOL by using Equation (3.5). DOL corrections were made for FG24 488 CASE, FG24 532 CASE, FG2 488 CASE, G-DP18 488 HSS and G-DP22 488 HSS, with the purpose to obtain a more accurate basis for evaluation of the transdermal diffusion studies. Throughout the rest of the report $I_{corrected}$ represents the mean intensity value in the tissue corrected for DOL.

$$I_{corrected} = \frac{I_{mean\text{-}sample}}{DOL} \qquad (3.5)$$

An identical correction was made for the fluorescence intensity values measured in the receptor phase (I_{RP}) for these five samples and are designated $I_{RP\ corrected}$ throughout the rest of the report.

3.2. Transdermal diffusion experiments

To study the diffusion of hydrophilic molecules into human skin a series of transdermal diffusion experiments were performed, and the results from the experiments are presented in the following sections. In sections 3.2.4, 3.2.6 and 3.2.7 the results from each single experiment are illustrated by a CLSM image showing the detected fluorescence in the tissue, a transillumination image showing the tissue structure, an intensity plot and a 3D surface plot. The intensity plot illustrates the detected fluorescence intensity as a function of tissue depth and the 3D surface plots illustrates the distribution of fluorescence intensities, and thus, the distribution of the test molecules in the tissue. For the diffusion kinetics experiments in section 3.2.5 the results are only illustrated by CLSM images and 3D surface plots. Only one set of images are chosen to represent each individual result. All images and raw data, for the line plots and mean fluorescence intensities, are given on the enclosed cd.

From the CLSM and 3D surface plots the distribution of each test sample is described relative to where increase in fluorescence in the skin tissues was detected. Figure 3.3 illustrates the skin layers expected to be present in the tissues used in the transdermal diffusion experiments.
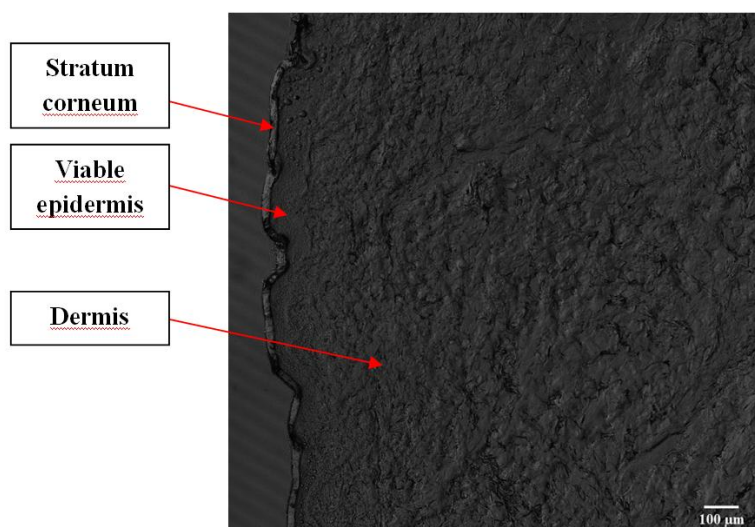
Figure 3.3: Transillumination image illustrating the skin layers in the tissues used in the transdermal diffusion experiments.

In all the transdermal diffusion experiments it was detected mean fluorescence intensity values with very high standard deviations (SD's). This may be due to skin heterogeneity and the independency between all the individual experiments that were performed. Heterogeneity may occur both between different or within the same body sites of an individual, and between identical body sites in different individuals (section 1.3), and could potentially influence the diffusion of molecules into human skin. For each of the experiments a new and individual piece of skin, with its individual pretreatment, was used. Therefore, each skin piece, from the same donor or not, mounted in individual Franz-type diffusion cells, gave rise to experiments with a high degree of independency. Holes and ruptures in the tissues, which would lead to black areas and falsely increase the intensity variations within the tissues, may have contributed to the high SD's. It should also be remembered that the corrections for I_{auto}, in tissues with applied Alexa 488 CASE, further increased these values, in accordance with Equation 2.5.

3.2.1. Control skin tissue

The skin tissues used in the transdermal experiments gave rise to autofluorescence at wavelengths similar to those used in the excitation and emission of the fluorescent dye conjugated to the test molecules. To investigate this phenomenon control experiments were performed for every donor, where only the vehicle, either 60% DMSO or 10% PEG200, was applied on skin from each individual donor. The autofluorescence intensities and the standard deviations (SD's) detected in the skins from the 9 different donors are given in Table 3.5. For donor A the fluorescence intensities were detected at two different wavelengths because FG

samples conjugated to both Alexa 488 and 532 CASE were used in the transdermal diffusion experiments performed on skin from that particular donor.

Table 3.5: Autofluorescence intensities and their incident standard deviation (SD) detected after penetration and diffusion of only the vehicles in skin from different donors.

Donor	Excitation/emission wavelengths (nm)	Vehicle applied as control	Mean autofluorescence intensity	SD
A	494/517 and 530/554	60% DMSO	11/19	6/14
B	494/517	60% DMSO	16	8
E	494/517	60% DMSO	9	5
F	494/517	60% DMSO	23	14
G	494/517	10% PEG200	17	10
H	494/517	60% DMSO	12	8
H	494/517	10% PEG200	13	8
I	494/517	60% DMSO	13	9
J	494/517	60% DMSO	13	7
K	494/517	60% DMSO	10	4
K	494/517	10% PEG200	11	5

The results from the control experiments, including CLSM and transillumination images, intensity plots, and 3D surface plots, will not be illustrated for each individual experiment in the following sections. Instead one representative control tissue has been chosen to illustrate the detection of autofluorescence in human skin (Figure 3.4).

a)   **b)**

c)   **d)**
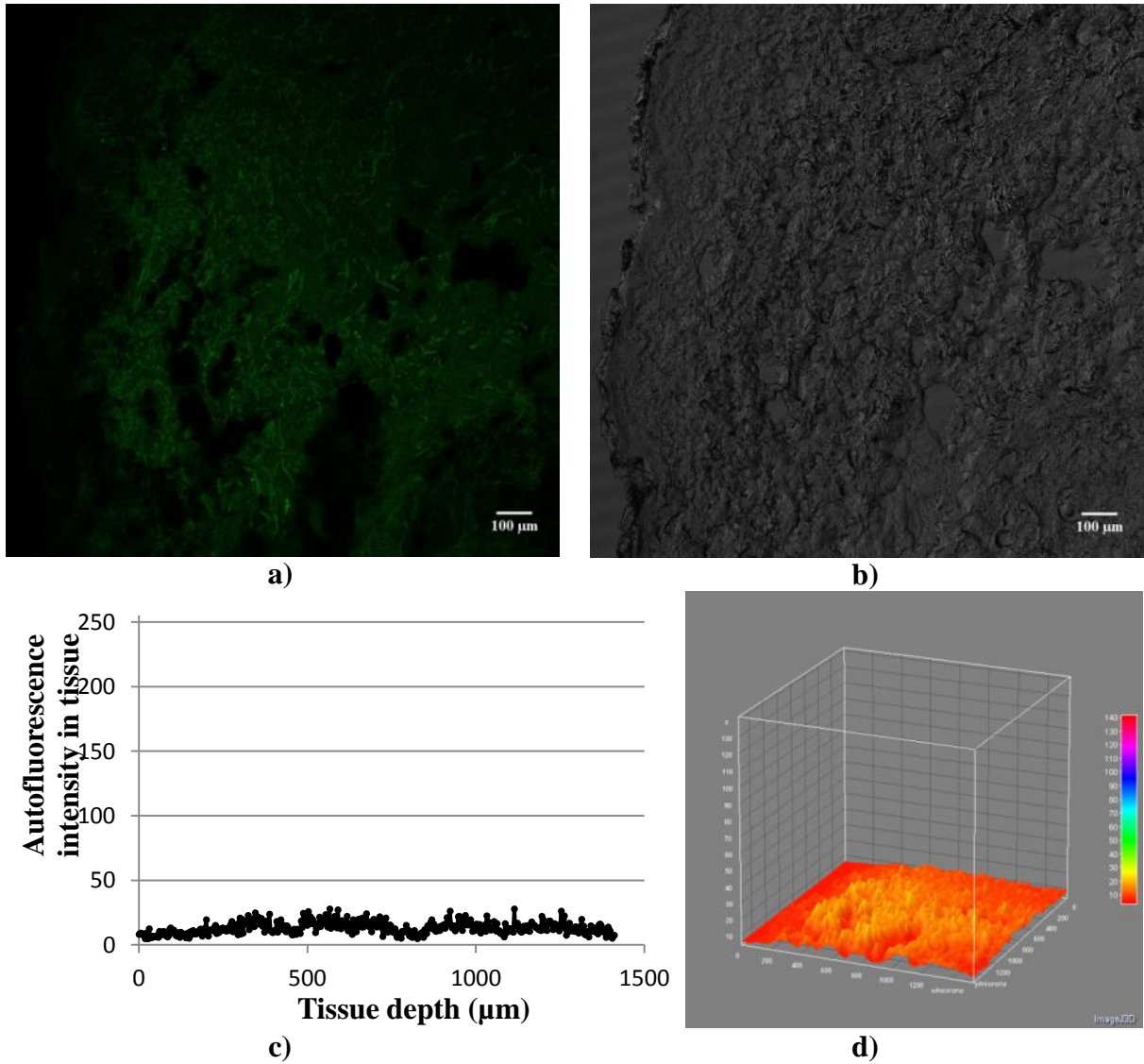
Figure 3.4: Results of a transdermal control experiment for the detection of skin autofluorescence. The only substance applied on the skin was 60% DMSO. **a)** CLSM image showing the fluorescence intensity in the tissue, **b)** transillumination image showing the tissue structure, **c)** intensity plot with fluorescence intensity as a function of tissue depth and **d)** 3D surface plot illustrating the distribution of autofluorescence in the tissue.

From the CLSM image (Figure 3.4a) an autofluorescence intensity (I_{auto}) of 14 ± 8 was detected. Autofluorescence in human skin is caused by a variety of known fluorophores, including components of the extracellular matrix (ECM), such as collagen and elastin (Section 1.6). The results in Figure 3.3 illustrate distribution of autofluorescence predominantly in the dermal skin layer. This may be explained by the content of collagen and elastin in the papillary dermis, and the dense and collagen rich connective tissue comprising the reticular dermis (Mitchell and Peel, 2009). The contribution of I_{auto} in the transdermal diffusion experiments was corrected for in $I_{mean\ tissue}$ values measured after transdermal diffusion of pure Alexa Fluor® dyes, giving corresponding $I_{mean\ sample}$ values (Equation 2.5). The contribution of

I_{auto} was not corrected for in the experiments performed with FG peptides and G-block oligomers because the fluorescence intensity values obtained from both the tissue and the receptor phase for these samples were corrected for DOL. As a consequence I_{auto} constituted < 4% of the measured fluorescence intensities, and autofluorescence contributions < 5% were determined to be negligible.

3.2.2. Thickness of skin from different donors

The skin thickness measured for the skins from different donors are averages of 10 measurements made at different sites throughout each skin sample, and are given in Table 3.6.

Table 3.6: Skin thickness of skin from different donors used in transdermal diffusion experiments.

Donor	Skin thickness (mm)
A	1.81
B	2.18
E	1.53
F	2.01
G	1.47
H	1.55
I	1.48
J	1.67
K	1.29

Significant variations in skin thickness were observed between the donors, and this may have influenced the rate of diffusion of the test molecules through the skin. One reason for this variation could be that the donors with thicker skins had been or were obese. This is a plausible reason considering that obesity has been found to give significant skin thickening (Laurent et al., 2007). It is not possible to predict accurately in which layers of the skin the difference in thickness originate from. It was observed considerable variations in the thickness of hypodermis among the donors, and it was likely to believe that this was influenced by the amount of body fat. However, this subcutaneous fat layer was removed prior to the transdermal experiments and therefore did not affect the diffusion of the test molecules. The intercellular penetration path through SC is much longer than the 10-15 layers of corneocytes typically found in SC (Hadgraft, 2004), but if thicker skin is a result of a thicker SC, this may potentially make the penetration path even longer and thus, cause the diffusion of topical applied molecules to be more difficult and time-consuming. A more time-consuming

diffusion can also be caused by thicker viable epidermis and/or dermis. Therefore thinner skin may contribute to more efficient diffusion of test substances compared to thicker skin.

The hand-operated digital slide gauge used to measure skin thickness can serve as basis for accurate length and thickness measurements. However, the soft tissue, particularly on the dermal side of the skin, made it difficult to predict if the skin was squeezed too much, giving lower and false skin measurements. A way to control this was to inspect whether or not the skin piece was immobilized in the slide gauge, but because of the soft and slippery tissue this was not easily determined either, and a standardized measuring method was difficult to obtain. In addition, the measurements could also be affected by remaining subcutaneous fat or stretch marks in the skin giving rise to higher or lower skin thicknesses, respectively.

3.2.3. Maximal fluorescence intensity in the receptor phase

The ability to penetrate the SC is an essential premise for the delivery of molecules to the deeper skin layers and the systemic circulation. Fluorescence in the receptor phase (I_{RP}) could give an indication whether the FG peptides and G-block oligomers remained in the tissue or were able to diffuse through all the layers of the skin tissue. The maximum possible fluorescence intensity in the receptor phase ($I_{RP\,max}$) was measured for the FG, G-block and pure Alexa Fluor$^®$ dye test samples to provide a basis of comparison with the I_{RP} values obtained after the transdermal diffusion experiments, and the results of the measurements are given in Table 3.7.

Table 3.7: $I_{RP\,max}$ for the samples used in transdermal experiments. $I_{RP\,max}$ values corrected for DOL is also included for the FG and G-block samples conjugated to Alexa Fluor$^®$ dyes.

Sample	Vehicle	$I_{RP\,max}$	$I_{RP\,max}$ corrected for DOL
FG24 488 CASE	60% DMSO	2441	321230
FG24 488 CASE	10% PEG200	1351	177771
FG24 532 CASE	60% DMSO	472	112449
FG2 488 CASE	60% DMSO	1429	62130
FG2 488 CASE	10% PEG200	2698	117299
G-DP18 488 HSS	60% DMSO	140	32637
G-DP18 488 HSS	10% PEG200	684	159049
G-DP22 488 HSS	60% DMSO	230	29103
G-DP22 488 HSS	10% PEG200	1036	131120
Alexa 488 CASE	60% DMSO	2997	-
Alexa 488 CASE	10% PEG200	2513	-
Alexa 488 HSS	60% DMSO	823	-
Alexa 488 HSS	10% PEG200	1577	-

3.2.4. The effect of pretreatment with laser – a pilot study

A pilot study was performed to investigate the effect of laser pretreatment on both transdermal diffusion and skin viability. An overview of the three different laser treatments is presented in Table 2.2. The results of the experiments performed in skin tissue after pretreatment with FG24 488 CASE are given in Figure 3.5 and 3.6, while the results from identical experiments performed with FG24 532 are given in Figure 3.7 and 3.8. The mean fluorescence intensity ($I_{corrected}$) values detected in the different tissues are given in the text and are also presented in Figure 3.9, as basis of comparison between the different tissues. The fluorescence intensities in the receptor phases ($I_{RP\ corrected}$) are presented in Figure 3.10. In addition, the results obtained from untreated skin are shown in Figure 3.9 and 3.10 (images and plots are not shown, but can be found on the enclosed cd).

Figure 3.5 shows CLSM images taken after diffusion of FG24 488 CASE, giving rise to $I_{corrected}$ values of 8314 ± 5890 and 11443 ± 6628 in the tissues after pretreatment with L1 and L2, respectively. This was significantly higher than the $I_{corrected}$ of 3682 ± 2031 detected in the tissue pre-treated with L3. In the L1 and L2 pre-treated tissues a small accumulation of high fluorescence intensities were observed in the cavities caused by the lasers. However, in all three tissues FG24 488 CASE was observed to have diffused deeper into the skin, and this observation was supported by the intensity and 3D surface plots in Figure 3.6. The fluorescence distribution in the tissues after pretreatment with L1 and L2 was very similar (Figure 3.6a, b), while pretreatment with L3 resulted in a more even, but relatively lower distribution throughout the tissue (Figure 3.6c). In the L2 pre-treated tissue (Figure 3.5b) it was also observed a rather dominating assembly of holes in the dermis. These holes were not taken into account in the measurement of $I_{corrected}$, and they were considered not to have influenced the diffusion of FG24 488 CASE into and through the tissue, as they most likely were ruptures originating from cryo sectioning.

In the experiment with FG24 532 CASE the results were different from the FG24 488 CASE study. Figure 3.7 shows CLSM images taken after diffusion of FG24 532 CASE, where the $I_{corrected}$ in tissues pre-treated with L1, L2 and L3 were 9624 ± 7765, 9595 ± 7904 and 8686 ± 6970, respectively. These values represented less variation among the three pretreatments, but nevertheless, L1 pretreatment resulted in the highest mean fluorescence intensity closely followed by L2, and then L3. The intensity and 3D surface plots, presented in Figure 3.8, illustrated that the test sample, to varying extent, was distributed both in the SC and in the

54

deeper dermal layers of the three tissues. From the results it was also observed that FG24 532 CASE to a larger extent was located in the outermost barrier of SC after all three pretreatments compared to FG24 488 CASE.

a)

b)

c)
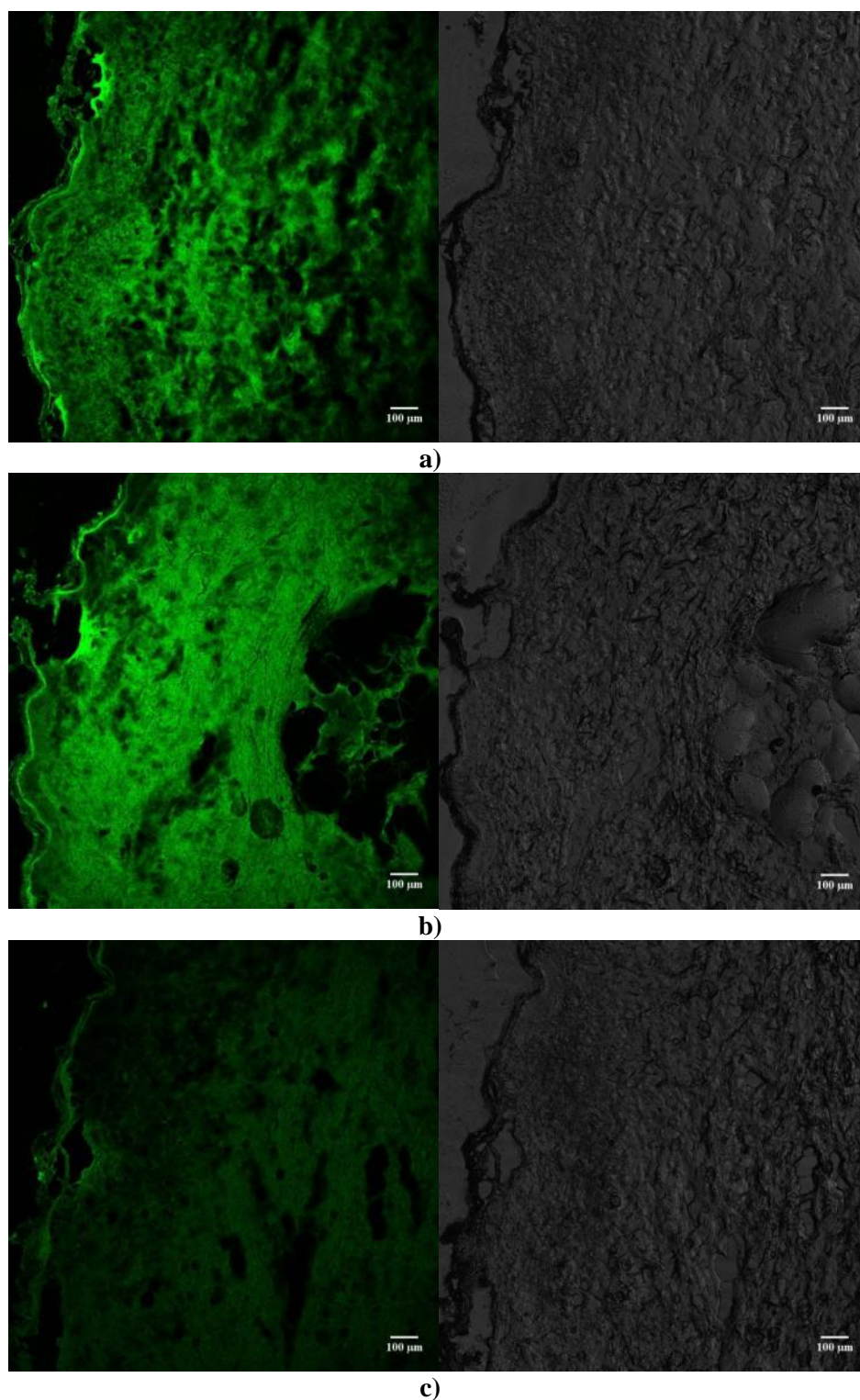
Figure 3.5: Results of transdermal diffusion by FG24 488 in a 60% DMSO vehicle into skin from donor A, after pretreatment with **a)** L1, **b)** L2 and **c)** L3. The CLSM images show the distribution of fluorescence in the tissue, and the transillumination images show the tissue structure.
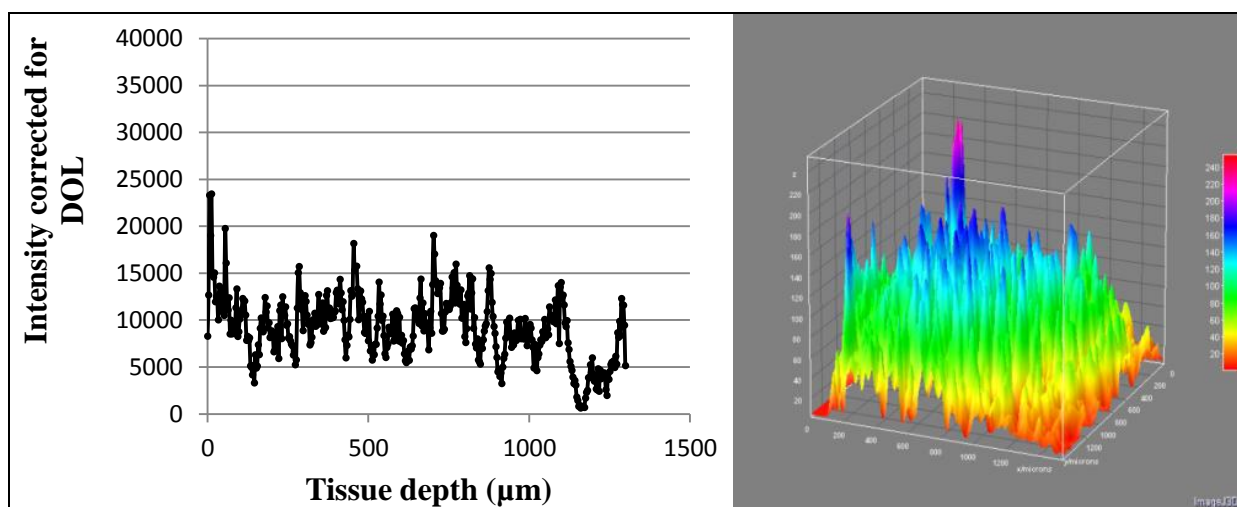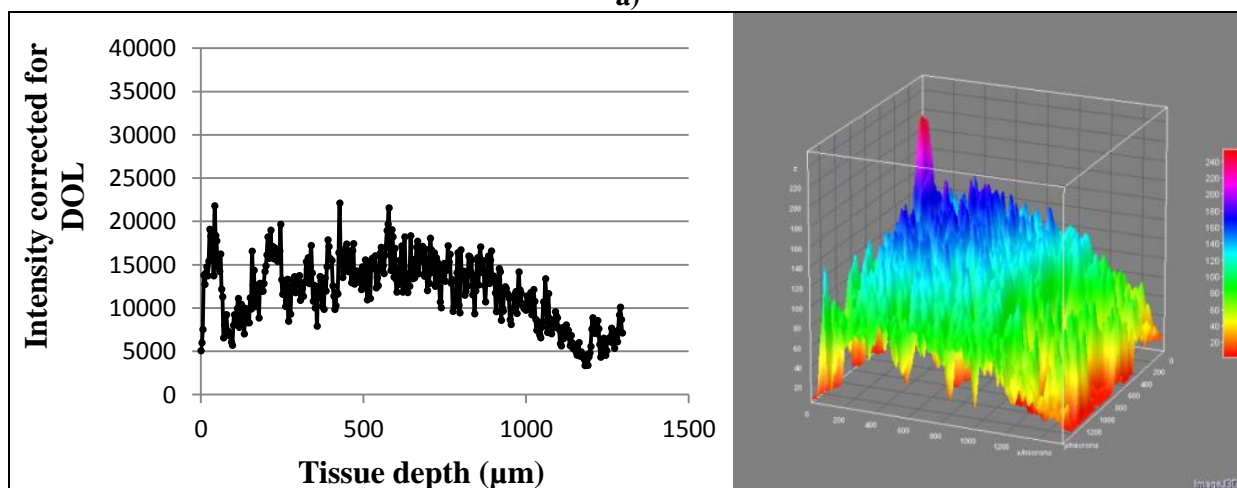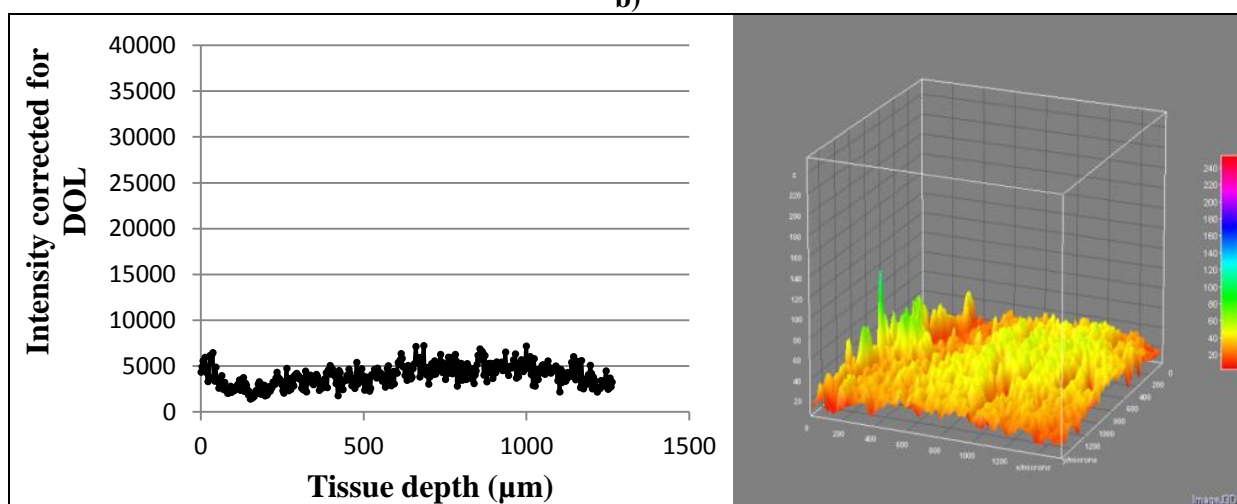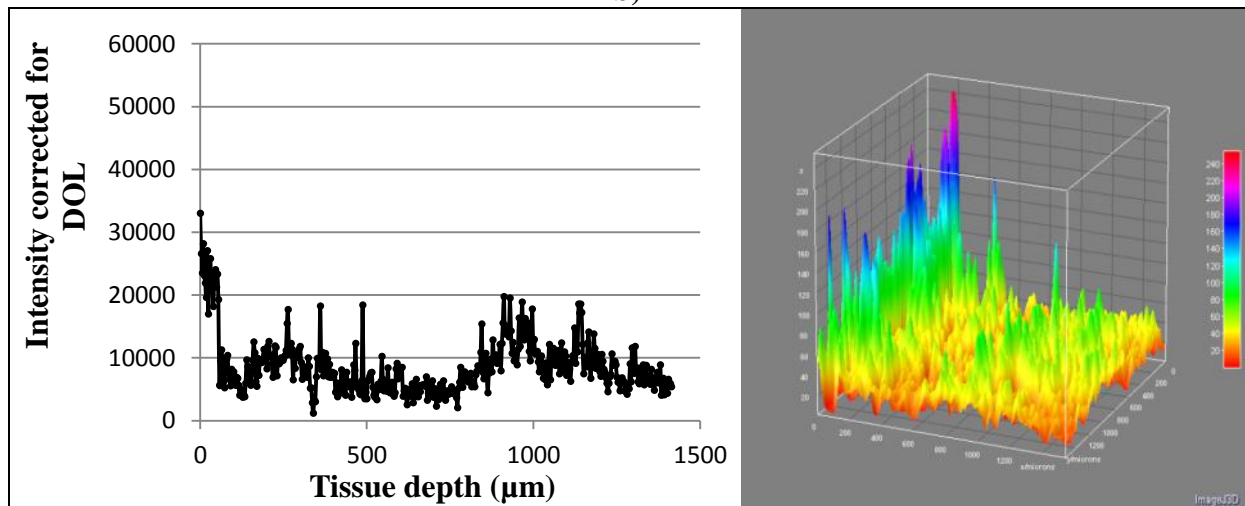
Figure 3.6: Intensity plots with fluorescence intensity as a function of tissue depth and 3D surface plots illustrating the distribution of FG24 488 CASE in the tissue after pretreatment with **a)** L1, **b)** L2 and **c)** L3.

56
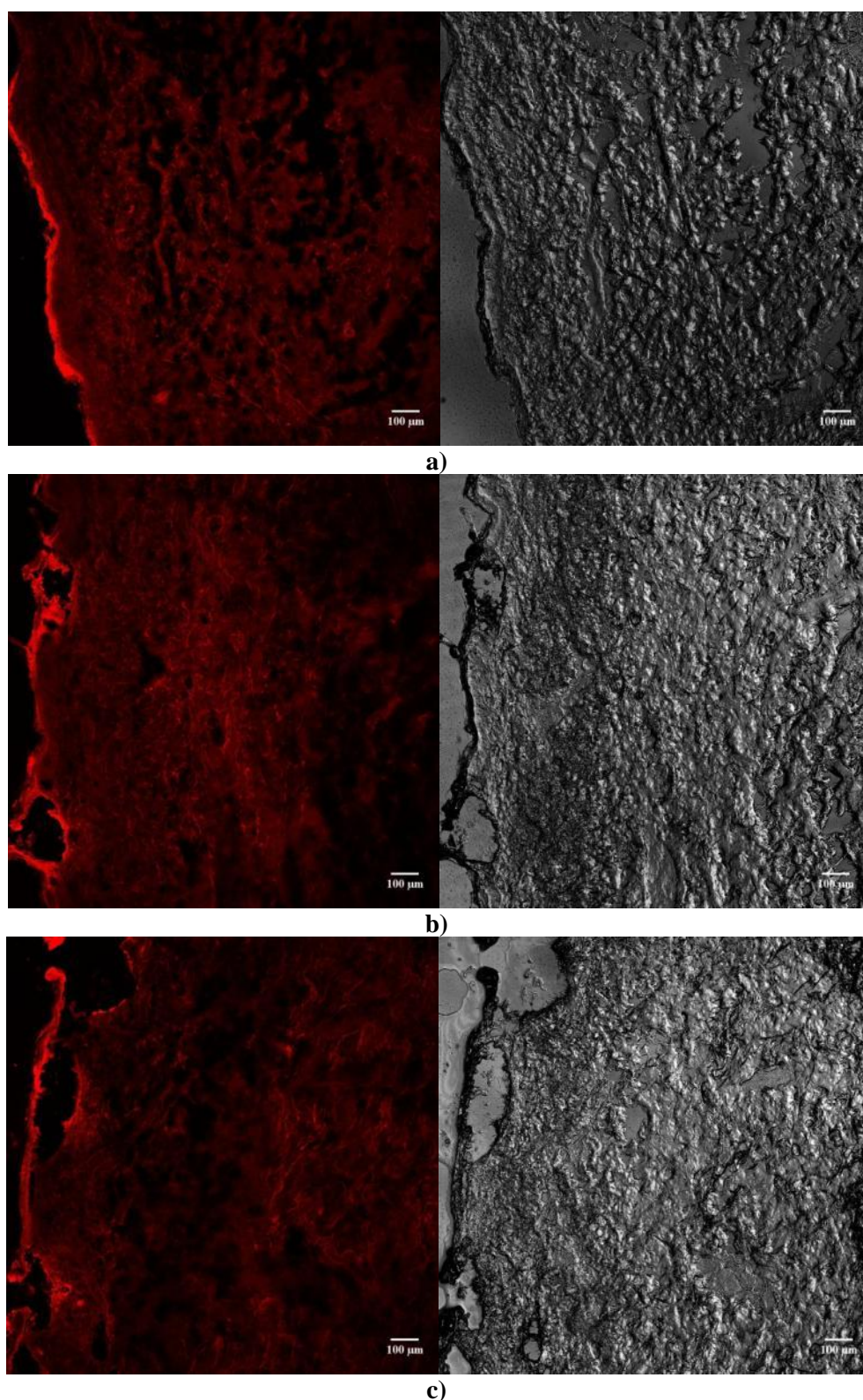
Figure 3.7: Results of transdermal diffusion by FG24 532 in a 60% DMSO vehicle into skin from donor A, after pretreatment with **a)** L1, **b)** L2 and **c)** L3. The CLSM images show the distribution of fluorescence in the tissue, and the transillumination images show the tissue structure.
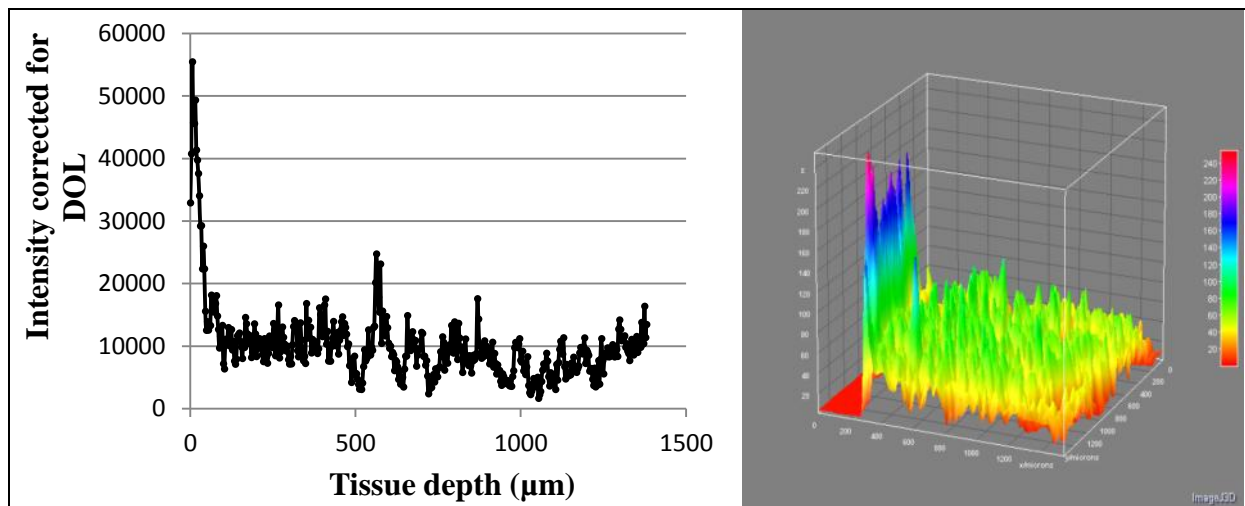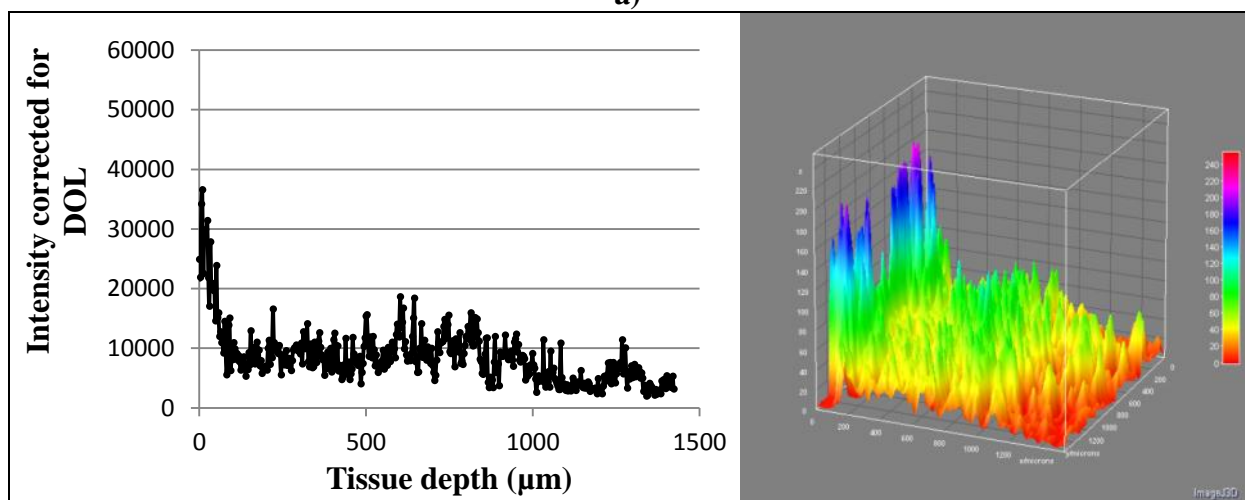
Figure 3.8: Intensity plots with fluorescence intensity as a function of tissue depth and 3D surface plots illustrating the distribution of the FG24 532 sample in the tissue after pretreatment with **a)** L1, **b)** L2 and **c)** L3.
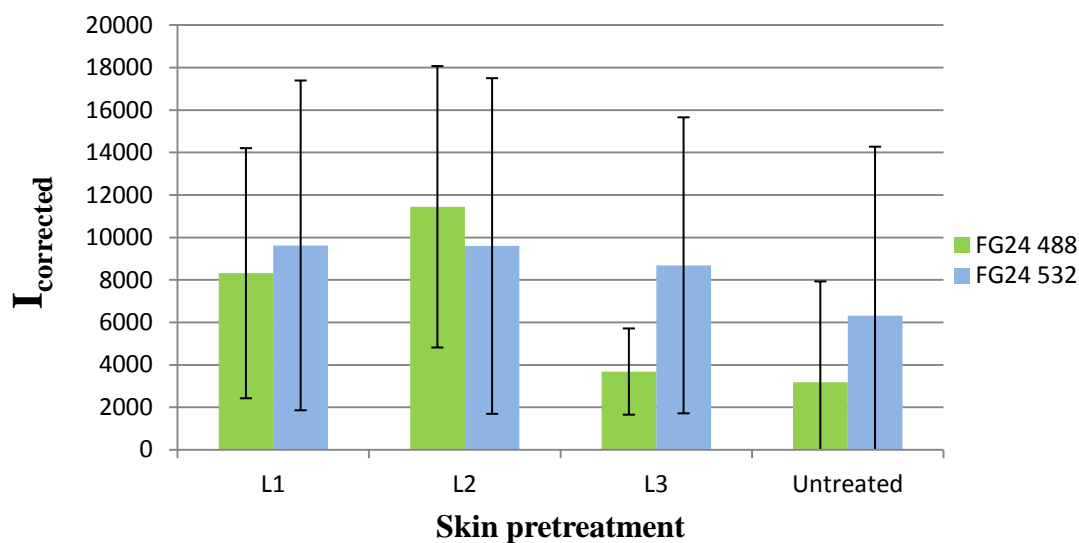
Figure 3.9: $I_{corrected}$ of FG24 488 and 532 CASE in tissues pre-treated with L1, L2 and L3.

The degree of SC barrier disruption was expected to be affected by the pulse energies and laser spot densities of the lasers applied in the study (Table 2.2). Upfront, it was likely to believe that L3 would give the highest degree of SC disruption and hence to the largest extent ease the diffusion of FG peptides into the skin. In the experiment, the L3 pre-treated tissues surprisingly resulted in the lowest $I_{corrected}$ values and the lowest fluorescence distribution of both peptides (FG24 488 and 532 CASE) compared to L1 and L2 (Figure 3.9). An interpretation of these results could be that the L3 pretreatment had physically enhanced diffusion of the peptides to a larger extent, by creating micro-channels enabling the peptides to diffuse all the way through the skin. This could further indicate that L1 and L2 enhanced the diffusion through SC, and into the deeper skin layers, but that the rate of diffusion was lower. This interpretation of the results was, however, contradictory to the results from fluorescence measurements in the receptor phase presented in Figure 3.10. These results showed that 40% and 39% (relative to $I_{RP\ max}$, Table 3.7) of applied FG24 488 CASE were detected to have diffused all the way through the tissues pre-treated with L1 and L2, compared to 28% through the tissue pre-treated with L3. For FG24 532 CASE, the results in Figure 3.10 show that approximately 27%, 43% and 28% of the applied samples reached the receptor phase in the tissues pretreated with L1, L2 and L3, respectively.
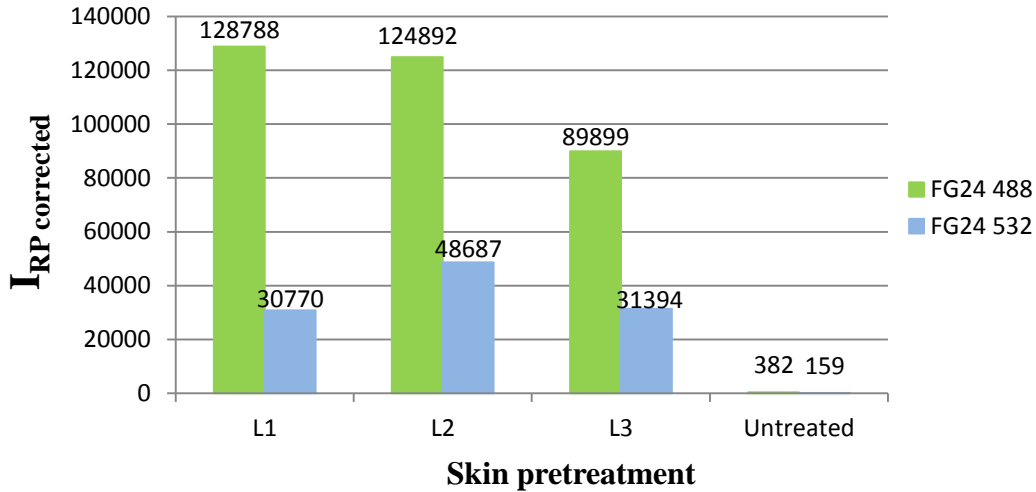
Figure 3.10: The fluorescence intensity in the receptor phase, I_{RP}, measured for FG24 488 and 532 CASE after diffusion through human abdominal skin.

The $I_{RP\ corrected}$ values of FG24 488 CASE (Figure 3.10) indicated that approximately the same amount of the sample had reached the receptor phase after diffusion through skin pre-treated with L1 and L2, and thus, that the diffusion rate was close to equal in both tissues. A possible interpretation of this could be that the lower pulse energy of L1 was compensated for by a higher spot density, enabling the same degree of enhancement as L2, which have higher pulse energy, but lower spot density. However, the distribution of fluorescence was generally higher throughout the tissue after pretreatment with L2, which could further indicate that, even though longitudinal diffusion through the tissues appeared to occur at the same rates, the diffusion across SC and the lateral diffusion of the sample in the tissue were more profound after this pretreatment.

A possible explanation of the lower $I_{corrected}$ and $I_{RP\ corrected}$ found in tissues after pretreatment with L3 may be the extensive skin damage caused by the high laser pulse energy, leading to disintegration and descaling of the SC (Figure 3.5c and Figure 3.7c). Even before applying test samples on tissues pre-treated with L3 there were a tendency of skin descaling in the laser treated area. The same tendencies, although less profound, were observed for L1 and L2, but not in the untreated tissue. Such skin damages could possibly diminish the penetration through SC, and especially the diffusion into deeper skin layers in areas displaying lack of contact between SC and the rest of the skin. In the laser treated tissues it was also observed dark fields, indicating necrosis in the viable epidermis and the upper dermis (not easily seen in the images presented on paper). Extensive necrosis could potentially plug the pores made by the laser, and further result in declined or zero diffusion rates of the model drugs.

60

After evaluating these results it was concluded that all three laser pretreatments enhanced the diffusion of the test samples into human skin compared to what was observed for untreated skin. But although L2 showed the most promising enhancement effect, L1 was chosen for further use in transdermal diffusion experiments. This was due to this pretreatment's ability to effectively penetrate the SC and allow for diffusion of the test samples deeper into the skin, without causing undesirable and severe damages to the skin.

This study also provided the opportunity to investigate and understand the effect of autofluorescence and therefore, test samples conjugated to fluorophores with different excitation/emission wavelengths were used (Table 2.1). It was anticipated that background signals caused by autofluorescence would be reduced in the tissues at higher wavelengths in the confocal laser scanning microscopy. However, the opposite was observed in this study, and in the tissues the contribution of autofluorescence was detected to be higher for FG24 532 CASE compared to FG24 488 CASE, as can be seen for donor A in Table 3.5. This suggests that even though autofluorescence generally decreases when imaging at wavelengths greater than 550 nm (Zeiss et al., 2012), fluorophores with excitation/emission wavelengths higher than 530/554 would be more appropriate when studying the impact of autofluorescence.

3.2.5. Evaluation of skin diffusion kinetics

The purpose of this study was to investigate the time it would take for a sample to diffuse through the SC and further into deeper skin layers, after pretreatment of the tissues with two different physical enhancement methods. The diffusion of Alexa 488 CASE and FG24 488 CASE, each in a 60% DMSO vehicle, was studied by varying the incubation time of tissues pre-treated with micro-needles and L1. A total of four experiments were performed, involving skin tissues from three different donors. In experiments performed with micro-needles the incubation time varied within an interval of 2-24 hours, while the incubation time varied within an interval of 20 minutes-6 hours in the experiments performed with L1. The results from the diffusion kinetic studies are presented in the following two subsections (3.2.5.1 and 3.2.5.2), and the experiments are summarized and further discussed in subsection 3.2.5.3.

3.2.5.1. Diffusion kinetics in tissue pre-treated with micro-needles

In this subsection the results of the diffusion kinetics experiments performed in skin pre-treated with micro-needles are presented. Skins from two different donors were used in the experiments, due to the small sizes of the abdominal skin pieces from donor E and F. Control tissues from each donor are included in the results. CLSM images and 3D surface plots from

transdermal diffusion of Alexa 488 CASE are given in Figures 3.11 and 3.12 and in Figures 3.15 and 3.16 for FG24 488 CASE. Tissues incubated for 2 and 6 hours were obtained from donor E, and tissues incubated for 12-24 hours from donor F.
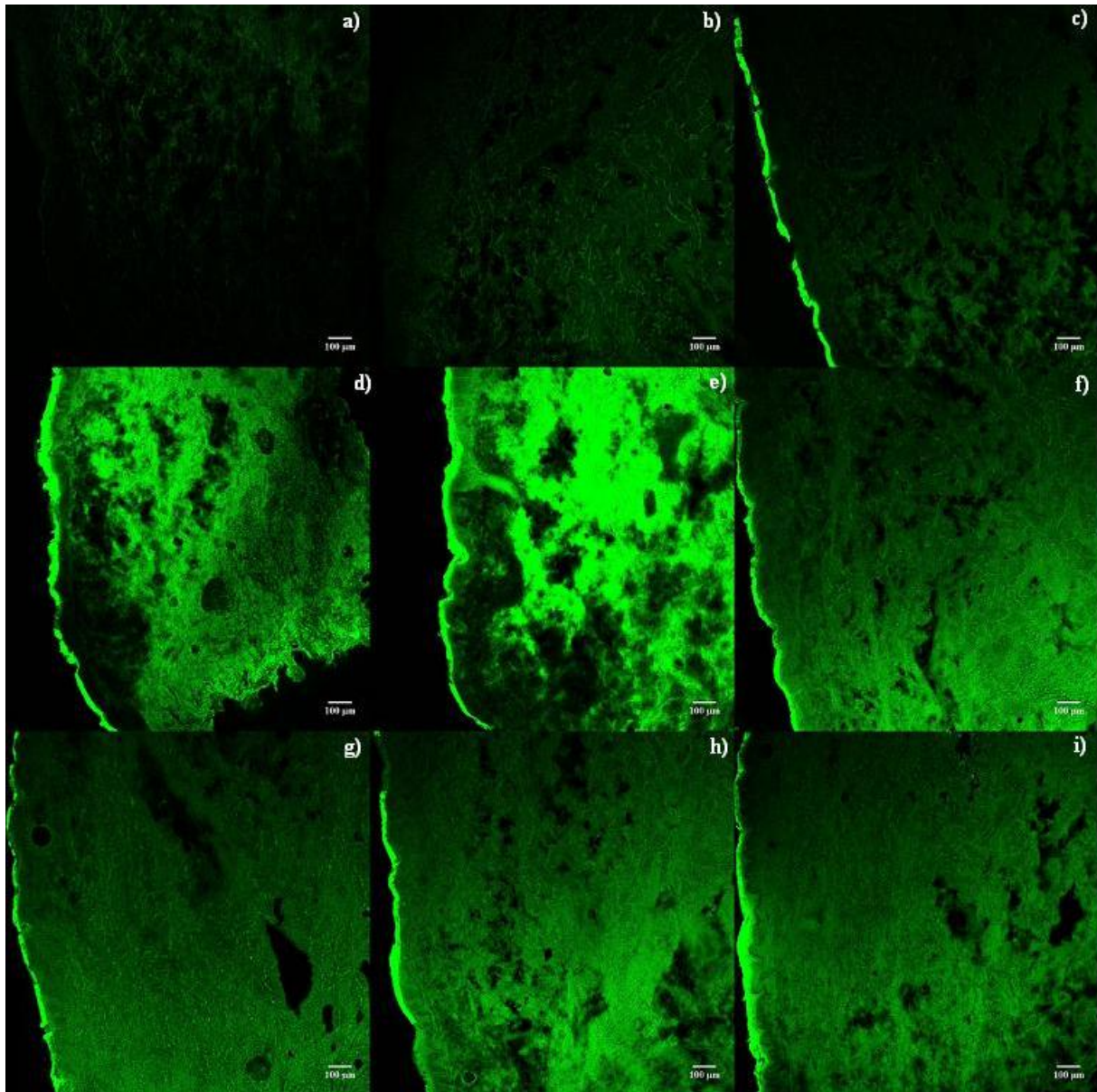
Figure 3.11: CLSM images illustrating diffusion of Alexa 488 CASE into skin tissue from donor E and F, after pretreatment with micro-needles. Image **a)** and **b)** are the control tissues, and image c) to i) represents the diffusion in skin incubated for **c)** 2 hours (donor E), **d)** 6 hours (donor E), **e)** 12 hours (donor F), **f)** 16 hours (donor F), **g)** 18 hours (donor F), **h)** 20 hours (donor F) and **i)** 24 hours (donor F).
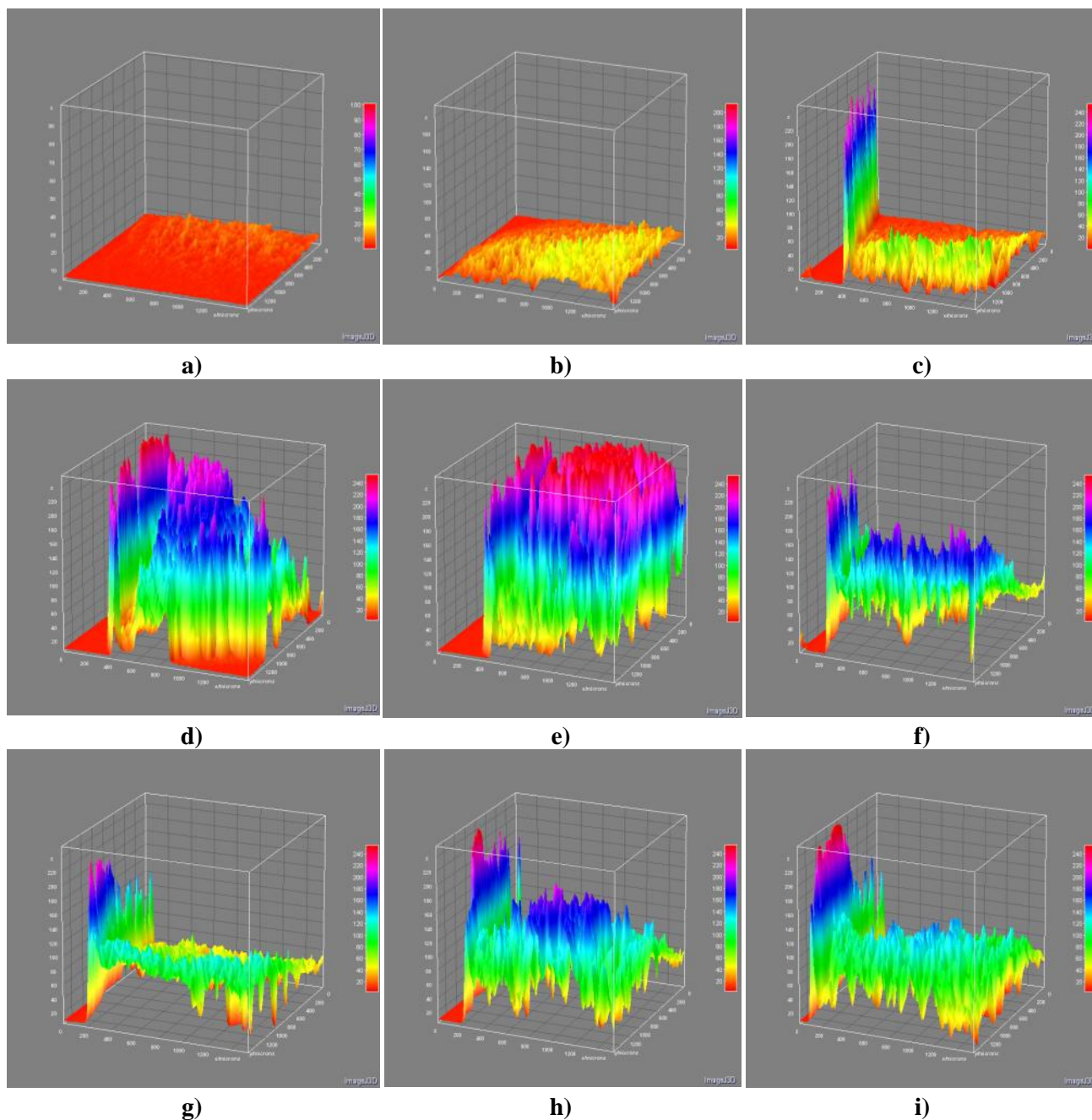
Figure 3.12: 3D surface plots showing the distribution of fluorescence intensity after diffusion of Alexa 488 CASE into skin tissue, after pretreatment with micro-needles. **a)** and **b)** are the control tissues, and c) to i) represents the diffusion of Alexa 488 CASE in skin incubated for **c)** 2 hours (donor E), **d)** 6 hours (donor E), **e)** 12 hours (donor F), **f)** 16 hours (donor F), **g)** 18 hours (donor F), **h)** 20 hours (donor F) and **i)** 24 hours (donor F).

Figures 3.11 and 3.12 demonstrate how Alexa 488 CASE diffused into the skin tissues after pretreatment with micro-needles. A minor increase in fluorescence in the tissue was observed after 2 hours of incubation, but most of the fluorescence was observed to be accumulated in the SC (Figures 3.11c and 3.12c). A similar, but varying degree of accumulation was also observed after 12-24 hours of incubation. After 6 hours an increase in fluorescence distribution both in the viable epidermis and dermis was observed, and the highest and most

evenly distributed fluorescence intensity was observed throughout the tissue after 12 hours of incubation (Figures 3.11 and 3.12 d, e). After 16 hours it was observed a decrease in fluorescence intensity, and even though there were some variance between tissues incubated for 16-24 hours, they all displayed lower fluorescence intensities distributed throughout the tissues (Figures 3.11 and 3.12 f-i).

In the tissues incubated for 2, 18 and 24 hours, Alexa 488 CASE was observed to be distributed in a fashion that resembled narrow pillars, spanning from the SC and into deeper layers of the tissues (Figure 3.12c, h, i). This pattern of diffusion was suggested to be caused by inconsistent barrier disruption after pretreatment with the manually operated micro-needle device, further discussed in section 3.2.10. Thus, these results illustrated the need for sufficient penetration of the SC to enable diffusion of the test sample deeper into the tissue. In these three tissues it was also observed that lateral diffusion of Alexa 488 CASE only occurred to a minor degree in the deeper dermal layer. An interpretation of this observation could be that micro-pores, created by the micro-needles, not only enabled diffusion through the outermost barrier, but also had an impact on the direction of diffusion deeper into the skin.

The $I_{mean-sample}$ detected in tissues incubated for 2-24 hours is presented as function of incubation time in Figure 3.13, together with the $I_{mean\ control}$ in the tissues from both donors. The $I_{mean-tissue}$ and $I_{mean-sample}$ values are given in Table E.1 in Appendix E.
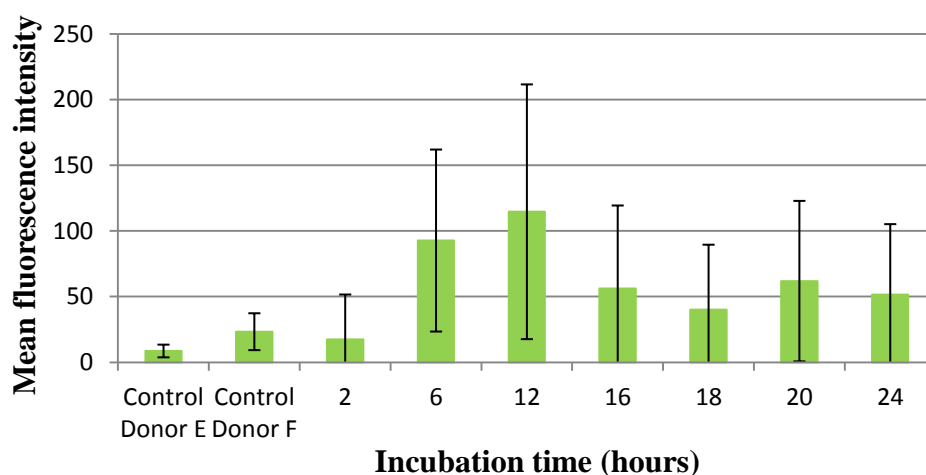
Figure 3.13: $I_{mean\ control}$ detected in the control tissues from donor E and F, and $I_{mean\ sample}$ values of Alexa 488 CASE detected in tissues after 2-24 hours of incubation.

Figure 3.13 supports the observation of increased fluorescence in the tissue already after 6 hours, and that a peak in mean fluorescence intensity was achieved after 12 hours.

Interestingly, the tissue incubated for 6 hours displayed higher intensity values compared to the tissues incubated for 16-24 hours. This could be due to that the tissues originated from two different donors with varying skin thickness. In addition, the heterogeneity in tissues from the same donor may have contributed both to the variation in diffusion efficiency into the skin tissues and the high standard deviations (SD's) observed in figure 3.13 (discussed in section 3.2).

The I_{RP} values measured in the receptor phases are given in Figure 3.14. After 12 hours of incubation an I_{RP} value of 7 was measured, corresponding to only 0.23% of $I_{RP\,max}$ (Table 3.7). This could mean that, even though a peak in $I_{mean\,sample}$ and an extended distribution of Alexa 488 CASE were observed after 12 hours, the diffusion rate was lower than 0.17 mm/hour (tissue thickness/hours of incubation). Therefore, a longer incubation time would likely result in diffusion of the sample through the skin and into the receptor phase. A high $I_{mean\,sample}$ and low I_{RP} could also indicate a high degree of lateral diffusion of the sample in the tissue. The highest I_{RP} value was measured after 20 hours of incubation, supporting the suggested need for longer incubation time to reach the receptor phase. However, the I_{RP} value corresponded to 8% of $I_{RP\,max}$, and thus only a minor portion of the sample was detected to have diffused all the way through the skin.

In general, the I_{RP} values were highly inconsistent, and showed no logical trend that could be correlated to the $I_{mean\text{-}sample}$ values and the distribution of Alexa 488 CASE in the tissues. The I_{RP} value obtained after 2 hours was higher compared to after 6, 12, 18 and 24 hours, and the I_{RP} value after 24 hours was lower compared to in the control experiment (donor F), indicating that the fluorescence was likely to be a result of autofluorescence caused by skin constituents. The inconsistency indicated unreliable measurements, which could be due to experimental errors, further discussed in subsection 3.2.5.3.
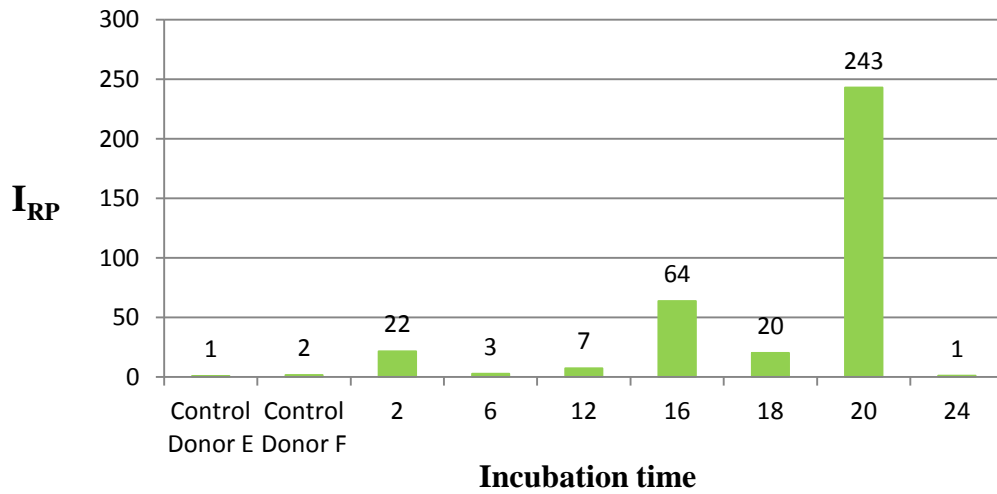
Figure 3.14: The fluorescence intensity in the receptor phase, I_{RP}, measured for the control tissues and for Alexa 488 CASE after 2-24 hours of incubation.
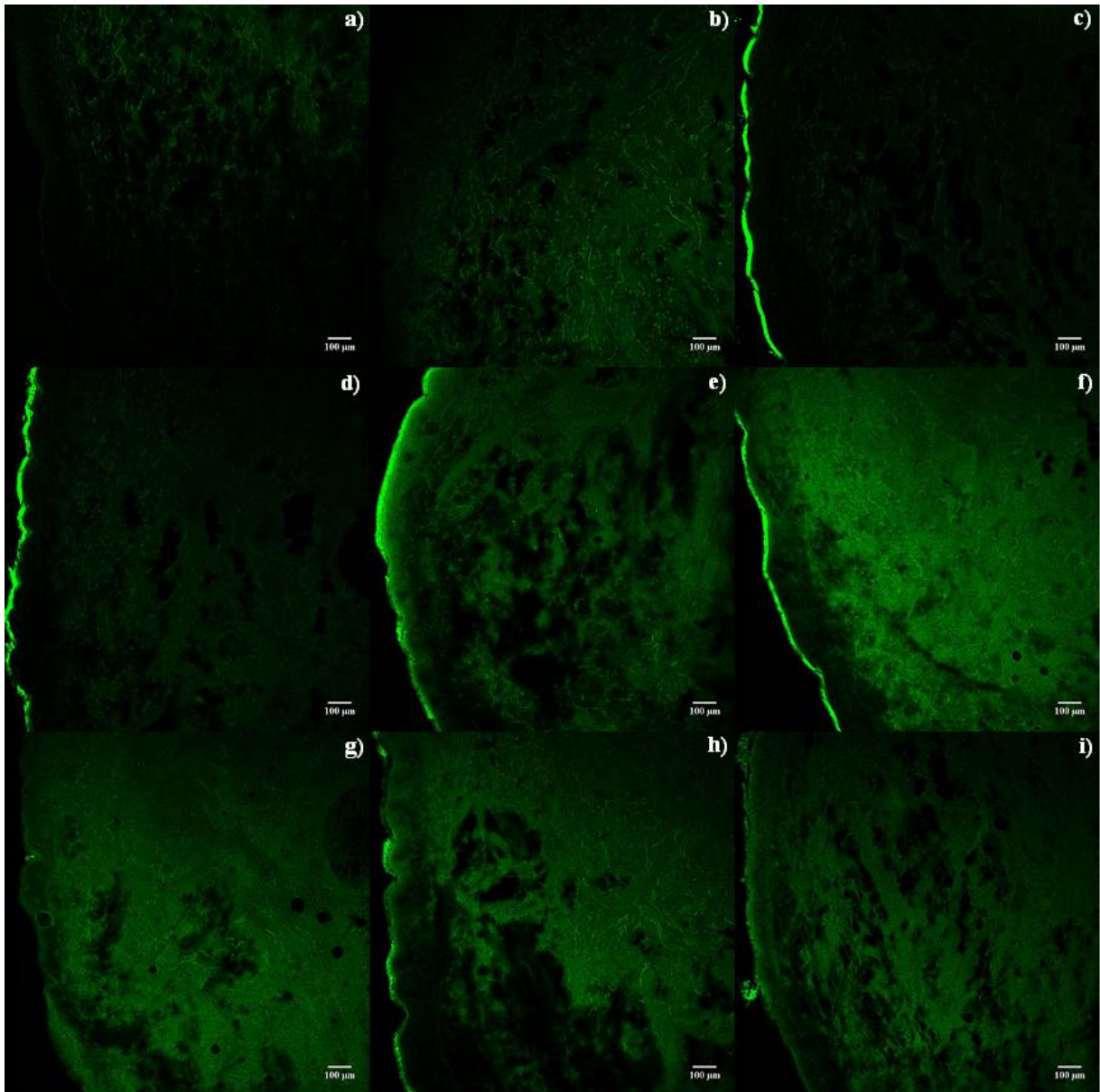
Figure 3.15: CLSM pictures illustrating diffusion of FG24 488 CASE into skin tissues from donor E and F, after pretreatment with micro-needles. The pictures **a)** and **b)** are the control tissues, and c) to i) represents the diffusion of FG24 488 CASE in skin incubated for **c)** 2 hours (donor E), **d)** 6 hours (donor E), **e)** 12 hours (donor F), **f)** 16 hours (donor F), **g)** 18 hours (donor F), **h)** 20 hours (donor F) and **i)** 24 hours (donor F).

a)	b)	c)
d)	e)	f)
g)	h)	i)
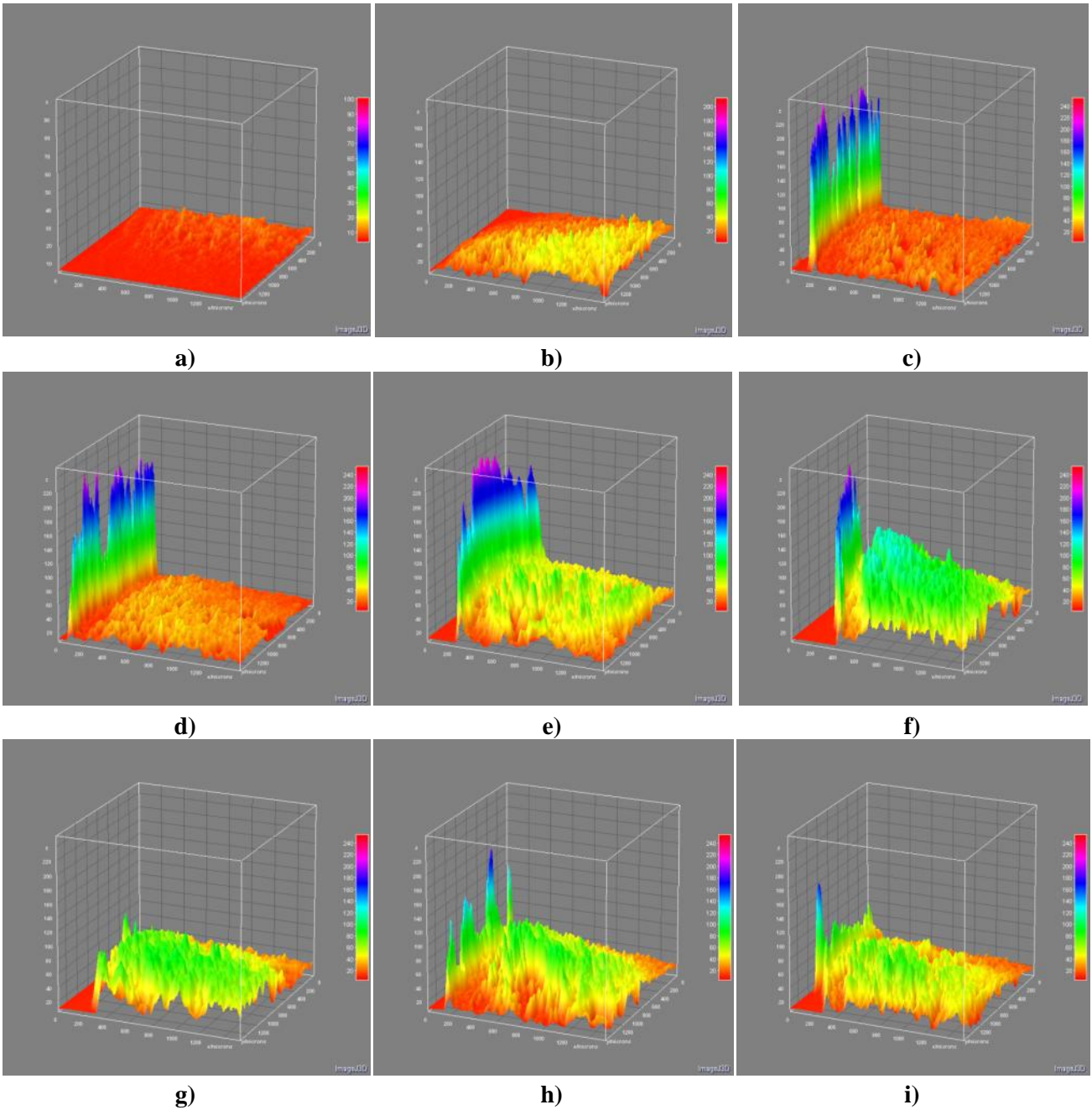
Figure 3.16: Surface plot showing the distribution of fluorescence intensity after diffusion of FG24 488 CASE into skin tissues from donor E and F, after pretreatment with micro-needles. **a)** and **b)** are the control tissue, and c) to i) represents the diffusion of Alexa 488 CASE in skin incubated for **c)** 2 hours (donor E), **d)** 6 hours (donor E), **e)** 12 hours (donor F), **f)** 16 hours (donor F), **g)** 18 hours (donor F), **h)** 20 hours (donor F) and **i)** 24 hours (donor F).

Figures 3.15 and 3.16 demonstrate how FG24 488 CASE diffused into skin tissues after pretreatment with micro-needles. In tissue from donor E, incubated for 2 and 6 hours, the distribution of fluorescence was concentrated in SC and no fluorescence indicating diffusion of FG24 488 CASE deeper into the tissue was observed (Figure 3.15c, d). These observations were supported by the 3D surface plots (Figure 3.16c, d). After 12 and 16 hours high fluorescence intensities were observed in the SC, but the applied sample was also observed to

be distributed deeper in the tissue (Figure 3.15d,e). The highest and most evenly distributed dermal fluorescence was observed after 16 hours (Figure 3.16e). At the same time this tissue displayed lower intensities in the viable epidermis compared to in the dermis, indicating that FG24 488 CASE was able to readily diffuse through the epidermal layer after overcoming the SC barrier. After 18, 20 and 24 hours of incubation a decrease in fluorescence were observed, both in the SC and in deeper in the tissues (Figures 3.15 and 3.16 g, h, i).

$I_{corrected}$, detected in the tissues after 2-24 hours of incubation, is presented as a function of incubation time in Figure 3.17, and the $I_{corrected}$ values are given in Table E.2 in Appendix E.
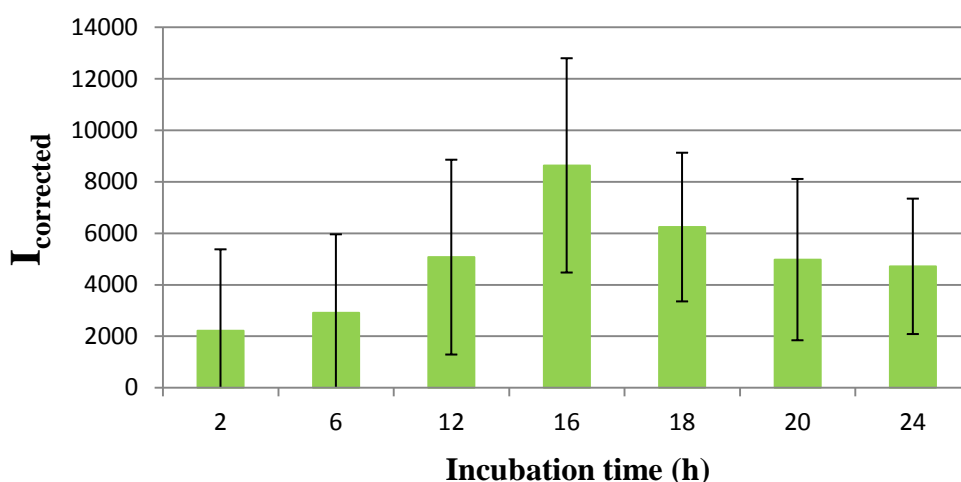
Figure 3.17: $I_{corrected}$ values of FG24 488 detected in tissues incubated for 2-24 hours.

Figure 3.17 supports the observations of increasing fluorescence with increasing incubation time in the time interval of 2-16 hours of incubation, and show that a peak in $I_{corrected}$ for FG24 488 CASE was achieved after 16 hours. It also illustrates a decrease in $I_{corrected}$ with increasing incubation time after 18-24 hours. The tissue incubated for 12 hours displayed higher intensity values compared to the tissues incubated for 20 and 24 hours, and this variation may have been due to the heterogeneity of each individual piece of tissue. Possible reasons for the variations in $I_{corrected}$ are discussed in subsection 3.2.5.3.

The I_{RP} values measured after 2-24 hours of incubation are given in Figure 3.18. After 16 hours of incubation an increase in fluorescence in the receptor phase was observed, but this increase only corresponded to 0.3% of $I_{RP\ max}$. This was similar to the results obtained for Alexa 488 CASE, and indicated that the rate of diffusion in the longitudinal direction was < 12.5 mm/hour. Increase in $I_{RP\ corrected}$ was also observed after 20 hours (0.4 % of $I_{RP\ max}$), and after 24 hours the highest value was measured. The $I_{RP\ corrected}$ did, however, only correspond

to 3% of $I_{RP\,max}$. A minor degree of inconsistency was observed for the $I_{RP\,corrected}$ values of FG24 488 CASE, including the lower value measured after 18 hours compared to after 16 hours. The reasons for this inconsistency were believed to be the same as for Alexa 488 CASE, discussed in subsection 3.2.5.3.
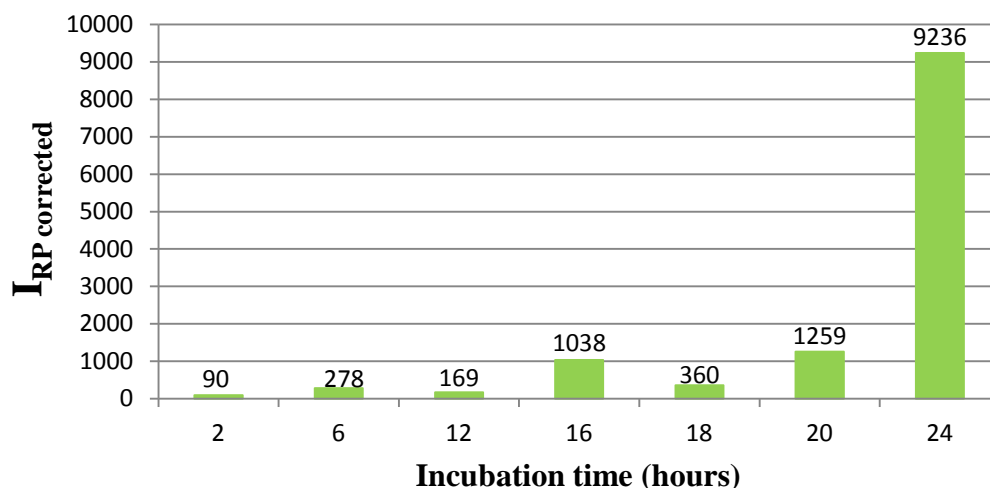

Figure 3.18: The $I_{RP\,corrected}$ values measured for FG24 488 CASE after 2-24 hours of incubation.

3.2.5.2. Diffusion kinetics in skin pre-treated with laser

In this subsection the results of the diffusion kinetics experiments performed in skin pre-treated with L1 (Table 2.2) are presented. CLSM images and 3D surface plots illustrating diffusion of Alexa 488 CASE in human skin tissues incubated for 20 minutes-6 hours are given in Figures 3.19 and 3.20. CLSM images and 3D surface plots illustrating diffusion of FG24 488 CASE in skin under identical terms, are given in Figures 3.23 and 3.24. The control tissue from donor J is included in the results.
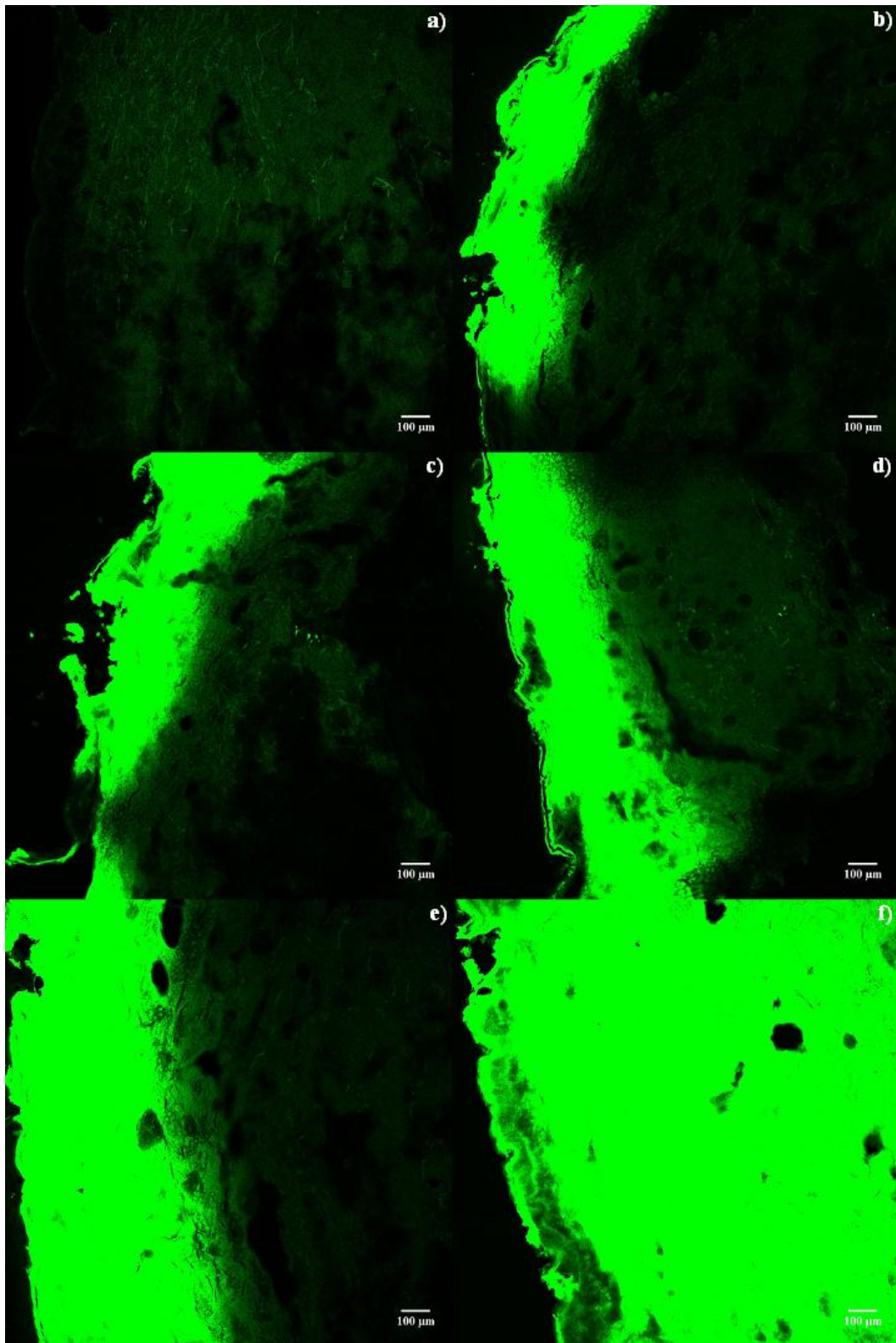
Figure 3.19: CLSM pictures illustrating diffusion of Alexa 488 CASE into skin tissue from donor J, after pretreatment with L1. Picture **a)** is the control tissue, b) to f) shows the diffusion of Alexa 488 incubated for **b)** 20 min, **c)** 40 min, **d)** 60min, **e)** 2 hours and **f)** 6 hours.
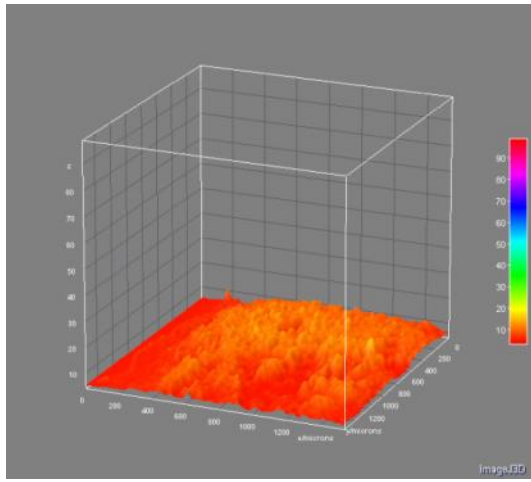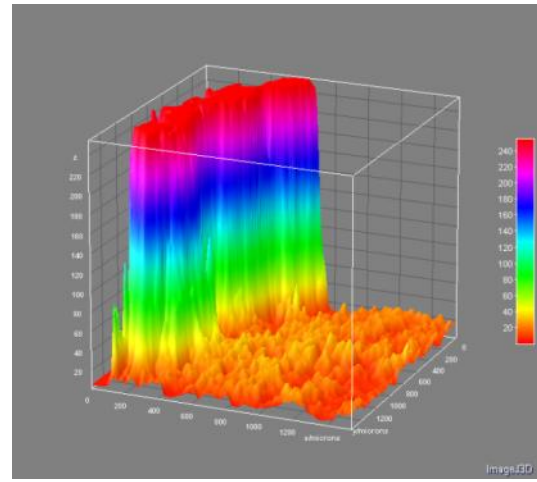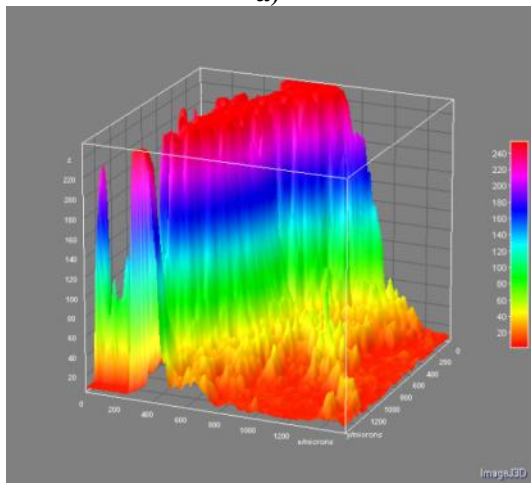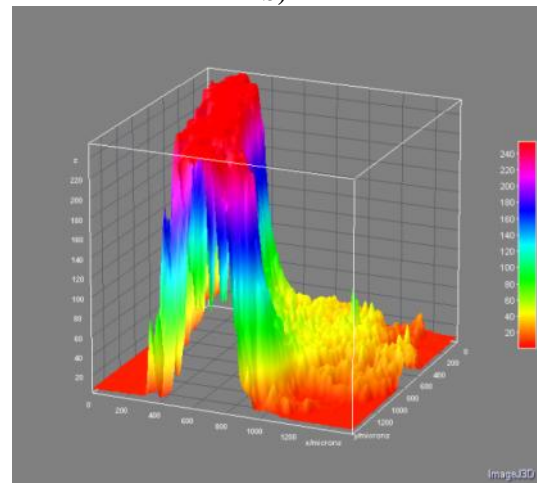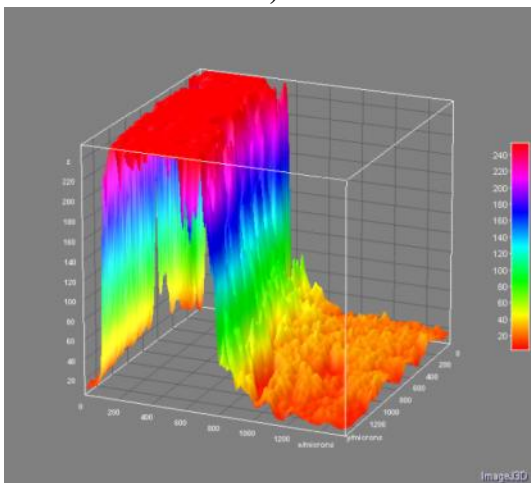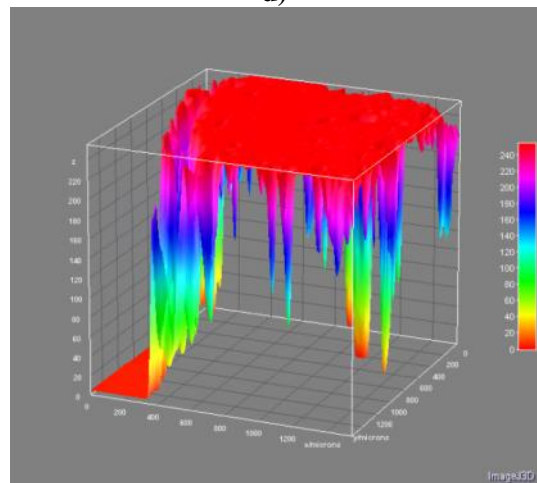
Figure 3.20: Surface plot illustrating the distribution of fluorescence intensity after diffusion of Alexa 488 CASE into skin tissues from donor J, after pretreatment with L1. Picture **a)** is the control tissue, b) to f) shows the diffusion of Alexa 488 incubated for **b)** 20 min, **c)** 40 min, **d)** 60min, **e)** 2 hours and **f)** 6 hours.

Figures 3.19 and 3.20 demonstrate an increase in fluorescence intensity distribution with increasing incubation time. After 20 minutes of incubation high intensity fluorescence was observed to be distributed throughout the epidermis (Figure 3.19b and 3.20b). The distribution of Alexa 488 CASE was observed to increase deeper into the tissue with increasing incubation time between 40 minutes-6 hours of incubation (Figure 3.19 and 3.20). After 6 hours the highest fluorescence intensities were observed to be distributed in the SC and evenly throughout the dermal layer. At the same time this tissue displayed lower intensities in the viable epidermis compared to in the dermis (Figures 3.19f and 3.20f), as was observed for FG24 488 CASE after pretreatment with micro-needles and 16 hours of incubation (subsection 3.2.5.1). Thus, disruption of the SC barrier enabled Alexa 488 CASE to readily diffuse through the epidermis and into the dermis.

$I_{mean\ sample}$ of Alexa 488 CASE, detected in tissues after 20 minutes-6 hours of incubation, is presented as a function of incubation time in Figure 3.21. The $I_{mean\ tissue}$ and $I_{mean\ sample}$ values are given in Table E.3, in Appendix E.
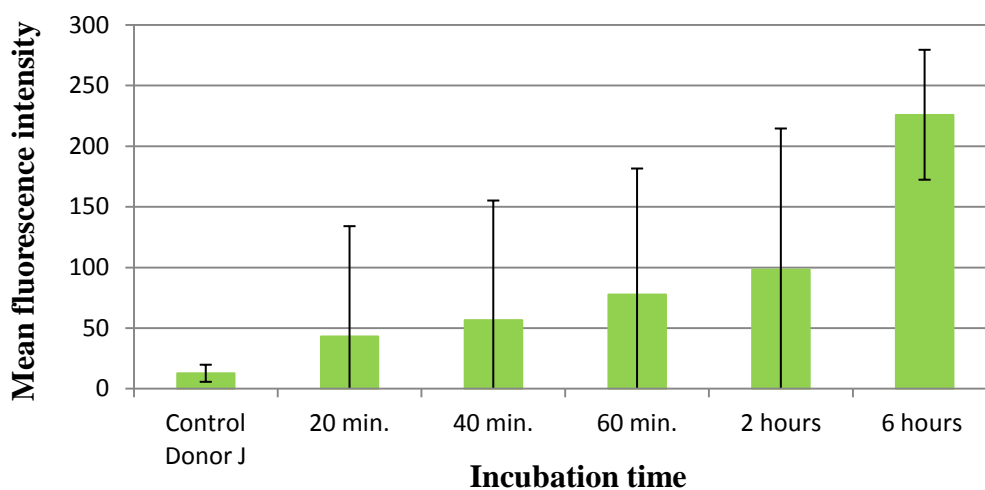

Figure 3.21: $I_{mean\ control}$ detected in the control tissue from donor J, and $I_{mean\ sample}$ values of Alexa 488 CASE detected in tissues after 20 minutes-6 hours of incubation.

Figure 3.21 clearly illustrates an increase in $I_{mean\ sample}$ with increasing incubation time, and demonstrates that the highest mean fluorescence intensity in the tissues was obtained after 6 hours of incubation (Figures 3.19f and 3.20f). This could imply that 6 hours of incubation was sufficient for diffusion of the sample all the way through the tissue and into the receptor phase. The I_{RP} measurements, given in Figure 3.22, somewhat confirmed this implication, as the only increase in fluorescence intensity in the receptor phase was observed after this

incubation time. However, the measured I_{RP} value only corresponded to 1 % of $I_{RP\,max}$, which once again emphasized that a high $I_{mean\,sample}$ and an even distribution of the sample throughout the deeper layers of the tissue was not equivalent with efficient diffusion into the receptor phase. The diffusion rate was therefore suggested to be < 0.28 mm/hour. This diffusion rate was higher compared to the ones suggested for diffusion of Alexa 488 CASE and FG24 488 CASE through skin tissues and into the receptor phase after pretreatment with micro-needles, given in subsection 3.2.5.1. The I_{RP} values measured after 40 minutes-2 hours were equal to the I_{RP} from the control tissue, and after 20 minutes it was even lower (one decimal used to indicate value > 0), indicating the presence of endogenous fluorophores in the receptor phase giving rise to autofluorescence.
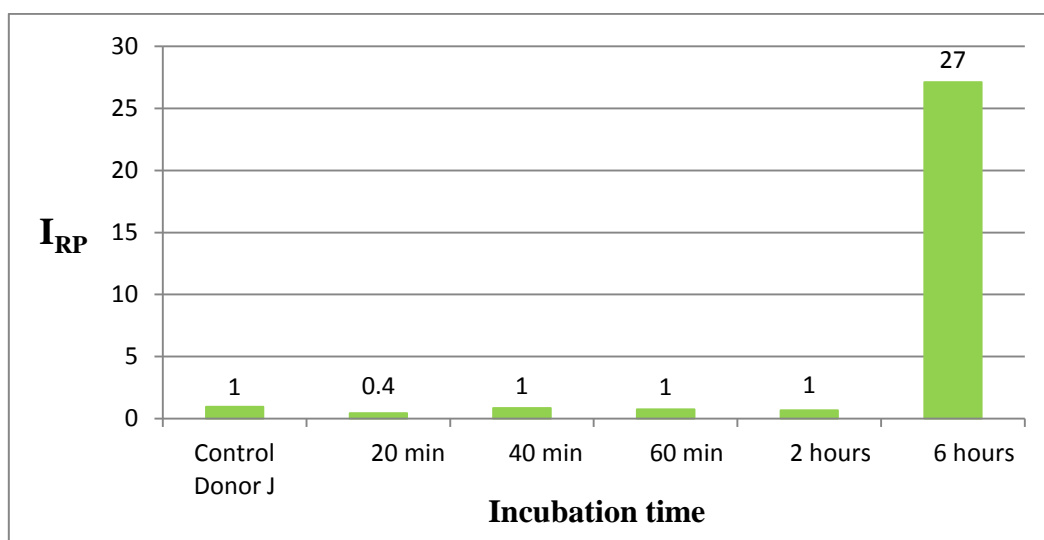
Figure 3.22: The fluorescence intensity in the receptor phase, I_{RP}, measured for the control tissue and for Alexa 488 CASE after 20 minutes - 6 hours of incubation.
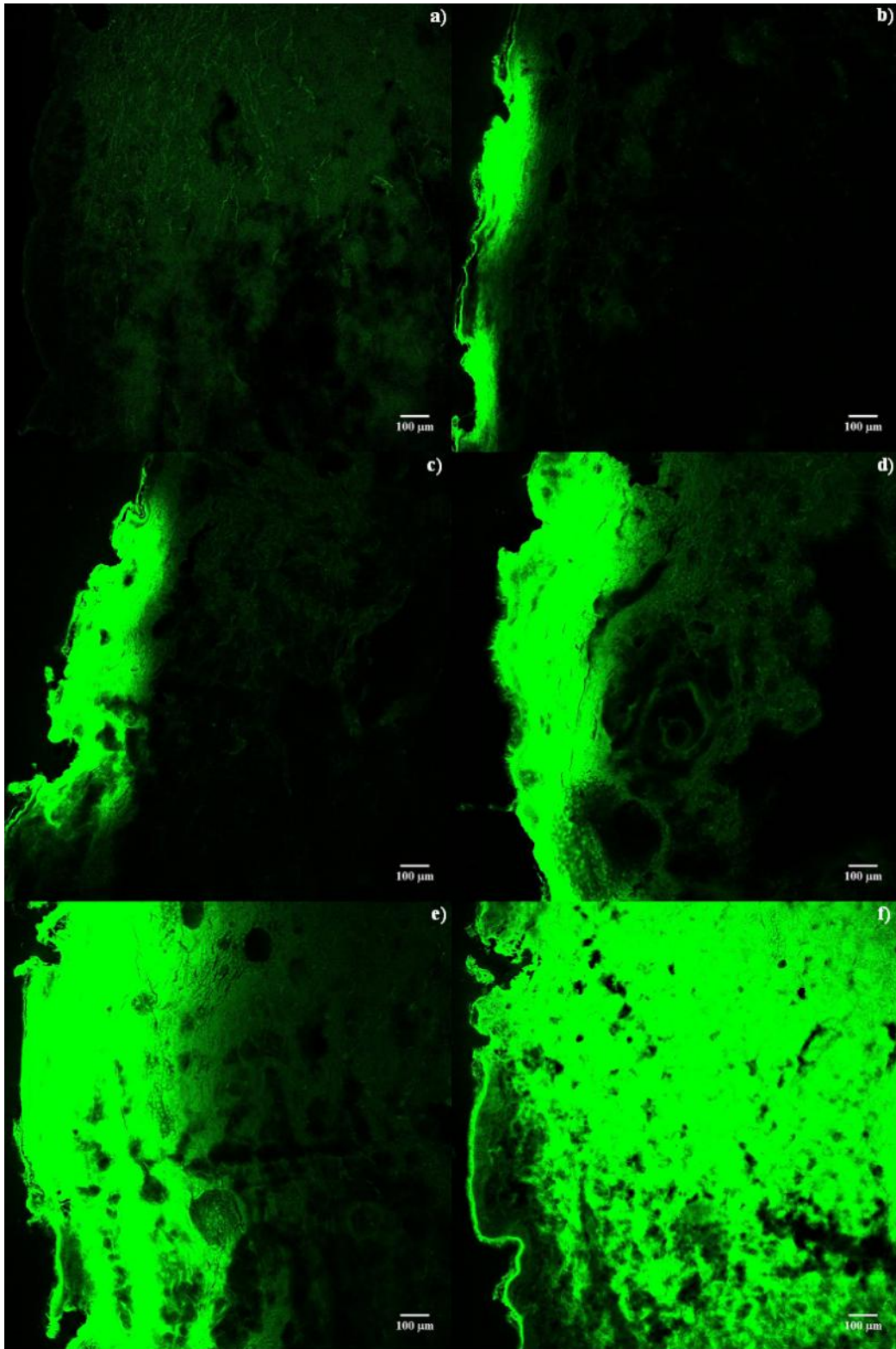
Figure 3.23: CLSM pictures illustrating diffusion of FG24 488 CASE into skin tissue from donor J, after pretreatment with L1. Picture **a)** is the control tissue, b) to f) shows the diffusion of FG24 488 incubated for **b)** 20 min, **c)** 40 min, **d)** 60min, **e)** 2 hours and **f)** 6 hours.
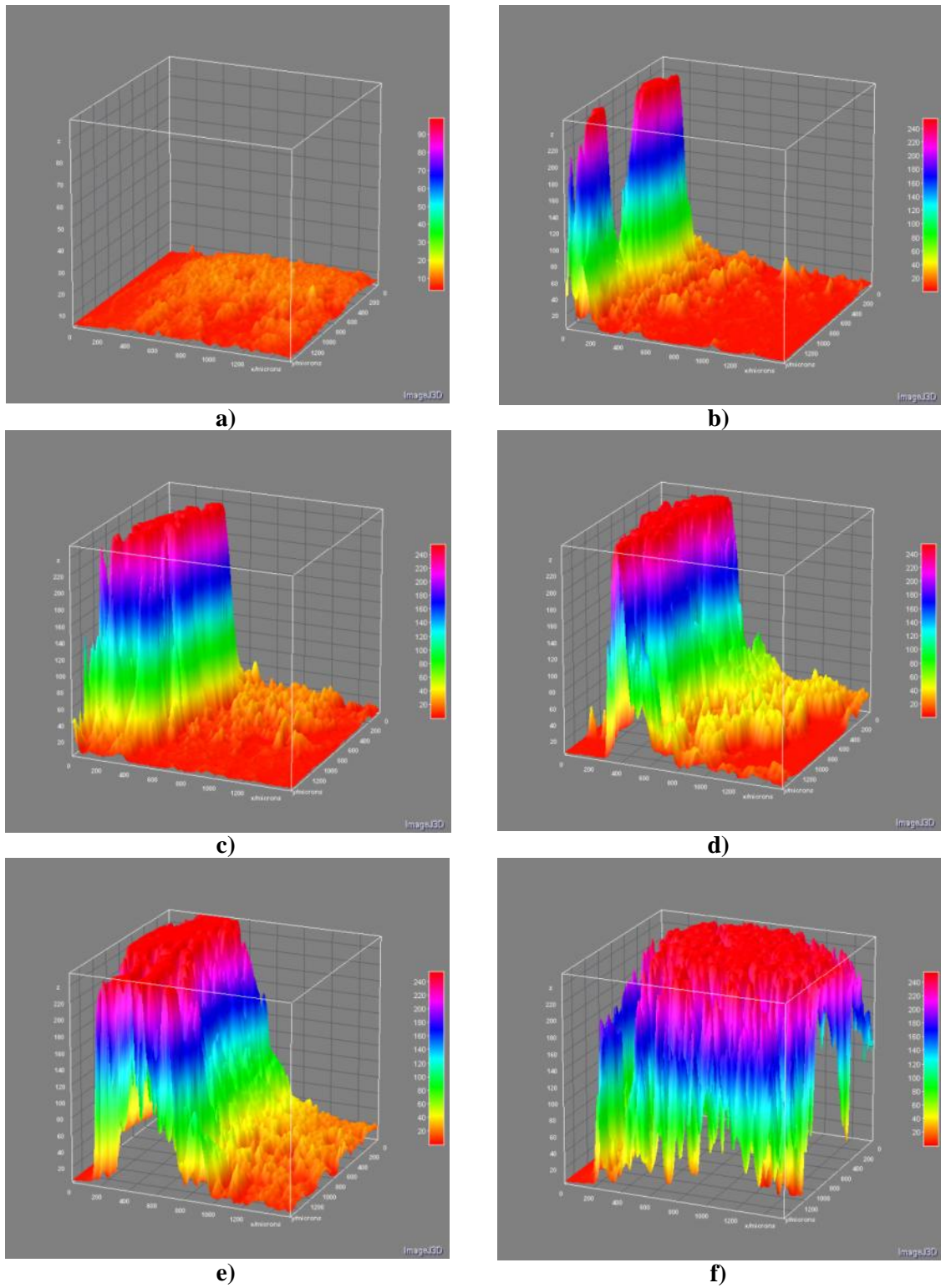
Figure 3.24: Surface plot illustrating the distribution of fluorescence intensity after diffusion of FG24 488 CASE into skin tissue from donor J, after pretreatment with L1. Picture **a)** is the control tissue, b) to f) shows the diffusion of FG24 488 incubated for **b)** 20 min, **c)** 40 min, **d)** 60min, **e)** 2 hours and **f)** 6 hours.

Figures 3.23 and 3.24 show how the distribution of fluorescence increased with increasing incubation time as a result of diffusion of FG24 488 CASE in skin tissues. This trend was similar to what was found for Alexa 488 CASE in skin tissues after pretreatment with L1, but the progression of diffusion seemed to be slower for the FG peptide sample. After 20 minutes of incubation high intensity fluorescence was observed to be distributed in the upper part of epidermis, and after 40 minutes FG24 488 CASE was primarily distributed throughout the layers of epidermis (Figures 3.23 and 3.24 b, c). An increasing distribution of high intensity fluorescence in both epidermis and in the upper dermis was observed after 1 and 2 hours of incubation, indicating diffusion of FG24 488 CASE beyond the SC and the viable epidermis, and into the dermis (Figures 3.23 and 3.24 d, e). The highest overall distribution of FG24 488 CASE was observed after 6 hours of incubation (Figure 3.23f and 3.24f).

In the tissue incubated for 6 hours (Figure 3.23f) a large cavity, caused by the laser treatment, was observed to span both the SC and the viable epidermis. Similar cavities were also observed in other tissues with this pretreatment. However, in this particular tissue, the distribution of high fluorescence intensities was observed to expand from the laser cavity to deeper layers of the dermis, while fluorescence was observed in the SC in the areas where the skin barrier was intact and deeper in the underlying dermis. An interpretation of this observation was that the diffusion of FG24 488 CASE primarily occurred through the cavity in the outer layers of the skin, and that lateral diffusion of FG24 488 CASE contributed to a more extensive distribution of the sample throughout the dermis.

$I_{corrected}$ of FG24 488 CASE, detected in tissues after 20 minutes-6 hours of incubation, is presented as a function of incubation time in Figure 3.25. The $I_{corrected}$ values are given in Table E.4, in Appendix E.
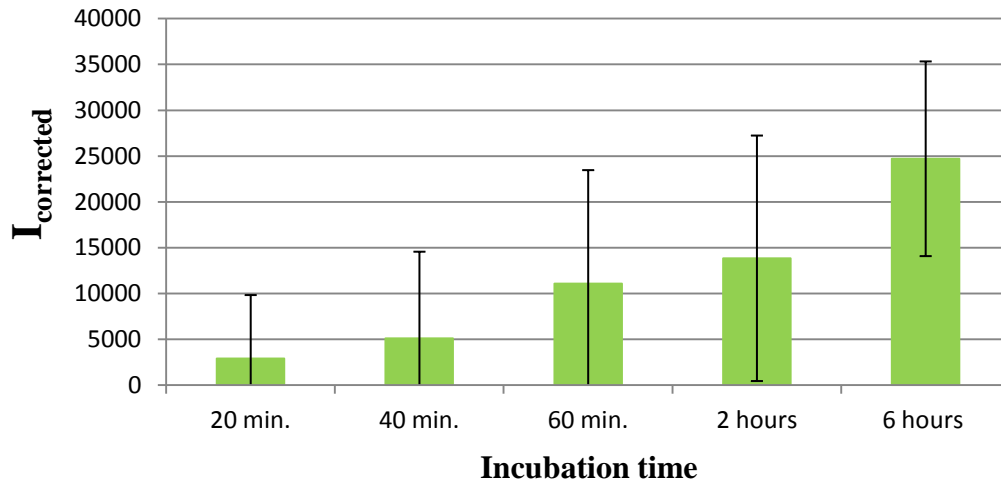
Figure 3.25: $I_{corrected}$ values of FG24 488 detected in tissues after 20 minutes-6 hours of incubation.

Figure 3.25 shows the trend of increasing $I_{corrected}$ values with increasing incubation time, and that the highest mean fluorescence was obtained after 6 hours of incubation. The I_{RP} measurements, given in Figure 3.26, showed the greatest increase in fluorescence intensity in the receptor phase after 6 hours of incubation, corresponding to 1.8% of $I_{RP\,max}$. The diffusion rate was therefore suggested to be < 0.28 mm/hour, the same as for Alexa 488 CASE in skin tissue after the same incubation time. However, the increase in I_{RP} measured after 1 hour, corresponding to 1.5% $I_{RP\,max}$, introduced a degree of inconsistency in the measurements. Possible reasons for this inconsistency are discussed in subsection 3.2.5.3.
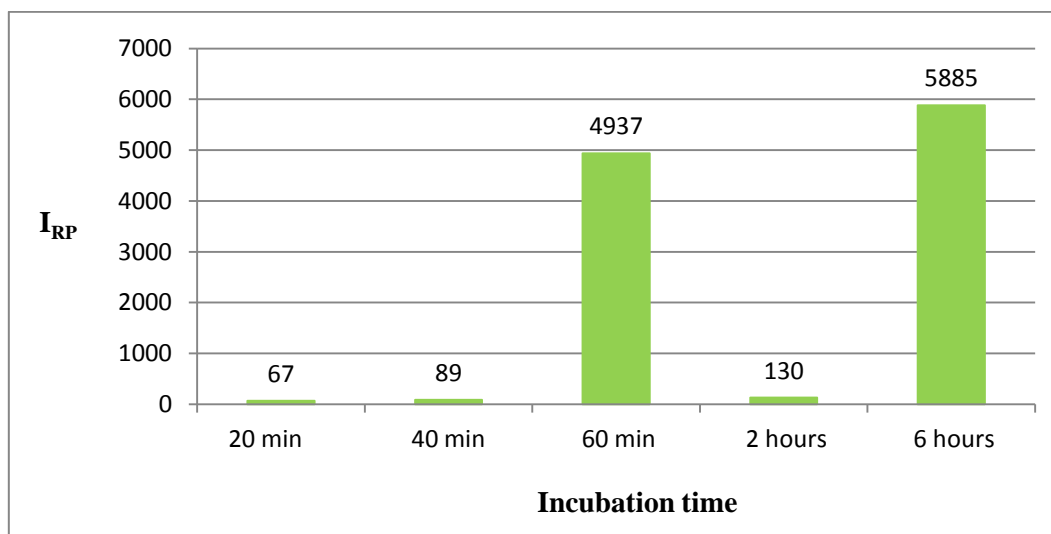
Figure 3.26: The $I_{RP\,corrected}$ values measured for FG24 488 CASE after 20 minutes-6 hours of incubation.

3.2.5.3. Summary of skin diffusion kinetics experiments

The diffusion kinetics of Alexa 488 CASE and FG24 488 CASE in skin tissues pre-treated with micro-needles and L1 are collectively compared and discussed in this subsection. The results of the kinetics experiments indicated the need for 12 and 6 hours of incubation to achieve the greatest distribution of Alexa 488 CASE throughout the skin tissues, after pretreatment with micro-needles and L1, respectively. For FG24 488 CASE the greatest distribution of fluorescence was achieved after 16 hours in skin pre-treated with micro-needles and 6 hours in skin pre-treated with L1.

The different incubation times needed for distribution throughout the tissues between the two samples may have been due to their differences in M_w. Bos and Meinardi (2000) introduced the "500 Dalton rule", and stated that passive skin absorption starts to decline rapidly around 500 Dalton (g/mol) due to molecular size in untreated skin. The M_w of Alexa 488 CASE is around 650 g/mol (Table 2.1), and thus it is likely to assume that Alexa 488 CASE diffuse into skin more rapidly compared to FG24 488 CASE, with an estimated M_w of 3000 g/mol. Da Silva *et. al* (2008) reported significant *ex vivo* skin penetration of taurin, a hydrophilic amino acid with a molecular weight of 125.48 g/mol, in untreated human breast skin after 1 hour. In comparison, the longer time needed for distribution of Alexa 488 CASE and FG24 488 CASE into deeper skin layers demonstrated the need for longer incubation time with increasing molecular weight. However, the results reported here were obtained from skin tissues where penetration through the outer skin barrier was physically enhanced, by the use of micro-needles and laser, prior to application of samples. Therefore, it cannot be assumed that a longer incubation time alone would be sufficient to achieve diffusion of larger molecules through untreated skin. However, for the following transdermal diffusion experiments it was introduced a standard incubation time of 22 hours. A longer incubation time was considered to be favorable for the use of test molecules of higher M_w compared to FG24 488 CASE. In addition, a longer incubation time could possibly provide the opportunity to study diffusion both **into** and all the way **through** human skin.

The effect of M_w in penetration of the SC should imply that FG24 488 CASE would be retained in the SC to a larger extent compared to Alexa 488 CASE. However, from the results after diffusion of the samples in skin tissues pre-treated with micro-needles (Figures 3.11 and 3.15), Alexa 488 CASE was observed to be more accumulated in the SC compared to FG24 488 CASE. This observation was most profound in tissues incubated for 18-24 hours. A

reason for this could be a varying degree of barrier disruption by the micro-needle device, discussed in section 3.2.10. Another explanation could be that, even though the SC barrier was disrupted, the higher M_w of FG24 488 resulted in slower diffusion into and through the SC compared to Alexa 488 CASE, leaving more of the sample to be wiped off on the skin surface after the given incubation time.

In the experiment performed with micro-needles and L1, the time span between each chosen time of incubation was not identical. This might have affected the results from the experiments performed with laser more profoundly, as the time span was increased from being 20 minutes during the first hour of incubation to 4 hours between 2 and 6 hours of incubation. Identical incubation time (6 hours) was observed to give the highest mean fluorescence intensities and the greatest distribution throughout the tissues after pretreatment with L1 for both Alexa 488 CASE and FG24 488 CASE. If assuming a correlation between M_w and incubation time, a shorter incubation time would be expected for Alexa 488 CASE compared to FG24 488. It can therefore be questioned if the highest $I_{mean\ sample}$ of Alexa 488 CASE was reached at an earlier time within this time span of 4 hours. Inclusion of an additional incubation time within the interval of 2-6 hours could perhaps have revealed this, while inclusion of an extra incubation time exceeding 6 hours could give an indication of whether or not the highest fluorescence distribution in fact was reached for both samples after 6 hours.

The skin tissues pre-treated with micro-needles were obtained from two different donors, and the average thickness of the two tissues varied, as shown in Table 3.6. Skin from donor F was measured to be 0.48 mm thicker than skin from donor E, which means that the longitudinal diffusion path towards the deeper skin layers and ultimately the receptor phase, were much longer for samples applied on skin from donor F. This may have influenced the results, and thus the interpretation of the diffusion kinetics of Alexa 488 CASE and FG24 488 CASE. In the experiments with applied Alexa 488 CASE this difference in skin thickness could likely be the reason why the tissue incubated for 6 hours displayed higher intensity values compared to the tissues incubated for 16-24 hours. The thinner skin of donor E may also have been the reason behind the higher I_{RP} values measured after 2 hours compared to after longer incubation times for Alexa 488 CASE, and the higher I_{RP} values after 6 hours compared to after 12 hours for FG24 488 CASE. Skin tissues prepared from one individual donor are likely to display a varying degree of heterogeneity. This may include varying thickness and nature of the SC throughout the skin of one single individual, but also visible variations, such

as stretch marks and amount and density of skin appendages. This could potentially influence the diffusion efficiency in the different skin tissues, and thus, also have influenced the results from the receptor phases. Skin heterogeneity is also mentioned in section 1.3 and 3.2.

The inconsistency observed in the I_{RP} measurements may have been caused by experimental errors. Contact between the skin pieces and the PBS buffer in the Franz cells is a requirement for efficient diffusion into the skin tissues and the receptor phase. Lack of such contact could be due to insufficient tightening of the screw clamps used to mount together the experimental set ups, and air bubbles in the interface between the skin tissue and the PBS buffer. In addition, spillage of excess sample from the epidermal surface of the tissues after incubation and into the receptor phase during dismounting of the Franz-cells, may have contributed to higher fluorescence in this phase in some experiments. Insufficient removal of the subcutaneous fat could also restrict, and even prevent, molecules from diffusing into the receptor phase, and thus give rise to incorrect I_{RP} measures.

The results of the diffusion kinetics experiments showed that Alexa 488 CASE was able to efficiently diffuse into human skin. Therefore, the fluorophore, conjugated to FG peptides, was not expected to cause any negative effects on the diffusion into skin tissues. Since only the Alexa 488 CASE fluorophore was studied, it could only be assumed that the same was true for Alexa 488 HSS bound to the G-block oligomers. The fluorophores would, however, contribute to a minor increase in M_w, which could further decrease the diffusion efficiency of the test molecules into human skin.

3.2.6. Diffusion experiments – fish gelatin peptides

The two FG peptides FG24 488 CASE and FG2 488 CASE were used to study diffusion of peptides into the skin (Table 2.3). Diffusion of each sample was studied in a total of 6 experiments. Two different vehicles, 60% DMSO and 10% PEG200, were used separately to investigate the diffusion through untreated skin and through skin pre-treated with micro-needles and L1. The skin tissues were obtained from different donors, as given in Table 2.3. The results from the transdermal diffusion experiments of FG24 488 CASE and FG2 488 CASE are given in subsection 3.2.6.1 and 3.2.6.2, respectively, and both are summarized in subsection 3.2.6.3.
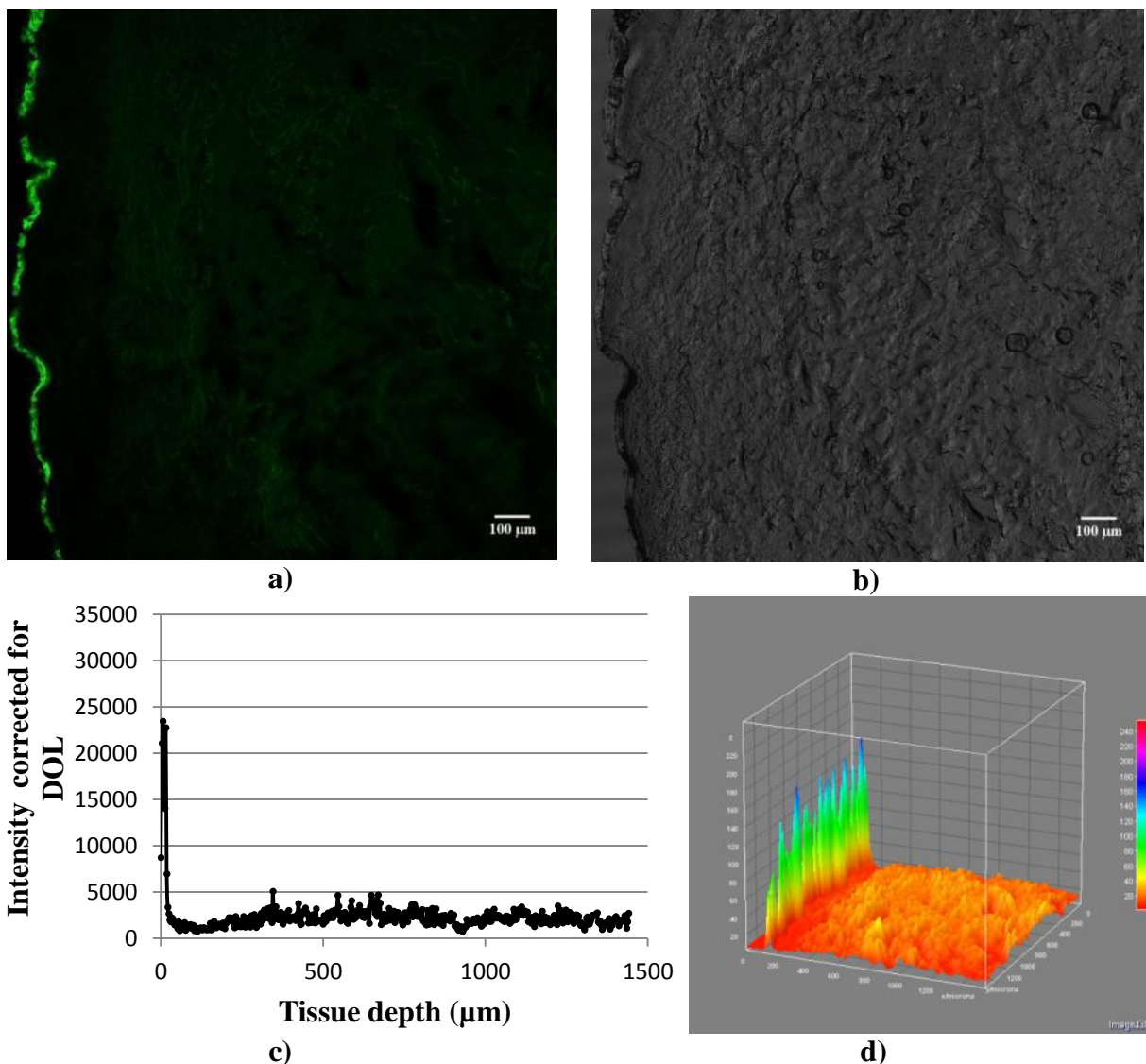
3.2.6.1. FG24 488 CASE

Transdermal diffusion of FG24 488 CASE in untreated skin

The results obtained from transdermal diffusion of FG24 488 CASE in a 60% DMSO and in a 10% PEG200 vehicle into untreated skin from donor H, are given in Figures 3.27 and 3.28, respectively.
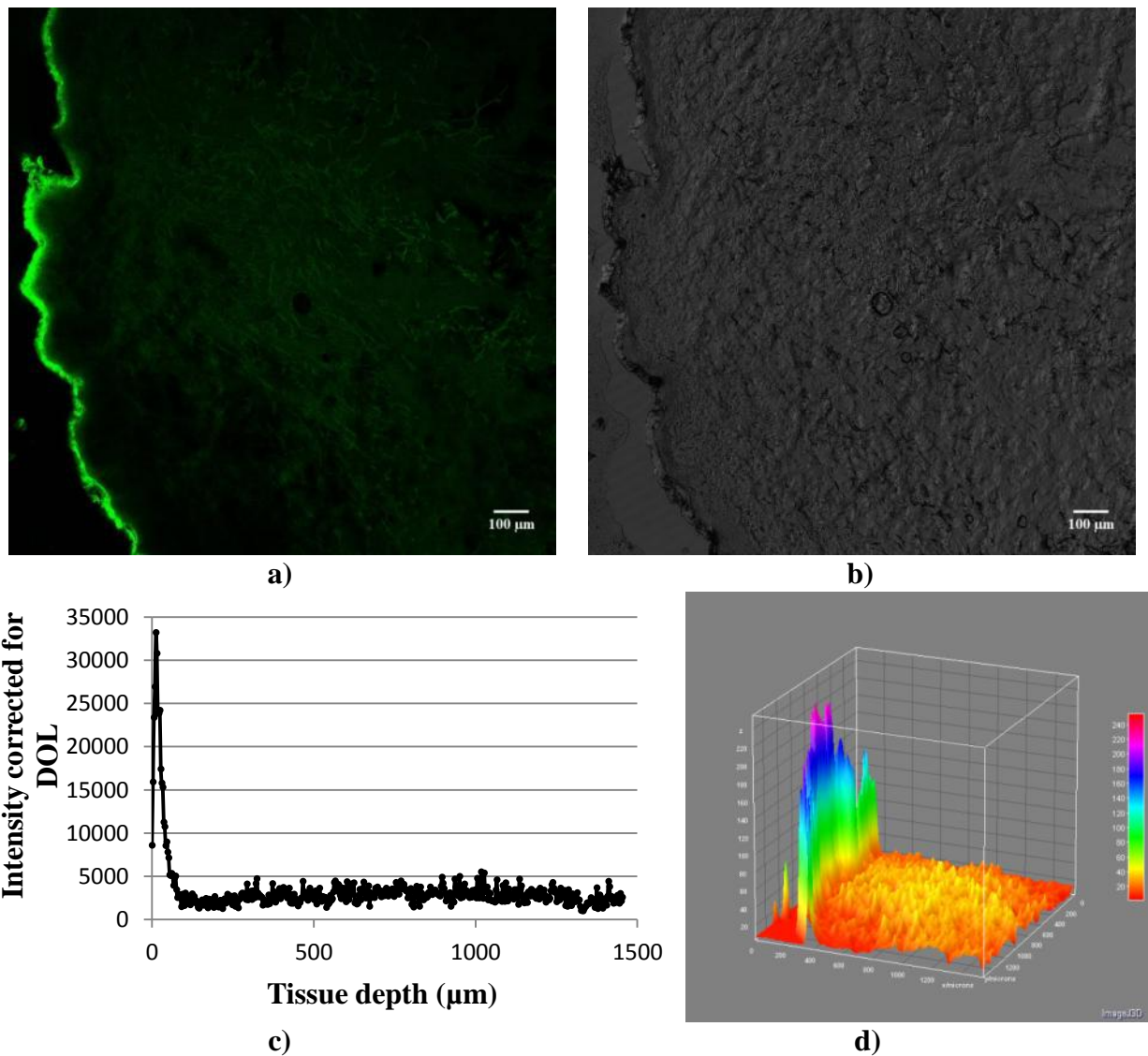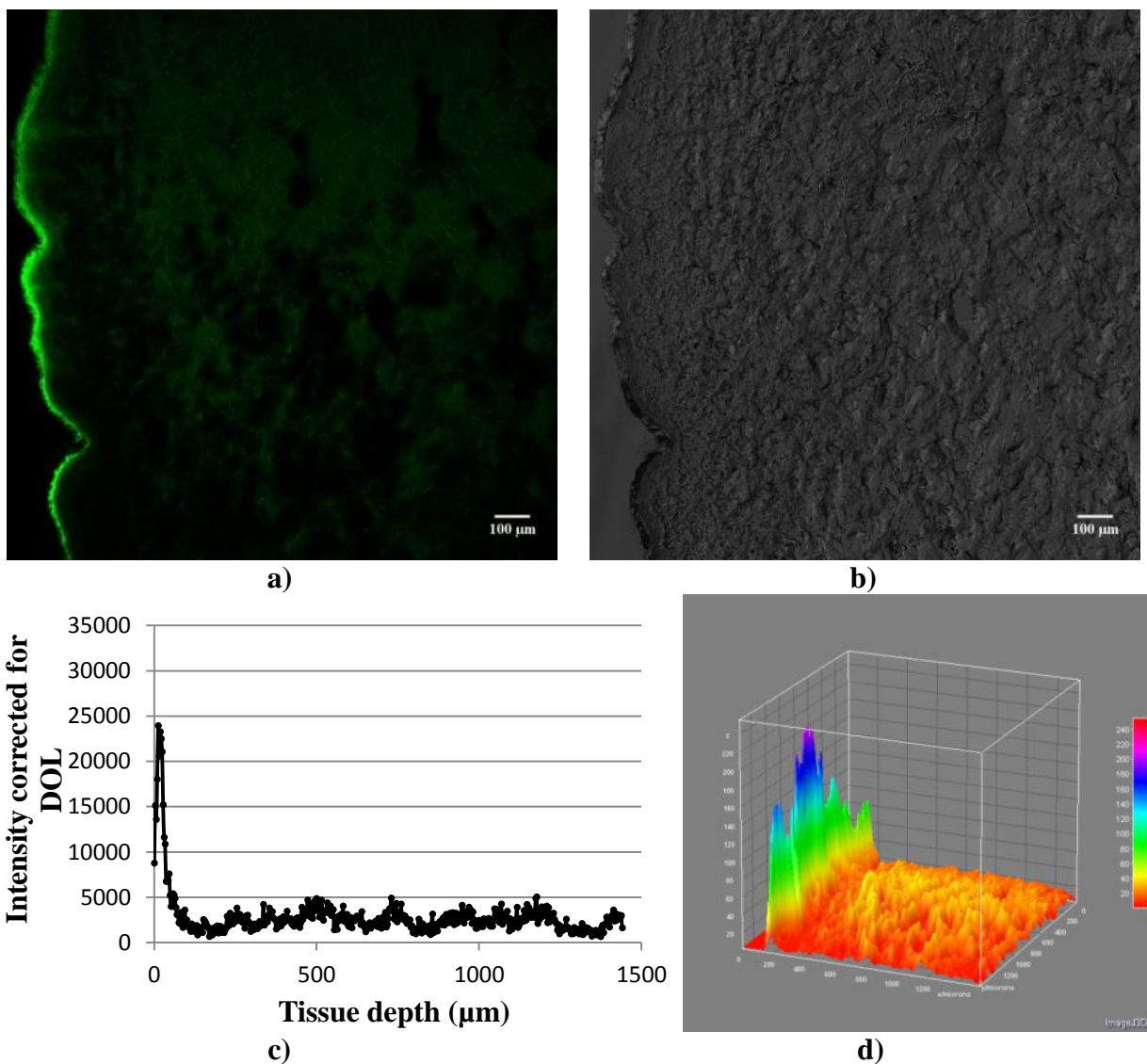

Figure 3.27: Results of transdermal diffusion by FG24 488 in a 60% DMSO vehicle into untreated skin from donor H. **a)** CLSM image showing the fluorescence intensity in the tissue, **b)** transillumination image showing the tissue structure, **c)** intensity plot where fluorescence intensity is given as a function of tissue depth and **d)** 3D surface plot illustrating the distribution of the FG24 488 sample in the tissue.

a)

b)

c)

d)

Figure 3.28: Results of transdermal diffusion by FG24 488 in a 10% PEG200 vehicle in untreated skin from donor H. **a)** CLSM image showing the fluorescence intensity in the tissue, **b)** transillumination image showing the tissue structure, **c)** intensity plot with fluorescence intensity as a function of tissue depth and **d)** 3D surface plot illustrating the distribution of the FG24 488 sample in the tissue.

Figure 3.27 demonstrates how FG24 488 CASE in a 60% DMSO vehicle was distributed in the tissue after diffusion. $I_{corrected}$ of FG24 488 CASE was detected to be 3225 ± 3450. From the CLSM image (Figure 3.27a) it was observed that the detected fluorescence predominantly was located in the SC. This observation was supported by the intensity and the surface plots (Figure 3.27 c, d). However, the surface plot also indicated a minor increase in distribution of the sample in the dermal layer compared to the control tissue (results from the control tissue are given on the enclosed cd). The two single intensity peaks observed in the lower left corner of the surface plot (Figure 3.267) may be due to tissue fragments torn off from the tissue during cryo sectioning.

Figure 3.28 illustrates the results after transdermal diffusion of FG24 488 CASE in a 10% PEG200 vehicle. The distribution of fluorescence was observed to be similar to the one seen for the sample in a 60% DMSO vehicle, illustrated in Figure 3.28a. However, the detected fluorescence intensities were lower for FG24 488 CASE in a 10% PEG200 vehicle, as can be seen by comparing the results from these two experiments (Figures 3.27 and 3.28 c, d). This observation was also supported by the $I_{corrected}$, detected to be 2350 ± 2174. The observations of fluorescence being predominantly located in the SC may indicate the ability of FG24 488 CASE to passively diffuse into this outermost skin layer. However, the sample seemed to be retained in SC and thus, further diffusion into deeper layers was apparently restricted.

Transdermal diffusion of FG24 488 CASE in skin after pretreatment with micro-needles

The results obtained from transdermal diffusion of FG24 488 CASE in a 60% DMSO vehicle and in a 10% PEG200 vehicle into skin from donor H, after pretreatment with micro-needles, are given in Figures 3.29 and 3.30, respectively.

Figure 3.29: Results of transdermal diffusion by FG24 488 in a 60% DMSO vehicle in skin from donor H, after pretreatment with micro-needles. **a)** CLSM image showing the fluorescence intensity in the tissue, **b)** transillumination image showing the tissue structure, **c)** intensity plot with fluorescence intensity as a function of tissue depth and **d)** 3D surface plot illustrating the distribution of the FG24 488 sample in the tissue.
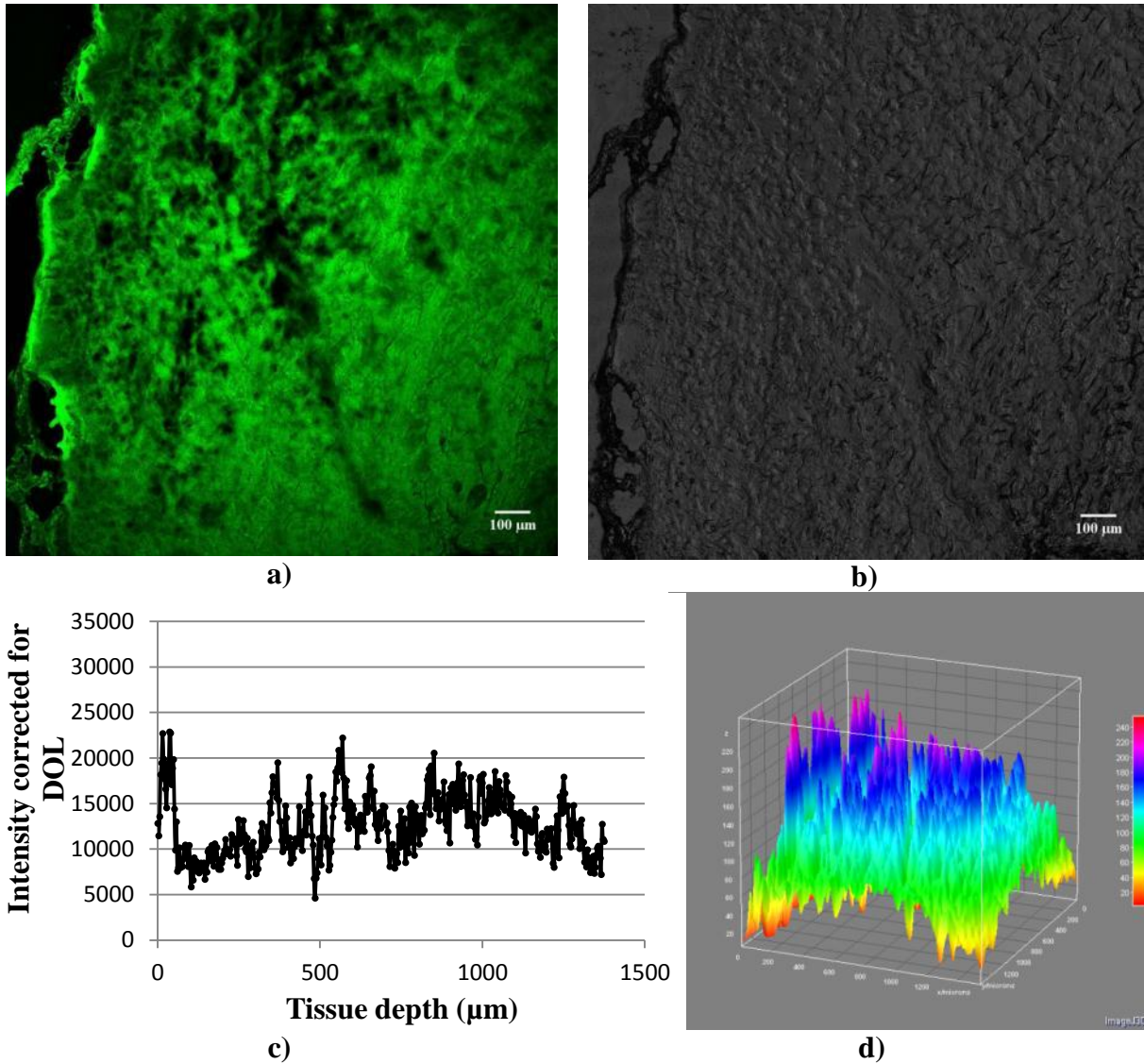
a)

b)

c)

d)
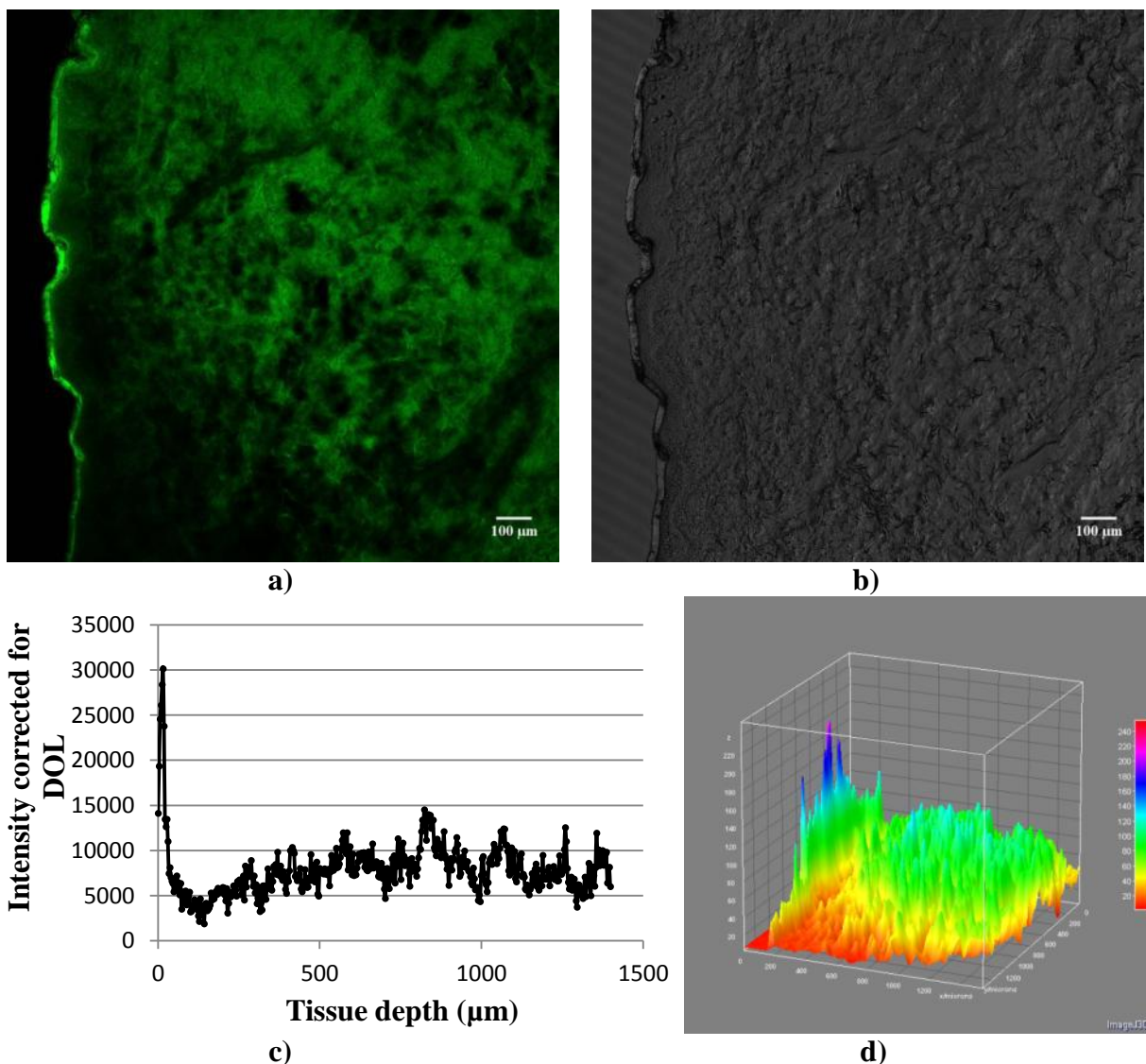
Figure 3.30: Results of transdermal diffusion by FG24 488 in a 10% PEG200 vehicle in skin from donor H, after pretreatment with micro-needles. **a)** CLSM image showing the fluorescence intensity in the tissue, **b)** transillumination image showing the tissue structure, **c)** intensity plot with fluorescence intensity as a function of tissue depth and **d)** 3D surface plot illustrating the distribution of the FG24 488 sample in the tissue.

Figure 3.29 demonstrates how FG24 488 CASE, applied in a 60% DMSO vehicle, was distributed in the tissue after diffusion. Fluorescence was observed to be predominantly, but unevenly, distributed in the SC (Figure 3.29 a, d). The $I_{corrected}$ of FG24 488 CASE was detected to be 2513 ± 2790. Although the higher distribution of fluorescence in SC most likely constituted the majority of this detected mean fluorescence, the results from the experiment indicated that FG24 488 CASE to a minor degree was able to diffuse through the SC and deeper into the skin (Figure 3.29d).

Figure 3.30 illustrates the results from transdermal diffusion of FG24 488 CASE in a 10% PEG200 vehicle. The $I_{corrected}$ for the sample was detected to be 6808 ± 4349, a value considerably higher than the one found after diffusion of the sample in a 60% DMSO vehicle. The fluorescence was observed to be distributed both in the SC and throughout the skin with varying intensities (Figure 3.30a). Distribution, and thus diffusion, of FG24 488 CASE deeper into the tissue was confirmed by the intensity and surface plots (Figure 3.30 c, d). In the viable epidermis and the underlying upper dermis considerably lower intensities was observed compared to in the SC and deeper into the dermis. This may indicate that after overcoming the SC barrier, FG24 488 CASE was able to diffuse more readily deeper into the tissue, which was indicated in the diffusion kinetics experiments also (section 3.2.5).

Transdermal diffusion of FG24 488 CASE in skin after pretreatment with L1

The results obtained from transdermal diffusion of FG24 488 CASE in a 60% DMSO vehicle into skin from donor B and FG24 488 CASE in a 10% PEG200 vehicle into skin from donor K, after pretreatment with L1, are given in Figures 3.31 and 3.32, respectively.

a)

b)

c)

d)

Figure 3.31: Results of transdermal diffusion by FG24 488 in a 60% DMSO vehicle in skin from donor B, after pretreatment with L1. **a)** CLSM image showing the fluorescence intensity in the tissue, **b)** transillumination image showing the tissue structure, **c)** intensity plot with fluorescence intensity as a function of tissue depth and **d)** 3D surface plot illustrating the distribution of the FG24 488 sample in the tissue.
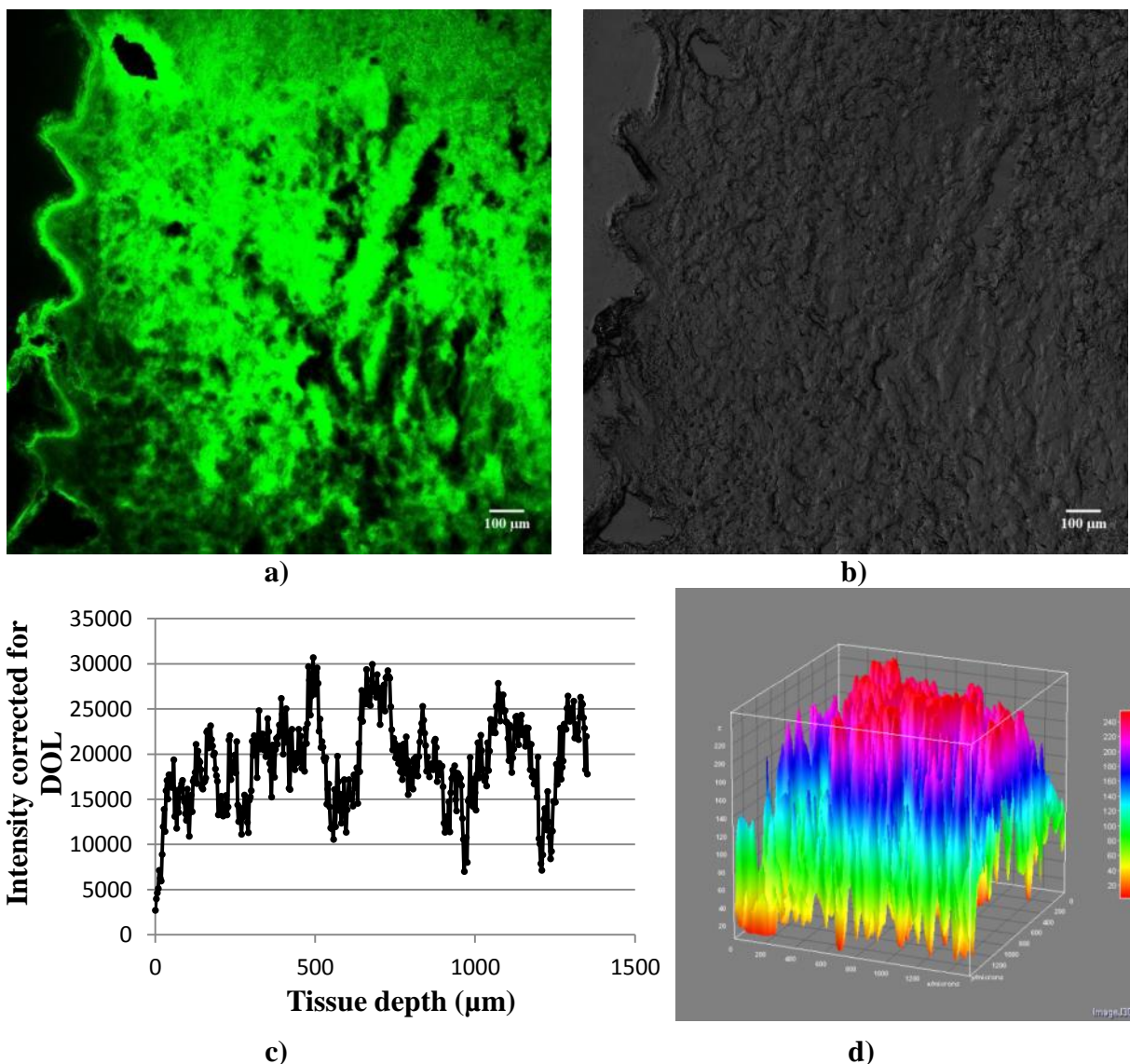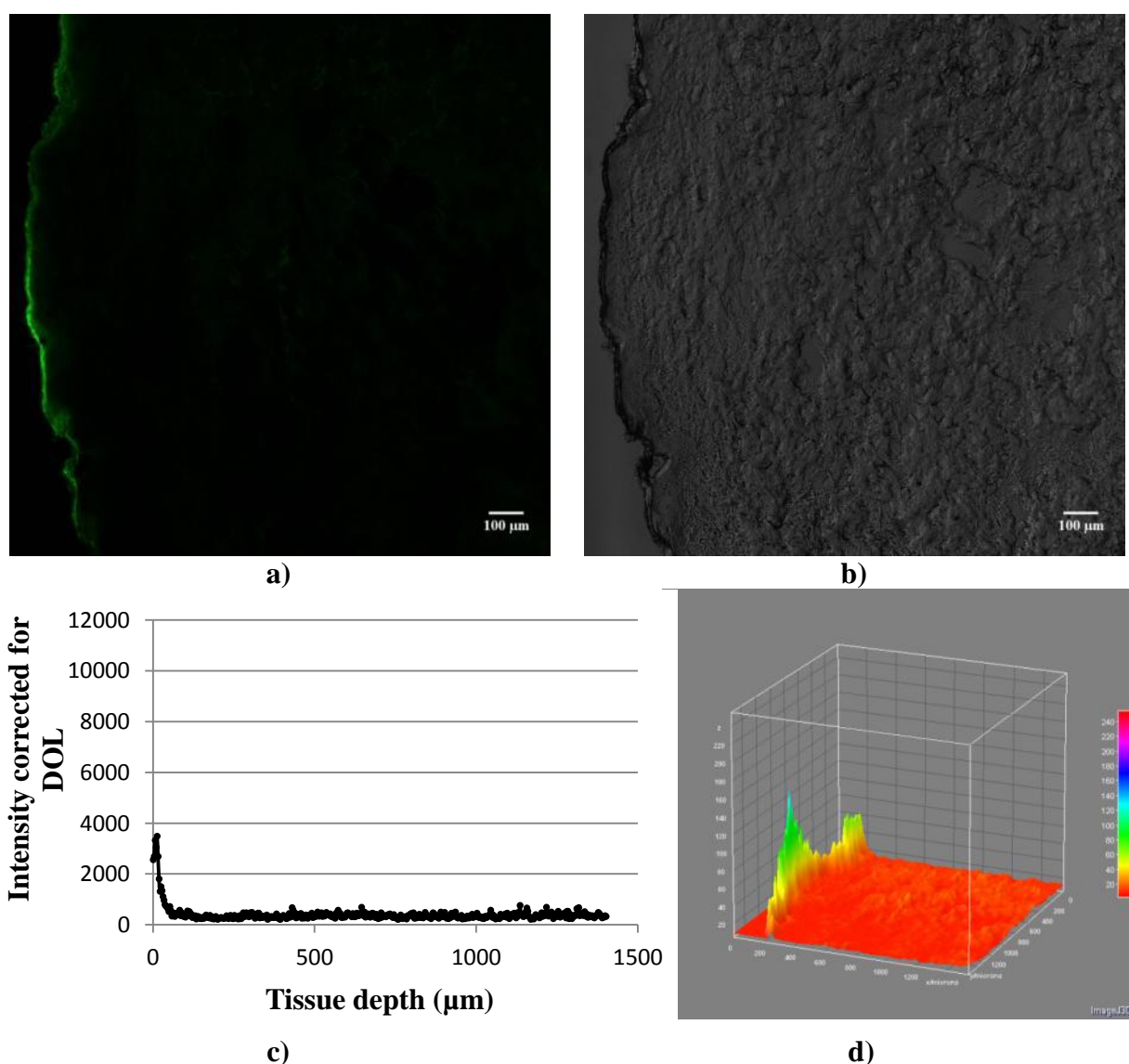
Figure 3.32: Results of transdermal diffusion by FG24 488 in a 10% PEG200 vehicle in skin from donor K, after pretreatment with L1. **a)** CLSM image showing the fluorescence intensity in the tissue, **b)** transillumination image showing the tissue structure, **c)** intensity plot with fluorescence intensity as a function of tissue depth and **d)** 3D surface plot illustrating the distribution of the FG24 488 sample in the tissue.

Figure 3.31 demonstrates how FG24 488 CASE in a 60% DMSO vehicle was distributed in the skin tissue. The highest fluorescence intensities were observed in the areas of SC where the barrier was intact and in the cavities originating from the laser treatment (Figure 3.31a). However, relatively high fluorescence intensities were also observed in the rest of the tissue (Figure 3.31 c, d), and the $I_{corrected}$ for FG24 488 CASE was detected to be 13102 ± 6479. Figure 3.32 demonstrates that FG24 488 CASE in a 10% PEG200 vehicle was able to diffuse more efficiently into the skin tissue compared to the same sample applied in a 60% DMSO vehicle. In this experiment $I_{corrected}$ for FG24 488 CASE was detected to be 18885 ± 10003. High fluorescence intensities were observed throughout the tissue, especially in and around

the laser cavity (Figure 3.32a), and the observations were supported by both the intensity and the surface plots (Figure 3.32 c, d).
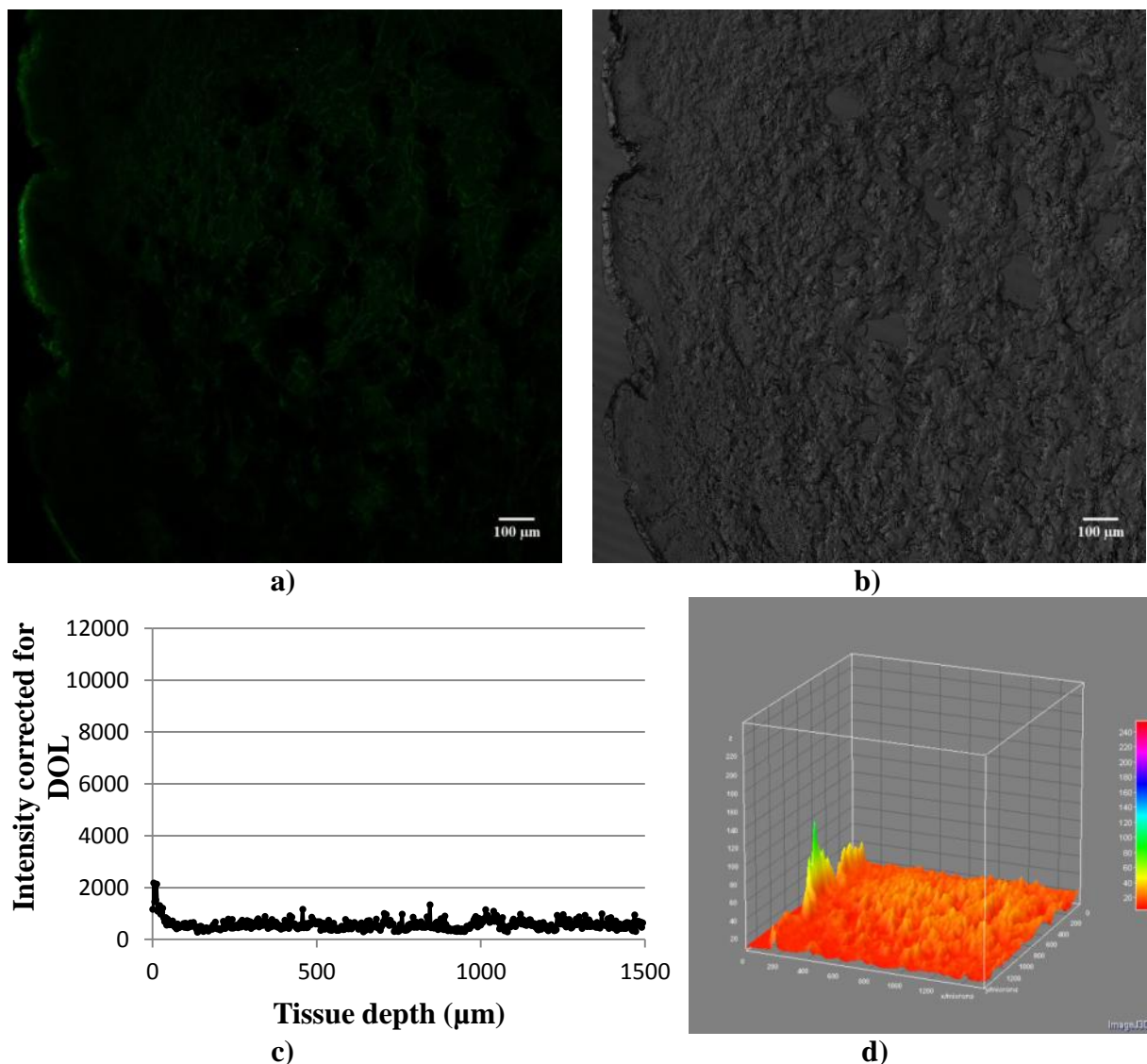
3.2.6.2. FG2 488 CASE

Transdermal diffusion of FG2 488 CASE in untreated skin

The results obtained from transdermal diffusion of FG2 488 CASE in a 60% DMSO and in a 10% PEG200 vehicle, into untreated skin from donor H, are given in Figures 3.33 and 3.34, respectively.

Figure 3.33: Results of transdermal diffusion by FG2 488 in a 60% DMSO vehicle into untreated skin from donor K. **a)** CLSM image showing the fluorescence intensity in the tissue, **b)** transillumination image showing the tissue structure, **c)** intensity plot with fluorescence intensity as a function of tissue depth and **d)** 3D surface plot illustrating the distribution of the FG2 488 sample in the tissue.

Figure 3.34: Results of transdermal diffusion by FG2 488 in a 10% PEG200 vehicle into untreated skin from donor K. **a)** CLSM image showing the fluorescence intensity in the tissue, **b)** transillumination image showing the tissue structure, **c)** intensity plot with fluorescence intensity as a function of tissue depth and **d)** 3D surface plot illustrating the distribution of the FG2 488 sample in the tissue.

Figure 3.33 demonstrates how FG2 488 CASE in a 60% DMSO vehicle was distributed in the tissue after diffusion. From the CLSM image (Figure 3.33a) very little fluorescence was observed, and $I_{corrected}$ was detected to be 407 ± 440. The low $I_{corrected}$ value seemed to be a result of the weak fluorescence observed in the SC. Diffusion of the sample deeper into the tissue was not observed, an observation supported by the intensity and surface plots (Figure 3.33 c, d). Figure 3.34 illustrates the results after diffusion experiments with FG2 48 CASE applied in a 10% PEG200 vehicle. $I_{corrected}$ was detected to be 554 ± 365, which was somewhat higher compared to what was found for the sample in a 60% DMSO vehicle. However, less fluorescence was observed in the SC (Figure 3.34a), and the intensity and surface plots

91

(Figure 3.34 c, d) indicated fluorescence deeper in the skin. Because of the M_w of the sample (Table 3.3) and the weak fluorescence intensies observed in the SC, it was assumed that the fluorescence detected in the deeper skin layers was autofluorescence, distributed in the dermal layer of this individual skin sample, rather than a result of diffusion of FG2 488 CASE.

Transdermal diffusion of FG2 488 CASE in skin after pretreatment with micro-needles

The results obtained from transdermal diffusion of FG2 488 CASE in a 60% DMSO and in a 10% PEG200 vehicle into skin from donor K, after pretreatment with micro-needles, are given Figures 3.35 and 3.36, respectively.
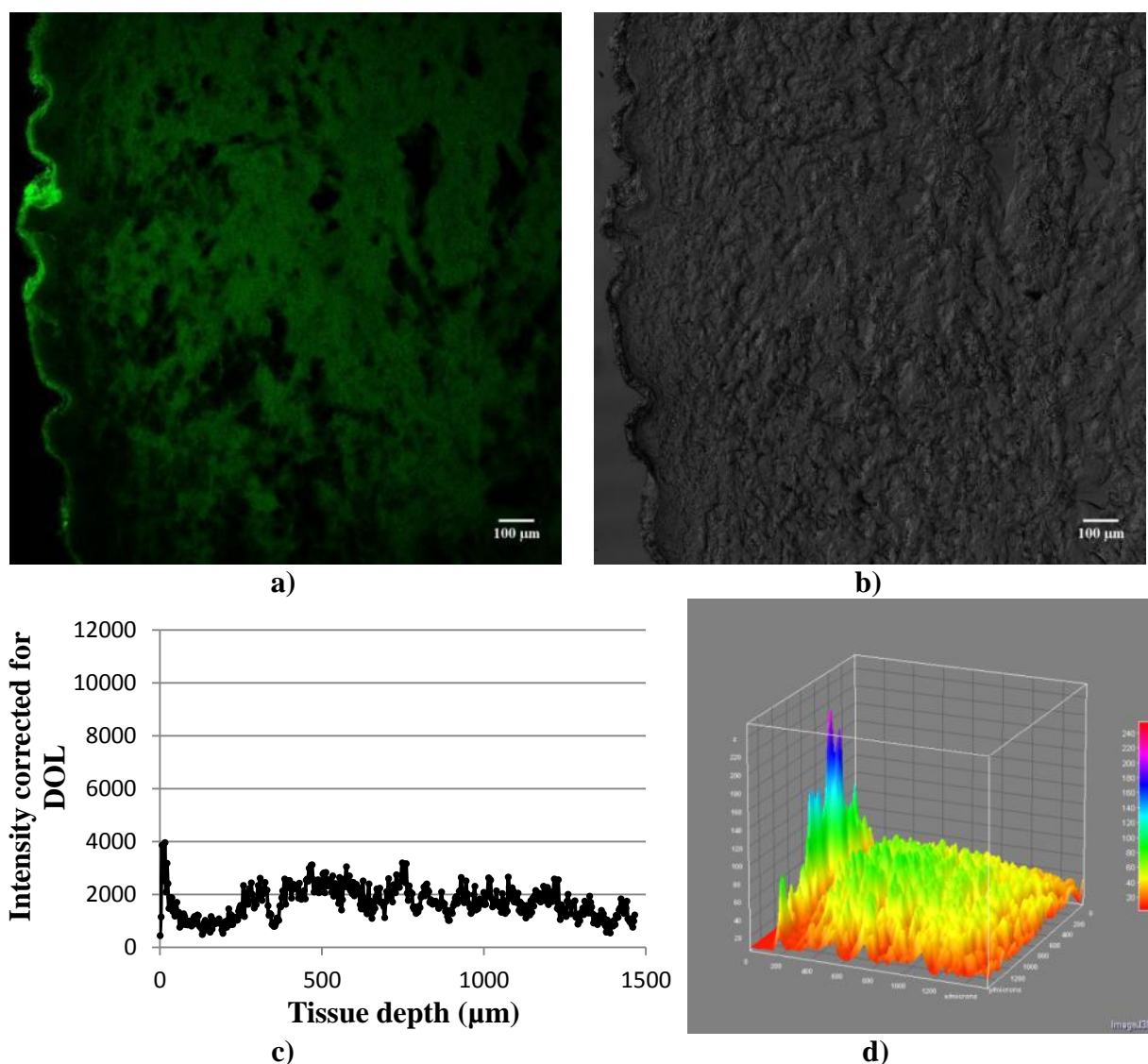
Figure 3.35: Results of transdermal diffusion by FG2 488 in a 60% DMSO vehicle into skin from donor K, after pretreatment with micro-needles. **a)** CLSM image showing the fluorescence intensity in the tissue, **b)** transillumination image showing the tissue structure, **c)** intensity plot with fluorescence intensity as a function of tissue depth and **d)** 3D surface plot illustrating the distribution of the FG2 488 sample in the tissue.

a)   **b)**

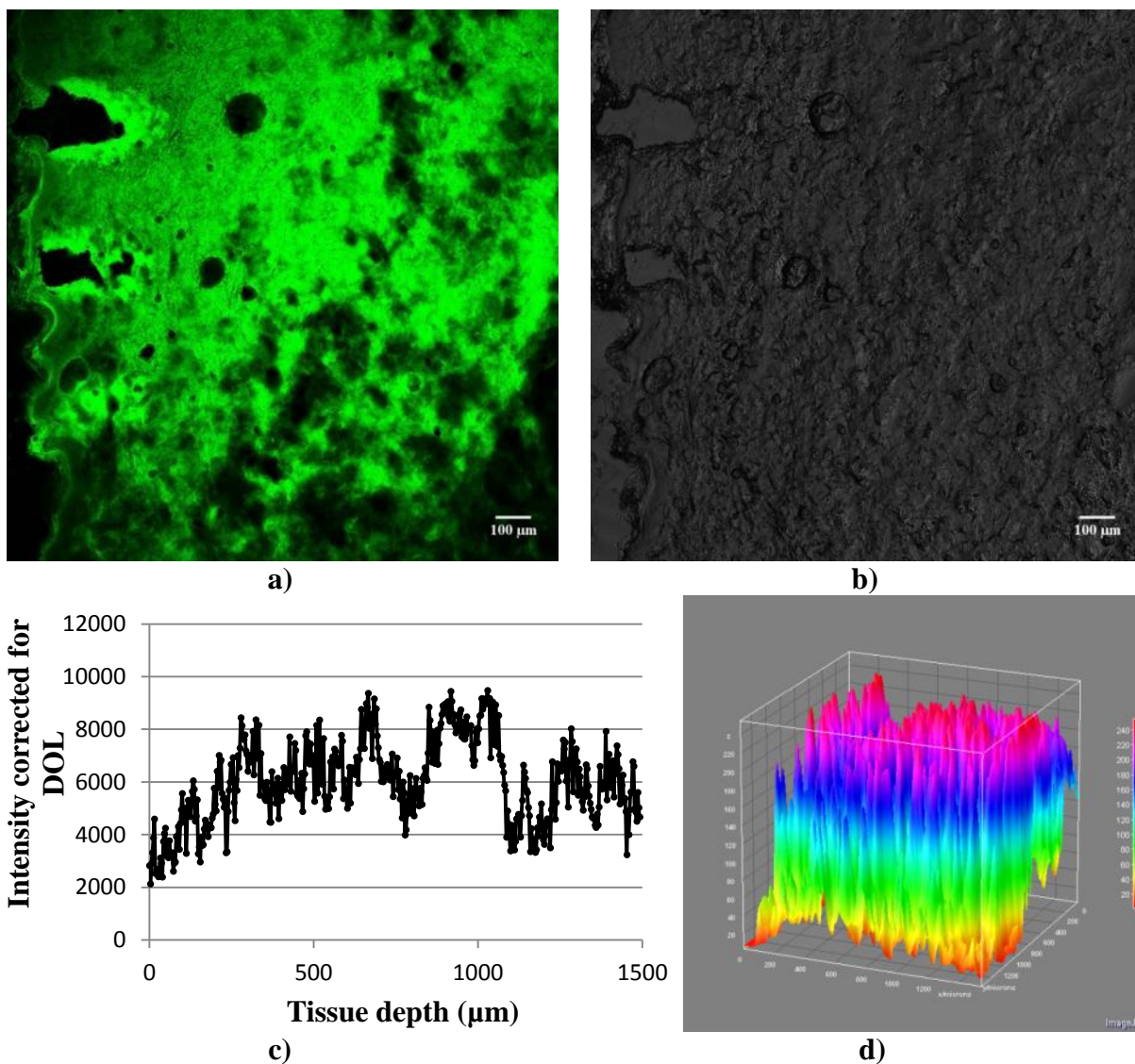**c)**   **d)**
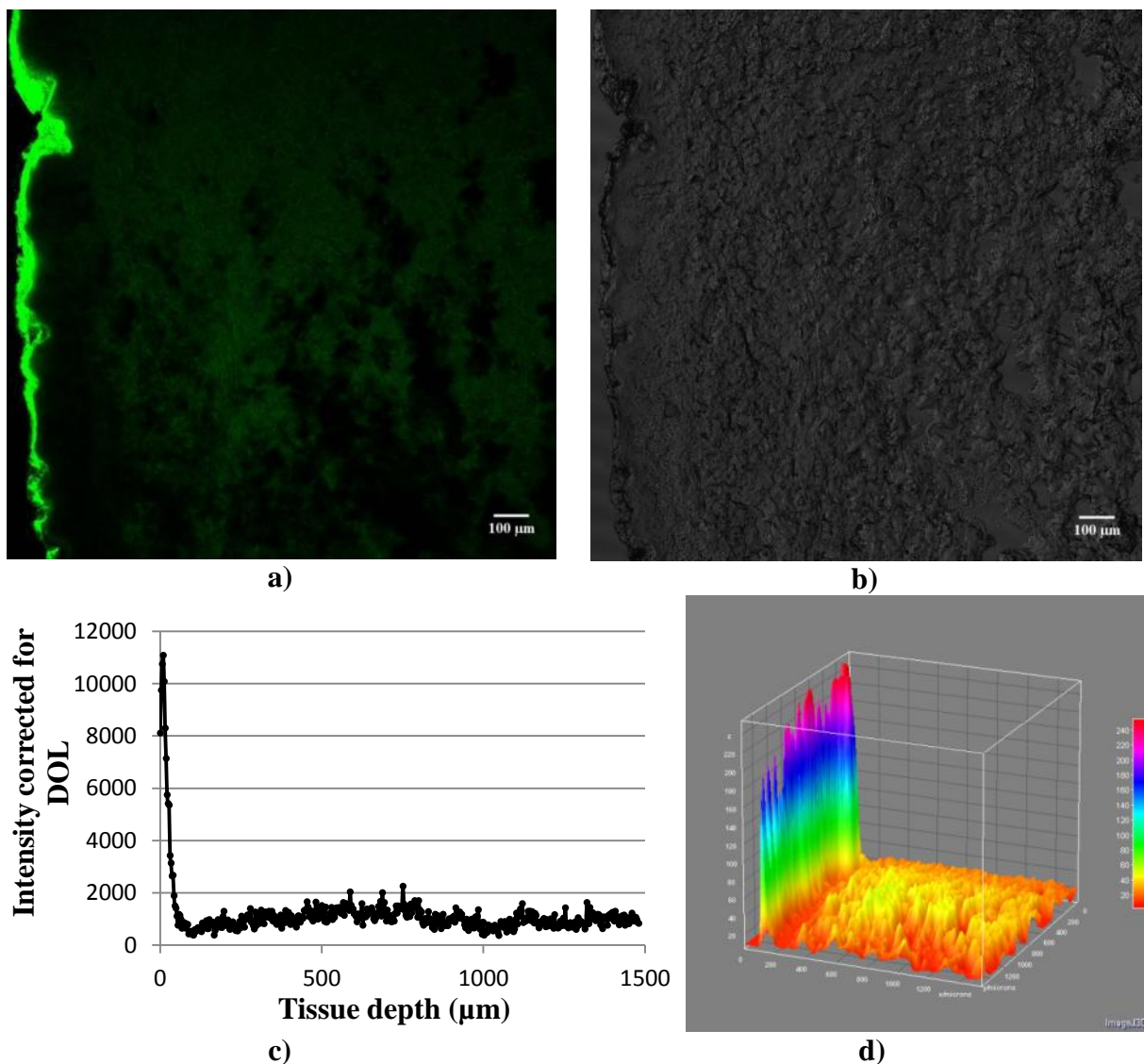
Figure 3.36: Results of transdermal diffusion by FG2 488 in a 10% PEG200 vehicle into skin from donor K, after pretreatment with micro-needles **a)** CLSM image showing the fluorescence intensity in the tissue, **b)** transillumination image showing the tissue structure, **c)** intensity plot with fluorescence intensity as a function of tissue depth and **d)** 3D surface plot illustrating the distribution of the FG2 488 sample in the tissue.

Figure 3.35 demonstrates the distribution of FG2 488 CASE in a DMSO vehicle in the skin tissue after the diffusion experiment. Fluorescence intensities were observed both in the SC and deeper into the tissue, and $I_{corrected}$ for FG2 488 CASE was detected to be 1631 ± 993. The intensity and surface plots (Figure 3.35 a, d) both illustrated that more fluorescence was distributed in one particular area of the SC. A minor cavity was observed in the SC in this area (Figure 3.35b) and was likely to be a result of penetration into SC by the micro-needle device. Because fluorescence also was observed to be distributed deeper into the tissue it was suggested that FG2 488 CASE, to some extent, was able to penetrate the SC and diffuse deeper into skin after pretreatment with micro-needles.

Diffusion of FG2 48 CASE in a 10% PEG vehicle resulted in an accumulation of the sample in the SC (Figure 3.36a). Distribution of fluorescence was not easily observed in the deeper layers of the tissue. The intensity and surface plots (Figure 3.36 c, d) both supported the observation of fluorescence accumulated in the SC, but also indicated a minor distribution deeper into the tissue. The $I_{corrected}$ of FG2 488 CASE was detected to be 1248 ± 1498, and the transillumination image (Figure 3.36b) showed perforations in the SC, suggesting that this sample could be able to diffuse through the barrier and deeper into the skin. But, even though the micro-needle pretreatment penetrated the skin barrier, and thus potentially overcame the size limitations associated with the SC barrier, the results presented here did not indicate efficient diffusion of FG2 488 CASE into the skin.

Transdermal diffusion of FG2 488 CASE in skin after pretreatment with L1

The results obtained from transdermal diffusion of FG2 488 CASE in a 60% DMSO and a 10% PEG200 vehicle into skin from donor K, after pretreatment with L1, are given in Figures 3.37 and 3.38, respectively.

a)

b)

c)

d)

Figure 3.37: Results of transdermal diffusion by FG2 488 in a 60% DMSO vehicle into skin from donor K, after pretreatment with laser **a)** CLSM image showing the fluorescence intensity in the tissue, **b)** transillumination image showing the tissue structure, **c)** intensity plot with fluorescence intensity as a function of tissue depth and **d)** 3D surface plot illustrating the distribution of the FG2 488 sample in the tissue.
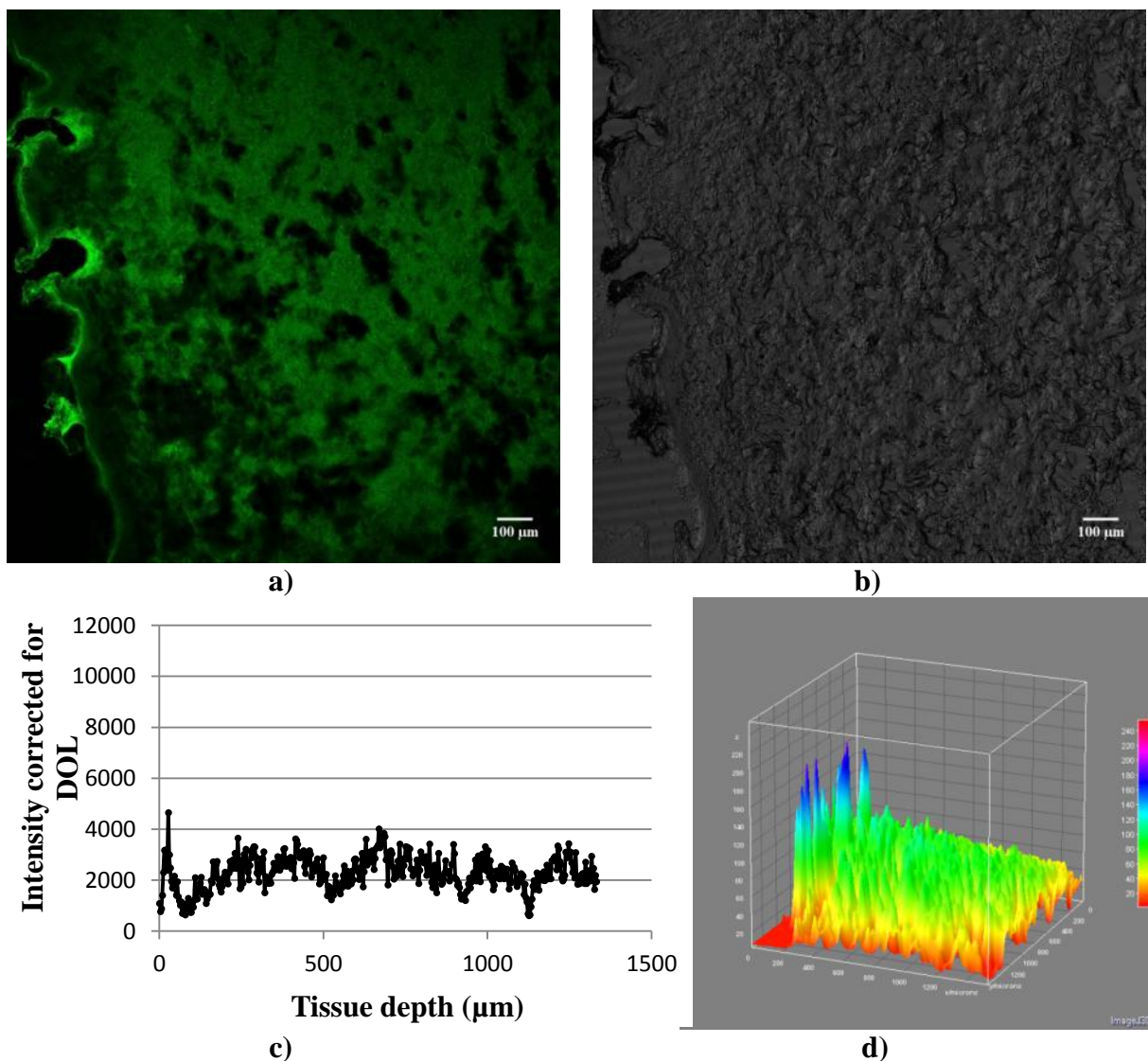
Figure 3.38: Results of transdermal diffusion by FG2 488 in a 10% PEG200 vehicle into skin from donor K, after pretreatment with laser **a)** CLSM image showing the fluorescence intensity in the tissue, **b)** transillumination image showing the tissue structure, **c)** intensity plot with fluorescence intensity as a function of tissue depth and **d)** 3D surface plot illustrating the distribution of the FG2 488 sample in the tissue.

Figure 3.37 demonstrates how FG2 488 CASE in a 60% DMSO vehicle was distributed in the skin tissue after diffusion. FG2 488 CASE was observed to be distributed with the highest fluorescence intensities in the laser cavities and deeper into the surrounding tissue (Figure 3.37a). The intensity plot (Figure 3.37c) confirmed diffusion in the longitudinal direction, and the surface plot (Figure 3.37d) showed high distribution of FG2 488 CASE throughout the entire tissue. Figure 3.38 illustrate how FG2 488 CASE in a 10% PEG200 vehicle was distributed in the tissue. Here, the highest fluorescence intensities were located in the SC and in the laser cavities (Figure 3.38a). The distribution of fluorescence throughout the tissue (Figure 3.38 c, d) was generally lower compared to what was observed in Figure 3.37,

indicating a difference in diffusion efficiency in the two different skin tissues. $I_{corrected}$ of FG2 488 CASE was detected to be 5538 ± 3185 when applied in a 60% DMSO vehicle, which was almost 2.5 times higher compared to the $I_{corrected}$ of 2178 ± 1329 detected for the same sample applied in a 10% PEG200 vehicle.

3.2.6.3. Summary of transdermal diffusion of fish gelatin peptides

Figure 3.39 demonstrate a correlation between skin treatment and detected fluorescence ($I_{corrected}$) in the tissues for FG24 488 CASE in a 10% PEG200 vehicle (blue). The lowest mean fluorescence intensity was observed in untreated skin, and $I_{corrected}$ was detected to be almost three times higher in skin pre-treated with micro-needles and eight times higher in skin pre-treated with L1. Almost a threefold higher $I_{corrected}$ was detected in skin pre-treated with L1 compared to micro-needles for the same sample. A similar correlation was not observed for FG24 488 CASE applied in a 60% DMSO vehicle (green), where $I_{corrected}$ was detected to be close to equal in untreated skin and skin pre-treated with micro-needles. However, $I_{corrected}$ obtained from skin pre-treated with laser was four and five times higher compared to $I_{corrected}$ detected in untreated skin and skin pre-treated with micro-needles, respectively.
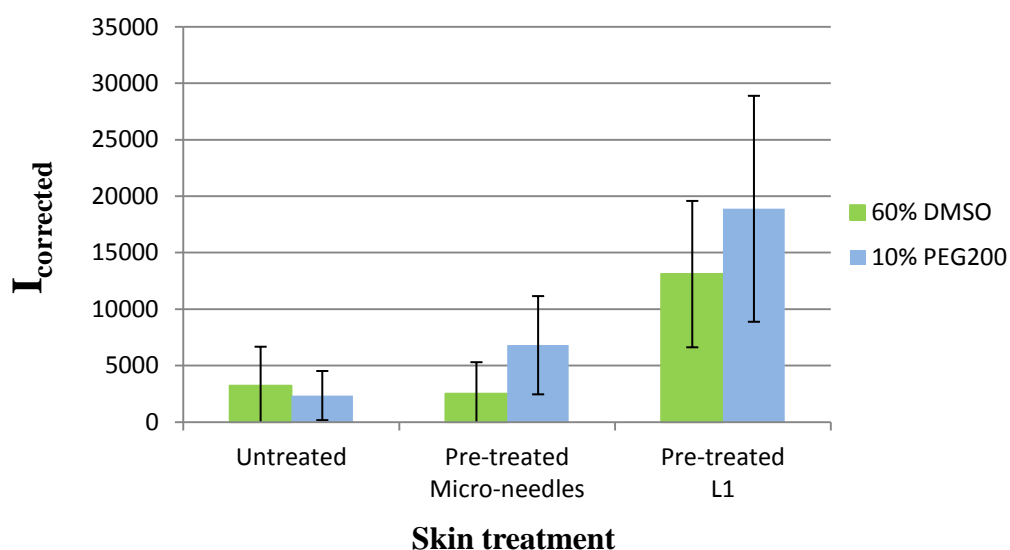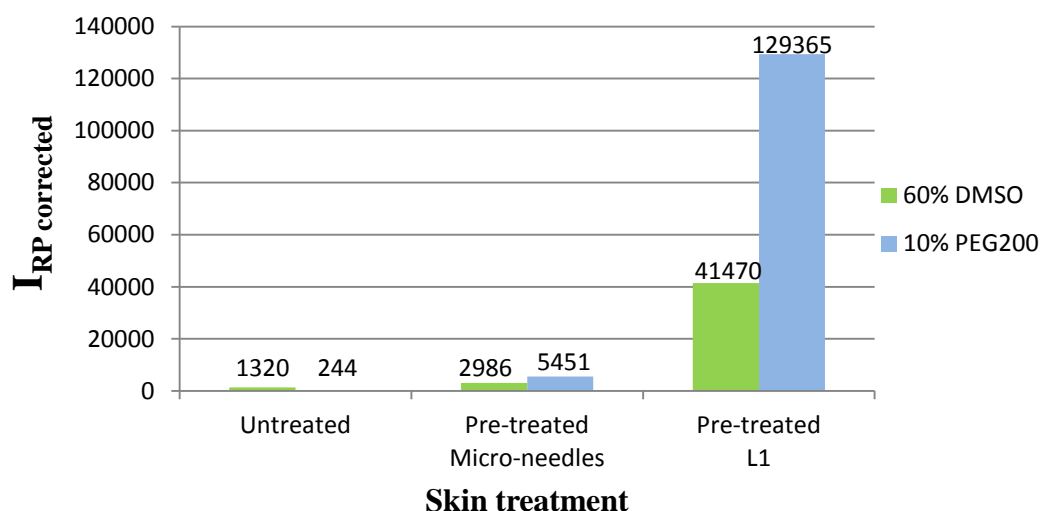

Figure 3.39: $I_{corrected}$ values for FG24 488 CASE applied on skin in a 60% DMSO and a 10% PEG200 vehicle after diffusion into untreated and pre-treated skin.

In untreated skin the FG24 488 CASE applied in a 60% DMSO was observed to result in a higher $I_{corrected}$ compared to when applied in a 10% PEG200 vehicle (Figure 3.39). An interpretation of this could be that the 60% DMSO vehicle enabled diffusion deeper into the tissue, which may be supported by the minor increase in dermal fluorescence observed in the

surface plot for this tissue (Figure 3.27d). However, it would be expected a higher degree of accumulation in the SC for the sample in both vehicles, due to the molecular weight of the sample (discussed in section 3.2.5.3). This could indicate that a smaller amount of sample was available for diffusion into the skin. A reason for this could be an incline of the Franz-cells during incubation, causing some of the sample to run off from the center of the application chamber. Such an experimental weakness could also explain why $I_{corrected}$ for FG24 488 CASE, applied in a 60% DMSO vehicle, was lower in skin pre-treated with micro-needles compared to in untreated skin. Thus, it could also be a potential reason for the difference in $I_{corrected}$ in the tissues pre-treated with micro-needles, where the value was almost a threefold higher for FG24 488 CASE applied in a 10% PEG200 vehicle. Varying degree of barrier disruption by the micro-needle device may also have affected the diffusion of the sample in the two skin tissues, and thus, contributed to the difference observed for the sample when applied in the two different vehicles.
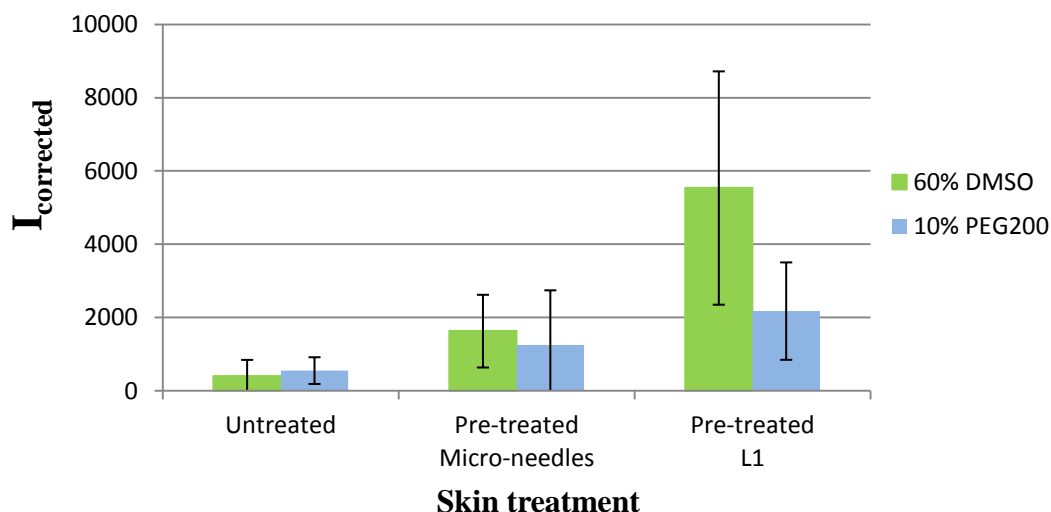
From the results in Figure 3.39 it was concluded that L1 to a larger extent enhanced the diffusion of FG24 488 CASE into human skin compared to micro-needles. This was supported by the fluorescence intensities detected in the receptor phase, illustrated in figure 3.40. Pre-treatment with micro-needles resulted in increased I_{RP} values compared to untreated skin for both vehicles. Diffusion of FG24 488 CASE in a 10% PEG200 vehicle into skin, after pretreatment with L1, resulted in an $I_{RP\ corrected}$ value corresponding to ~73% of $I_{RP\ max}$. This value was almost twenty-four times higher compared to the one detected after pretreatment with micro-needles. When 60% DMSO was used as vehicle, pretreatment with L1 resulted in an $I_{RP\ corrected}$ value almost fourteen times higher compared to micro-needles, a value corresponding to 13% of $I_{RP\ max}$. From this it was concluded that L1 not only enabled the most efficient diffusion of FG24 488 CASE into the skin, but also all the way through the tissue, compared to diffusion in untreated skin and skin pre-treated with micro-needles.

Figure 3.40: $I_{RP\ corrected}$ values for FG24 488 CASE applied on skin in both the 60% DMSO and the 10% PEG200 vehicle after diffusion into untreated and pre-treated skin.

In all the pre-treated tissues the highest $I_{corrected}$ values were observed for FG24 488 applied in a 10% PEG200 vehicle. This was the opposite of what was found in the untreated skin tissues, and could indicate that after overcoming the SC barrier, the sample diffused more efficiently deeper in the skin, when applied in a PEG200 vehicle. The variations in $I_{corrected}$ and I_{RP} of FG24 488 CASE in the laser treated skin tissues may also be due to the fact that the tissues originated from two different donors (B and K), and that the difference in skin thickness was 0.89 mm (Table 3.6). This could explain the lower diffusion efficiency observed for FG24 488 CASE when applied on skin tissue from donor B in a 60% DMSO vehicle, as discussed in subsection 3.2.5.3. Variations in distribution, $I_{corrected}$ and I_{RP} of FG24 488 CASE in tissues with the same pre-treatments may also have been due to the heterogeneity of the skin tissues, the independency between each single experiment, and experimental errors, also discussed in subsection 3.2.5.3.

Figure 3.41 demonstrates a correlation between skin treatment and the $I_{corrected}$ for FG2 488 CASE detected in the different tissues. The lowest $I_{corrected}$ was observed in untreated skin for both vehicles. For the sample applied in a 60% DMSO vehicle, $I_{corrected}$ was observed to increase with factors of four and fourteen after pretreatments with micro-needles and L1, respectively. After diffusion of FG2 488 CASE applied in a 10% PEG200 vehicle into skin with the same pretreatments, $I_{corrected}$ was detected to be approximately two and four times higher.
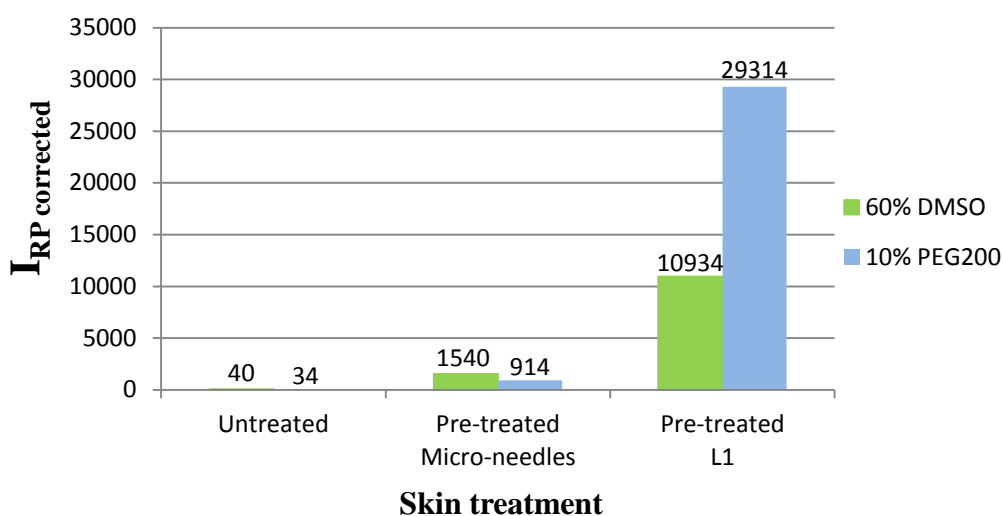
Figure 3.41: $I_{corrected}$ values for FG2 488 CASE applied on skin in both the 60% DMSO and the 10% PEG200 vehicle after diffusion into untreated and pre-treated skin.

From the results presented for FG2 488 CASE (Figures 3.33 and 3.34) it was concluded that the sample was unable to passively penetrate the SC barrier in untreated skin and diffuse deeper into the tissues. This was probably due to the molecular weight of the sample, which is in accordance with the size limitations in passive absorption through untreated skin, reported by Bos and Meinardi (2000) and discussed in subsection 3.2.5.3. The molecular weight may also have been the reason for the low extent of FG2 488 CASE distribution in deeper skin layers after pre-treatment with micro-needles. This pretreatment should in theory allow for larger molecules to diffuse through the SC and deeper into the skin, but efficient diffusion was not observed. This may further indicate a lower diffusion rate of this peptide sample compared to smaller peptides, such as FG24 488 CASE, and reflects the potential need for longer incubation time with increasing molecular size to achieve increased dermal distribution, also discussed in section 3.2.5.3. This is in accordance with that M_w have been found to be the main determinant for the maximum delivery or flux of drug solutions into and through human skin, as reported by Magnusson et.al (2004).

One interpretation of the $I_{corrected}$ detected in the laser treated tissues was that FG2 488 CASE applied in a 60% DMSO vehicle diffused more efficiently compared to the same sample in a 10% PEG200 vehicle. However, this interpretation was contradictory to the results from the fluorescence measurements in the receptor phase, given in Figure 3.42, where a higher I_{RP} value was obtained for the sample applied in a 10% PEG200 vehicle. Therefore, when these two results were interpreted collectively it was clear that FG2 488 CASE in a 10% PEG200 vehicle diffused into and through the skin tissue with a higher rate compared to diffusion in a

60% DMSO vehicle. The higher diffusion rate caused a larger amount of sample to diffuse all the way through the tissue and into the receptor phase, and thus, could be the reason why a smaller amount was distributed in the tissue. The two different vehicles are further evaluated in section 3.2.9. In addition, the heterogeneity of the tissues, the independency between each of the experiments, and experimental errors, discussed in subsection 3.2.5.3, may have contributed to the variations in skin diffusion through the laser treated tissues. These factors may also have influenced the results obtained from untreated skin and skin pre-treated with micro-needles.

Figure 3.42: $I_{RP\ corrected}$ values for FG2 488 CASE applied on skin in both the 60% DMSO and the 10% PEG200 vehicle after diffusion into untreated and pre-treated skin.

The $I_{RP\ corrected}$ values of FG2 488 CASE for both vehicles after diffusion in untreated skin were very low, and may primarily have been a result of cellular components giving rise to autofluorescence. Pre-treatment with micro-needles resulted in increased I_{RP} values compared to untreated skin for both the 60% DMSO and the 10% PEG200 vehicle. In the tissues pre-treated with L1 diffusion of the sample in a 10% PEG200 vehicle resulted in an $I_{RP\ corrected}$ value corresponding to 25% of $I_{RP\ max}$, a value nineteen times higher compared to the one detected after pretreatment with micro-needles. For the same pretreatment the sample applied in a 60% DMSO vehicle resulted in an $I_{RP\ corrected}$ value almost six times higher compared to after pretreatment with micro-needles, a value corresponding to ~18 % of $I_{RP\ max}$.

From the results after transdermal diffusion of FG2 488 CASE, it was concluded that L1 enhanced the diffusion of the sample into human skin to a larger extent compared to micro-needles, which was the same conclusion drawn for FG24 488 CASE. These skin pretreatments are further evaluated in section 3.2.10. A final remark must be made to

emphasize the effect of M_w on transdermal diffusion of FG peptides. From the presented results M_w was determined to be the predominant reason for the generally lower distribution and $I_{corrected}$ and $I_{RP\ corrected}$ values (the $I_{corrected}$ values was of course also influenced by DOL) of FG2 488 CASE compared to FG24 488 CASE, regardless of vehicles and skin treatments.

3.2.7. Diffusion experiments – G-block oligomers

The two G-block oligomers G-DP18 and G-DP22 were used to study the diffusion of polysaccharides into the skin. Diffusion of each sample was studied in a total of 4 experiments. Two different vehicles, 60% DMSO and 10% PEG200, were used separately to investigate the diffusion through untreated skin and through skin pre-treated with micro-needles. The skin tissues were obtained from different donors (Table 2.3). The results from the transdermal diffusion experiments of G-DP18 488 HSS and G-DP22 488 HSS are given in subsection 3.2.7.1 and 3.2.7.2, respectively, and both are summarized in subsection 3.2.7.3.
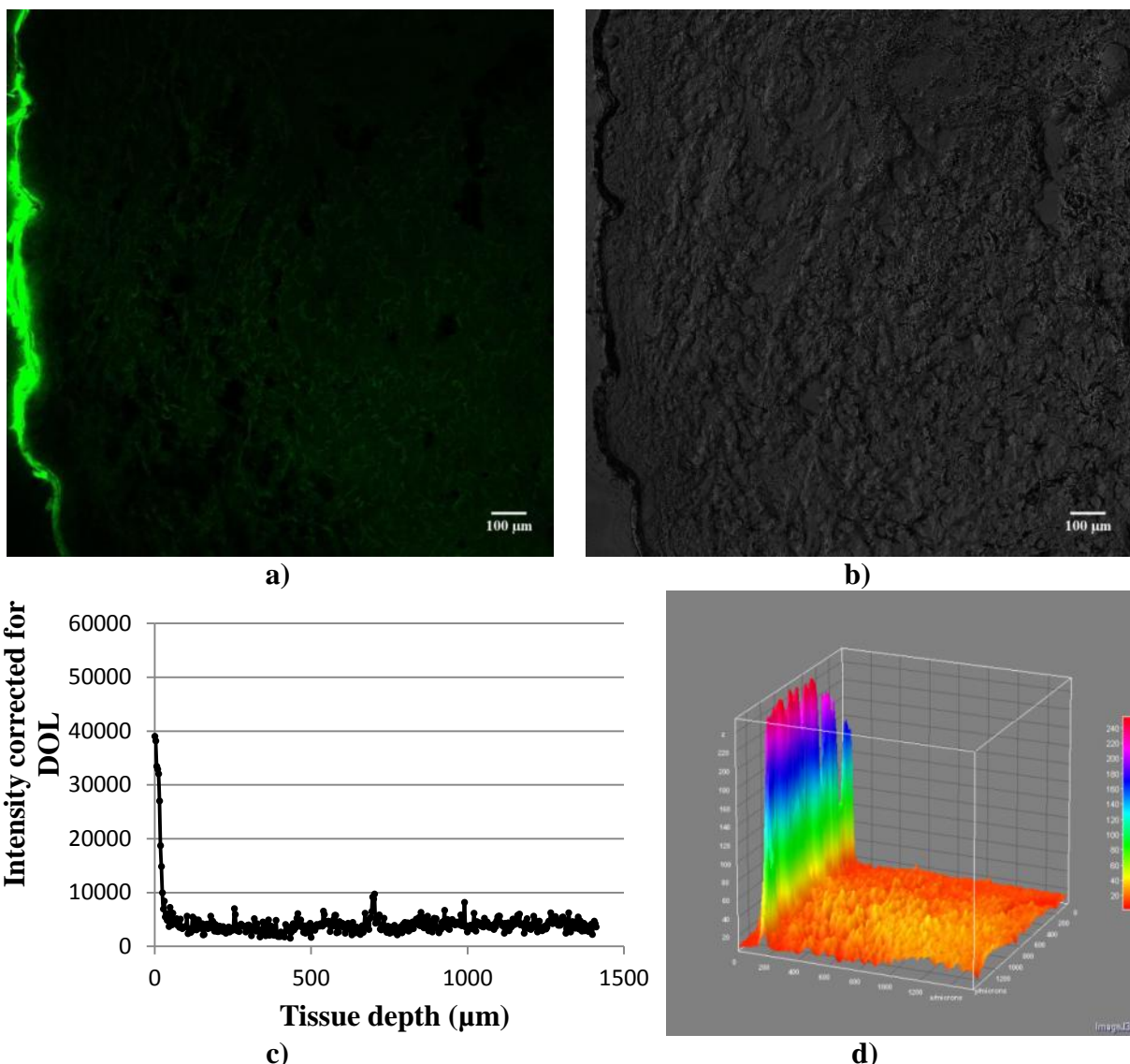
3.2.7.1. G-DP18

Transdermal diffusion of G-DP18 488 HSS in untreated skin

The results obtained from transdermal diffusion of G-DP18 488 HSS in a 60% DMSO vehicle into untreated skin from donor I and in a 10% PEG200 vehicle into untreated skin from donor G, are given in Figures 3.43 and 3.44, respectively.

a)

b)

c)

d)
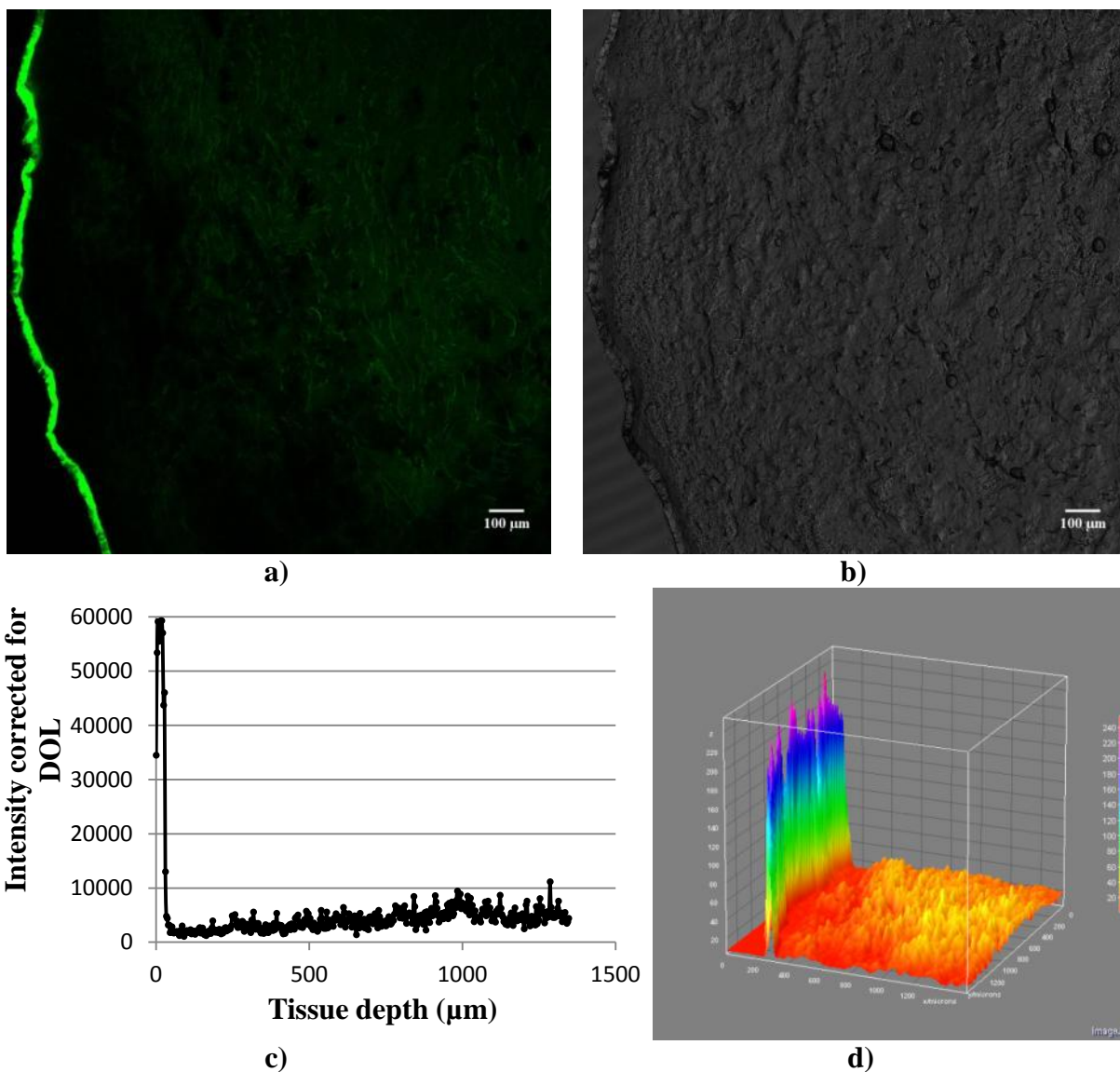
Figure 3.43: Results of transdermal diffusion by G-DP18 488 HSS in a 60% DMSO vehicle into untreated skin from donor I. **a)** CLSM image showing the fluorescence intensity in the tissue, **b)** transillumination image showing the tissue structure, **c)** intensity plot with fluorescence intensity as a function of tissue depth and **d)** 3D surface plot illustrating the distribution of the G-DP18 sample in the tissue.
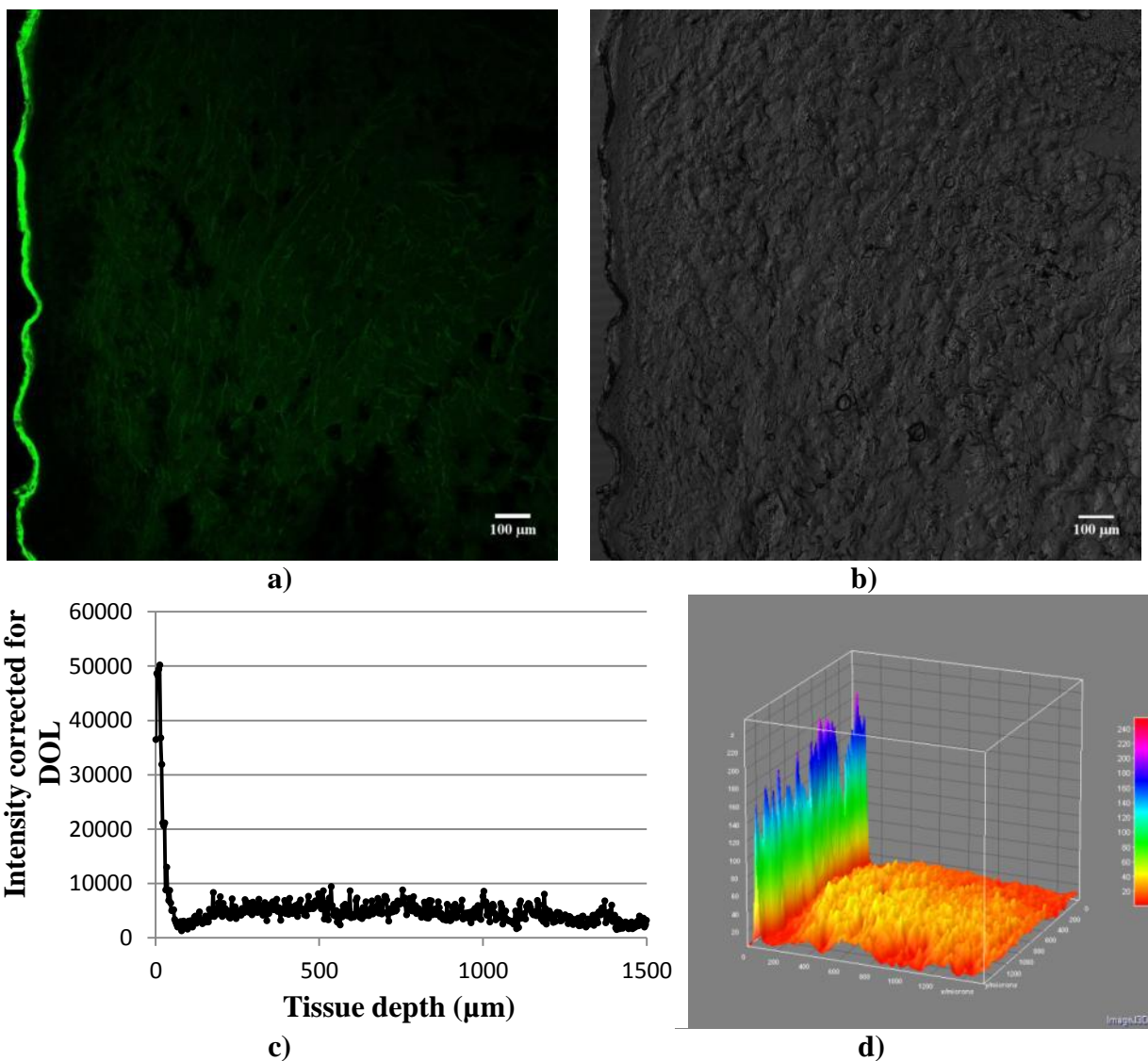
Figure 3.44: Results of transdermal diffusion by G-DP18 in a 10% PEG200 vehicle into untreated skin from donor G. **a)** CLSM image showing the fluorescence intensity in the tissue, **b)** transillumination image showing the tissue structure, **c)** intensity plot with fluorescence intensity as a function of tissue depth and **d)** 3D surface plot illustrating the distribution of the G-DP18 sample in the tissue.

Figure 3.43 demonstrates how G-DP18 488 HSS in a 60% DMSO vehicle was distributed in the tissue after diffusion. From the CLSM image (Figure 3.43a) high intensity fluorescence was observed in the SC. The intensity and surface plots (Figure 3.43 c, d) confirmed this observation, and indicated a minor distribution of fluorescence deeper in the tissue. This dermal distribution was interpreted to be caused by endogenous fluorophores resulting in autofluorescence, rather than diffusion of FG2 488 CASE. $I_{corrected}$ of the sample, detected to be 4883 ± 6646, was concluded to be a result of the accumulation of G-DP18 488 in the SC. Figure 3.44 illustrated similar results after diffusion of G-DP18 488 HSS in a 10% PEG200 vehicle and $I_{corrected}$ was detected to be 4944 ± 6571. However, the intensity plot (Figure

3.44c) illustrated lower fluorescence intensities in the SC, which could indicate that a smaller amount of the sample in a 10% PEG200 vehicle had penetrated into the SC. But the observed lower fluorescence intensities should not result in a higher $I_{corrected}$. The opposite was observed from the surface plot (Figure 3.44d), giving rise to inconsistent results. This inconsistency could be explained by comparing the CLSM and transillumination images in Figure 3.44, which clearly demonstrate that excess sample is located on the surface of the skin tissue. The fluorescence from this excess was believed to cause a faulty high $I_{corrected}$ value and contribute to the high fluorescence intensities observed in the outermost layer of the tissue in the surface plot.

Transdermal diffusion of G-DP18 488 HSS in skin pre-treated with micro-needles

The results obtained from transdermal diffusion of G-DP18 488 HSS in a 60% DMSO vehicle into skin from donor I and in a 10% PEG200 vehicle into skin from donor G, after pretreatment with micro-needles, are given in Figures 3.45 and 3.46, respectively.

a)

b)

c)

d)

Figure 3.45: Results of transdermal diffusion by G-DP18 in a 60% DMSO vehicle into skin from donor I, after pretreatment with micro-needles. **a)** CLSM image showing the fluorescence intensity in the tissue, **b)** transillumination image showing the tissue structure, **c)** intensity plot with fluorescence intensity as a function of tissue depth and **d)** 3D surface plot illustrating the distribution of the G-DP18 sample in the tissue.
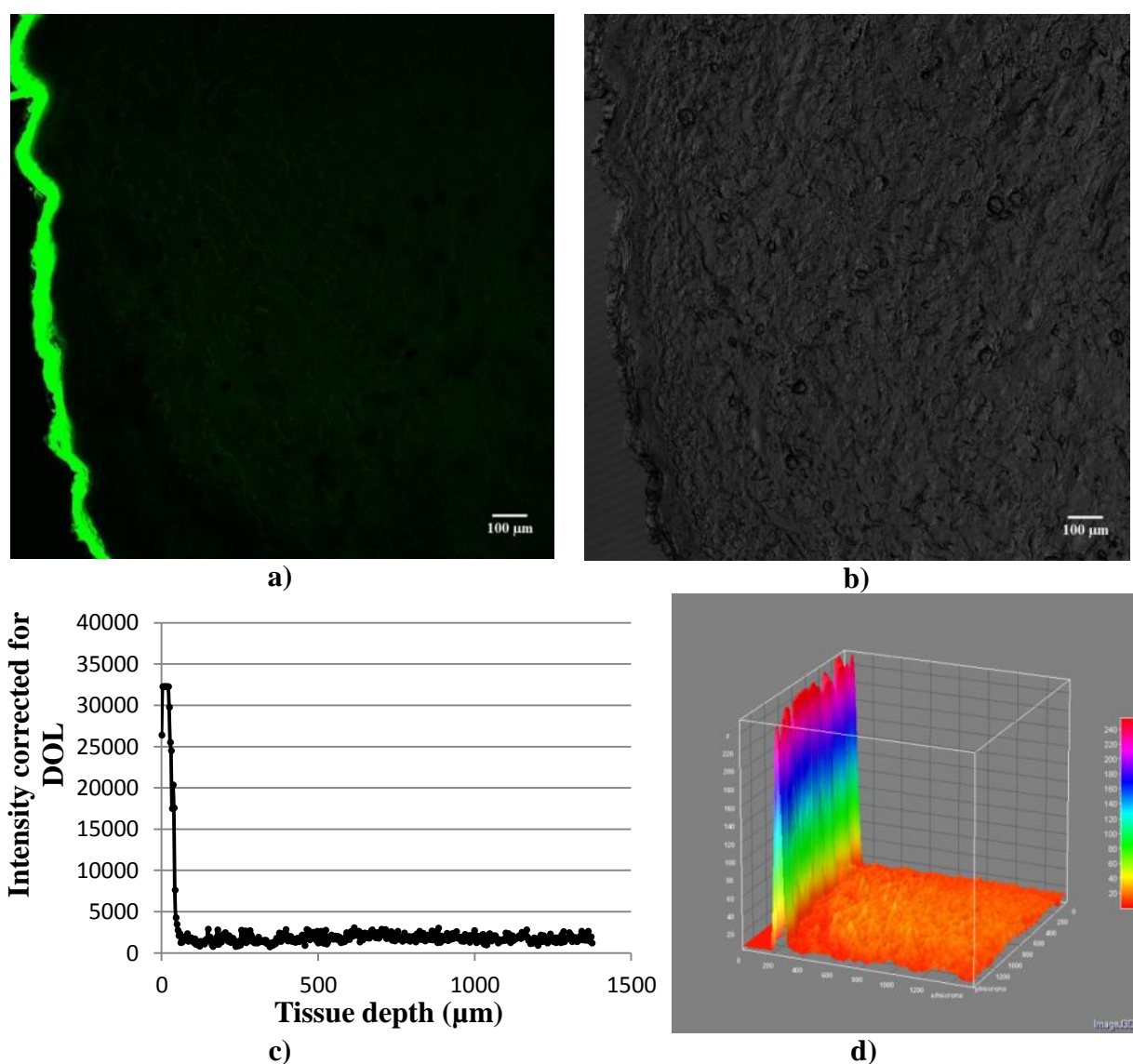
a)

b)

c)

d)
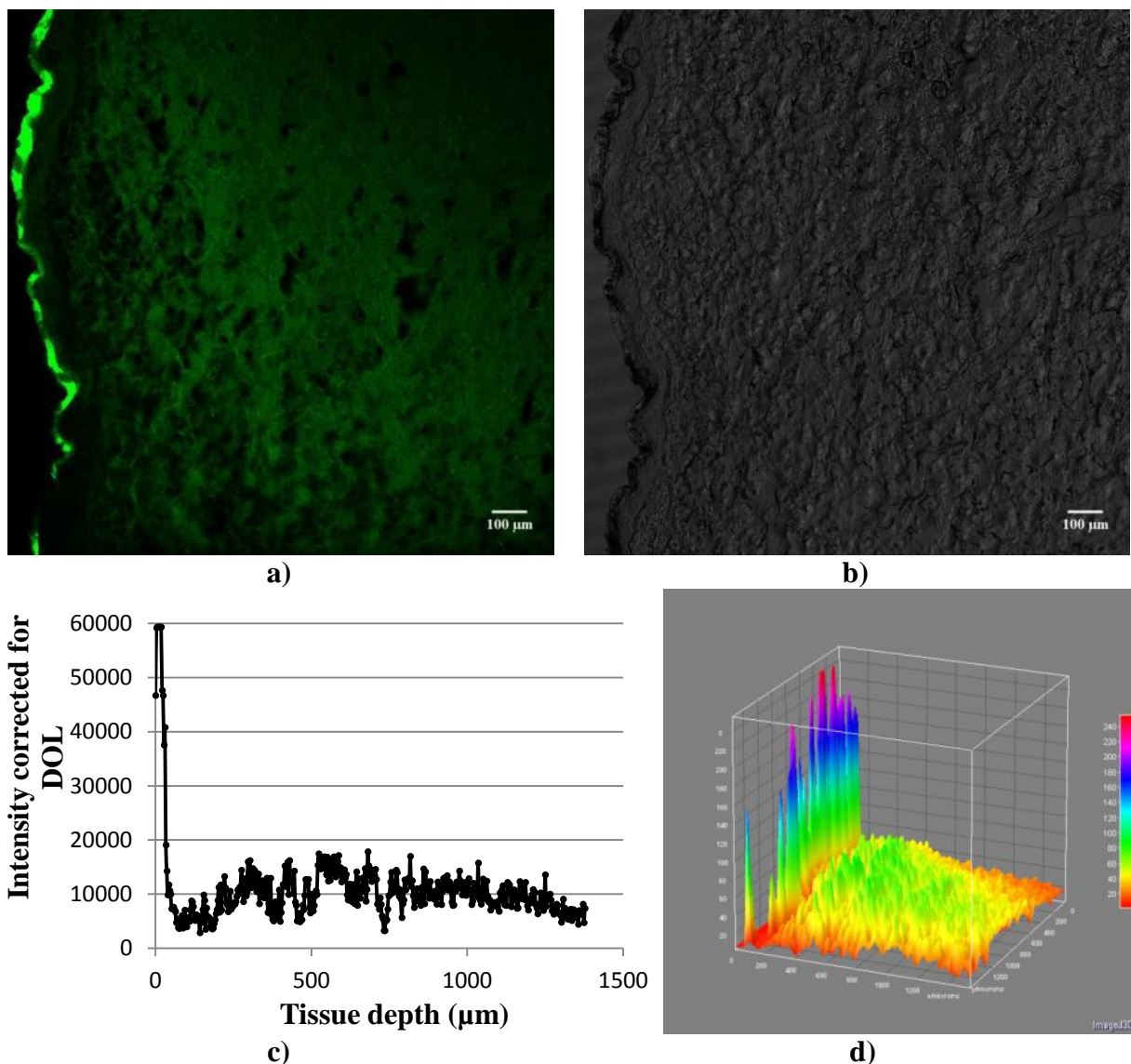
Figure 3.46: Results of transdermal diffusion by G-DP18 in a 10% PEG200 vehicle into skin from donor G, after pretreatment with micro-needles. **a)** CLSM image showing the fluorescence intensity in the tissue, **b)** transillumination image showing the tissue structure, **c)** intensity plot with fluorescence intensity as a function of tissue depth and **d)** 3D surface plot illustrating the distribution of the G-DP18 sample in the tissue.

Figure 3.45 demonstrates how G-DP18 488 HSS in a 60% DMSO vehicle was distributed in the tissue after diffusion. High intensity fluorescence was observed to be evenly distributed in the SC (Figure 3.45a). The intensity and surface plots (Figure 3.45 c, d) confirmed this observation, and also indicated a minor distribution deeper into the tissue, primarily in the upper dermis. $I_{corrected}$ of G-DP18 HSS in a 60% DMSO vehicle was detected to be 5002 ± 5820, a value considerably lower compared to $I_{corrected}$, detected to be 9239 ± 6280, for the same sample in a 10% PEG200 vehicle. The results after diffusion of G-DP18 488 HSS in the PEG200 vehicle, presented in Figure 3.46, illustrated that the highest fluorescence intensities were unevenly distributed in the SC. The intensity plot (Figure 3.46c) supported this

107

observation, but also indicated diffusion of G-DP18 488 HSS deeper into the tissue. This was in accordance with the fluorescence distribution observed in the surface plot (Figure 3.46d).
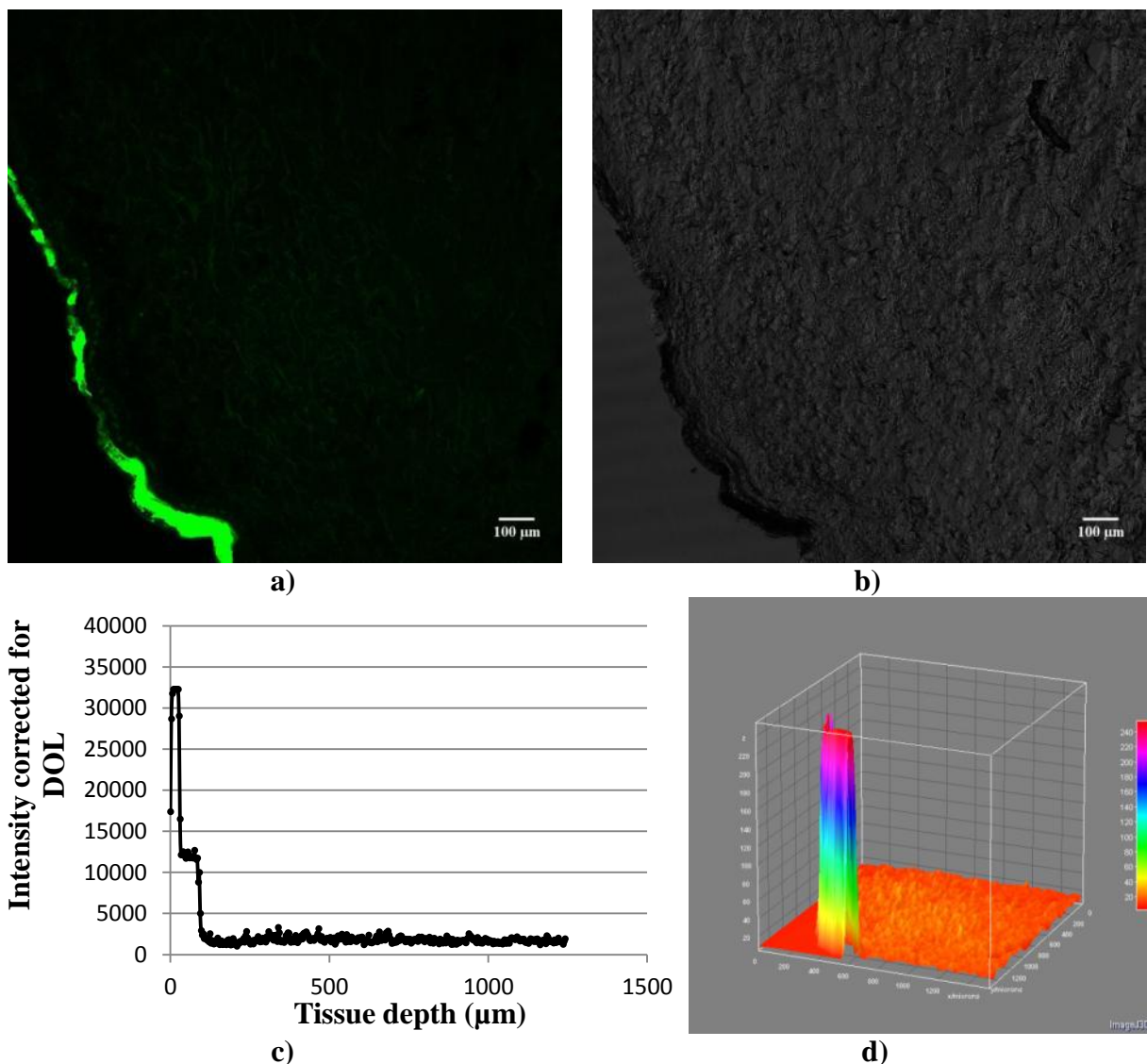
3.2.7.2. G-DP22

Transdermal diffusion of G-DP22 488 HSS in untreated skin

The results obtained from transdermal diffusion of G-DP22 488 HSS in a 60% DMSO vehicle into untreated skin from donor I and in a 10% PEG200 vehicle into untreated skin from donor G, are given in Figures 3.47 and 3.48, respectively.

Figure 3.47: Results of transdermal diffusion by G-DP22 in a 60% DMSO vehicle into untreated skin from donor I. **a)** CLSM image showing the fluorescence intensity in the tissue, **b)** transillumination image showing the tissue structure, **c)** intensity plot with fluorescence intensity as a function of tissue depth and **d)** 3D surface plot illustrating the distribution of the G-DP22 sample in the tissue.
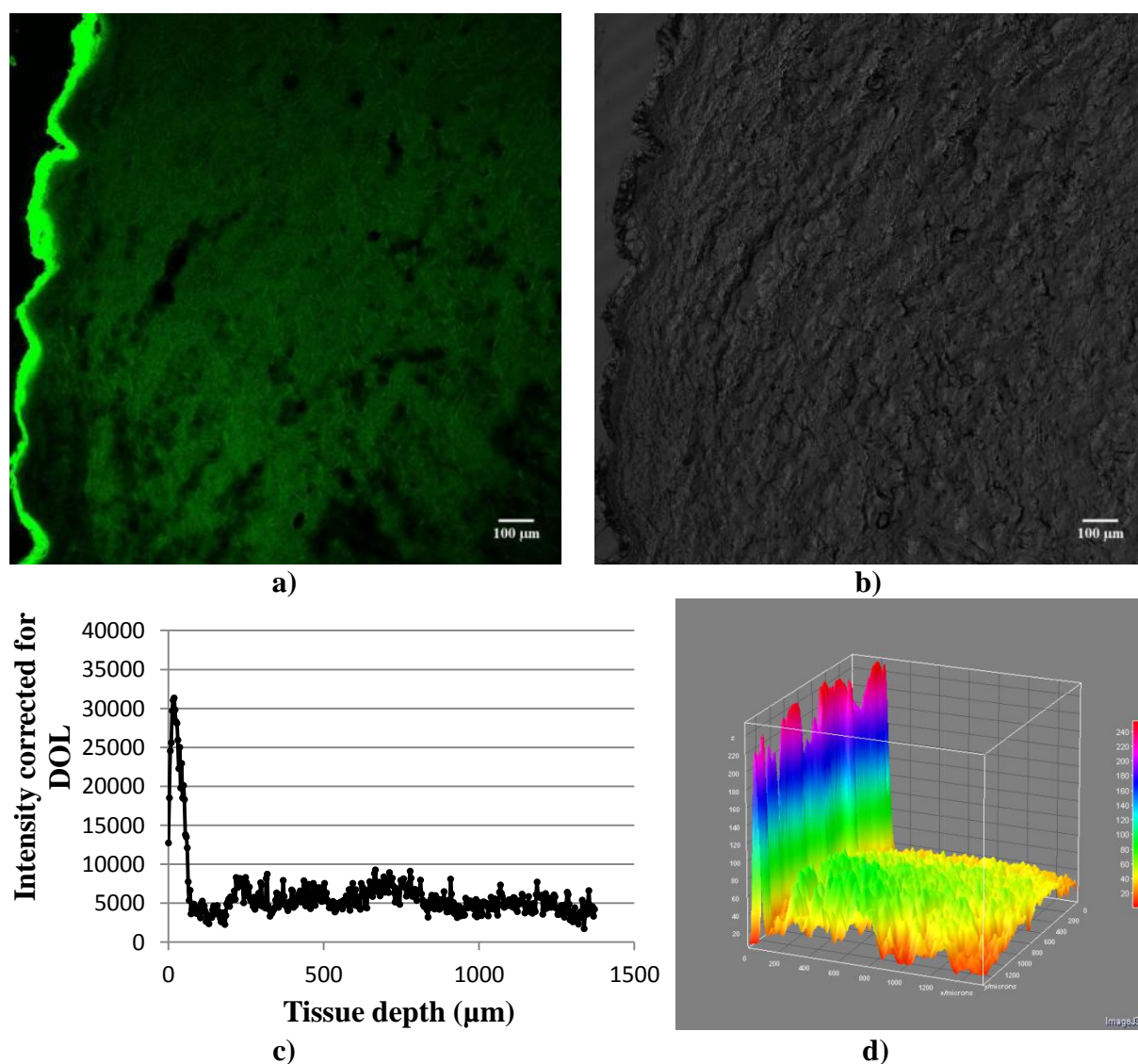
Figure 3.48: Results of transdermal diffusion by G-DP22 in a 10% PEG200 vehicle into untreated skin from donor G. **a)** CLSM image showing the fluorescence intensity in the tissue, **b)** transillumination image showing the tissue structure, **c)** intensity plot with fluorescence intensity as a function of tissue depth and **d)** 3D surface plot illustrating the distribution of the G-DP22 sample in the tissue.

Figure 3.47 demonstrates how G-DP22 488 HSS in a 60% DMSO vehicle was distributed in the tissue after diffusion. High intensity fluorescence was observed to be distributed only in the SC (Figure 3.47a). $I_{corrected}$ of the sample was detected to be 2866 ± 5318, and was assumed to be a result of the accumulation of fluorescence in the SC barrier. The results after diffusion of G-DP22 488 HSS in a 10% PEG200 vehicle, presented in Figure 3.48, illustrated a similar trend of fluorescence only being observed in the SC. However, the distribution of fluorescence intensities throughout the barrier was more uneven and $I_{corrected}$ was detected to be 2226 ± 3625. Extended distribution of high fluorescence was observed in one specific area of the SC, which can be seen in the lower left corner of the CLSM image (Figure 3.48a). In

the same area the SC was observed to display a darker region in the transillumination image (Figure 3.48b), indicating overlapping or compressed tissue. This could result in falsely high fluorescence intensities.

Transdermal diffusion of G-DP22 488 HSS in skin pre-treated with micro-needles

The results obtained from transdermal diffusion of G-DP22 488 HSS in a 60% DMSO vehicle into skin from donor I and in a 10% PEG200 vehicle into skin from donor G after pretreatment with micro-needles, are given in Figures 3.49 and 3.50, respectively.

a)

b)

c)

d)

Figure 3.49: Results of transdermal diffusion by G-DP22 in a 60% DMSO vehicle into skin from donor I, after pretreatment with micro-needles. **a)** CLSM image showing the fluorescence intensity in the tissue, **b)** transillumination image showing the tissue structure, **c)** intensity plot with fluorescence intensity as a function of tissue depth and **d)** 3D surface plot illustrating the distribution of the G-DP22 sample in the tissue.
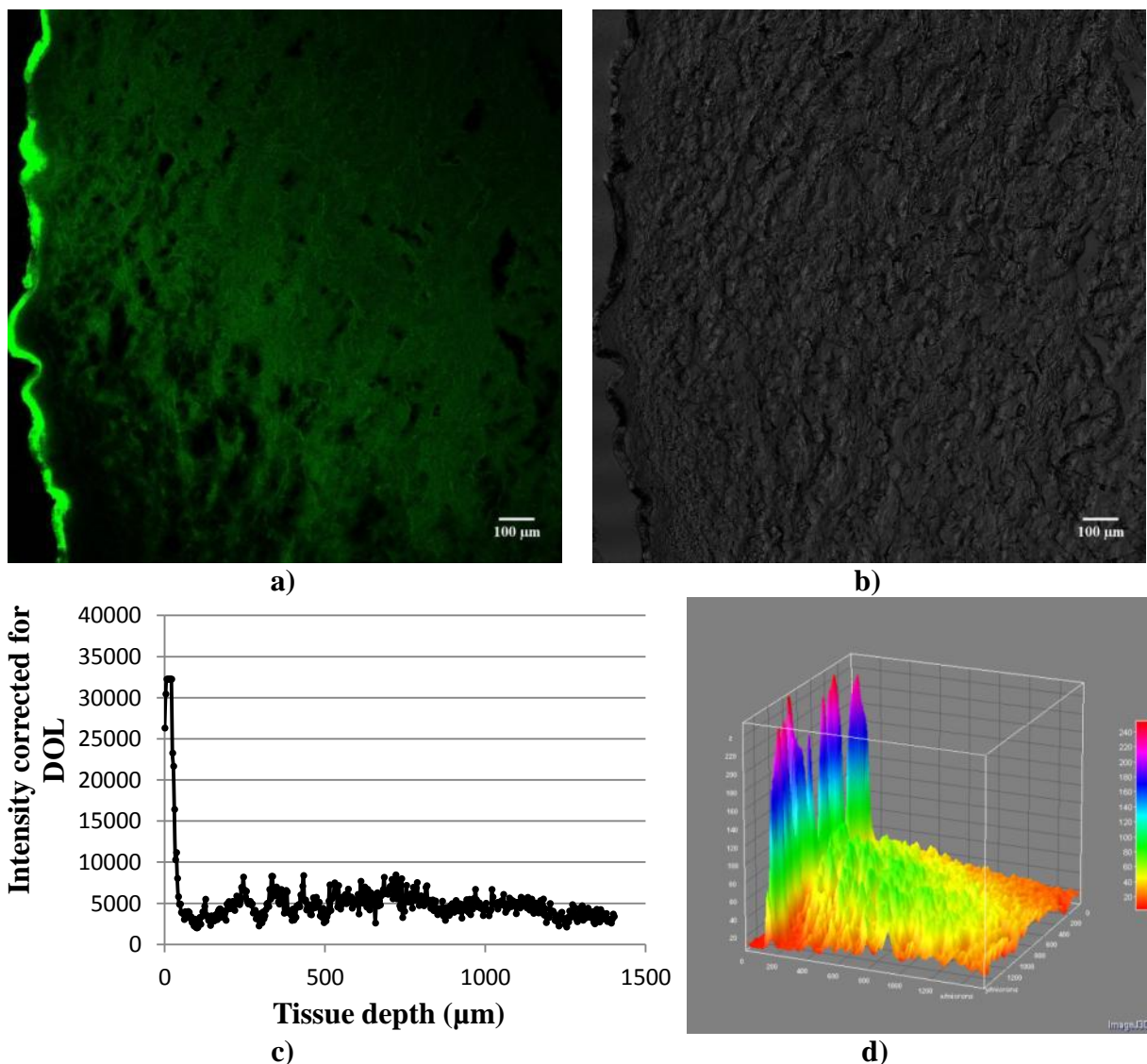
Figure 3.50: Results of transdermal diffusion by G-DP22 in a 10% PEG200 vehicle into skin from donor G, after pretreatment with micro-needles. **a)** CLSM image showing the fluorescence intensity in the tissue, **b)** transillumination image showing the tissue structure, **c)** intensity plot with fluorescence intensity as a function of tissue depth and **d)** 3D surface plot illustrating the distribution of the G-DP22 sample in the tissue.

Figure 3.49 demonstrates the distribution of G-DP22 488 HSS applied in a 60% DMSO vehicle after the diffusion experiment. High intensity fluorescence was observed to be distributed throughout the SC (Figure 3.49a), and this observation was confirmed by the intensity and surface plots (Figure 3.49 c, d). From the CLSM image and the two plots it was also observed distribution of fluorescence deeper in the tissue, and $I_{corrected}$ was detected to be 6290 ± 4679. Diffusion of G-DP22 488 HSS in a 10% PEG200 vehicle was observed to result in a more uneven and lower distribution of fluorescence throughout the SC (Figure 3.50a). $I_{corrected}$ of the sample applied in this vehicle was detected to be 5219 ± 3990, which was lower compared for the sample applied in a 60% DMSO vehicle. However, the extent of dermal

111

distribution of the sample was observed to be close to equal in the tissues regardless of the vehicle used and the difference in detected $I_{corrected}$ values (Figures 3.49d and 3.50d).

### 3.2.7.3. Summary of transdermal diffusion of G-block oligomers

Figure 3.51 demonstrates the difference in $I_{corrected}$ for G-DP18 488 HSS in untreated and pre-treated skin when applied in the two different vehicles. The $I_{corrected}$ for G-DP18 488 HSS in a 60% DMSO vehicle was almost the same in both untreated skin and skin pre-treated with micro-needles, and little difference was detected in untreated skin for the sample regardless of the vehicle used. However, a profound difference in $I_{corrected}$ was detected for G-DP18 488 HSS after pre-treatment with micro-needles, as the $I_{corrected}$ value was almost a twofold higher for the sample applied in a 10% PEG200 vehicle compared to in a 60% DMSO vehicle. Thus, the same difference was observed between untreated skin and skin pre-treated with micro-needles for the sample in a 10% PEG200 vehicle. From the results in untreated skin (Figures 3.43 and 3.44) it was concluded that G-DP18 488 HSS was unable to penetrate the SC and diffuse deeper into the tissues during the 22 hours of incubation. The I_{RP} values, given in Figure 3.52, did not indicate diffusion through untreated skin either, and the conclusion was considered to be plausible.
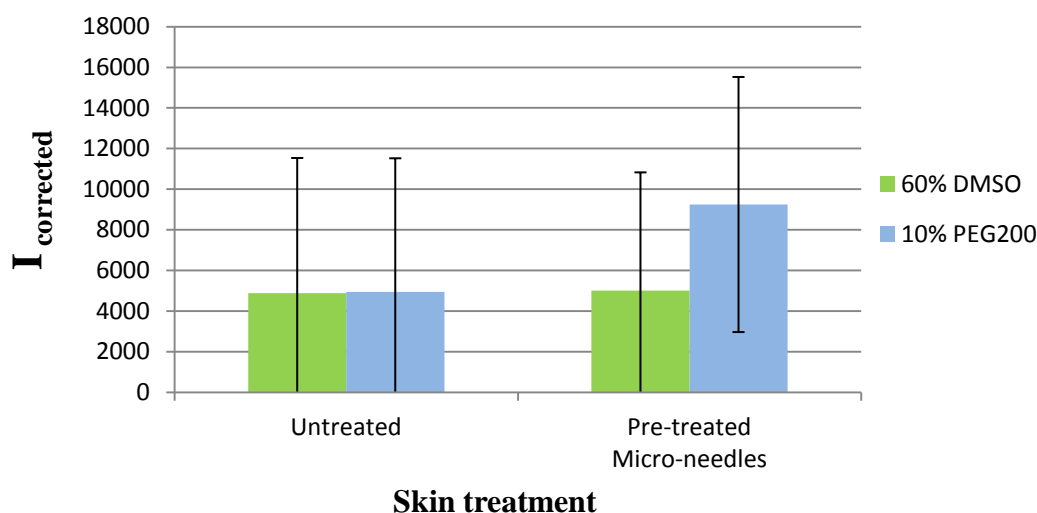
Figure 3.51: $I_{corrected}$ values for G-DP18 488 HSS applied on skin in both the 60% DMSO and the 10% PEG200 vehicle after diffusion into untreated and pre-treated skin.

G-DP18 488 HSS in a 60% DMSO vehicle resulted in a similar $I_{corrected}$ in both untreated and pre-treated skin. By comparing the surface plots of the two tissues (Figures 3.43d and 3.45d), it was determined that distribution of the sample was observed in the epidermis and the upper dermis in the tissue pre-treated with micro-needles. Weak fluorescence was also observed

deep in the untreated tissue, but this was believed to mainly be caused by autofluorescence. This indicated that the micro-needles enhanced the penetration through the SC, and allowed for the sample to diffuse deeper down. This was also confirmed by the $I_{RP\ corrected}$ values, though both values were low relative to $I_{RP\ max}$. Applied on skin pre-treated with micro-needles, G-DP18 488 HSS in this vehicle resulted in an $I_{RP\ corrected}$ value corresponding to ~7% of $I_{RP\ max}$, while the value corresponded to ~2% of $I_{RP\ max}$ when applied on untreated skin. G-DP18 488 HSS applied in a 10% PEG200 vehicle resulted in the highest $I_{RP\ corrected}$ value (Figure 3.52). But this value only corresponded to 3% of $I_{RP\ max}$, which once again illustrated that a higher dermal distribution was not equivalent with diffusion of the sample all the way through the tissue. However, it was concluded that micro-needles enhanced diffusion of G-DP18 488 HSS into human skin.
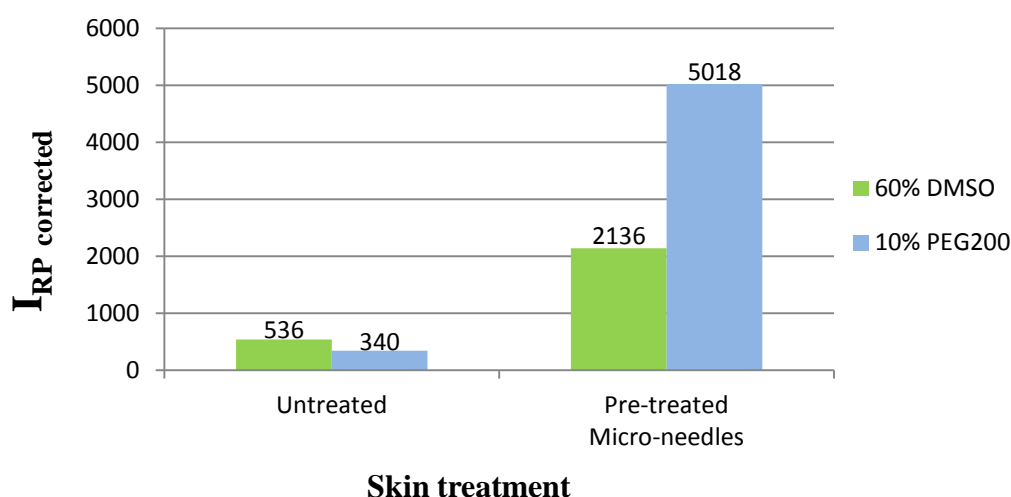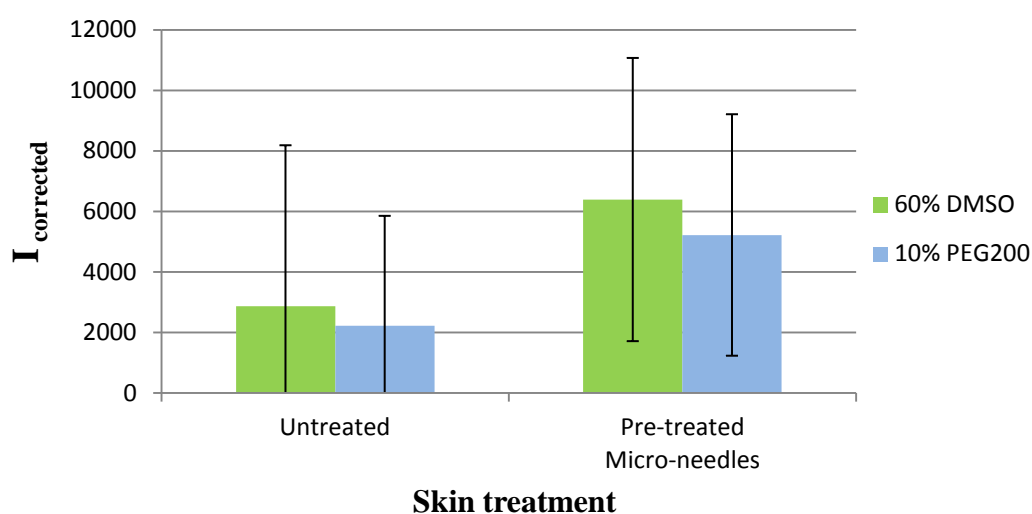

Figure 3.52: $I_{RP\ corrected}$ values for G-DP18 488 HSS applied on skin in both the 60% DMSO and the 10% PEG200 vehicle after diffusion into untreated and pre-treated skin.

The difference in $I_{corrected}$ observed in tissues pre-treated with micro-needles was profound. This difference could be due to the two different vehicles and varying degree of barrier disruption by the micro-needle device, as already emphasized for the experiments performed with FG peptides (subsection 3.2.6.3). An uneven distribution of G-DP18 488 HSS in a 10% PEG200 vehicle compared to the distribution of the same sample in a 60% DMSO vehicle was observed in skin tissues pre-treated with micro-needles (Figures 3.45a and 3.46a). The uneven distribution could be due to a more effective penetration enhancement by the micro-needles in this tissue, enabling more of the sample to diffuse through the SC barrier. This explanation may be supported by the observed increase in dermal distribution (Figure 3.46d). A similar distribution was also observed for FG24 488 CASE (Figure 3.28) and an

experimental weakness regarding the Franz-cell was suggested to be one possible cause, as discussed in subsection 3.2.6.3. However, this would mean that the difference in $I_{corrected}$ would have been even higher if larger amounts of G-DP18 488 HSS in the 10% PEG200 vehicle were located in the center of the application chamber during incubation.

Figure 3.53 demonstrates a correlation between the detected $I_{corrected}$ and skin treatment for G-DP22 488 HSS. Similar as for FG2 488 CASE, the lowest $I_{corrected}$ was observed in untreated skin tissues. $I_{corrected}$ was observed to be approximately a twofold higher in skin pre-treated with micro-needles compared to in untreated skin for the sample in both vehicles.

Figure 3.53: $I_{corrected}$ values for G-DP22 488 HSS applied on skin in both the 60% DMSO and the 10% PEG200 vehicle after diffusion into untreated and pre-treated skin.

From the results presented for G-DP22 488 HSS it was concluded that the sample was unable to penetrate the SC barrier in untreated skin and diffuse deeper into the tissue, regardless of the vehicle used (Figures 3.47 and 3.48). The $I_{corrected}$ values were therefore believed to be a result of the accumulation of the sample in the SC. The low $I_{RP\ corrected}$ values obtained from these two experiments, given in Figure 3.54, supported this conclusion and thus confirmed that the sample was unable to diffuse into and through untreated skin regardless of the vehicle used. It was further concluded that G-DP22 488 HSS diffused into skin pre-treated with micro-needles, a conclusion based on the results, presented in Figures 3.49 and 3.50, and the increased $I_{corrected}$ values in these tissues compared to in the untreated skin tissues. However, the $I_{RP\ corrected}$ values indicated that the diffusion of the sample applied in a 60% vehicle occurred at a higher rate compared to when applied in a 10% PEG200 vehicle, as these values corresponded to 11% and 2% of $I_{RP\ max}$, respectively.
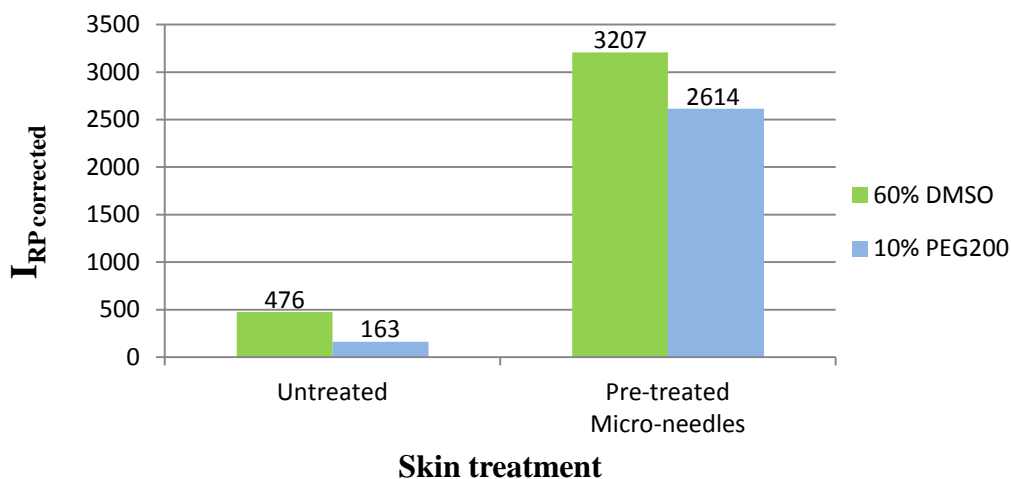
Figure 3.54: $I_{RP\ corrected}$ values for G-DP18 488 HSS applied on skin in both the 60% DMSO and the 10% PEG200 vehicle after diffusion into untreated and pre-treated skin.

A trend of higher $I_{corrected}$ values obtained for G-DP22 488 HSS applied in a 60% DMSO vehicle was observed (Figure 3.53). The differences in $I_{corrected}$ in tissues with the same skin treatment could be due to the two vehicles used, and in skin pre-treated with micro-needles a varying degree of barrier disruption may have contributed to the observed differences. The vehicles and skin pretreatments will be further evaluated in section 3.2.9 and 3.2.10, respectively. However, the dermal distribution, both in regards to extent and fluorescence intensities, of the sample in both vehicles (Figures 3.49d and 3.50d) was very similar. Variations in distribution, $I_{corrected}$, and I_{RP} of the G-block oligomers in tissues with the same pre-treatments may also be due to the heterogeneity of the skin tissues, the independency between each single experiment and experimental errors, discussed in subsection 3.2.5.3.

The skins in the experiments performed with G-DP18 488 HSS and G-DP22 488 HSS originated from two different donors (G and I). The possible effect of difference in skin thickness on diffusion efficiency has already been discussed in subsection 3.2.5.3. The thickness of the skins from donor G and I was almost equal (Table 3.6), the difference was only 0.01 mm. Therefore, the impact of this difference was believed to be minimal. However, the tissues may have possessed even higher degrees of heterogeneity compared to tissues from one individual donor. This may have contributed to the difference observed between the G-block oligomer samples applied in a 60% DMSO and a 10% PEG200 vehicle in both untreated and pre-treated skin.

Earlier in this subsection it was concluded that both G-DP18 488 HSS and G-DP22 488 HSS was unable to penetrate the SC and diffuse deeper into untreated skin tissues. This was

interpreted to be due to the molecular weight of the samples, and was in accordance with the "500 Dalton rule" introduced by Bos and Meinardi (2000) and discussed in subsection 3.2.5.3. It should be remarked that this interpretation was based on the samples M_n and not M_w, as for the FG peptides. However, M_w was expected to be higher compared to M_n for the oligomers, making the assumption plausible.

3.2.8. Evaluation of the model drugs

Of the two FG peptides, FG24 488 CASE displayed the highest $I_{corrected}$ values regardless of pretreatments performed on the skins (section 3.2.6.3). A similar trend was observed for the G-block oligomers, where G-DP18 488 HSS generally displayed the highest $I_{corrected}$ values, indicating that the molecular size of the model drugs was determining for the efficiency of skin diffusion. These observations were in accordance with molecular weight being the main determinant for diffusion across skin (Magnusson et al., 2004), and the size limitations in skin absorption reported by Bos and Meinardi (2000), already discussed in subsection 3.2.5.3. The impact of molecular weight was also likely to be decisive for the low $I_{corrected}$ values obtained after diffusion of FG2 into skin. However, FG24 488 CASE applied in a 60% DMSO vehicle was suggested to have diffused deeper into untreated skin. A possible cause for this could be the polydispersity of the test sample, meaning that molecules with a lower M_w than the estimated average may have been able to diffuse through the SC and deeper into the skin. Interestingly, the $I_{corrected}$ values of G-DP18 488 HSS were higher compared to for FG24 488 CASE, which also were contradictory to the reported effect of molecular weight on transdermal diffusion. However, this contradiction may be a result of the underestimation of DOL for the G-block samples (section 3.1.5), which consequently resulted in an overestimation of $I_{corrected}$, and thus falsely high mean fluorescence intensities in the tissues. It should also be taken into consideration that FG24 488 CASE generally resulted in more extended distribution in the dermal skin layer compared to G-DP18 488 HSS.

High $I_{corrected}$ values of G-DP18 and G-DP22 could indicate enhanced transdermal delivery similar to the enhancement of mucosal drug delivery, reported by Taylor and Draget (2011) (section 1.5.2.) A potential enhancement effect of G-block would, however, be restricted to the extracellular matrix (ECM) in the deeper skin layers and thus, G-blocks would first need to efficiently penetrate the SC. From the surface plots (subsections 3.2.7.1 and 3.2.7.2), no distribution of G-DP18 and G-DP22 were observed deeper in the tissue in untreated skin, and in skin pre-treated with micro-needles a greater dermal distribution was observed for

FG24 488 CASE (subsection 3.2.6.1) compared to the two G-block samples (subsections 3.2.7.1 and 3.2.7.2).

The G-block samples were also observed to result in higher fluorescence intensities and more extended accumulation in the SC, compared to the FG peptides. A possible interpretation of these observations could be that FG peptides diffused into skin more efficiently compared to G-block oligomers. FG peptides display a weak net positive charge at physiological pH and possess an amphiphilic nature due to their content of both hydrophilic and hydrophobic amino acids. Under identical conditions, the hydrophilic G-block oligomers are polyanionic. Therefore, a higher diffusion efficiency would be expected for the FG peptides across the hydrophobic skin barrier, since molecules with hydrophobic properties are reported to diffuse more efficiently through the barrier compared to hydrophilic molecules (Bos and Meinardi, 2000). The more extended and rigid conformation of G-block oligomers compared to the more flexible FG peptides may also have influenced the diffusion efficiency. However, neither of the model drugs fit into the ideal drug characteristics suggested for successful transdermal delivery (section 1.3), and their varying properties was one of the reason for choosing them as model drugs.

Theoretically, the diffusion of charged FG peptides and G-blocks may be affected by electrostatic interactions in the deeper skin layers. Negatively charged components in the ECM could restrict the entry of negatively charged G-block molecules, but if these molecules were able to enter the matrix, electrostatic repulsion could also efficiently move them into the receptor phase. The net positive charge of the FG peptides could cause them to be retained due to electrostatic attraction, and thus limit diffusion deeper into and through the skin. From the results presented in this report it was difficult to determine the exact impact of the charged nature of the model drugs, and the effect of size and degree of barrier disruption, was considered to have a larger impact on transdermal diffusion.

3.2.9. Evaluation of the vehicles

60% DMSO and 10% PEG200 was applied as vehicles for the model drugs in the transdermal diffusion experiments. DMSO and PEG are both classified as chemical enhancers, which are known to reduce the barrier properties of the SC and increase skin permeability (section 1.3). The use of known chemical enhancers as vehicles could potentially enhance the diffusion of the test samples into untreated skin or contribute to a synergistic enhancement effect in the pre-treated skin tissues.

From the results of the transdermal diffusion experiments a general trend of higher $I_{corrected}$ in the tissues was observed for FG24 488 CASE and G-DP18 488 HSS applied in a 10% PEG200 vehicle. The opposite trend was observed for FG2 488 CASE and G-DP22 488 HSS, and could possibly indicate a correlation between molecular weight and enhancement effect by the vehicles. However, even though higher dermal distribution was obtained for FG2 488 CASE in a 60% DMSO vehicle, the I_{RP} value for the sample in a 10% PEG200 vehicle was higher, indicating more efficient diffusion of the sample in this vehicle. The highest I_{RP} values (also relative to $I_{RP\ max}$), were observed for FG2 488 CASE and FG24 488 CASE in 10% PEG200, after diffusion through laser treated skin, and this could further support the indication of more efficiently diffusion of the samples in this vehicle. PEG is categorized in the chemical enhancement group of alcohols, which enhance skin permeability through a variety of mechanisms, including extraction of lipids and improvement of drug partitioning into the skin.

The partition coefficient (P) will be determined by the properties of both the drug and the vehicle (section 1.4), and an increase of P is known to increase the skin permeability. For successful transdermal delivery, moderate lipophilicity (log P 1-3) is suggested as one of the ideal characteristics of the compound to be delivered (section 1.3). The partition coefficients of solute between the vehicles and the skin for the model drugs were not known in this study. However, it was believed that the vehicles would have a higher affinity for the SC compared to the model drugs. This could further alter the partition coefficient of the model drugs and potentially enable them to diffuse in this skin layer. Deeper in the tissues it was likely that the drugs possessed a higher affinity for the ECM and thus, could diffuse into and be distributed in the matrix and potentially be taken up in the blood stream.

The vehicles were not observed to result in profound differences, or increase, in $I_{corrected}$ (as a result of dermal distribution) in the untreated skin tissues, indicating that the vehicles alone were not able to enhance the diffusion of the model drugs into skin. This further made it difficult to conclude which of the vehicles that were most suited for transdermal delivery of the model drugs. However, the highest $I_{corrected}$ and I_{RP} were observed in tissues where 10% PEG200 was used as vehicle. Further, PEG is non-toxic and non-immunogenic and already known to be used in pharmaceutical applications such as dermal ointments and creams (section 1.3), indicating compatibility with the skin. This makes PEG200 to an appealing choice of vehicle. DMSO, on the other hand, can cause rash and skin irritations (section 1.3) and has been shown to be toxic to the keratinocytes in the skin at constant exposure of high

concentrations (Aspevik, 2010). But regardless of all this, the effect of the two different vehicles on transdermal diffusion should be further studied before any conclusions are made.

3.2.10. Evaluation of the effect of pretreatment

The transdermal diffusion experiments revealed that the model drugs were unable to efficiently penetrate the SC and diffuse deeper into untreated skin. Micro-needles were observed to enhance transdermal diffusion of all the test samples. However, the need for manual operation of the micro-needle device made it difficult to achieve an identical and constant pressure for each pretreatment. Thus, a standardized method for skin penetration enhancement by micro-needles, resulting in consistent depths of penetration in each of the skin tissues, was difficult to obtain.

Laser treatment (L1, Table 2.2) was included in the transdermal diffusion experiments to obtain a highly standardized enhancement method. The laser created penetration patterns, where the density of laser spots, the distance between spots, and spot depth and diameter were identical in all the tissues after this pretreatment was performed. This penetration enhancement not only allowed distribution of FG peptides throughout the skin tissues, but also enabled efficient diffusion all the way through the tissues. FG2 488 CASE, with an estimated average M_w of 8000 g/mol, was observed to diffuse into and through the skin tissues pre-treated with L1. The M_w of this sample was 16 times higher than the M_w of 500 Dalton introduced by Bos and Meinardi (2000) as the limit value for passive diffusion into untreated skin, which illustrated the profound effect of this pretreatment. Diffusion of FG24 488 CASE in laser treated skin resulted in the highest $I_{corrected}$ and $I_{RP\ corrected}$ (also relative to $I_{RP\ max}$). However, transdermal diffusion of G-block oligomers was not studied in laser treated skin, and comparison between the oligomers and the peptides could only be made for untreated skin and skin pre-treated with micro-needles.

The penetration enhancement techniques used in the transdermal diffusion experiments showed enhancing effects *in vitro*, but they are not easily transferable for use in *in vivo* experiments or treatments. Micro-needles have been introduced as a promising approach to achieve increased skin permeability and transdermal delivery of drugs that otherwise would be restricted by the SC barrier. The micro-needles reported for *in vivo* use, such as in patches, only penetrates the SC and into the epidermis and are therefore not associated with pain or discomfort. However, the micro-needles used in the transdermal diffusion experiments were long enough to penetrate into the dermal layers of the skin, which could cause both pain and

119

bleeds if used on humans (Badran et al., 2009). The manufacturer also strongly emphasizes that the use of this micro-needle device should be performed by trained and licensed skin care professionals (Dermaroller, 2012). The laser treatment may cause a variety of adverse effects, including pain and burns. In addition, the apparatus used in such pretreatments are expensive, and treatment is restricted to clinical settings where it should be performed by professionals, as described in section 1.3.2. Taking all of this into account, both penetration enhancement techniques are likely to reduce patient compliance due to the risk of painful treatments, and laser treatments also exclude the possibility for self administering of drugs.

3.3. Future prospects

The FG peptides and G-block oligomers used as model drugs all demonstrated ability to diffuse in human skin, and it would therefore be of interest to further investigate these molecules as model drugs. It would also be preferable to perform each individual experiment more than once. It could also be advantageous to produce monodisperse test samples with the same molecular weights, as this would provide a better basis for comparison of the peptides and the oligomers. This could further make it possible to better evaluate the effect of the other physicochemical properties of the biopolymers on transdermal diffusion. It would also be of interest to perform studies to investigate the upper molecular weight limit for diffusion into and through pre-treated skin.

If further transdermal diffusion studies are to be performed as in the work presented in this report, effort should be made to minimize the experimental weaknesses and risks of errors associated with the experimental set-up. Decline of the Franz-type diffusion cells during incubation should be prevented and a better system for removal of skin tissues from the diffusion cells after incubation should be introduced, to avoid spillage of fluorescently labeled sample molecules into the receptor phase.

In this study physically penetration enhancement methods showed to have profound effect on transdermal diffusion. However, the micro-needles and laser treatments that were used are not readily transferable for use in *in vivo*. It was also found that the handhold micro-needle device resulted in varying degree of barrier disruption compared to the standardized laser treatment. It would therefore be beneficial to develop fully standardized penetration enhancement techniques, to enable efficient diffusion of molecules larger than 500 g/mol (Da) through the SC and deeper into the skin, which are readily transferable for use in *in vivo* transdermal drug delivery.

A step forward from studying transdermal diffusion *in vitro* could be to perform similar experiments *in vivo*, using experimental animals such as mice. This would especially be interesting for studying transdermal delivery of drugs for systemic effect. However, development of experimental assays for tracing of the model drugs in the bloodstream is required. In addition, animal experiments for research purposes must be licensed, which further requires a thoroughly elaborated experimental design.

4. Conclusion

This study demonstrated that water soluble molecules were able to diffuse into skin when physically penetration enhancement techniques were used to overcome the skin barrier. The results from the transdermal diffusion experiments demonstrated that $\overline{M}_W$ and degree of SC barrier disruption were the main determinants for successful diffusion of the model drugs into human skin. Of the four model drugs chosen for use in the experiments, the smallest FG peptide sample, with an estimated average molecular weight of 3000 g/mol, applied on laser pre-treated skin in a 10% PEG200 vehicle, resulted in the most efficient diffusion into and through human skin. Laser treatment was found to have the most profound enhancing effect on transdermal diffusion of FG peptides, as it enabled efficient diffusion both into and through the skin during the 22 hours of incubation introduced in the experiments. Micro-needles enhanced diffusion of FG peptides and G-block oligomers into skin to a varying extent, and thus indicated varying degree of barrier disruption by this device. None of the model drugs demonstrated efficient diffusion into untreated skin, although the results for FG24 488 CASE might have indicated a minor dermal diffusion in the tissue. It was therefore concluded that the vehicles alone did not enhance diffusion through the SC. However, the most efficient diffusion of model drugs in pre-treated skin were detected for samples applied on skin in a 10% PEG200 vehicle. Taking into account that this compound is non-toxic and non-immunogenic, PEG may be considered to be more applicable as vehicle compared to DMSO, known to be a skin irritant and potentially toxic, in transdermal diffusion experiments.

List of references

ALBANI, J. R. 2007. *Principles and applications of fluorescence spectroscopy,* Oxford ; Ames, Iowa, Blackwell Science.

ALBERTS, B., JOHNSON, A., LEWIS, J., RAFF, M., ROBERTS, K. & WALTER, P. 2002. *Molecular biology of the cell,* New York, Garland Science.

ANTOSOVA, Z., MACKOVA, M., KRAL, V. & MACEK, T. 2009. Therapeutic application of peptides and proteins: parenteral forever? *Trends in Biotechnology,* 27**,** 628-635.

ASPEVIK, T. 2010. *Transdermal administration of hydrophilic biopolymers.* Master's thesis, Norwegian University of Science and Technology (NTNU).

AULTON, M. E. 2007. *Aulton's pharmaceutics: the design and manufacture of medicines,* Edinburgh, Churchill Livingstone.

BABEL, W. 1996. Gelatin - A versatile biopolymer. *Chemie in Unserer Zeit,* 30**,** 86-95.

BADRAN, M. M., KUNTSCHE, J. & FAHR, A. 2009. Skin penetration enhancement by a microneedle device (Dermaroller®) in vitro: Dependency on needle size and applied formulation. *European Journal of Pharmaceutical Sciences,* 36**,** 511-523.

BAL, S. M., CAUSSIN, J., PAVEL, S. & BOUWSTRA, J. A. 2008. In vivo assessment of safety of microneedle arrays in human skin. *European Journal of Pharmaceutical Sciences,* 35**,** 193-202.

BARNES, R. K., VIEGAS, T. X. & HARRIS, M. J. 2008. *Poly(ethylene glycol)* [Online]. Access Science: McGraw Hill Companies. Available: http://www.accessscience.com/content/Poly(ethylene%20glycol)/534400 [Accessed 14.05. 2012].

BARRY, B. W. 2001. Novel mechanisms and devices to enable successful transdermal drug delivery. *European Journal of Pharmaceutical Sciences,* 14**,** 101-114.

BENSON, H. A. 2005. Transdermal drug delivery: penetration enhancement techniques. *Current Drug Delivery,* 2**,** 23-33.

BENSON, H. A. & NAMJOSHI, S. 2008. Proteins and peptides: strategies for delivery to and across the skin. *J Pharm Sci,* 97**,** 3591-610.

BOS, J. D. & MEINARDI, M. M. H. M. 2000. The 500 Dalton rule for the skin penetration of chemical compounds and drugs. *Experimental Dermatology,* 9**,** 165-169.

BOUWSTRA, J., GOORIS, G. & PONEC, M. 2002. The lipid organisation of the skin barrier: Liquid and crystalline domains coexist in lamellar phases. *Journal of Biological Physics,* 28**,** 211-223.

BROWN, M. B., MARTIN, G. P., JONES, S. A. & AKOMEAH, F. K. 2006. Dermal and transdermal drug delivery systems: Current and future prospects. *Drug Delivery,* 13**,** 175-187.

CHRISTENSEN, B. E. 2010a. Light scattering. *Compendium in TBT4135 Biopolymer chemistry.* Trondheim: NTNU.

CHRISTENSEN, B. E. 2010b. Size-exclusion chromatography (SEC). *Compendium in TBT4135 Biopolymer chemistry.* NTNU.

CLARK, D. P. 2005. *Molecular biology,* Amsterdam, Elsevier Academic Press.

CONE, R. A. 2009. Barrier properties of mucus. *Advanced Drug Delivery Reviews,* 61**,** 75-85.

COX, G. 2007. *Optical imaging techniques in cell biology,* Boca Raton, Fla., CRC/Taylor & Francis.

DA SILVA, D. L. P., THIAGO, S. B., PESSOA, F. A., MRESTANI, Y., RUTTINGER, H. H., WOHLRAB, J. & NEUBERT, R. H. H. 2008. Penetration profile of taurine in the human skin and its distribution in skin layers. *Pharmaceutical Research,* 25**,** 1846-1850.

DERMAROLLER. 2012. *Medical Dermaroller* [Online]. Available: http://www.dermaroller.com/en/medical-dermaroller [Accessed 10.05. 2012].

DETTMAR, P. W., STRUGALA, V. & CRAIG RICHARDSON, J. 2011. The key role alginates play in health. *Food Hydrocolloids,* 25**,** 263-266.

DONNELLY, R. F., SINGH, T. R. R. & WOOLFSON, A. D. 2010. Microneedle-based drug delivery systems: Microfabrication, drug delivery, and safety. *Drug Delivery,* 17**,** 187-207.

DOWNING, D. T. 1992. Lipid and protein structures in the permeability barrier of mammalian epidermis. *Journal of Lipid Research,* 33**,** 301-313.

DRAELOS, Z. D. 2005. *Cosmeceuticals,* Philadelphia, Elsevier Saunders.

DRAGET, K. I., MOE, S. T., SKJÅK-BRÆK, G. & SMIDSRØD, O. 2006. Alginate. *In:* STEPHEN, A. M., PHILLIPS, G. O. & WILLIAMS, P. A. (eds.) *Food Polysaccharides and Their Applications.* 2.nd ed. Boca Raton, Florida, USA: CRC Press.

DRAGET, K. I., SMIDSRØD, O. & SKJÅK-BRÆK, G. 2005. Alginates from Algae. *In:* STEINBÜCHEL, A. & RHEE, S. K. (eds.) *Polysaccharides and Polyamides in the*

Food Industry. Properties, Production, and Patents. Weinheim, Germany: Wiley-VCH Verlag GmbH & Co.

DRAGET, K. I. & TAYLOR, C. 2011. Chemical, physical and biological properties of alginates and their biomedical implications. *Food Hydrocolloids,* 25**,** 251-256.

EIKEN, K. B. 2011. *Levering av vannløselige molekyler gjennom hud - Diffusjon av molekyler gjennom stratum corneum.* Master's thesis, Norwegian University of Science and Technology.

ERTESVÅG, H. & VALLA, S. 1998. Biosynthesis and applications of alginates. *Polymer Degradation and Stability,* 59**,** 85-91.

ESCOBAR-CHAVEZ, J. J., BONILLA-MARTINEZ, D., VILLEGAS-GONZALEZ, M. A., MOLINA-TRINIDAD, E., CASAS-ALANCASTER, N. & REVILLA-VAZQUEZ, A. L. 2011. Microneedles: A Valuable Physical Enhancer to Increase Transdermal Drug Delivery. *Journal of Clinical Pharmacology,* 51**,** 964-977.

EYSTURSKARO, J., HAUG, I. J., ULSET, A. S. & DRAGET, K. I. 2009. Mechanical properties of mammalian and fish gelatins based on their weight average molecular weight and molecular weight distribution. *Food Hydrocolloids,* 23**,** 2315-2321.

FALLER, A., SCHÜNKE, M., SCHÜNKE, G. & TAUB, E. 2004. *The human body: an introduction to structure and function,* Stuttgart, Thieme.

FLORENCE, A. T. & ATTWOOD, D. 2006. *Physicochemical principles of pharmacy,* London, Pharmaceutical Press.

FLUHR, J. W., BANKOVA, L. & ELIAS, M. 2005. Stratum Corneum pH and Ions - Distribution and Importance. *In:* FLUHR, J. W., ELSNER, P., BERARDESCA, E. & MAIBACH, H. I. (eds.) *Bioengineering of the skin: Water and the Stratum Corneum.* 2.nd ed. Florida, USA: CRC Press LLC.

GOLD, M., H. 2010. Update on fractional laser technology. *J Clin Aesthet Dermatol,* 3**,** 42-50.

GROSS, J. H. 2011. Matrix-Assisted Laser Desorption/Ionization. *Mass spectrometry: a textbook.* Berlin: Springer-Verlag.

GUDMUNDSSON, M. 2002. Rheological properties of fish gelatins. *Journal of Food Science,* 67**,** 2172-2176.

GUPTA, J., GILL, H. S., ANDREWS, S. N. & PRAUSNITZ, M. R. 2011. Kinetics of skin resealing after insertion of microneedles in human subjects. *Journal of Controlled Release,* 154**,** 148-155.

HADGRAFT, J. 2004. Skin deep. *European Journal of Pharmaceutics and Biopharmaceutics,* 58**,** 291-299.

HAQ, M., SMITH, E., JOHN, D., KALAVALA, M., EDWARDS, C., ANSTEY, A., MORRISSEY, A. & BIRCHALL, J. 2009. Clinical administration of microneedles: skin puncture, pain and sensation. *Biomedical Microdevices,* 11**,** 35-47.

HAUG, A., LARSEN, B. & SMIDSRØD, O. 1967. *Studies on the sequence of uronic acid residues in alginic acid*, Acta Chemica Scandinavia.

HAUG, I. J. & DRAGET, K. I. 2009. Gelatin. *In:* PHILLIPS, G. O. & WILLIAMS, P. A. (eds.) *Handbook of Hydrocolloids (2nd Edition).* Woodhead Publishing.

HAUG, I. J., DRAGET, K. I. & SMIDSROD, A. 2004. Physical and rheological properties of fish gelatin compared to mammalian gelatin. *Food Hydrocolloids,* 18**,** 203-213.

HAUGLAND, R. P., SPENCE, M. T. Z., JOHNSON, I. D. & BASEY, A. 2005. *The handbook : a guide to fluorescent probes and labeling technologies,* Oregon, USA, Molecular Probes.

HENRY, S., MCALLISTER, D. V., ALLEN, M. G. & PRAUSNITZ, M. R. 1998. Microfabricated microneedles: A novel approach to transdermal drug delivery. *Journal of Pharmaceutical Sciences,* 87**,** 922-925.

HOLTAN, S., BRUHEIM, P. & SKJAK-BRAEK, G. 2006. Mode of action and subsite studies of the guluronan block-forming mannuronan C-5 epimerases AlgE1 and AlgE6. *Biochemical Journal,* 395**,** 319-329.

HÆDERSDAL, M., SAKAMOTO, F. H., FARINELLI, W. A., DOUKAS, A. G., TAM, J. & ANDERSON, R. R. 2010. Fractional CO2 laser-assisted drug delivery. *Lasers in Surgery and Medicine,* 42**,** 113-122.

INVITROGEN. 2010. *The Molecular Probes® Handbook-11th Edition* [Online]. Invitrogen. Available: http://www.invitrogen.com/site/us/en/home/References/Molecular-Probes-The-Handbook.html [Accessed 11.04. 2012].

KALLURI, H. & BANGA, A. K. 2011. Transdermal Delivery of Proteins. *Aaps Pharmscitech,* 12**,** 431-441.

KARANDE, P. & MITRAGOTRI, S. 2009. Enhancement of transdermal drug delivery via synergistic action of chemicals. *Biochimica Et Biophysica Acta-Biomembranes,* 1788**,** 2362-2373.

KARIM, A. A. & BHAT, R. 2009. Fish gelatin: properties, challenges, and prospects as an alternative to mammalian gelatins. *Food Hydrocolloids,* 23**,** 563-576.

KAUSHIK, S., HORD, A. H., DENSON, D. D., MCALLISTER, D. V., SMITRA, S., ALLEN, M. G. & PRAUSNITZ, M. R. 2001. Lack of pain associated with microfabricated microneedles. *Anesthesia and Analgesia,* 92**,** 502-504.

LAURENT, A., MISTRETTA, F., BOTTIGIOLI, D., DAHEL, K., GOUJON, C., NICOLAS, J. F., HENNINO, A. & LAURENT, P. E. 2007. Echographic measurement of skin thickness in adults by high frequency ultrasound to assess the appropriate microneedle length for intradermal delivery of vaccines. *Vaccine,* 25**,** 6423-6430.

LEE, W. R., SHEN, S. C., LAI, H. H., HU, C. H. & FANG, J. Y. 2001. Transdermal drug delivery enhanced and controlled by erbium : YAG laser: a comparative study of lipophilic and hydrophilic drugs. *Journal of Controlled Release,* 75**,** 155-166.

MACKIE, R. M. 2003. *Clinical dermatology,* Oxford, Oxford University Press.

MAGNUSSON, B. M., ANISSIMOV, Y. G., CROSS, S. E. & ROBERTS, M. S. 2004. Molecular size as the main determinant of solute maximum flux across the skin. *Journal of Investigative Dermatology,* 122**,** 993-999.

MCGRATH, J. A., EADY, R. A. J. & POPE, F. M. 2010. Anatomy and Organization of Human Skin. *In:* ROOK, A. & BURNS, T. (eds.) *Rook's textbook of dermatology.* 8th ed. Chichester: Wiley-Blackwell.

MITCHELL, B. & PEEL, S. 2009. *Histology: an illustrated colour text,* Edinburgh, Churchill Livingstone Elsevier.

MOSER, K., KRIWET, K., NAIK, A., KALIA, Y. N. & GUY, R. H. 2001. Passive skin penetration enhancement and its quantification in vitro. *European Journal of Pharmaceutics and Biopharmaceutics,* 52**,** 103-112.

NA, R. H., STENDER, I. M., HENRIKSEN, M. & WULF, H. C. 2001. Autofluorescence of human skin is age-related after correction for skin pigmentation and redness. *Journal of Investigative Dermatology,* 116**,** 536-540.

NAMJOSHI, S., CACCETTA, R. & BENSON, H. A. E. 2008. Skin peptides: Biological activity and therapeutic opportunities. *Journal of Pharmaceutical Sciences,* 97**,** 2524-2542.

NELSON, D. L., LEHNINGER, A. L. & COX, M. M. 2008. *Lehninger principles of biochemistry,* New York, Freeman.

NOTMAN, R., DEN OTTER, W. K., NORO, M. G., BRIELS, W. J. & ANWAR, J. 2007. The permeability enhancing mechanism of DMSO in ceramide Bilayers simulated by molecular dynamics. *Biophysical Journal,* 93**,** 2056-2068.

OTTERLEI, M., OSTGAARD, K., SKJAKBRAEK, G., SMIDSROD, O., SOONSHIONG, P. & ESPEVIK, T. 1991. Induction of Cytokine Production from Human Monocytes Stimulated with Alginate. *Journal of Immunotherapy,* 10**,** 286-291.

PATHAN, I. B. & SETTY, C. M. 2009. Chemical Penetration Enhancers for Transdermal Drug Delivery Systems. *Tropical Journal of Pharmaceutical Research,* 8**,** 173-179.

PRAESSLER, J. & FLUHR, J. W. 2005. Occlusion. *In:* FLUHR, J. W., ELSNER, P., BERARDESCA, E. & MAIBACH, H. I. (eds.) *Bioengineering of the skin - Water and the Stratum Corneum.* 2. nd ed. Florida, USA: CRC Press LLC.

PRAUSNITZ, M. R. 2004. Microneedles for transdermal drug delivery. *Advanced Drug Delivery Reviews,* 56**,** 581-587.

PRAUSNITZ, M. R., MITRAGOTRI, S. & LANGER, R. 2004. Current status and future potential of transdermal drug delivery. *Nature Reviews Drug Discovery,* 3**,** 115-124.

ROBINSON, P. 2005. Skin. *In:* PHILIP, W. (ed.) *Encyclopedia of Toxicology (Second Edition).* New York: Elsevier.

SCHRIEBER, R. & GAREIS, H. 2007. *Gelatine handbook: theory and industrial practice,* Weinheim, Germany.

SMIDSRØD, O. & MOE, S. T. 2008. *Biopolymer chemistry,* Trondheim, Tapir Academic Press.

SONG, T. T., NELSON, M. R., HERSHEY, J. N. & CHOWDHURY, B. A. 2004. Subcutaneous tissue depth differences between males and females: The need for gender based epinephrine needle. *Journal of Allergy and Clinical Immunology,* 113**,** S241.

SUBEDI, R. K., OH, S. Y., CHUN, M. K. & CHOI, H. K. 2010. Recent Advances in Transdermal Drug Delivery. *Archives of Pharmacal Research,* 33**,** 339-351.

TANNER, T. & MARKS, R. 2008. Delivering drugs by the transdermal route: review and comment. *Skin Research and Technology,* 14**,** 249-260.

TAYLOR, J. R. 1997. *An introduction to error analysis: the study of uncertainties in physical measurements,* Sausalito, Calif., University Science Books.

THOMAS, B. J. & FINNIN, B. C. 2004. The transdermal revolution. *Drug Discovery Today,* 9**,** 697-703.

VEIS, A. 1964. *The macromolecular chemistry of gelatin,* New York, Academic Press

WEBSTER, J. & OXLEY, D. 2005. Peptide Mass Fingerprinting - Protein Identification Using MALDI-TOF Mass Spectrometry. *In:* ZANDERS, E. D. (ed.) *Chemical Genomics: Reviews and protocols.* New Jersey, USA: Humana Press.

WEIFA. 2012. *Ibux gel* [Online]. Available: http://www.weifa.no/Vare-produkter/Smertefeber/Ibux-Gel--Lindrer-smerter-og-hevelser-rett-pa-stedet/ [Accessed 10.05. 2012].

WICKETT, R. R. & VISSCHER, M. O. 2006. Structure and function of the epidermal barrier. *American Journal of Infection Control,* 34**,** S98-S110.

WILLIAMS, A. 2003. *Transdermal and topical drug delivery: from theory to clinical practice,* London, Pharmaceutical Press.

WILLIAMS, A. C. & BARRY, B. W. 2004. Penetration enhancers. *Advanced Drug Delivery Reviews,* 56**,** 603-618.

ZEISS, C., DICKINSON, M. E., HESSLING, R. & DAVIDSON, M. W. 2012. *Practical Considerations for Spectral Imaging* [Online]. Carl Zeiss Microscopy Online Campus: Carl Zeiss Microscopy, LLC, North America. Available: http://zeiss-campus.magnet.fsu.edu/print/spectralimaging/considerations-print.html [Accessed 19.05. 2012].

List of Appendices

Enclosed cd

CLSM images and surface plots of the control tissues

CLSM images

Excel files including:

- Raw data for the intensity plots
- Raw data for mean fluorescence intensity values
- Raw data for I_{RP} values

MALDI-TOF

- Raw data
- Operator Manual

Appendix A: SEC-MALLS

The weight average molecular weight (M_w) and the number average molecular weight (M_n) of fish gelatin (FG) peptides were determined by SEC-MALLS analyses (section 3.1.1). The analyses were performed by Ann-Sissel Teialeret Ulset, Staff Engineer at the Department of biotechnology, NTNU. The experimental procedure is given in section 2.2.3.1. The raw data from the analyses are given in this appendix.

A.1 Initial FG
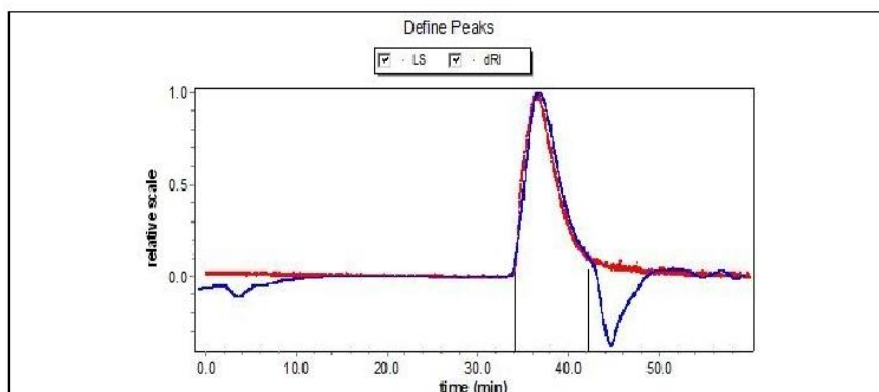
CONFIGURATION

Light scattering instrument: DAWN HELEOS
    Cell type: K5
    Laser wavelength: 658.0 nm
    Calibration constant: 2.8301e-5 1/(V cm)
RI Instrument: Optilab rEX
UV Instrument: n/a
Solvent: water
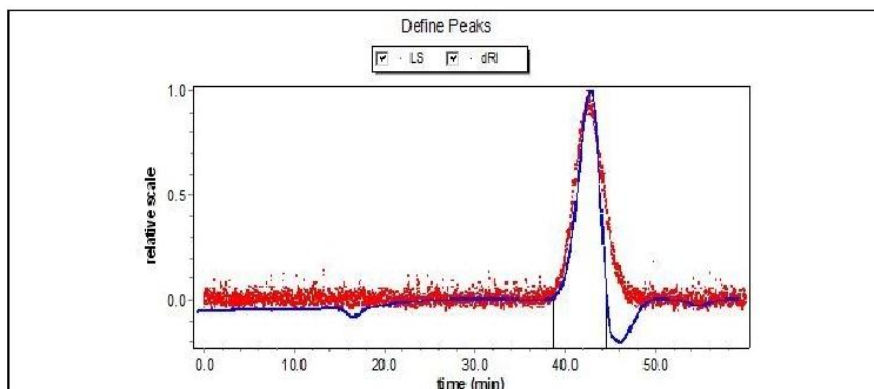   **Refractive index:** 1.331
Flow rate: 0.500 mL/min

PROCESSING

Processing time: Wednesday March 28, 2012 12:38 PM @tzres.dll,-321
Collection time: Friday September 30, 2011 06:10 PM @tzres.dll,-321
Detectors used: 6 7 8 9 10 11 12 13 14 15
Concentration detector: RI
Mass results fitting: none (fit degree: n/a)
Radius results fitting: none (fit degree: n/a)

	Peak 1
Peak limits (min)	34.022 - 42.262
dn/dc (mL/g)	0.190
A_2 (mol mL/g²)	1.000e-3
UV ext. (mL/(g cm))	0.000
Model	Zimm
Fit degree	1
Injected mass (g)	1.0000e-4
Calc. mass (g)	1.1188e-4

RESULTS

Peak 1
Polydispersity
  Mw/Mn 1.021(0.9%)
  Mz/Mn 1.046(2%)
Molar mass moments (g/mol)
  Mn 1.172e+5(0.7%)
  Mp 1.179e+5(0.4%)
  Mv n/a
  Mw 1.197e+5(0.7%)
  Mz 1.226e+5(1%)
rms radius moments (nm)
  Rn 23.1(5%)
  Rw 23.2(5%)
  Rz 23.3(5%)

A.2 FG1
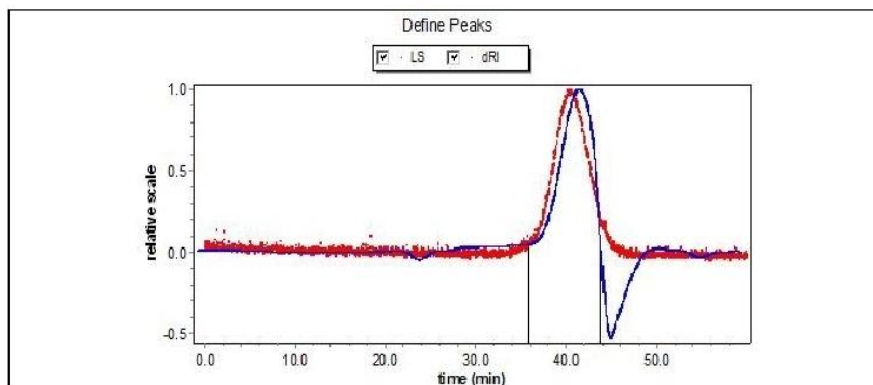
CONFIGURATION

Light scattering instrument: DAWN HELEOS
  Cell type: K5
  Laser wavelength: 658.0 nm
  Calibration constant: 2.8301e-5 1/(V cm)
RI Instrument: Optilab rEX
UV Instrument: n/a
Solvent: water
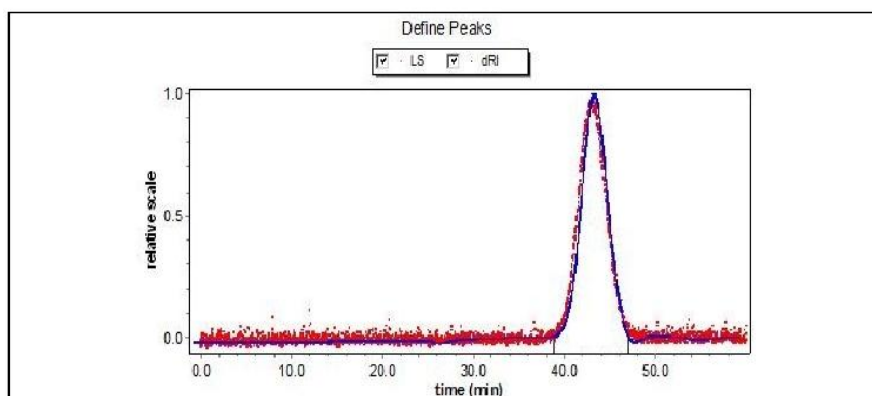 **Refractive index:** 1.331
Flow rate: 0.500 mL/min

PROCESSING

Processing time: Wednesday March 28, 2012 12:37 PM @tzres.dll,-321
Collection time: Saturday October 01, 2011 01:02 PM @tzres.dll,-321
Detectors used: 6 7 8 9 10 11 12 13 14 15
Concentration detector: RI
Mass results fitting: none (fit degree: n/a)
Radius results fitting: none (fit degree: n/a)

	Peak 1
Peak limits (min)	35.750 - 43.765
dn/dc (mL/g)	0.190
A_2 (mol mL/g²)	1.000e-3
UV ext. (mL/(g cm))	0.000
Model	Zimm
Fit degree	1
Injected mass (g)	2.0000e-4
Calc. mass (g)	1.2737e-4

RESULTS

Peak 1
Polydispersity
  Mw/Mn 1.120(3%)
  Mz/Mn 1.260(5%)
Molar mass moments (g/mol)
  Mn 1.257e+4(2%)
  Mp 1.146e+4(1%)
  Mv n/a
  Mw 1.408e+4(2%)
  Mz 1.584e+4(5%)
rms radius moments (nm)
  Rn 5.5(246%)
  Rw 6.3(189%)
  Rz 7.5(143%)

A.3 FG2
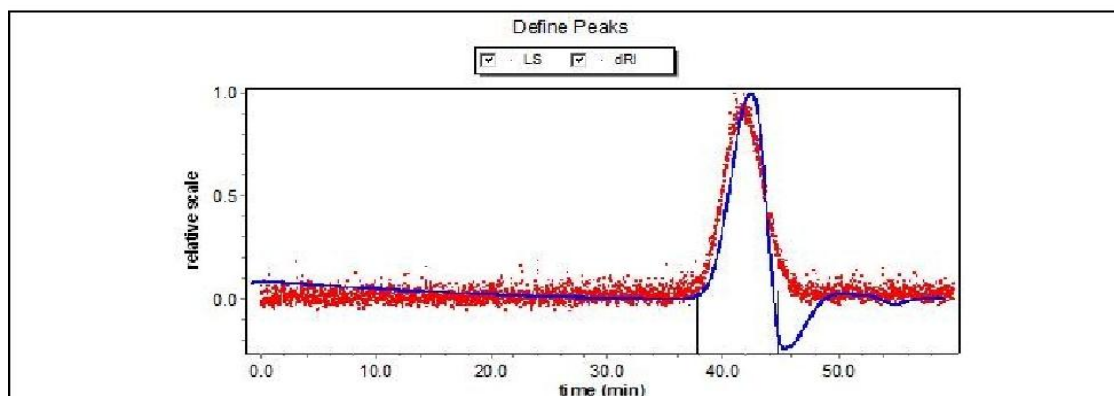
CONFIGURATION

Light scattering instrument: DAWN HELEOS
      Cell type: K5
      Laser wavelength: 658.0 nm
      Calibration constant: 2.8301e-5 1/(V cm)
RI Instrument: Optilab rEX
UV Instrument: n/a
Solvent: water
      Refractive index: 1.331
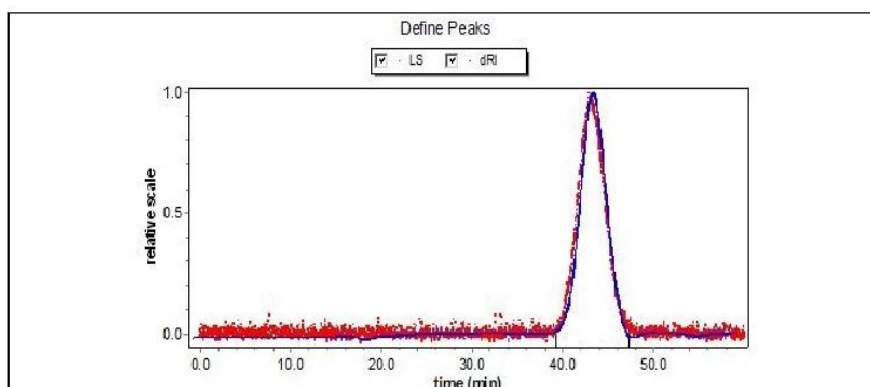**Flow rate:** 0.500 mL/min

PROCESSING

Processing time: Monday May 21, 2012 11:07 AM @tzres.dll,-321
Collection time: Friday September 30, 2011 08:16 PM @tzres.dll,-321
Detectors used: 6 7 8 9 10 11 12 13 14 15
Concentration detector: RI
Mass results fitting: none (fit degree: n/a)
Radius results fitting: none (fit degree: n/a)

	Peak 1
Peak limits (min)	37.741 - 44.831
dn/dc (mL/g)	0.190
A_2 (mol mL/g²)	1.000e-3
UV ext. (mL/(g cm))	0.000
Model	Zimm
Fit degree	1
Injected mass (g)	2.0000e-4
Calc. mass (g)	1.0908e-4

RESULTS

Peak 1

Polydispersity

Mn	9.025e+3(3%)
Mp	8.670e+3(3%)
Mv	n/a
Mw	1.000e+4(4%)
Mz	1.285e+4(12%)

rms radius moments (nm)

Rn	8.7(166%)
Rw	10.4(125%)
Rz	13.7(86%)

A.4 FG4

CONFIGURATION

Light scattering instrument: DAWN HELEOS
    Cell type: K5
    Laser wavelength: 658.0 nm
    Calibration constant: 2.8301e-5 1/(V cm)
RI Instrument: Optilab rEX
UV Instrument: n/a
Solvent: water
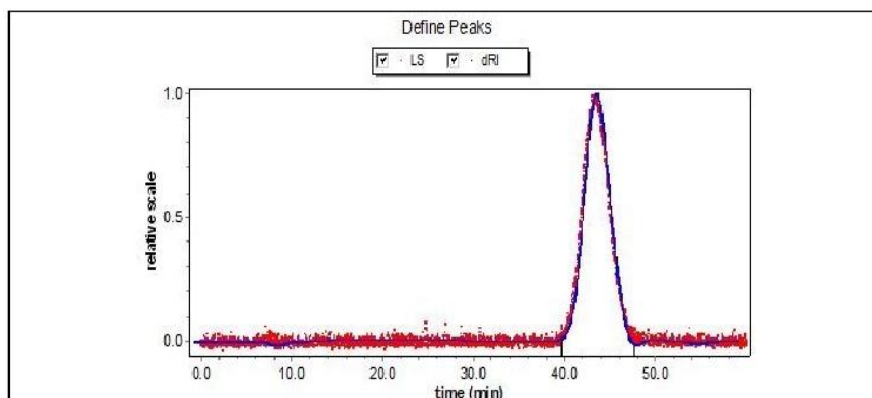   **Refractive index:** 1.331
Flow rate: 0.500 mL/min

PROCESSING

Processing time: Wednesday March 28, 2012 12:33 PM @tzres.dll,-321
Collection time: Saturday October 01, 2011 06:45 AM @tzres.dll,-321
Detectors used: 6 7 8 9 10 11 12 13 14 15
Concentration detector: RI
Mass results fitting: none (fit degree: n/a)
Radius results fitting: none (fit degree: n/a)

	Peak 1
Peak limits (min)	38.695-44.431
dn/dc (mL/g)	0.190
A_2 (mol mL/g²)	1.000e-3
UV ext. (mL/(g cm))	0.000
Model	Zimm
Fit degree	1
Injected mass (g)	2.0000e-4
Calc. mass (g)	1.0050e-4

RESULTS

	Peak 1
Polydispersity	
Mw/Mn	1.061(4%)
Mz/Mn	1.167(9%)
Molar mass moments (g/mol)	
Mn	6.083e+3(3%)
Mp	5.099e+3(2%)
Mv	n/a
Mw	6.452e+3(3%)
Mz	7.099e+3(9%)
rms radius moments (nm)	
Rn	n/a
Rw	n/a
Rz	n/a

A.5 FG6

CONFIGURATION

Light scattering instrument: DAWN HELEOS
    Cell type: K5
    Laser wavelength: 658.0 nm
    Calibration constant: 2.8301e-5 1/(V cm)
RI Instrument: Optilab rEX
UV Instrument: n/a
Solvent: water
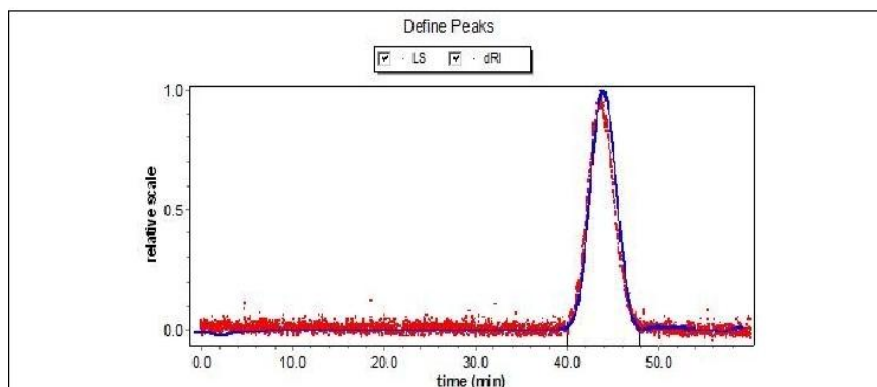   **Refractive index:** 1.331
Flow rate: 0.500 mL/min

PROCESSING

Processing time: Wednesday March 28, 2012 12:28 PM @tzres.dll,-321
Collection time: Friday September 30, 2011 10:22 PM @tzres.dll,-321
Detectors used: 6 7 8 9 10 11 12 13 14 15
Concentration detector: RI
Mass results fitting: none (fit degree: n/a)
Radius results fitting: none (fit degree: n/a)

	Peak 1
Peak limits (min)	38.836 - 46.963
dn/dc (mL/g)	0.190
A_2 (mol mL/g²)	1.000e-3
UV ext. (mL/(g cm))	0.000
Model	Zimm
Fit degree	1
Injected mass (g)	6.0000e-4
Calc. mass (g)	4.0742e-4

RESULTS

Peak 1
Polydispersity
  Mw/Mn 1.034(4%)
  Mz/Mn 1.079(8%)
Molar mass moments (g/mol)
  Mn 4.078e+3(3%)
  Mp 3.897e+3(1%)
  Mv n/a
  Mw 4.218e+3(3%)
  Mz 4.399e+3(8%)
rms radius moments (nm)
  Rn n/a
  Rw n/a
  Rz n/a

A.6 FG8

Light scattering instrument: DAWN HELEOS
    Cell type: K5
    Laser wavelength: 658.0 nm
    Calibration constant: 2.8301e-5 1/(V cm)
RI Instrument: Optilab rEX
UV Instrument: n/a
Solvent: water
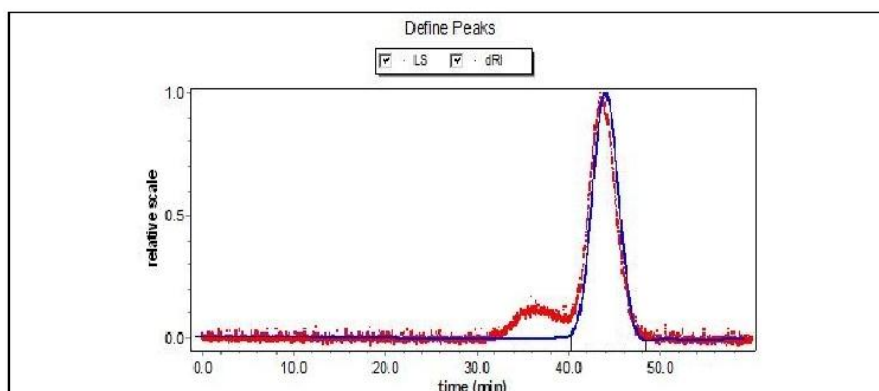   **Refractive index:** 1.331
Flow rate: 0.500 mL/min

PROCESSING

Processing time: Wednesday March 28, 2012 12:29 PM @tzres.dll,-321
Collection time: Friday September 30, 2011 11:25 PM @tzres.dll,-321
Detectors used: 6 7 8 9 10 11 12 13 14 15
Concentration detector: RI
Mass results fitting: none (fit degree: n/a)
Radius results fitting: none (fit degree: n/a)

	Peak 1
Peak limits (min)	39.331 - 47.398
dn/dc (mL/g)	0.190
A_2 (mol mL/g^2)	1.000e-3
UV ext. (mL/(g cm))	0.000
Model	Zimm
Fit degree	1
Injected mass (g)	6.0000e-4
Calc. mass (g)	3.9015e-4

RESULTS

	Peak 1
Polydispersity	
Mw/Mn	1.036(3%)
Mz/Mn	1.109(7%)
Molar mass moments (g/mol)	
Mn	3.990e+3(2%)
Mp	3.802e+3(1%)
Mv	n/a
Mw	4.134e+3(2%)
Mz	4.425e+3(7%)
rms radius moments (nm)	
Rn	n/a
Rw	n/a
Rz	n/a

A.7 FG12

VIII

A.8 FG16

Light scattering instrument: DAWN HELEOS
    Cell type: K5
    Laser wavelength: 658.0 nm
    Calibration constant: 2.8301e-5 1/(V cm)
RI Instrument: Optilab rEX
UV Instrument: n/a
Solvent: water
    Refractive index: 1.331
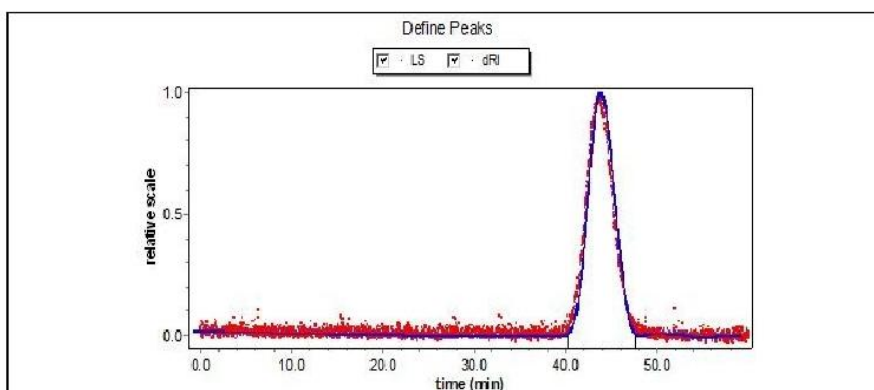**Flow rate:** 0.500 mL/min

Processing time: Wednesday March 28, 2012 12:30 PM @tzres.dll,-321
Collection time: Saturday October 01, 2011 01:31 AM @tzres.dll,-321
Detectors used: 6 7 8 9 10 11 12 13 14 15
Concentration detector: RI
Mass results fitting: none (fit degree: n/a)
Radius results fitting: none (fit degree: n/a)

	Peak 1
Peak limits (min)	40.002 - 47.827
dn/dc (mL/g)	0.190
A_2 (mol mL/g²)	1.000e-3
UV ext. (mL/(g cm))	0.000
Model	Zimm
Fit degree	1
Injected mass (g)	6.0000e-4
Calc. mass (g)	4.3461e-4

         Peak 1
Polydispersity
  Mw/Mn 1.046(4%)
  Mz/Mn 1.199(13%)
Molar mass moments (g/mol)
  Mn 2.641e+3(3%)
  Mp 2.645e+3(1%)
  Mv n/a
  Mw 2.764e+3(3%)
  Mz 3.166e+3(13%)
rms radius moments (nm)
  Rn n/a
  Rw n/a
  Rz 9.0(164%)

A.9 FG18

CONFIGURATION

Light scattering instrument: DAWN HELEOS
    Cell type: K5
    Laser wavelength: 658.0 nm
    Calibration constant: 2.8301e-5 1/(V cm)
RI Instrument: Optilab rEX
UV Instrument: n/a
Solvent: water
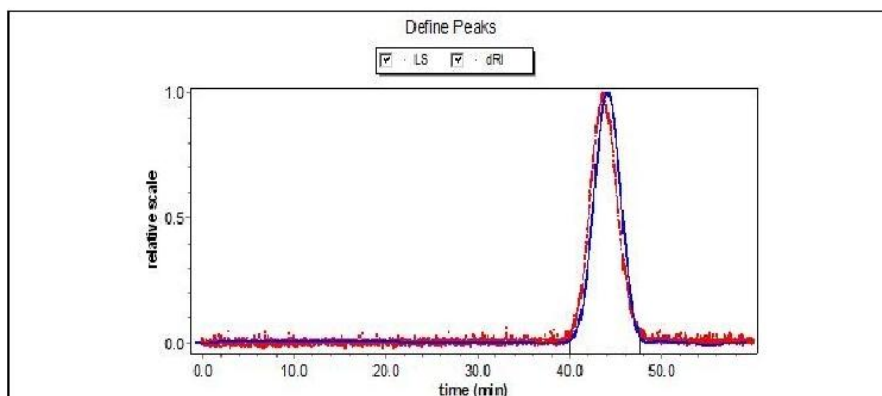   **Refractive index:** 1.331
Flow rate: 0.500 mL/min

PROCESSING

Processing time: Wednesday March 28, 2012 12:32 PM @tzres.dll,-321
Collection time: Saturday October 01, 2011 02:34 AM @tzres.dll,-321
Detectors used: 6 7 8 9 10 11 12 13 14 15
Concentration detector: RI
Mass results fitting: none (fit degree: n/a)
Radius results fitting: none (fit degree: n/a)

	Peak 1
Peak limits (min)	40.285 - 48.527
dn/dc (mL/g)	0.190
A_2 (mol mL/g²)	1.000e-3
UV ext. (mL/(g cm))	0.000
Model	Zimm
Fit degree	1
Injected mass (g)	1.0000e-3
Calc. mass (g)	6.9434e-4

RESULTS

Peak 1
Polydispersity
  Mw/Mn 1.067 (3%)
  Mz/Mn 1.354 (10%)
Molar mass moments (g/mol)
  Mn 2.537e+3 (2%)
  Mp 2.574e+3 (0.8%)
  Mv n/a
  Mw 2.708e+3 (2%)
  Mz 3.435e+3 (9%)
rms radius moments (nm)
  Rn n/a
  Rw n/a
  Rz n/a

X

A.10 FG20

CONFIGURATION

Light scattering instrument: DAWN HELEOS
    Cell type: K5
    Laser wavelength: 658.0 nm
    Calibration constant: 2.8301e-5 1/(V cm)
RI Instrument: Optilab rEX
UV Instrument: n/a
Solvent: water
    Refractive index: 1.331
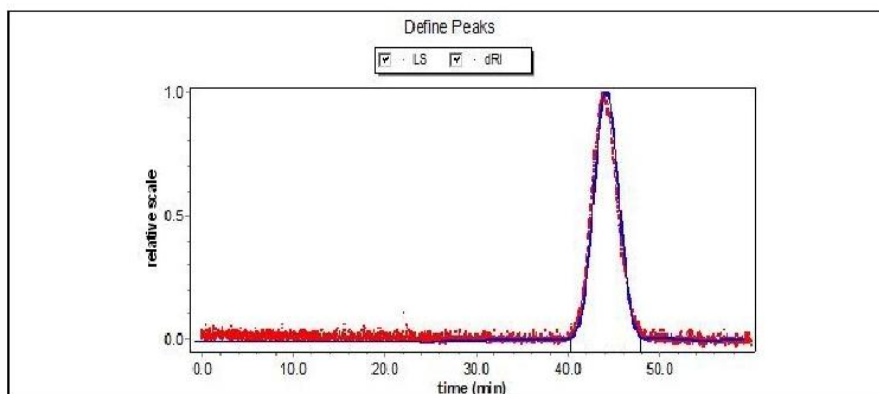**Flow rate:** 0.500 mL/min

PROCESSING

Processing time: Wednesday March 28, 2012 12:32 PM @tzres.dll,-321
Collection time: Saturday October 01, 2011 03:37 AM @tzres.dll,-321
Detectors used: 6 7 8 9 10 11 12 13 14 15
Concentration detector: RI
Mass results fitting: none (fit degree: n/a)
Radius results fitting: none (fit degree: n/a)

	Peak 1
Peak limits (min)	40.239 - 47.572
dn/dc (mL/g)	0.190
A_2 **(mol mL/g²)**	1.000e-3
UV ext. (mL/(g cm))	0.000
Model	Zimm
Fit degree	1
Injected mass (g)	5.0000e-4
Calc. mass (g)	4.7975e-4

RESULTS

Peak 1
Polydispersity
  Mw/Mn   1.038(3%)
  Mz/Mn   1.100(7%)
Molar mass moments (g/mol)
  Mn   2.839e+3(2%)
  Mp   2.794e+3(1%)
  Mv   n/a
  Mw   2.947e+3(3%)
  Mz   3.125e+3(7%)
rms radius moments (nm)
  Rn   n/a
  Rw   n/a
  Rz   4.5(501%)

A.11 FG24

CONFIGURATION

Light scattering instrument: DAWN HELEOS
    Cell type: K5
    Laser wavelength: 658.0 nm
    Calibration constant: 2.8301e-5 1/(V cm)
RI Instrument: Optilab rEX
UV Instrument: n/a
Solvent: water
    Refractive index: 1.331
Flow rate: 0.500 mL/min

PROCESSING

Processing time: Wednesday March 28, 2012 12:34 PM @tzres.dll,-321
Collection time: Saturday October 01, 2011 08:51 AM @tzres.dll,-321
Detectors used: 6 7 8 9 10 11 12 13 14 15
Concentration detector: RI
Mass results fitting: none (fit degree: n/a)
Radius results fitting: none (fit degree: n/a)

	Peak 1
Peak limits (min)	39.884 - 47.584
dn/dc (mL/g)	0.190
A_2 (mol mL/g²)	1.000e-3
UV ext. (mL/(g cm))	0.000
Model	Zimm
Fit degree	1
Injected mass (g)	1.0000e-3
Calc. mass (g)	7.4639e-4

RESULTS

           Peak 1
Polydispersity
 Mw/Mn 1.077(2%)
 Mz/Mn 1.180(5%)
Molar mass moments (g/mol)
 Mn 2.409e+3(2%)
 Mp 2.373e+3(0.7%)
 Mv n/a
 Mw 2.594e+3(2%)
 Mz 2.844e+3(4%)
rms radius moments (nm)
 Rn n/a
 Rw n/a
 Rz 4.0(427%)

A.12 FG36

Light scattering instrument: DAWN HELEOS
     Cell type: K5
     Laser wavelength: 658.0 nm
     Calibration constant: 2.8301e-5 1/(V cm)
RI Instrument: Optilab rEX
UV Instrument: n/a
Solvent: water
     Refractive index: 1.331
Flow rate: 0.500 mL/min

PROCESSING

Processing time: Wednesday March 28, 2012 12:33 PM @tzres.dll,-321
Collection time: Saturday October 01, 2011 05:43 AM @tzres.dll,-321
Detectors used: 6 7 8 9 10 11 12 13 14 15
Concentration detector: RI
Mass results fitting: none (fit degree: n/a)
Radius results fitting: none (fit degree: n/a)

	Peak 1
Peak limits (min)	40.244 - 47.944
dn/dc (mL/g)	0.190
A_2 (mol mL/g^2)	1.000e-3
UV ext. (mL/(g cm))	0.000
Model	Zimm
Fit degree	1
Injected mass (g)	1.0000e-3
Calc. mass (g)	7.4072e-4

RESULTS

       Peak 1
Polydispersity
 Mw/Mn 1.033(3%)
 Mz/Mn 1.085(6%)
Molar mass moments (g/mol)
 Mn 2.248e+3(2%)
 Mp 2.204e+3(0.9%)
 Mv n/a
 Mw 2.324e+3(2%)
 Mz 2.440e+3(6%)
rms radius moments (nm)
 Rn n/a
 Rw n/a
 Rz n/a

Appendix B: MALDI-TOF

The weight average molecular weight (M_w) and the number average molecular weight (M_n) of fish gelatin (FG) peptides were determined by MALDI-TOF analyses (section 3.1.2). The analyses were performed by Kåre Andre Kristiansen, Senior Engineer at the Department of biotechnology, NTNU. The experimental procedure is given in section 2.2.3.2. The MALDI-TOF spectra are given in this appendix, and the raw data are given on the enclosed CD. The mass spectra peaks are only labeled for FG4, FG12 and FG24. This is because labeling of the peaks in the other spectra caused overlapping values and made the results disorderly.

B.1   FG1
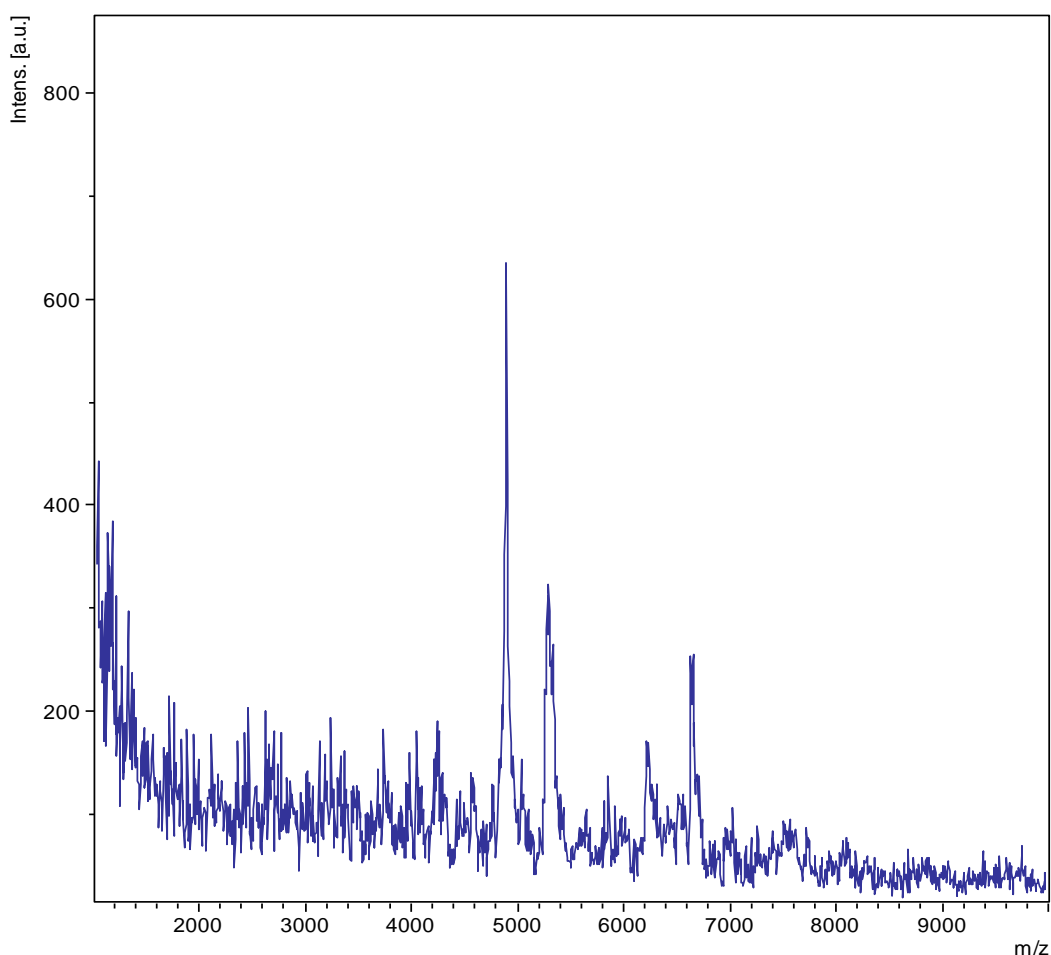
Figure B.1: MALDI-TOF spectrum for FG1. The x-axis and y-axis display the mass-to-charge (m/z) ratio and intensity.

B.2 FG2
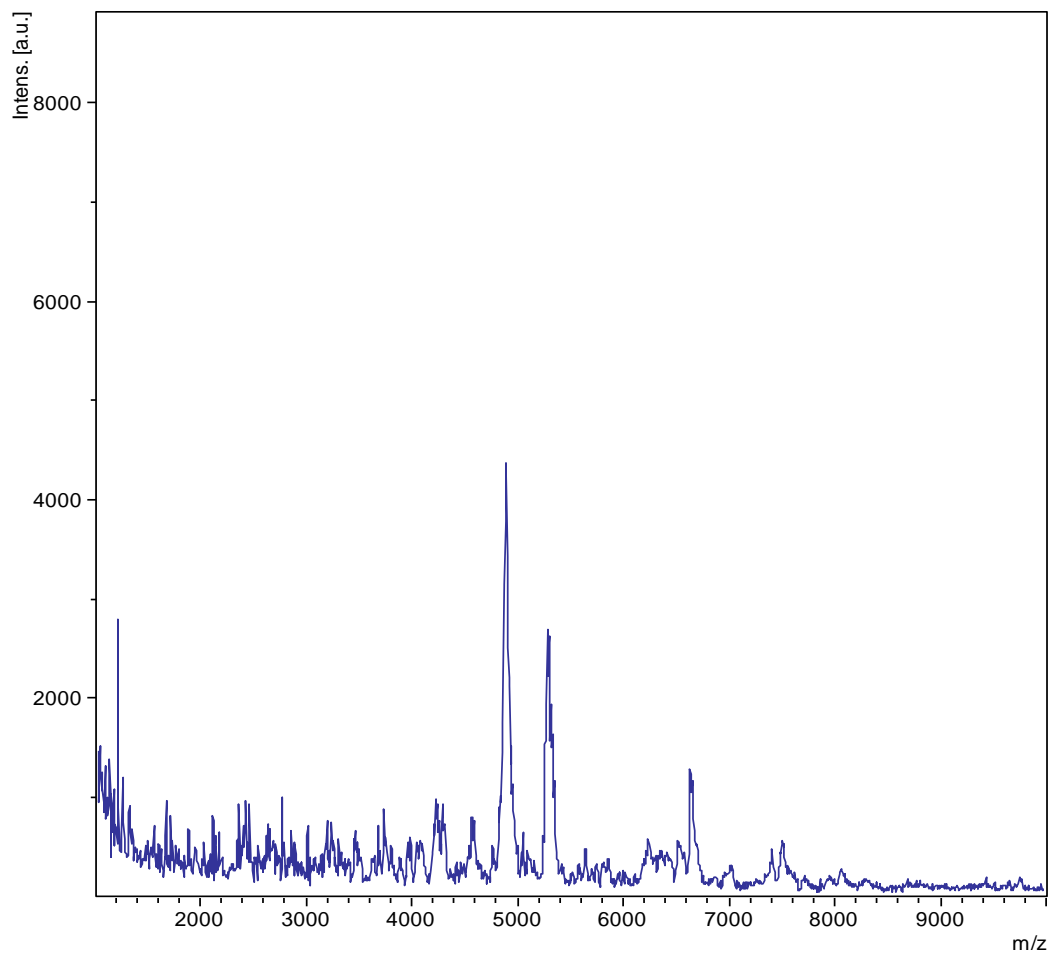
Figure B.2: MALDI-TOF spectrum for FG2. The x-axis and y-axis display the mass-to-charge (m/z) ratio and intensity.
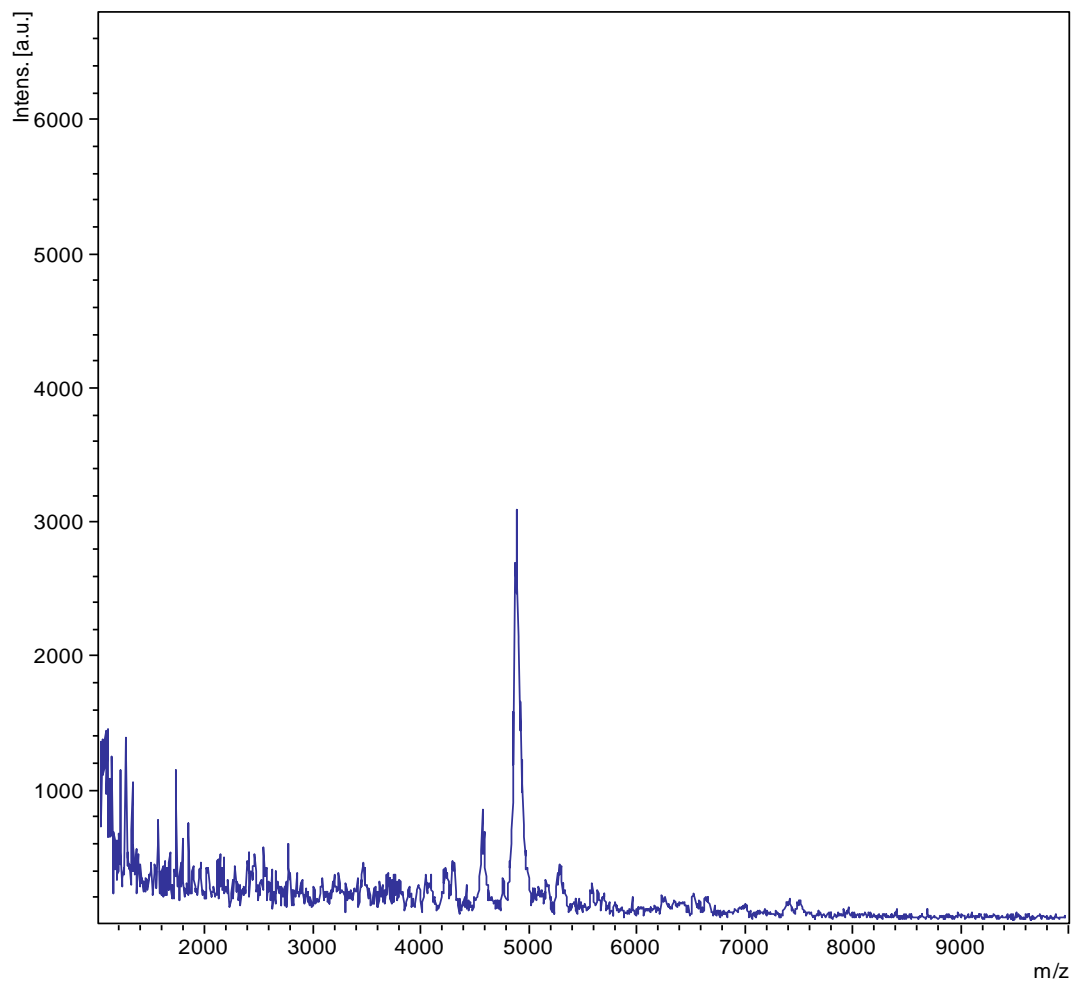
B.3 FG4
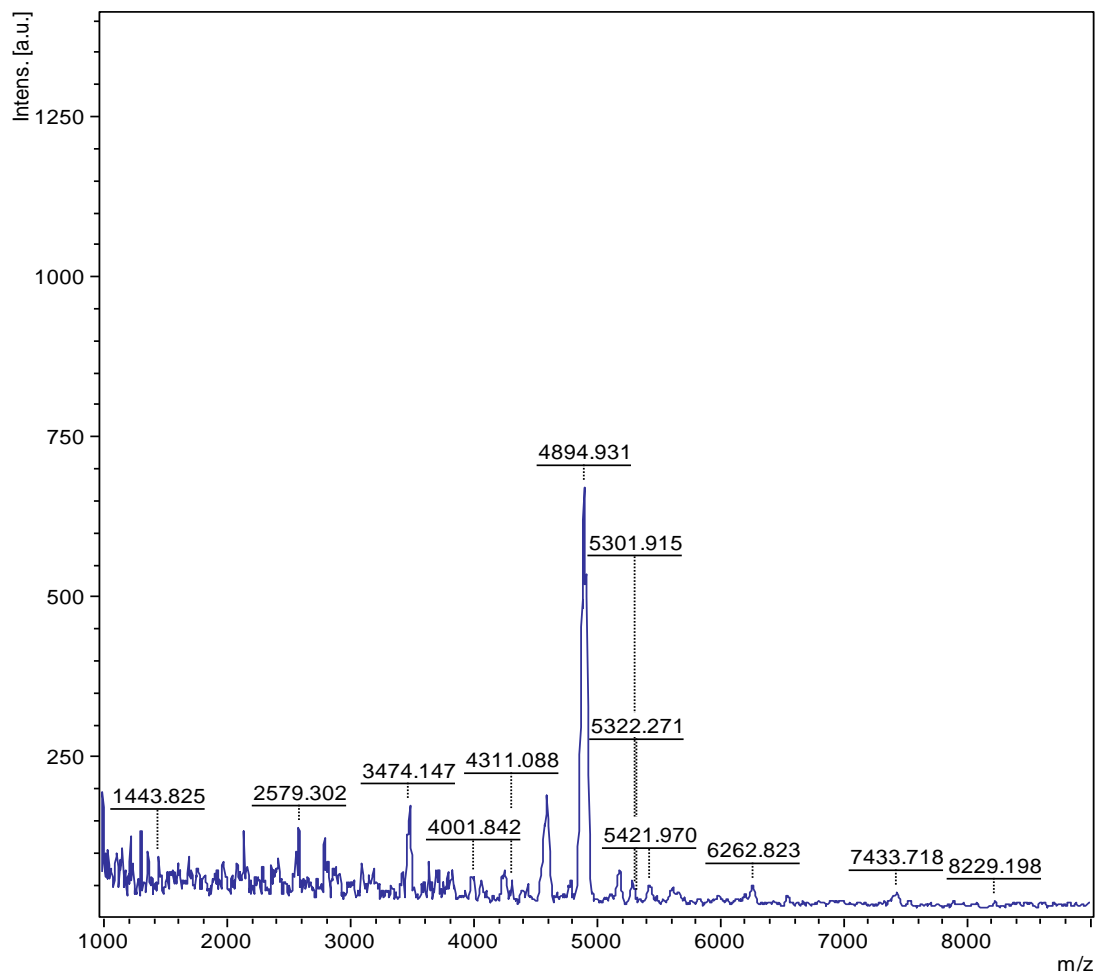
Figure B.3: MALDI-TOF spectrum for FG4. The x-axis and y-axis display the mass-to-charge (m/z) ratio and intensity. The values in the spectrum indicate the molecular weight represented by the peaks.
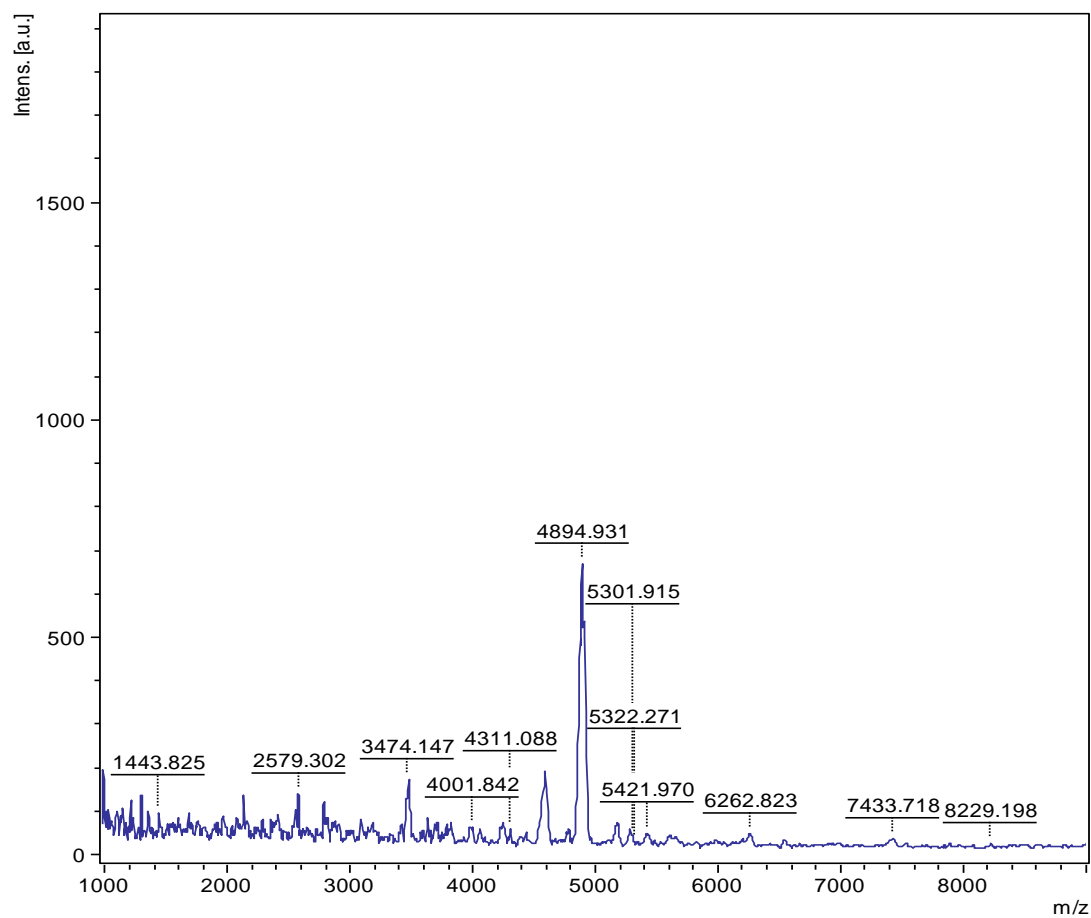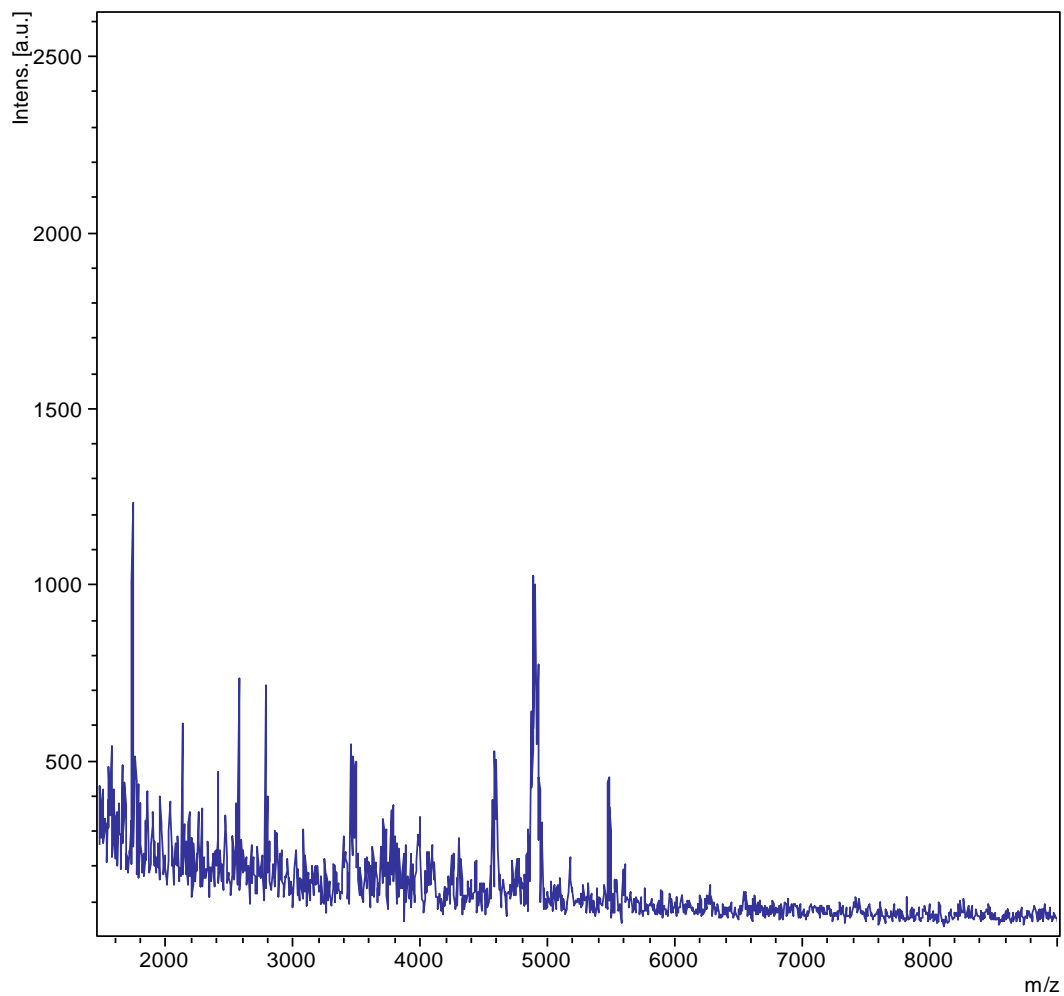
B.4 FG6
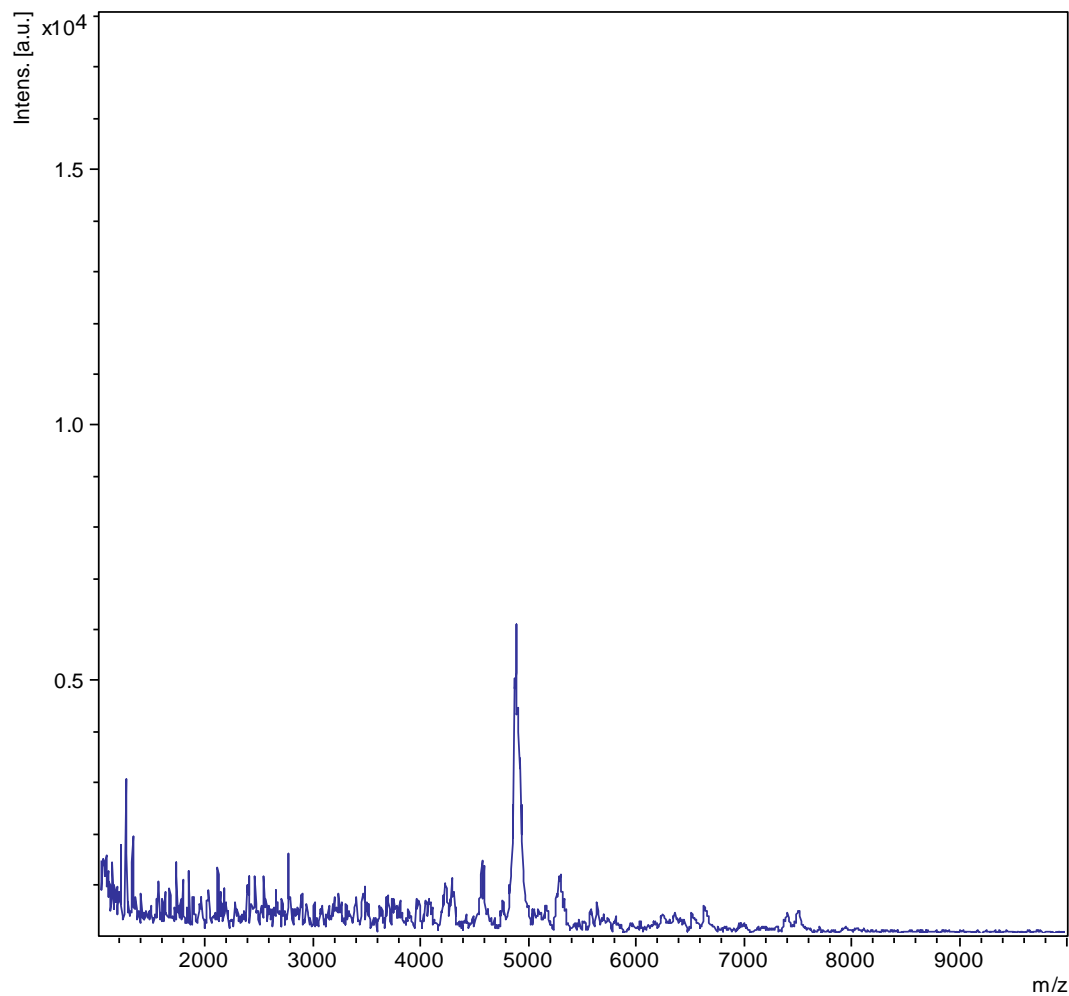
Figure B.4: MALDI-TOF spectrum for FG6. The x-axis and y-axis display the mass-to-charge (m/z) ratio and intensity.

B.5 FG8

Figure B.5: MALDI-TOF spectrum for FG8. The x-axis and y-axis display the mass-to-charge (m/z) ratio and intensity.
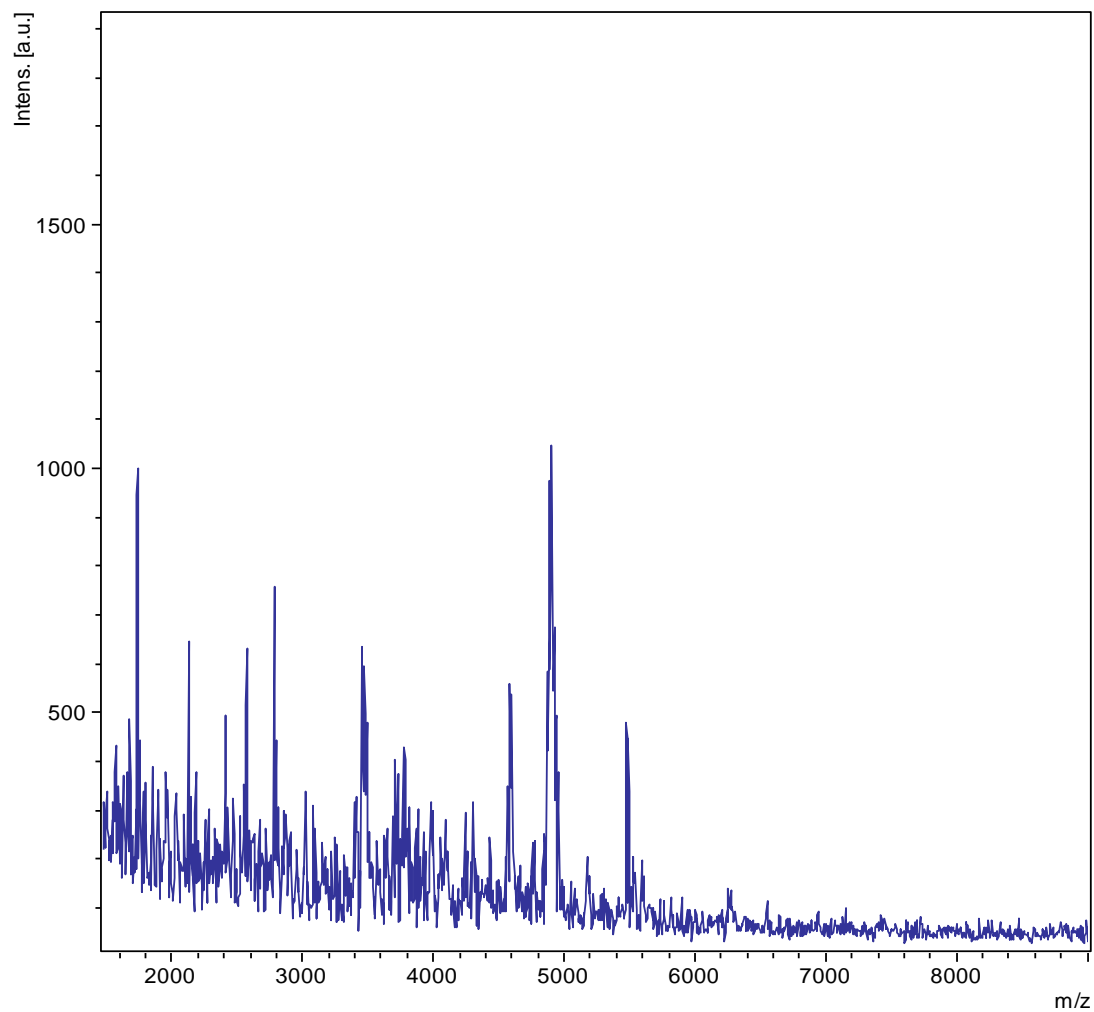
B.6 FG12

Figure B.6: MALDI-TOF spectrum for FG12. The x-axis and y-axis display the mass-to-charge (m/z) ratio and intensity. The values in the spectrum indicate the molecular weight represented by the peaks.
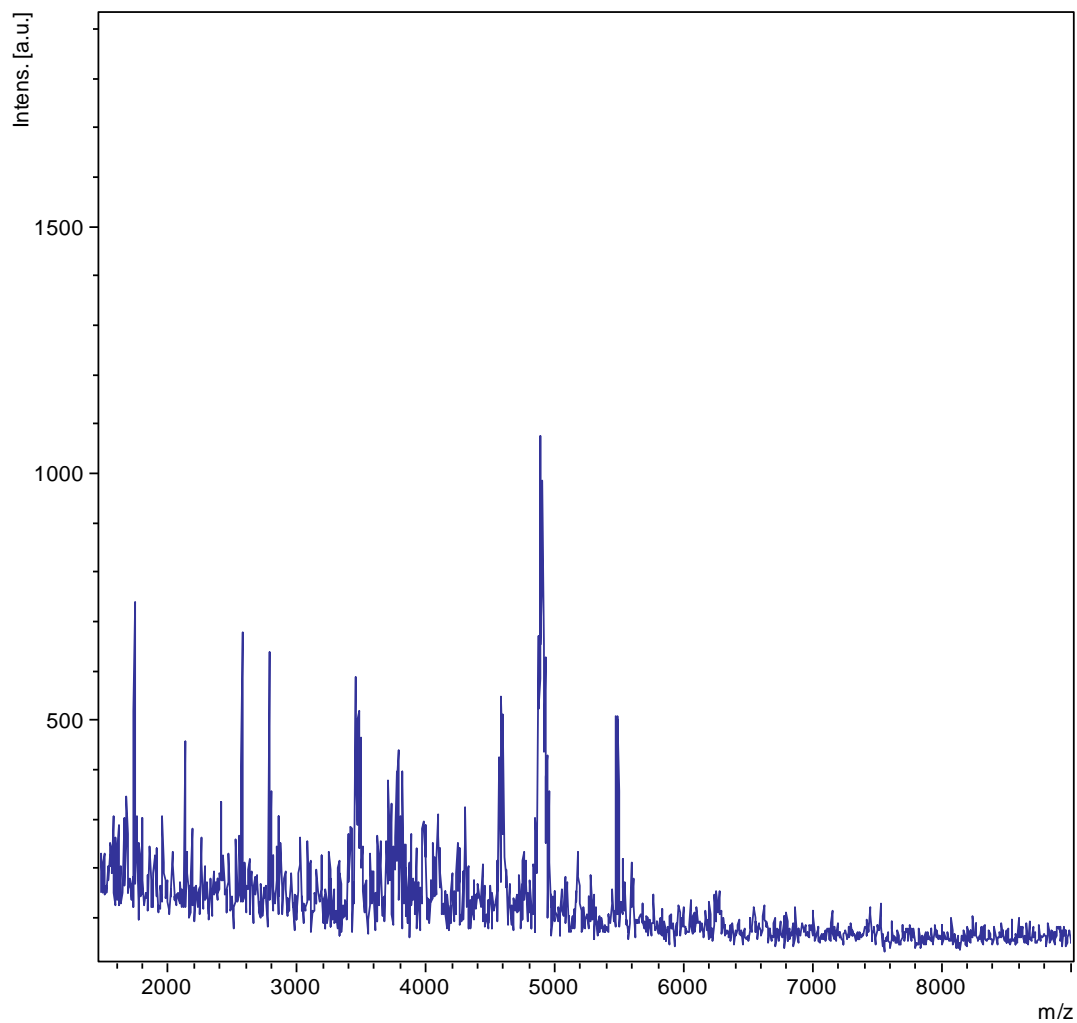
B.7   FG16

Figure B.7: MALDI-TOF spectrum for FG16. The x-axis and y-axis display the mass-to-charge (m/z) ratio and intensity.
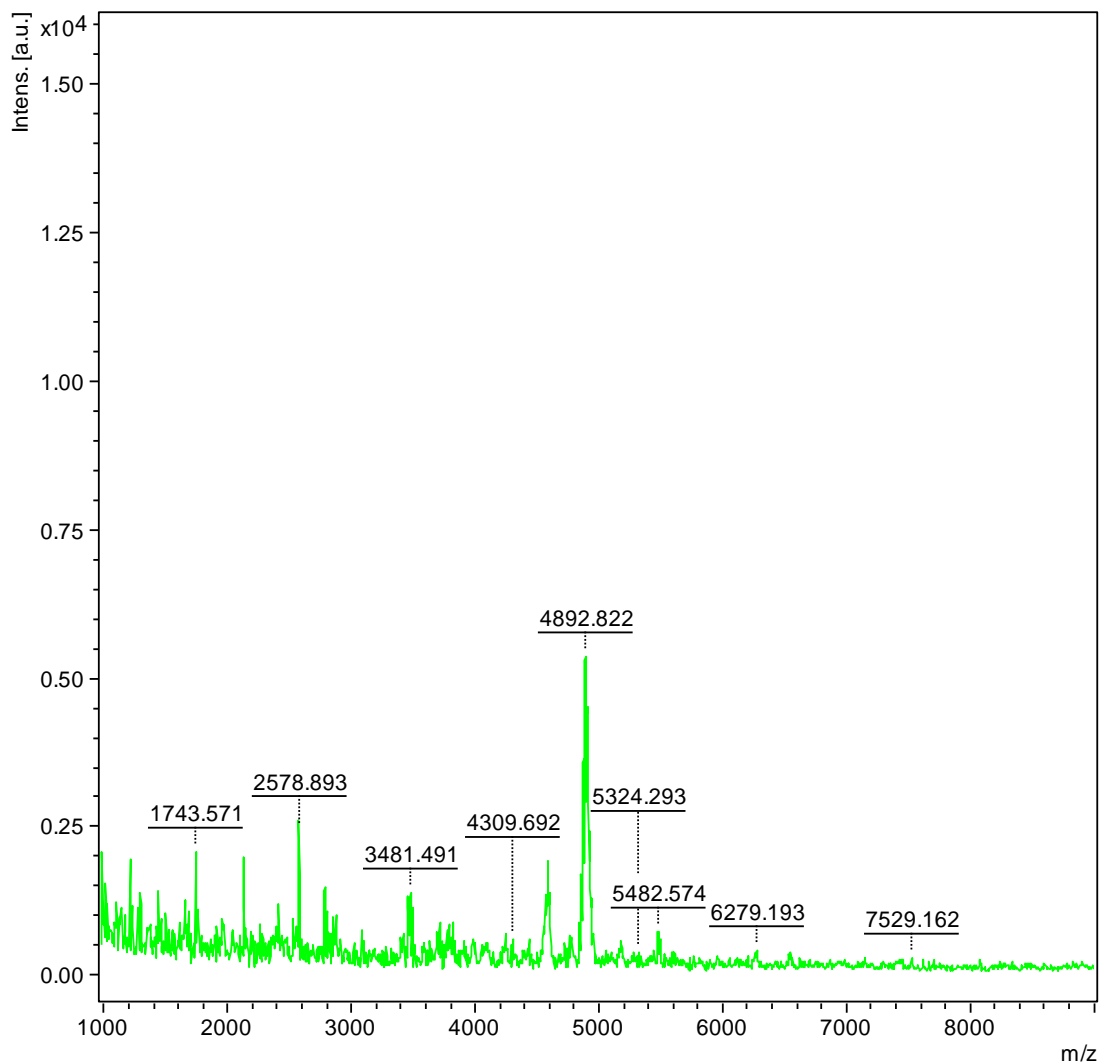
B.8 FG18

Figure B.8: MALDI-TOF spectrum for FG18. The x-axis and y-axis display the mass-to-charge (m/z) ratio and intensity.
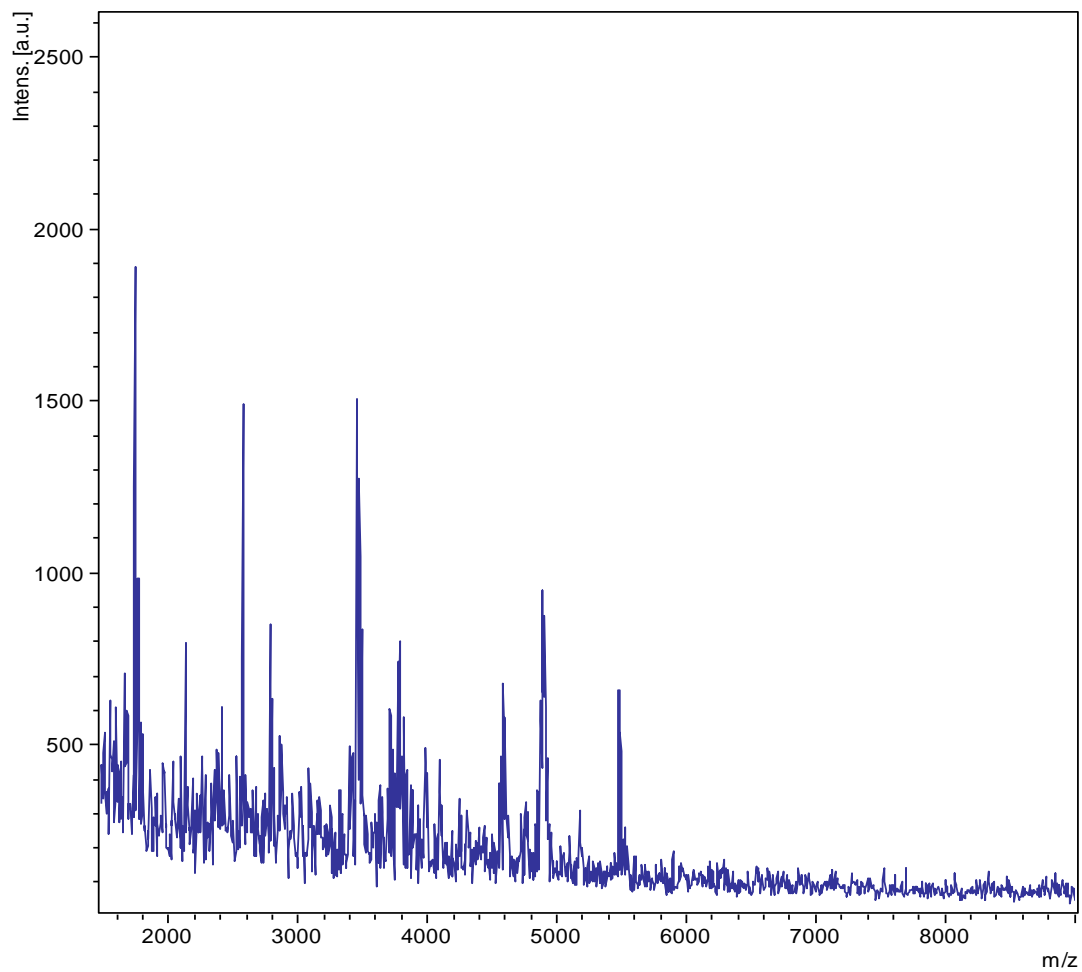
B.9   FG20

Figure B.9: MALDI-TOF spectrum for FG20. The x-axis and y-axis display the mass-to-charge (m/z) ratio and intensity.

B.10 FG24

Figure B.10: MALDI-TOF spectrum for FG24. The x-axis and y-axis display the mass-to-charge (m/z) ratio and intensity. The values in the spectrum indicate the molecular weight represented by the peaks.

B.11 FG36

Figure B.11: MALDI-TOF spectrum for FG36. The x-axis and y-axis display the mass-to-charge (m/z) ratio and intensity.

Appendix C: ^{1}H-NMR

The M_n of G-DP18 and G-DP22 were determined from the results of the ^{1}H-NMR analyses performed prior to this study (Eiken, 2011). The analysis resulted in two ^{1}H-NMR spectra, one for G-DP18 and one for G-DP22, which are given in Figures C.1 and C.2, respectively. The fractions of G- and M monomers, and the number average degree of polymerization (DP_n) given in Table C.1.

C.1: ^{1}H-NMR spectrum of G-DP18

The ^{1}H-NMR spectra of the G-block sample G-DP18.
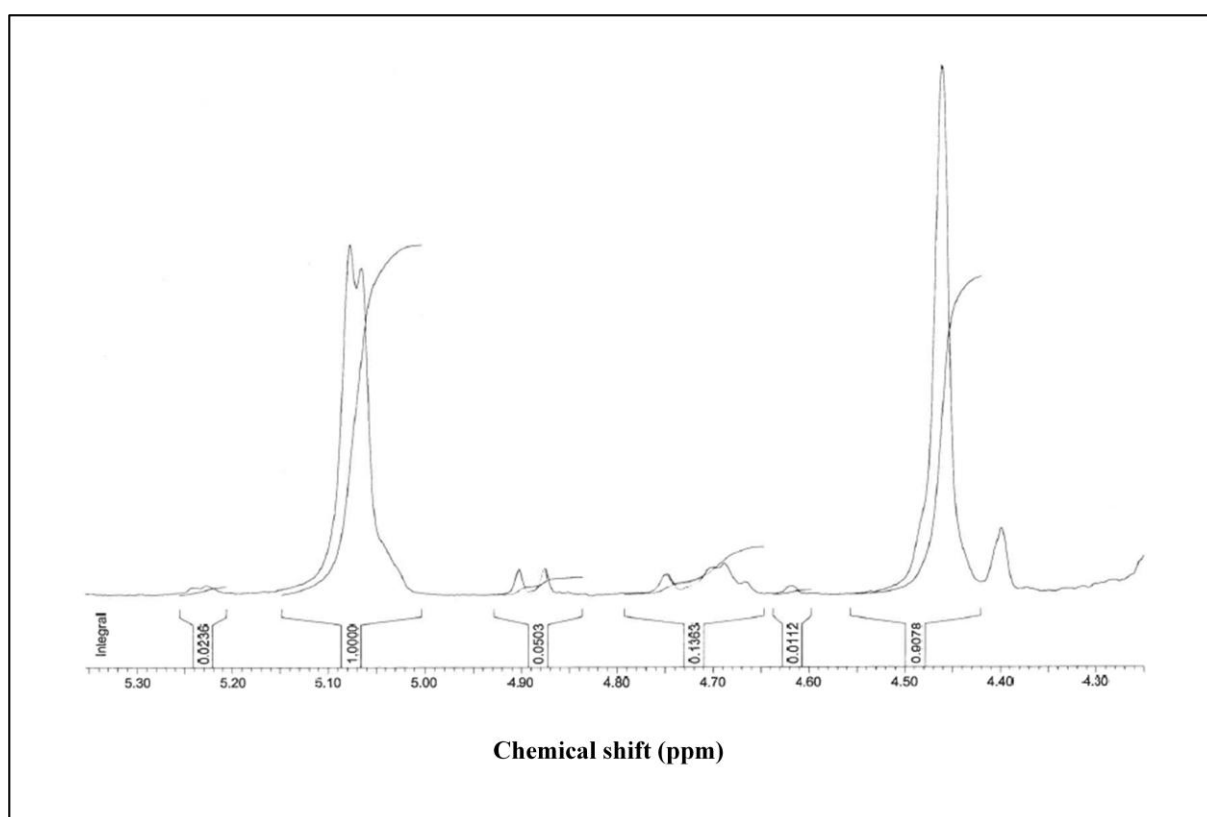

Figure C.1: ^{1}H-NMR spectra of the G-block sample G-DP18, showing integral limits and corresponding values (Eiken, 2011).

C.2: ^{1}H-NMR spectrum of G-DP22
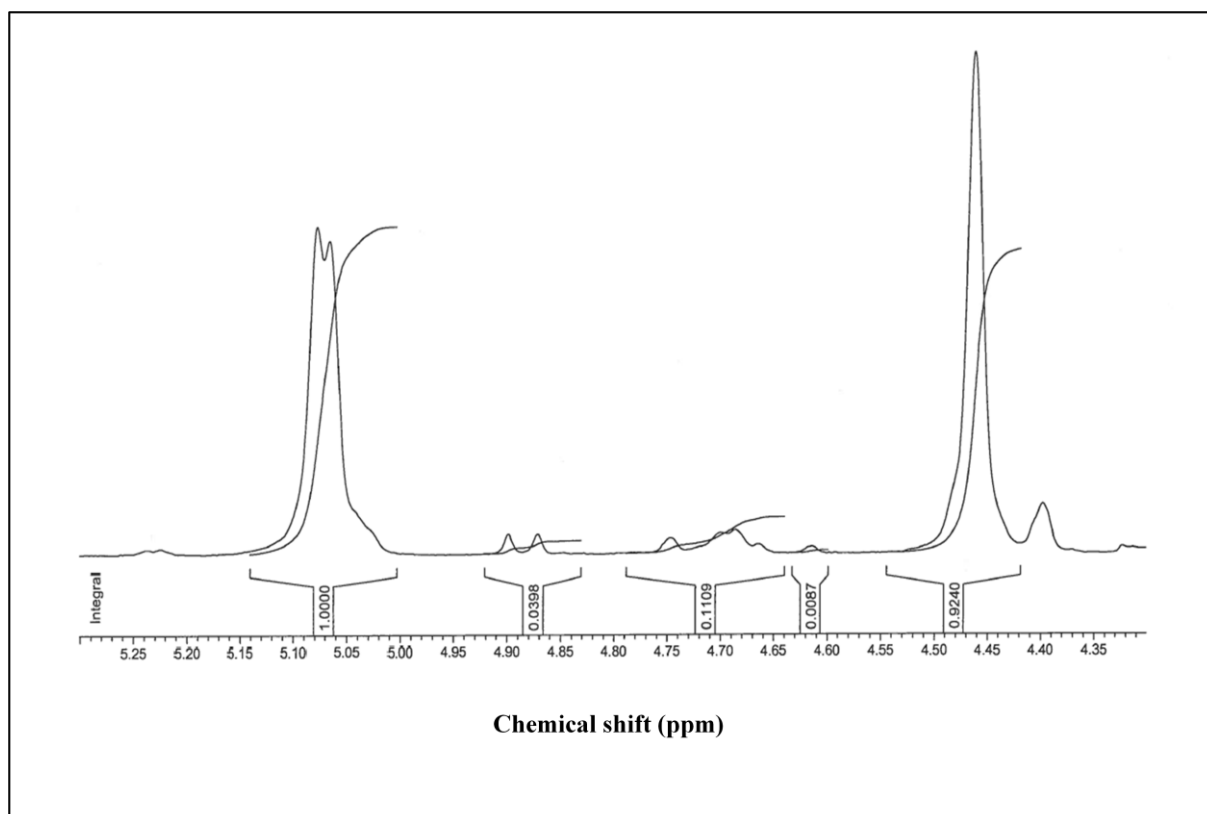
The ^{1}H-NMR spectra of the G-block sample G-DP18.

Figure C.2: ^{1}H-NMR spectra of the G-block sample G-DP22, showing integral limits and corresponding values (Eiken, 2011).

Table C.1: The number average degree of polymerization (DP_n) and fractions of G and M monomers in the G-block samples G-DP18 and G-DP22 (Eiken, 2011)

Sample	F_G (internal)	F_M	F_{GG}	F_{MG} F_{GM}	F_{MM}	F_G (reduced)	F_G (total)	DP_n
G-DP18	0.90	0.10	0.82	0.083	0.012	0.056	0.96	18
G-DP22	0.92	0.08	0.85	0.070	0.007	0.045	0.97	22

Appendix D: Absorbance values – DOL

The degree of labeling (section 2.2.4) was calculated for the FG and G-block samples according to Equation 2.3. The A_{max} values for the samples, measured at the λ_{max} of the respective dyes, are given in Table D.1.

Table D.1: A_{max} measured for the FG peptides and G-block oligomers applied in transdermal diffusion experiments. The measured values were used to calculate the DOL of the samples.

Sample	A_{max}
FG24 488 CASE	0.0076
FG24 532 CASE	0.0042
FG2 488 CASE	0.023
G-DP18 488 HSS	0.0043
G-DP22 488 HSS	0.0079

Appendix E: Mean fluorescence intensity values - diffusion kinetics experiments

The diffusion of Alexa 488 CASE and FG24 488 CASE, each in a 60% DMSO vehicle, was studied by varying the incubation time of tissues pre-treated with micro-needles and L1. These experiments were performed to investigate the time it would take for a sample to diffuse through the SC and further into deeper skin layers. The mean fluorescence intensity in the tissues ($I_{mean\ tissue}$) and the $I_{mean\ sample}$ ($I_{mean\ tissues}$ corrected for I_{auto}) for Alexa 488 CASE, after diffusion into skin pre-treated with micro-needles and laser from donor E and F, are given in Table E.1 and E.2, respectively. $I_{corrected}$ for FG24 488 CASE, after diffusion into skin pre-treated with micro-needles and laser, are given in Table E.2 and E.4, respectively.

Table E.1: $I_{mean\text{-}tissue}$ and $I_{mean\text{-}sample}$ of Alexa 488 CASE in skin tissues pre-treated with micro-needles, from donor E and F, after 2-24 hours of incubation.

Incubation time (hours)	$I_{mean\text{-}tissue}$	$I_{mean\text{-}sample}$
2	26 ± 29	17 ± 19
6	101 ± 64	92 ± 69
12	138 ± 83	115 ± 97
16	79 ± 49	56 ± 63
18	63 ± 35	40 ± 49
20	85 ± 47	62 ± 61
24	75 ± 40	52 ± 54

Table E.2: $I_{corrected}$ FG24 488 CASE in skin tissues pre-treated with micro-needles, from donor E and F, after 2-24 hours of incubation.

Incubation time (hours)	$I_{corrected}$
2	2219 ± 3159
6	2919 ± 3043
12	5075 ± 3784
16	8639 ± 4162
18	6243 ± 2888
20	4979 ± 3133
24	4717 ± 2630

Table E.3: $I_{mean-tissue}$ and $I_{mean-sample}$ of Alexa 488 CASE in skin tissues pre-treated with laser (L1), from donor J, after 20 minutes-6 hours.

Incubation time	$I_{mean-tissue}$	$I_{mean-sample}$
20 minutes	56 ± 84	43 ± 91
40 minutes	69 ± 91	56 ± 98
1 hour	90 ± 97	77 ± 104
2 hours	111 ± 109	98 ± 116
6 hours	239 ± 47	226 ± 226

Table E.4: $I_{corrected}$ of FG24 488 CASE in skin tissues pre-treated with laser (L1), from donor J, after 20 minutes-6 hours.

Incubation time	$I_{corrected}$
20 minutes	2923 ± 6930
40 minutes	5104 ± 9478
1 hour	11093 ± 12392
2 hours	13862 ± 13394
6 hours	24724 ± 10621